THESIS APPROVAL

GRADUATE SCHOOL, KASETSART UNIVERSITY

Doctor of Engineering (Water Resources Engineering)
DEGREE

Water Resources Engineering
FIELD

Water Resources Engineering
DEPARTMENT

TITLE: The Effects of Land Cover Changes on Flooding

NAME: Mr. Wisuwat Taesombat

THIS THESIS HAS BEEN ACCEPTED BY

..... **THESIS ADVISOR**
(Associate Professor Nutchanart Sriwongsitanon, Ph.D.)

..... **COMMITTEE MEMBER**
(Professor Ian H. Fisher, Ph.D.)

..... **COMMITTEE MEMBER**
(Associate Professor Kobkiat Pongput, Ph.D.)

..... **COMMITTEE MEMBER**
(Professor Nipon Tangtham, Ph.D.)

..... **DEPARTMENT HEAD**
(Assistant Professor Surachai Lipiwattanakarn, M.ASc.)

APPROVED BY THE GRADUATE SCHOOL ON .....

..... **DEAN**
(Associate Professor Gunjana Theeragool, D.Agr.)

THESIS

THE EFFECTS OF LAND COVER CHANGES ON FLOODING

WISUWAT TAESOMBAT

A Thesis Submitted in Partial Fulfillment of
the Requirements for the Degree of
Doctor of Engineering (Water Resources Engineering)
Graduate School, Kasetsart University
2010

Wisuwat Taesombat 2010: The Effects of Land Cover Changes on Flooding.
Doctor of Engineering (Water Resources Engineering), Major Field:
Water Resources Engineering, Department of Water Resources Engineering.
Thesis Advisor: Associate Professor Nutchanart Sriwongsitanon, Ph.D. 199 pages.

Land cover is considered to be an important factor affecting the frequency and severity of flooding in a river basin. An assessment of how changes in land cover over time affected flood behaviour from 1988 to 2005 in the upper Ping river basin in Northern Thailand was undertaken in this study. Correlations between these land cover changes and rainfall-runoff behaviour for flood and flow events taking place during this period were examined. To quantify land cover, nine LANDSAT-5TM images taken during the dry season (January or February) were obtained and processed to examine inter-annual land cover changes. From the networks of daily read rainfall data and stream gaugings available across the basin, 68 rainfall stations and 11 runoff stations were selected to evaluate peak flow rate and Rainfall-Runoff Factor (RRF) for flood events. For individual sub-catchments, strong nonlinear correlations between the overall RRF and peak flow rates for flood events were found. These RRF to peak flow relationships varied from year to year with different land cover for each sub-catchment. From these relationships within a particular sub-catchment, relationships between different land cover and RRF for the 2, 5, 10 and 25 year ARI peak flood events were determined. The results showed that RRF increased with increasing forest proportion for these specified peak flood conditions on nine out of eleven sub-catchments. On the other hand, the RRF associated with these peak flood events decreased as agricultural and disturbed forest areas increased. The influence of land cover on RRF was however found to be very different between flood and flow events. RRF is higher with for high forest cover under flood events (greater than around one year ARI); but for flow events (less than around one year ARI), RRF is lower when forest cover is high. The correlations between RRF and percentage of forest cover for flood and flow events were then generated for the scenarios runs to see the effect of forest cover on flood and flow hydrographs. Two scenarios of deforestation in 2005 and 2010 and one scenario of aforestation in 2005 were applied on the selected flood event in 2001. Flood inundation maps for these three scenarios and the baseline flood event in 2001 were prepared by GIS software using the input data of the maximum water level at each cross-section determined by FLDWAV together with the DEM data of the basin. The result of flood maps confirmed that deforestation tend to relieve flooding for both flood peak magnitude as well as flood volume but aforestation showed a reverse effect. To be expected, an impact of deforestation and aforestation on flow hydrograph showed an opposite direction as presented within flood events. It seems as if the catchment has a flood saturation threshold: for a flood exceeding the threshold then a high proportion of the rainfall is transformed to runoff. These thresholds are most likely controlling by soil saturation within the basin. For smaller events lower than the saturation threshold a much lower proportion of rainfall is transformed to runoff. As the forest cover increases, this seems to magnify this effect making RRF even larger for flood events and smaller for small events. This finding revealed a very new understanding of the effect of changing land cover on flood behaviour for different catchment saturation conditions within the basin.

/ /

Student's signature Thesis Advisor's signature

ACKNOWLEDGEMENTS

This thesis is a result of my studies at inspiring university namely the Department of Water Resources Engineering at Kasetsart University (KU) in the period of November 2004 to March 2010.

I am greatly indebted to my thesis advisor Assoc. Prof. Dr. Nutchanart Sriwongsitanon, for her valuable suggestions, encouragement, advice and understanding through my study experience. I would also like to thank the other members of my committee, Prof. Dr. Ian H. Fisher, Assoc. Prof. Dr. Kobkiat Pongput, and Prof. Dr. Nipon Tangtham at KU, and Prof. Eric Valentine, Dr. Sandeep G. Patil, and Mr. Phil Totterdell at Charles Darwin Unversity (CDU), NT, Australia. Dr.Michael Waters is also thanked for his suggestions and reviewing this thesis, and Assoc. Prof. Dr. Chavalit Chaleeraktrakoon from the Graduate School at KU for reviewing this thesis.

I would like to sincerely thank Assoc. Prof. Santi Tongpumnuk and Assoc. Prof. Dr. Bancha Kwanyuen who head the Department of Irrigation Engineering at KU, other instructors and staffs for their support and encouragement. This thesis was mainly financially supported by the Kasetsart University Research Development Institute, and the thesis and dissertation support fund of the Graduate School at KU. For LANDSAT-5TM images, were supplied by the Geo-Informatics and Space Technology Department Agency (Public Organization), GISTDA. Moreover, I would like to acknowledge the efforts of many people who contributed to this thesis, without them, the work would never have been completed.

Finally, this thesis is dedicated to my family especially my mother, Mrs.Thongpool, who encouraged and supported me in all my needs, my father, Mr.Wirasak, my younger brother, Doctor Wipusit, my friends, and my colleagues for their invaluable supports.

Wisuwat Taesombat

March 2010

TABLE OF CONTENTS

Page

LIST OF TABLES

LIST OF TABLES (CONTINUED)

LIST OF TABLES (CONTINUED)

LIST OF FIGURES

LIST OF FIGURES (CONTINUED)

LIST OF FIGURES (CONTINUED)

LIST OF FIGURES (CONTINUED)

THE EFFECTS OF LAND COVER CHANGES ON FLOODING

INTRODUCTION

A flood can be considered as a natural phenomenon whereby excessive catchment runoff causes a river to overflow its banks. Flood waters can spread to agricultural, residential, industrial and commercial areas, can cause economic and social damage and especially can cause risks with regard to human life. In Thailand, there is a potential for serious flooding every year on low lying landscapes because of the monsoon climate. Land cover is one of the main factors affecting the hydrological characteristics of a river basin, especially those characteristics that affect flood magnitude and flood frequency. Thailand as a developing and agricultural country is currently facing significant land cover changes that may tend to increase the flood magnitude and occurrence.

Internationally, there has been much concern for quite some time that deforestation of upland catchments may alter downstream flood hydrology. This concern has been fostered by the strong evidence that deforestation leads to increased flooding on scales smaller than 2 km^2 (Bosch and Hewlett, 1982). However, for larger catchments the situation is more complex. The limited number of studies that have quantified effects of land cover changes on flood behaviour report a diversity of results, with some studies reporting that deforestation is linked with an increased severity of flooding, a number of other studies finding no definitive change in flood behaviour, and some studies even showing evidence that flooding reduces as deforestation occurs.

Lin and Wei (2008) provide a good example of a large scale study showing a trend of increased flooding with decreasing forest cover. They showed evidence that deforestation in the Willow catchment (2,860 km^2) in Canada significantly increased mean and peak flows between 1957 and 2005 during spring periods; however, the mean and peak flows in summer and winter were not significantly affected. More broadly, in a study based on a dataset of national statistics of land cover change and

flood characteristics, Bradshaw *et al.* (2007) concluded that deforestation is strongly correlated with flood occurrence and severity in developing countries. However, Van Dijk *et al*. (2009), re-examined this data set and concluded that the understanding of how deforestation impacts on hydrology for large scale catchments is far from complete. They went on to cite many recent studies on large-scale catchments that found no significant changes in hydrology even after deforestation of up to 50% of the catchment. Furthermore, they found that where changes did occur, these were not directly attributable to deforestation. Van Dijk *et al.* (2009) concluded that until now, there has not been convincing empirical evidence or theoretical argument that removal of trees is likely to increase severe flooding in developing countries.

Case studies that showed flood flows on large-scale catchments were not significantly affected by land cover change include Buttle and Metcalfe (2000) found only limited flow responses to land cover changes of 5 to 25%, for catchments in Northeastern Ontario, Canada, with no definitive changes in annual flood peak. Dyhr-Nielsen (1986), also showed no significant trends in hydrology in the Pasak river basin in Central Thailand, where changes in forest cover of up to 50% were observed. Wilk *et al*. (2001) did not find any significant change in hydrological behavior after deforestation in the Nam Pong river basin in Northeastern Thailand when forest cover declined from 80% in 1957 to 27% in 1995. Finally, Adamson (2005) reports no definitive changes in the observed river hydrology of the Mekong river basin have occurred over the last 90 years despite the significant land cover changes in the basin during that period.

Few studies have shown deforestation to be linked to a decrease in peak flows; however a particularly significant study that did report this trend was conducted on the upper Penticton experimental basin in British Columbia, Canada (Austin, 1999).

This diversity of results is not surprising given that large catchments display significant temporal and spatial variability in many inter-related hydrological factors including rainfall, evapotranspiration, interception rates, overland flow rates and infiltration rates (Cosandy *et al*., 2005). Furthermore, when land cover changes occur

on a catchment, they are usually fragmented in time and space, impacting the hydrologic cycle through the clearing of vegetated areas in some areas and planting in others, as well as by geomorphologic changes due to the construction of roads, drainage channels and other infrastructure (Calder and Alyward, 2006).

Until 30 years ago, the heterogeneous nature of land cover changes across large catchments made their accurate assessment difficult. However, remote sensing now provides an invaluable tool for accurately detecting land cover change. LANDSAT-5 Thematic Mapper (TM) in particular is now a well established technique used with wide success internationally to detect interannual land cover changes for a variety of purposes. Examples include the detection of land cover change due to urban expansion, military base development and the political and cultural revolutions in Shijiazhuang city in China (Xiao *et al*., 2006), measuring environmental impacts of urban expansion in large Chinese cities, such as Beijing (Liu *et al*., 2000) and Guangzhou (Weng, 2002; Carlson & Arthur, 2000; Shen *et al*., 2003). In the United Kingdom, Grey *et al*. (2003) used remote sensing in mapping urban areas to analyze links between urban growth and land use/land cover change in South Wales. In Thailand TM has received widespread application, such as the accurate assessment by Ratanopad and Kainz (2006) of land cover change from 1995 to 2004 in Mahasarakham province of North-Eastern Thailand.

Quantifying flood behavior at the catchment scale is also difficult. Rainfall causing floods tends to occur infrequently and stochastically in time and space, meaning each flood is associated with a different spatio-temporal pattern of rainfall leading up to and during the event. Furthermore, rainfall and stream flow measuring techniques are both resource intensive and are limited to locations suitable for recording rainfall and stream gauging stations across the catchment.

For many years, engineers and researchers have been trying to understand the physical characteristics of river basins and to simulate flood behavior in the form of flood hydrographs to be able to predict and mitigate flooding and its effects for many years. To simulate the flood hydrograph more correctly, two model components - the

hydrologic and hydraulic models normally require. A hydrologic model can estimate flood discharges of various magnitudes while a hydraulic model can determine the extent, depth, and velocity of flooding (O'Connor and Costa, 2004). These two types of models have their own development to increase the accuracy for flood estimates.

This thesis aims to investigate the relationship between the land cover changes and flood characteristics in order to improve the understanding on the impacts of land cover changes on flood and flow events across the Upper Ping river basin (UPRB). flood management on the upper Ping river basin (UPRB). The UPRB is one of the main tributaries of the largest river basin within Thailand, the Chao Phraya, which drains more than one-third of the country's land area, making it Thailand's largest river basin. With Thailand's economic development, there is increasing concern for land cover changes and flooding in the Chao Praya basin. For example, between 25 and 30 September 2005, Typhoon Damrey devastated the UPRB, displacing 24,395 people and causing around 100 million baht (3 million US dollars) of widespread economic damage across Chiang Mai Province (Department of Disaster Prevention and Mitigation, 2005).

The UPRB occupies an area of approximately 25,370 km^2 upstream of the Bhumibol Reservoir between 16^o 54’ and 19^o 51’ N latitude, 97^o 48’ and 99^o 36’ E longitude. The UPRB is dominated by well forested steep mountains in a generally North – South alignment. Historically, the UPRB was nearly 90% forested, but by 2006 forest cover had declined to 72% (Royal Forest Department, 2006). Over the last 30 to 40 years, there has been significant deforestation on the UPRB for agricultural purposes and expansion of new urban communities. Much of this deforestation has been driven by economic development in and around Chiang Mai, a city of 2 million people, which is Northern Thailand's most important economic urban centre and is located in the north-central area of the UPRB.

The UPRB is subject to annual flooding due to heavy seasonal rains from both the South West monsoon and tropical storms related to typhoon events in the South China Sea. The average annual rainfall and runoff of the basin between years 1988

and 2005 are 1,174 mm and 6.8 billion m^3, respectively (Taesombat and Sriwongsitanon, 2010a).

This thesis was carried out using the following tools: numerical models (the hydrologic and hydrodynamic models) and Geoinformatics comprising RS, GIS, and GPS. The IHACRES and FLDWAV models were selected to estimate flood hydrographs at each lateral location and flood properties (flow rate and water level) at important locations, respectively, in the UPRB. The study river reach is between the gauging stations P.20 (Chiang Dao District) and P.73 (Chom Thong District). Annual land cover changes for the period of 1988-2005 in the UPRB were investigated by an application of Geoinformatics. Historical relationships between land cover changes and flood characteristics were examined using the multiple regression technique. Land cover change scenarios were investigated to determine their effects on flood characteristics. Finally, draft proposed land cover scenarios were prepared for consideration by local authorities for the improved flood management of the UPRB in order to alleviate flood damage and enhance the sustainable development of the basin.

OBJECTIVES

1. To study the theory and concept of the well known hydrologic and hydrodynamic public domain models and to choose the suitable models to suit Thailand river basins to be used for flood estimation and flood routing investigation for the UPRB.

2. To setup the hydrologic and hydrodynamic models for the study basin for an investigation of flood hydrograph characteristics at each runoff station and downstream areas for the flood events from 1988 to 2005. Hydrologic and hydraulic parameters were examined for their differences within these flood events.

3. To apply the technique of Geoinformatics (RS, GIS, and GPS) to investigate annual land cover changes from 1988 to 2005 in the study basin. Future land cover changes were predicted using the historical recorded data.

4. To investigate the historical relationship between annual land cover change and flood characteristics in the study basin. These relationships were used to predict future flooding using the predicted future land cover changes in the basin.

5. To prepare land cover change scenarios to alleviate possible flooding that would occur in the UPRB.

Scopes

1. The hydrologic public domain model to be used for flood characteristic investigation was selected by the literature review.

2. The comparison between the well known hydrodynamic public domain models were carried out and the suitable model were chosen to suit Thailand river basins. The performance comparison between the selected hydrodynamic public

domain model and the MIKE 11-HD model were verified by applying these models in the UPRB.

3. Annual land cover changes in the same period of flood characteristic investigation were identified using LANDSAT-5 Thematic Mapper satellite imagery.

4. Measurement rainfall and meteorological data at different stations over the study area were generated into areal average values using the ANUSPLIN spatial interpolation software and the digital elevation model (DEM) of topography, before they were input to the selected hydrologic public domain model.

5. Topographic map (scales 1:50,000 and 1:4,000), land cover maps, and other related information to support the hydrologic and hydrodynamic investigation and annual land cover changes detection of the UPRB in GIS format prepared by related government agencies were acquired. The accuracy of each map was verified.

6. To setup the selected hydrologic and hydrodynamic models to investigate flood characteristics in the UPRB for the period 1988-2005. The relationship between flood characteristics and annual land cover changes in that period were examined.

7. The results gained from the relationship between historical flood characteristics and annual land cover changes were used to investigate appropriate land cover planning by trialing scenarios. Land cover change scenarios for flood management of the UPRB were prepared to alleviate flood damage for the basin sustainable development.

About This Thesis

Much of the materials presented in this thesis have already appeared in publication as follow:

1. Taesombat and Sriwongsitanon (2006) An Evaluation of the Effectiveness of Hydrodynamic Models Application for Flood Routing Investigation in the Upper Ping River Basin. Engineering Journal Kasetsart 20(60), 74-82: Sub-section 2.4.2 “Hydraulic model for flood routing investigation” in the Literature Review section (p.35)

2. Taesombat and Sriwongsitanon (2009) Areal Rainfall Estimations using Spatial Interpolation Techniques. ScienceAsia 35(3), 268-275: Sub-section “1.2 Spatial Interpolation over the study area by ANUSPLIN software” in the Materials and Methods section (p.89), and Sub-section “1. Areal rainfall estimations using spatial interpolation technique” in the Results and Discussion section (p.118).

3. Taesombat and Sriwongsitanon (2010a) Flood Investigation for the upper Ping river basin using the Mathematical Models. Kasetsart Journal (Natural Science) 44(1), 152-166: Sub-section “2. Selection of hydrologic and hydrodynamic public domain models” in the Materials and Methods section (p.91), and in the Results and Discussion section (p.124).

4. Taesombat and Sriwongsitanon (2010b) Flood Estimation for Ungauged Catchments using IHACRES. Submitted to ScienceAsia: Sub-section “3. Examine relationships between flood characteristics and catchment characteristics” in the Materials and Methods section (p.96), and in the Results and Discussion section (p.129).

5. Taesombat and Sriwongsitanon (2010c) An Investigation on the Land Cover Changes in the Upper Ping River Basin using Geoinformatics. Submitted to Kasetsart Journal (Natural Science): Sub-section “4.1 Classification of Land Cover

Changes in the UPRB using the Geoinformatics" in the Materials and Methods section (p.102), and in the Results and Discussion section (p.140).

6. Taesombat, Waters and Sriwongsitanon (2010) Relationships between Land Cover and Rainfall Runoff Factor. Submitted to Global Change Biology: Sub-section "4.2 Examination of the Relationship between Land Use and Flood Characteristics." in the Materials and Methods section (p.106), and Sub-section "4.2 Correlations between Land Cover Change and Peak Flow Rates" in the Results and Discussion section (p.146).

7. Taesombat and Sriwongsitanon (2010d) Effects of Land Cover Changes on Flooding. Submitted to Global Change Biology: Sub-section "5. Effects of Land Cover Changes on Flooding." in the Materials and Methods section (p.109), and in the Results and Discussion section (p.158).

LITERATURE REVIEW

1. Study Area

Northern Thailand is a critical area for a number of sustainable development issues. The mountainous landscape still has relatively high forest cover and is home to a very diverse cultural mixture of long-term residents and more recent migrants and settlers. It contains the upper reaches of most of the major watersheds feeding into the Chao Phraya river system, including the largest of these, the Ping river basin (USER, 2006).

The Ping river basin is subdivided into the upper and lower portions by the Bhumibol dam. This dam was constructed across the Ping river at Sam Ngao District of Tak Province in 1958 and completed in 1964. This dam has a height of 154 m, crest length of 486 m and maximum retention capacity of 13.46 billion m^3. This dam is the first and largest multipurpose concrete arch dam constructed in Thailand. This dam is setup as the lower boundary of investigations in this thesis.

The UPRB covers an area of approximately 25,370 km^2 in the provinces of Chiang Mai and Lamphun, Northern Thailand and is located between 16^o 54' – 19^o 51' N latitude and 97^o 48' – 99^o 36' E longitude. The UPRB is mostly covered by forest and steep mountains, which are aligned in a North – South direction along the basin. The forest area has declined to 72% of the total area in 2006 (Royal Forest Department, 2006). The climate is monsoon type, with a rainy season from May to October and supplementary rains from occasional westward storm depressions originating in the Indian Ocean. Mean daily temperatures for the period 1975 to 2004, recorded at the Chiang Mai meteorological station, varied from 14°C in January to 36°C in April.

The Ping river originates in Chiang Dao District in the north of Chiang Mai Province and flows downstream to the south to become the inflow for the Bhumibol Dam. The average annual rainfall and runoff of the basin are around 1,174 mm and

6.8 billion m^3, respectively. The UPRB is one of the main sources of water supply for the people living in the basin and downstream areas. However, this river basin has always faced several flood problems each year because of heavy rains from both monsoon and tropical storms.

Chiang Mai is a city of economic significance for Thailand that is located in the north-central area of this river basin, resulting in internal migration of a large number of non-natives from other parts of Thailand into the area to make a living. This leads to problems of deforestation for agricultural purposes and expansion of new communities which makes it difficult to develop sustainable land cover planning and management. Declining forest cover within the basin area has apparently contributed to the occurrence of several natural disasters such as floods and landslides and poses a greater threat of adverse impact every year.

1.1 Topography characteristics

The general topography of the UPRB is steeply mountain covered with forest as shown in Figure 1. This river basin includes the Inthanon Mountain which stands 2,575 m (8,448 ft) above mean sea level and is Thailand's highest peak. The Ping river which originates in the mountains of Chiang Dao District where it has an altitude range of 500 to 1,300 m above mean sea level and a river bed slope approximately 1:40. The river portion in the mountains of Mae Taeng District has an altitude range of 320 to 500 m above mean sea level and a river bed slope of approximately 1:50. The river portion in the flat area of Mae Taeng District, Mae Rim District and Chiang Mai City has an altitude range of 260 to 300 m above mean sea level and a river bed slope approximately 1:1,800. The last river portion in the flat area before flowing into Bhumibol dam has an altitude range of 140 to 260 m above mean sea level and a river bed slope of approximately 1:1,590.

The UPRB comprises 14 first tributary and river line sub-catchments. Table 1 shows the area of each sub-catchment in the UPRB.

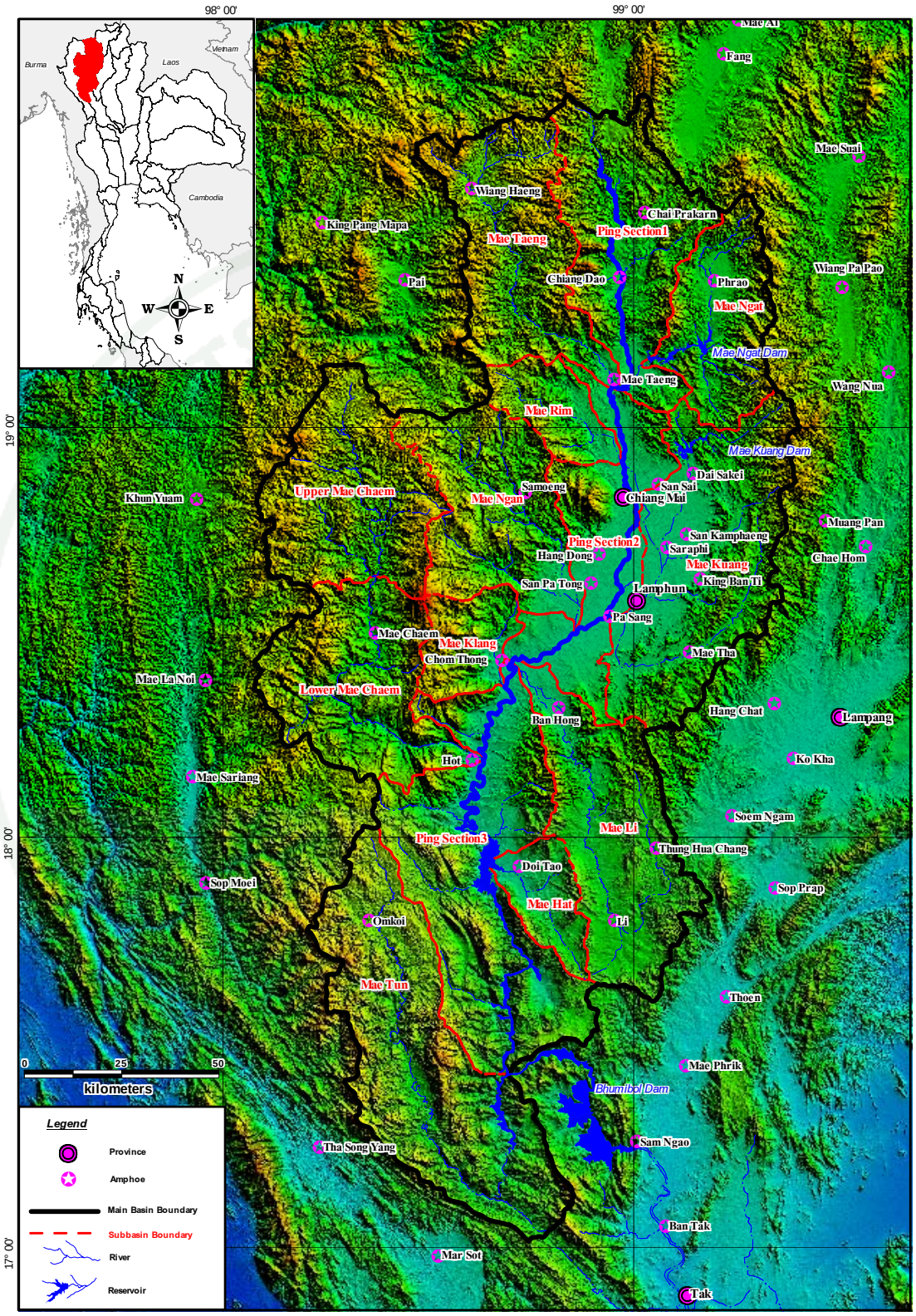

Figure 1 The topographical map of the UPRB.

Table 1 The area of each sub-catchment in the UPRB.

Order	Sub-catchment	Tributary(T) / Main-river(M)	Area (km^2)
1	Upper Ping	M	1,972.33
2	Nam Mae Ngat	T	1,282.39
3	Nam Mae Taeng	T	1,955.63
4	Ping section 2	M	1,723.15
5	Nam Mae Rim	T	565.45
6	Nam Mae Kuang	T	2,680.05
7	Nam Mae Ngan	T	1,731.68
8	Nam Mae Li	T	2,079.86
9	Nam Mae Klang	T	615.84
10	Ping section 3	M	3,179.72
11	Upper Mae Chaem	T	1,965.24
12	Lower Mae Chaem	T	1,930.26
13	Nam Mae Hat	T	520.76
14	Nam Mae Tun	T	3,167.27
Total area of the UPRB			**25,369.63**

1.2 Land cover

Based on the last land cover data collected from the Land Development Department (LDD) in 2000, Land cover area in the UPRB derived from LANDSAT-5 TM can be classified into 5 main types. First, forest covers 79.5% of the total area. (see Figure 2) Second, agriculture consists of paddy, crop, fruit, horticulture, mixed swidden cultivation, active shifting cultivation, old clearing and pastoral covers 15.2% of the total area. Urban and water bodies covers 3.1% and 0.8%, respectively. The last type, other areas comprise such as mine, well, etc. and cover 1.5% of the total area. Table 2 shows the area of each land cover type in the UPRB.

1.3 Hydrological characteristics

The average annual runoff and rainfall for the UPRB from 1970 to 2000 are 6,815 million m^3 and 1,174 mm, respectively. There are 123 rainfall stations located across this basin and the surrounds in 6 provinces, namely Chiang Mai, Chiang Rai, Lamphun, Lampang, Mae Hong Son and Tak provinces. A total of 80 runoff stations are located in the basin. Data are recorded by many government agencies, the Department of Water Resources (DWR), Royal Irrigation Department (RID), Thai Meteorology Department (TMD), and the Electricity Generating Authority of Thailand (EGAT). The location of the rainfall and runoff stations in the UPRB and the surroundings are shown in Figure 3 and Figure 4, respectively.

Chiang Mai and Lamphun Provinces have been settled and irrigated for paddy rice farming for more than 700 years. Since the early 1980s Chiang Mai's commercial and urban areas have grown dramatically affecting impropriated land cover changes. The degradation of forest and an expansion of urban, agricultural and industrial areas, caused by an increase in the population of Chiang Mai and Lamphun provinces, are suspected to be the main causes affecting flood characteristics and increasing flood magnitude.

Table 2 The area of each land cover type in the UPRB in year 2000.

Order	**Land cover type**	**Area**	
		km^2	**%**
1	Forest	20,165.26	79.5
2	Agriculture	3,847.95	15.1
3	Urban	779.78	3.1
4	Water bodies	197.95	0.8
5	Other area	378.69	1.5
Total area of the UPRB		**25,369.63**	**100.0**

Source: Land Development Department (2000).

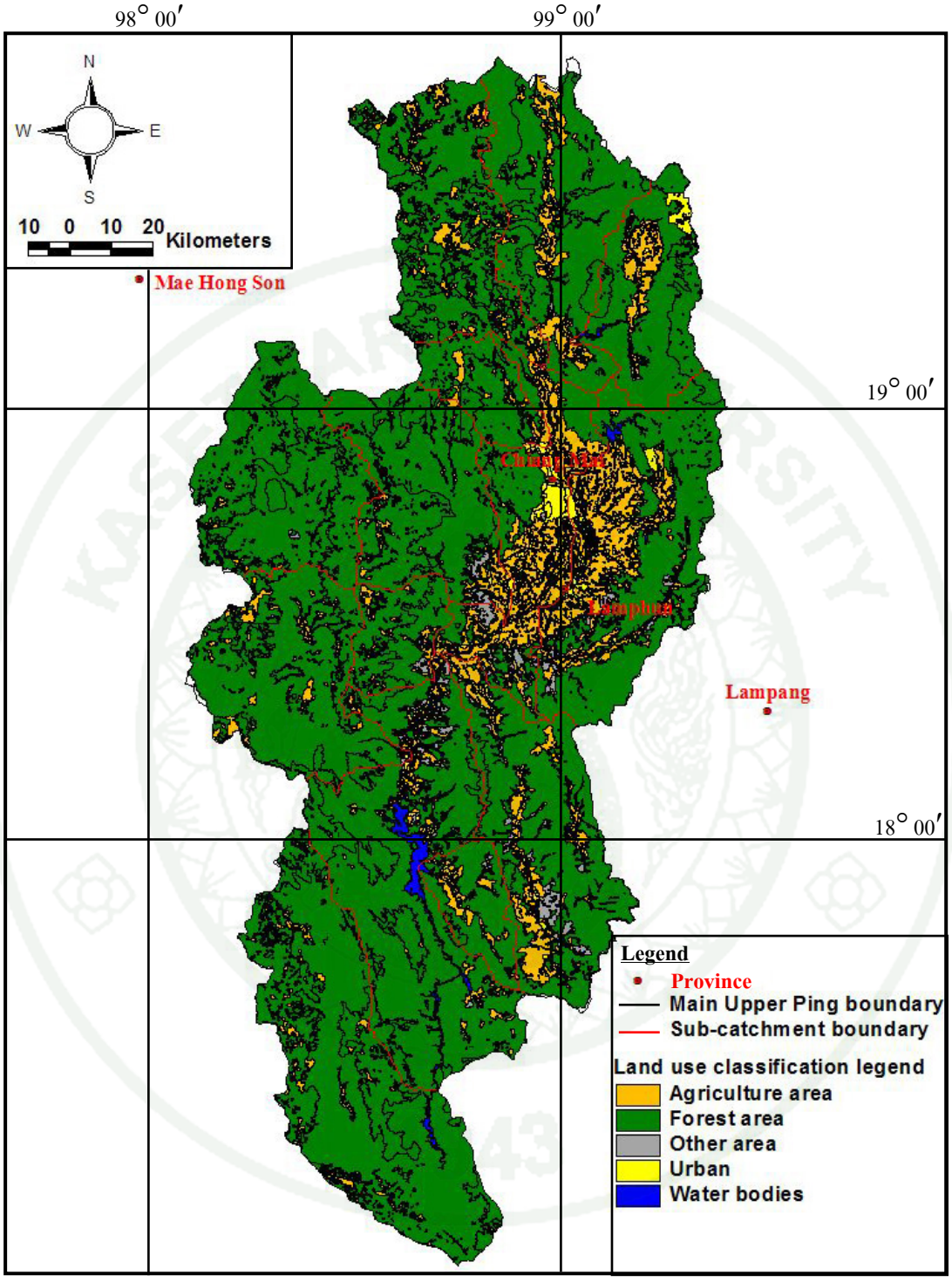

Figure 2 The land cover map of the UPRB in year 2000.

Source: Land Development Department (2000).

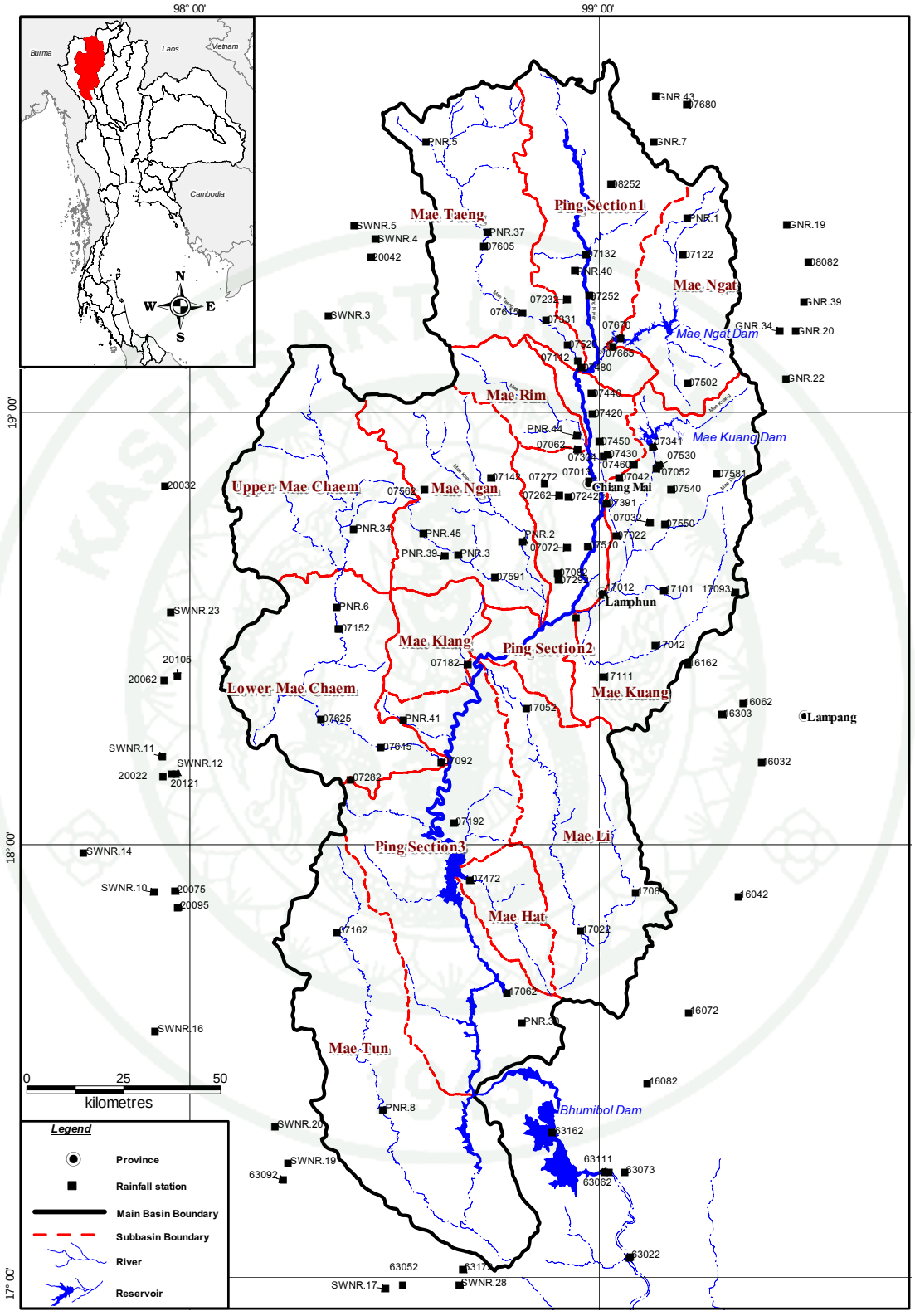

Figure 3 The location of the rainfall stations in the UPRB and the surroundings.

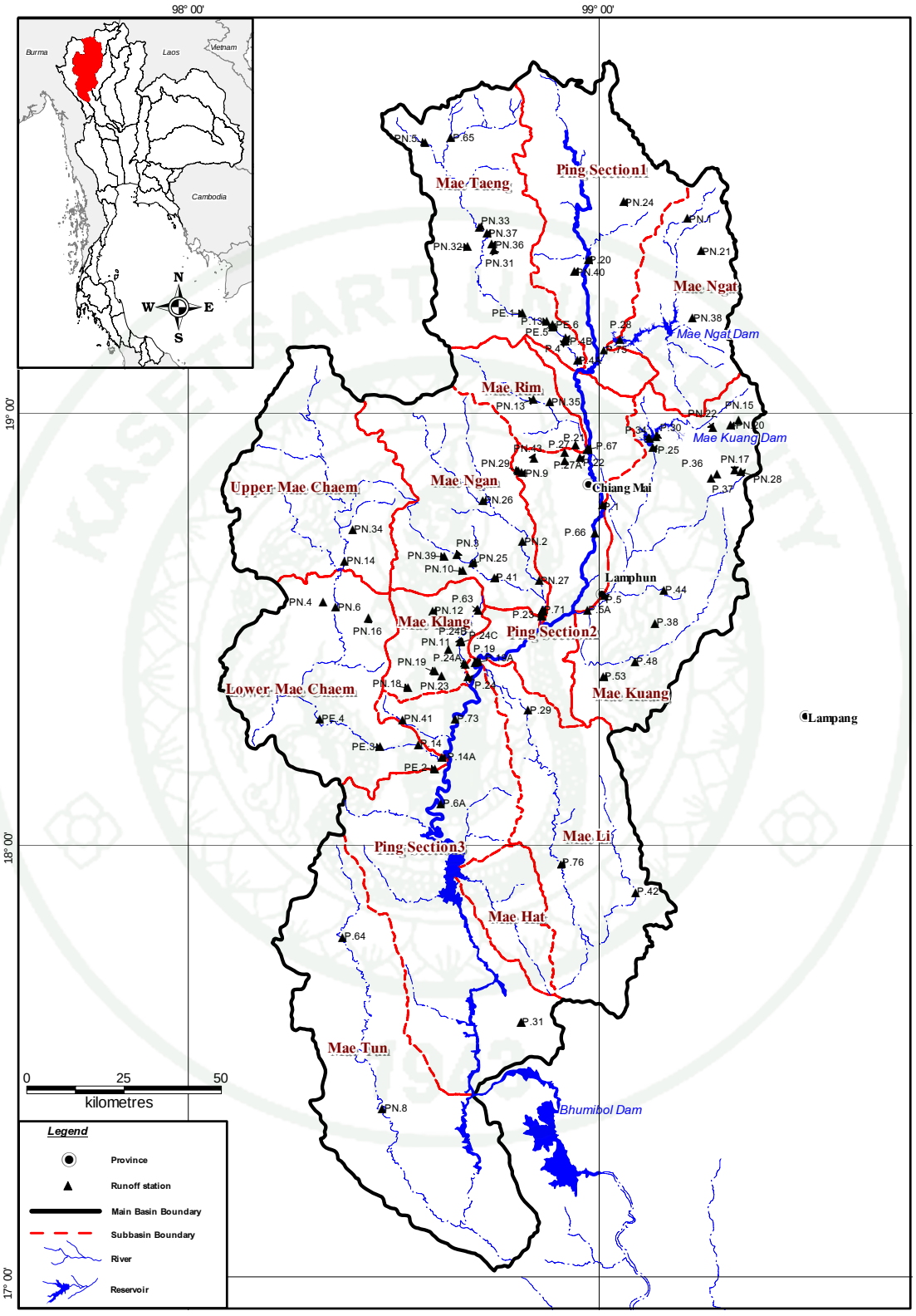

Figure 4 The location of the runoff stations in the UPRB.

2. Related Previous Research

2.1 Flood Management

Large floods can cause substantial loss of life and social and economic damage. From the past to present, government agencies responsible for flood mitigation have generally focused on structural measures because of their effectiveness to alleviate flood effects. However, often the structural measures may have some negative environment effects. On the other hand, non-structural measures such as catchment and flood management and flood warning systems, tend to have less effects on environment than structural measures, are more sustainable as solutions, and are of increasing interest among researchers and planners (DHI, 2003).

For effective flood management, it is necessary to use a multi-faceted approach, including structural and non-structural measures such as the following:

1) Management of the river basin by conserving the natural storage in the vegetation and soil upstream, and wetland areas downstream.

2) Structural interventions to increase the storage and conveyance of flood waters, and to protect the inhabitants of flood vulnerable areas.

3) Monitoring the hydrological conditions in the river basin.

4) Operation of upstream reservoirs and downstream detention areas to contain flood waters

5) Land cover planning in the floodplain, restricting urban and industrial development and allocating areas for the storage of flood waters

Taken as a whole, flood management involves an environmentally sensitive approach, protecting the ecology while permitting sustainable exploitation of the natural land and water resources.

The aim of this thesis will focus on non-structural measures particularly flood management on the areas affecting by land cover changes. The UPRB is chosen for detailed investigation as mentioned earlier.

2.2 Flood characteristics

Flood characteristics are considered such as depth, velocity and duration at specific locations in a catchment. Each catchment has its own unique characteristics related to topography, land cover and geology. These characteristics vary widely, from the slow-rising, long duration floods associated with most large catchments to fast-rising "flash floods" usually seen on small catchments. To understand flood characteristics we need to account for the key hydrologic processes occurring on a catchment.

Hydrologic processes determine the distribution of water after precipitation onto the land and before its return to the oceans. These main processes include precipitation, interception, evaporation, transpiration, evapotranspiration, infiltration, percolation, overland flow (surface runoff), interflow (subsurface flow), and groundwater flow as shown in Figure 5.

As the atmosphere becomes saturated, water is released back to earth as rain, snow, sleet, or hail. The rate of precipitation is influenced by topography; mountainous regions receive more rainfall than the flat areas. Precipitation is a natural phenomenon and humans can do very little to either control or change it. Precipitated water may intercept on leaves and branches in vegetation areas and evaporate before it reaches the ground. Some of the factors that affect evaporation include: air and water temperatures, wind, solar radiation, and relative humidity. Evaporation occurs from any surface where water is present in some form, including surfaces of bare soil, vegetation area, ponds, lakes, streams, and oceans. Transpiration which is the uptake water in soil absorbed by roots of plants and entitled out of the plants from their stomata. It is a natural by-product of photosynthesis and accounts for ten percent of the water evaporation on globally (Kern Mediation Group, 2006).

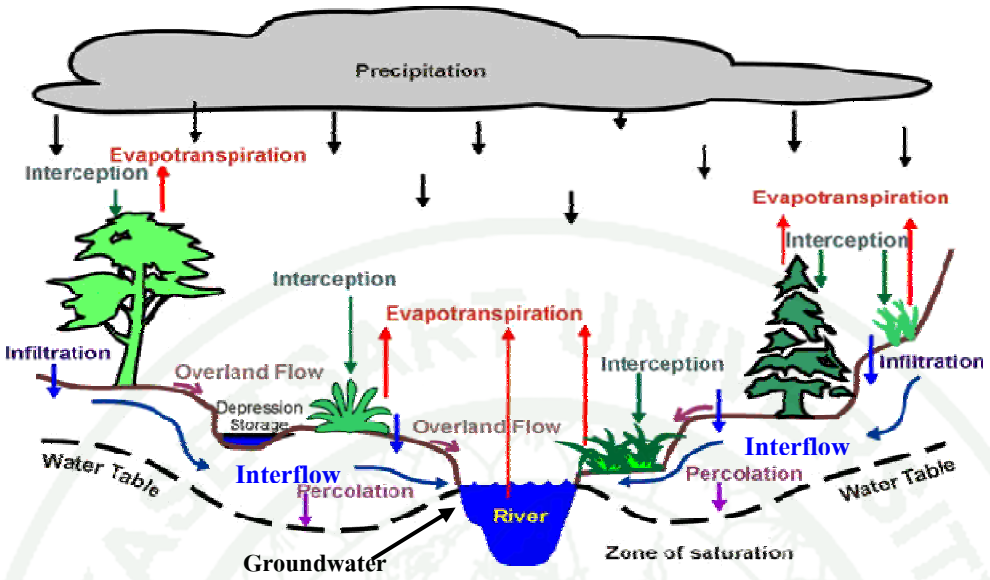

Figure 5 Hydrologic processes.

Source: R-Can Environmental Inc. (2006)

The combined loss of water from soil and vegetation by evaporation and transpiration is called evapotranspiration. This process accounts for more than half of the water transported back to the atmosphere. The rest of the water infiltrates or runs off into water bodies, such as streams, lakes and oceans. The rate at which water seeps through soil depends on certain soil properties such as soil water content, texture, density, organic matter content, hydraulic conductivity, and porosity. Soil surface conditions also affect the rate of infiltration. For instance, forested area, or pasture have greater infiltration rate than paved urban areas. In addition, topography, slope and the roughness of land surface influence infiltration. The groundwater in a saturated zone is recharged by the percolation process which is vertical and lateral movements of water caused by gravity through spaces between soil and rock layers through the overlaying unsaturated zone.

When the precipitation rate exceeds the infiltration rate, or when soil is saturated, water begins to move down slope on ground surfaces. Most surface runoff

enters streams and rivers and eventually flows into oceans. Surface runoff is also known as overland flow. In addition, interflow is a lateral movement of percolated water through soil and continues to follow the slope. This water is eventually discharged into rivers, streams, and lakes. Groundwater is a body of water found in a deep saturated zone that flows laterally and eventually merges with rivers, streams, lakes, and oceans.

Land cover changes due to human activities such as the introduction and expansion of grazing, agroforestry, cultivation, and urban development, including construction of road pavements, have greatly reduced the rate of infiltration and have increased surface runoff. So, human activities in the past several decades have dramatically affected flood characteristics in many river basins.

More surface runoff means less water percolates down to recharge groundwater supply. With increased surface runoff, a greater volume of water runs into streams and rivers at a faster rate, causing a sudden influx of water downstream. This higher volume of surface runoff not only increases the severity and frequency of flooding, but also degrades the environment by carrying a greater amount of sediments and pollutants from surface erosion.

2.3 Effects of land cover changes on flood characteristics

Land cover changes in developing counties, such as Thailand greatly affect flood characteristics which tend to increase peak flow magnitudes and occurrences and decrease recharge to groundwater. Generally, this is caused by not only long-term development such as deforestation, but also short-term development such as urbanization. Forest cover in the northern region of Thailand particularly Chiang Mai and Lamphun provinces dramatically decreased during the period of 1993 to 1997 as shown in Table 3. The total area of deforest in Chiang Mai and Lamphun provinces was 435 km^2 (271,875 rai) over this period.

Table 3 Forest cover of Chiang Mai and Lamphun provinces during 1993-1997

Province	Total Province area[1]	Conservatively estimated forest area[2]	Forest cover area[3]					
			1993		1995		1997	
			Area	%	Area	%	Area	%
Chiang Mai	20,107.06	19,555.83	14,420	71.72	14,232	70.78	14,060	69.93
Lamphun	4,505.88	2,928.06	2,207	48.98	2,155	47.83	2,132	47.32
Total	**24,612.94**	**22,483.89**	**16,627**	**67.55**	**16,387**	**66.58**	**16,192**	**65.79**

Remark Area unit is km^2.

(1) Collected from the Royal Thai Survey Department, Thailand.

(2) Announced in the Secretariat of the Cabinet, Thailand.

(3) Interpreted from LANDSAT-5TM.

Source: Royal Forestry Department (2005)

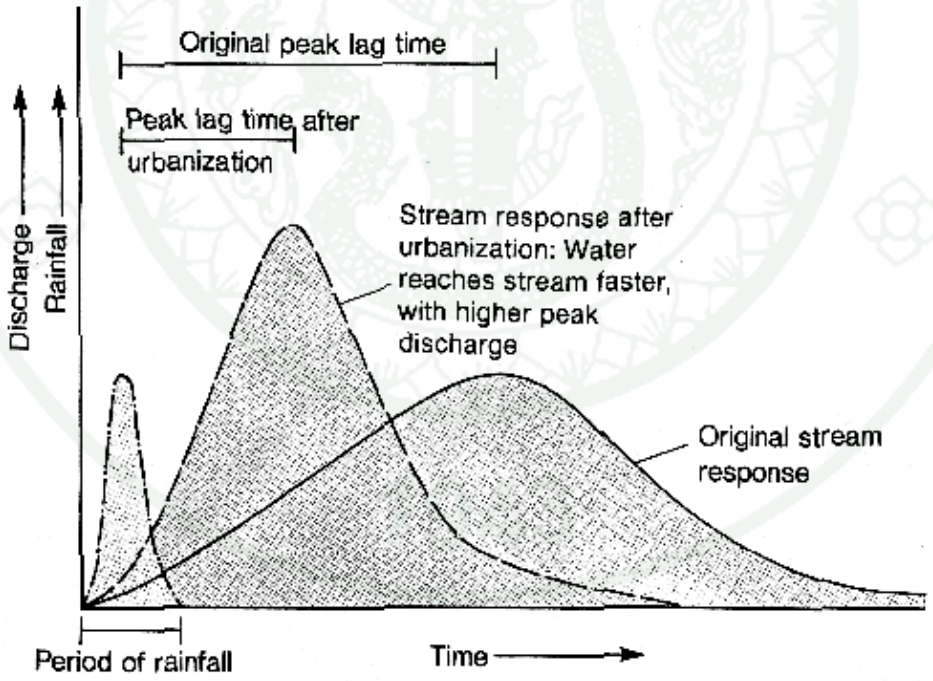

Figure 6 Hydrograph reflecting modification of stream response to precipitation following urbanization.

Source: Connecticut Geology (2005)

Regarding to Figure 6, urbanization causes peak discharge to increase and the lag time to peak to decrease. Urbanization is the development of land into residential, commercial, and industrial areas. Urban developments cause profound changes to natural conditions by altering the terrain, modifying the vegetation and soil characteristics, construction of buildings, drainage systems, and flood control structures. Flood characteristics therefore change, usually an increase of impervious area due to urban development.

Hydrologic impact due to urbanization affects the flood characteristics by increasing peak flow magnitudes and occurrences, and decreasing base flows. An increase in total impervious area decreases the volume of precipitation allowed to infiltrate into the soil during a storm event, increasing the volume of surface runoff. If the surface runoff is directly connected to the stream system through roads or storm drains, an increase in the peak flow magnitude will occur in a shorter time-period than in an undisturbed stream system. Also, the increase in surface runoff and decrease in infiltration reduces the natural groundwater storage that becomes available for base flow in the dry season.

Moreover, land cover changes affect both water quantity and quality. The effects have significant implications for the overall environment, society and economy, because of the intrinsic links between inland waters and their catchments. For water quantity, the key environmental effects of inland waters on water extraction and storage include the following (Resource Planning and Development Commission, 2003):

1) Altering river flows and groundwater to levels that are not sustainable for dependent aquatic ecosystems and human use.

2) The alteration of natural hydrological patterns and processes within and between rivers, streams, wetlands and groundwaters.

3) Due to the construction of in-stream dams and weirs, a changed flow regime through river regulation can affect the geomorphology of river systems, for example, by changing channel width and rates of erosion and scouring.

The scope of this thesis will focus only on the effects of water quantity, in particular change in the magnitudes and occurrences of water flows, due to land cover changes.

Thailand is lacking in-depth investigations with empirical prediction on the relationship between forest cover and rainfall and the relationship between forests and water yields such studies are needed. Because long-term records of changes in water yields corresponding to land cover changes are rare in order to formulate a national and regional policy on forest and land resource management (Tangtham, 1994).

Tangtham (1994) summarized the hydrological role of forests in Thailand as following;

1) High altitude forests or the so-called "cloud forests" such as the hill-evergreen forests in the north and the montane forests of Doi Inthanon National Park, Chiang Mai province these forests have higher rainfall frequency and abundance than other areas. There are two conditions to suggest that forests generate rainfall. First, montane forests in very high altitudes (over 2,000 m above mean sea level) can harvest clouds. Second, deforestation of vast tracts of land could reduce the probability of rainfall from water cycling.

2) Upland watershed areas in the northern of Thailand which have deep soils and are covered by hill-evergreen forests that regulate 70% of the wet period flow and 30% of the annual runoff during the dry season. This type of forest could be classified as the best water conservation forest in Thailand.

3) Due to the forests' regulation of groundwater recharge, on slopes of upland watersheds in Northern Thailand, groundwater levels have been observed to rise after the upper slopes were cleared for cultivation, because of a decrease in evapotranspiration and maintenance of soil structure and high permeability. However, this rising water table is a temporary phenomenon. It gradually falls when the topsoil of cultivated areas becomes compacted and generates larger amounts of overland flow which is drained directly to stream channels.

Although in-depth investigations on the effects of land cover changes on flood characteristics is lacking in Thailand river basins, there are some empirical findings from Ratanasuwan (2001) who used GIS and RS to investigate the impact of land cover change on monthly streamflow quality in the Mae Chaem river basin (P.14), Chiang Mai province by using Arc-Info, ArcView-GIS and ERDAS imagine softwares. Mae Chaem river basin is a sub-basin of the UPRB and occupies an area of 3,896 km^2. Ten LANDSAT-5 TM path 131 row 47 images for the period of 1988 to 1997 were used to classify land cover types on the study area. Streamflow and rainfall data were collected for the same period. The relationship between the streamflow quantity and the annual change of land cover were determined by regression analysis. Six land cover categories were identified as forest, agricultural, old clearing (including secondary forest), shifting cultivation, urban and water areas. Table 4 shows land cover area for each category, annual average discharge at P.14 gauging station occupied an area of 3,853 km^2 and annual average areal rainfall computed by isohyetal method of 10 rainfall stations around study area for the period of 1988 to 1997.

Ratanasuwan's results show that there were 22 patterns of land cover change that influenced the streamflow quantity. 14 patterns forced the water quantity to be decreased, while the other 4 patterns behave in the opposite way. In addition, the remaining 4 patterns had no concrete effect on the streamflow quantity. (see Table 5.) He suggested that to increase the monthly streamflow quantity, there are two approaches for land cover planning in this river basin. (1) minimizing the shifting cultivation area and (2) allowing the old clearing and secondary forest to develop into

healthy forest. The increasing rate of water quantity will be around 1.1% per year. At the end of his research, he recommended that the study of land cover changes by GIS and RS should include a mathematical model to compute the streamflow quantity. The monitoring and planning of land cover needs tools to run continuously as a decision support system, because changes occurs continuously both of spatial and temporal scales.

Some international research have recently begun to study the hydrological impact of land cover changes within river basins by using a hydrological rainfall-runoff model whose parameters are determined on the basis of satellite image, digital terrain model and digital maps.

Schultz (1995) developed a physically based rainfall-runoff model to allow most model parameters to be estimated from catchment characteristics which are derived from digital soil maps, digital terrain model and LANDSAT image data. Thus changes that may be expected in the flood hydrograph due to changes in land cover. The soil storage capacity for each soil type was derived from the seven channels of the LANDSAT image and soil porosity was derived from digital soil maps. Five land cover classes: forest, cropland, water, pasture and built up areas were identified, and the root depths of vegetation cover for each pixel in Nims catchment (264 km^2), Germany were determined.

A flood event in 1989 on the Nims catchment was selected to compute flood hydrographs from precipitation by the rainfall-runoff model. Two scenarios were considered a) the urbanized area is significantly increased and b) all trees above 400 m above mean sea level are assumed to be dead. Results were shown that in both scenarios a) and b) flood conditions became more severe, i.e. the rising limb became steeper, the peak considerably higher, and the flood volume significantly larger. He concluded that both types of land cover change produce a significant deterioration in flood conditions.

Table 4 Annual changes in land cover area, rainfall and runoff in Mae Chaem river basin for the period of 1988 to 1997.

Year	Each land cover area is in a unit of km^2 (% in parenthesis)							Rainfall	Runoff
	FR	AG	SC	SH	UB	WT	Total	mm	cms
1988	3,366.3	95.5	101.2	305.9	26.0	0.5	3,895.5	1,026.9	30.27
	(86.42)	(2.45)	(2.60)	(7.85)	(0.67)	(0.01)	(100.0)		
1989	3,383.6	54.0	169.1	251.8	36.3	0.6	3,895.5	883.0	28.95
	(86.86)	(1.39)	(4.34)	(6.46)	(0.93)	(0.02)	(100.0)		
1990	3,311.9	27.6	192.2	309.5	53.6	0.6	3,895.5	740.0	28.30
	(85.02)	(0.71)	(4.93)	(7.95)	(1.38)	(0.02)	(100.0)		
1991	3,111.8	29.6	391.3	293.3	69.0	0.5	3,895.5	652.7	33.35
	(79.88)	(0.76)	(10.04)	(7.53)	(1.77)	(0.01)	(100.0)		
1992	3,104.1	27.3	110.0	537.9	116.1	0.3	3,895.5	862.9	25.59
	(79.68)	(0.70)	(2.82)	(13.81)	(2.98)	(0.01)	(100.0)		
1993	3,112.7	24.1	404.1	227.9	126.5	0.3	3,895.5	618.5	19.64
	(79.90)	(0.62)	(10.37)	(5.85)	(3.25)	(0.01)	(100.0)		
1994	2,893.9	58.9	215.5	594.9	131.8	0.6	3,895.5	795.9	44.07
	(74.29)	(1.51)	(5.53)	(15.27)	(3.38)	(0.01)	(100.0)		
1995	3,235.1	23.5	115.9	377.7	143.1	0.2	3,895.5	750.5	45.51
	(83.05)	(0.60)	(2.97)	(9.70)	(3.67)	(0.01)	(100.0)		
1996	3,324.7	25.7	116.4	282.9	145.6	0.2	3,895.5	636.9	34.60
	(85.35)	(0.66)	(2.99)	(7.26)	(3.74)	(0.01)	(100.0)		
1997	3,076.1	55.9	272.0	341.3	149.7	0.6	3,895.5	752.7	25.78
	(78.97)	(1.43)	(6.98)	(8.76)	(3.84)	(0.01)	(100.0)		

Remark The symbols of 6 categories of land cover such as forest (FR), agricultural (AG), old clearing including secondary forest (SC), active shifting cultivation (SH), urban (UB) and water bodies (WT) areas.

Source: Ratanasuwan (2001)

Table 5 Effects of land cover changes on streamflow quantity in Mae Chaem river basin.

Patterns	Streamflow quantity effects	Changes of land cover types		
1	Increasing surface runoff	FR	→	UB
		FR	→	AG
		FR	→	SH
		FR	→	SC
		AG	→	UB
		SC	→	SH
		SC	→	UB
		SH	→	UB
2	Increasing water storage	SC	→	WT
		FR	→	WT
		SH	→	WT
		AG	→	WT
		UB	→	WT
3	Increasing water consumption	AG	→	SC
4	Decreasing water consumption	SC	→	AG
		SC	→	FR
5	Decreasing evaporation	WT	→	SC
		SH	→	SC
6	No concrete effect	WT	→	AG
		WT	→	SH
		WT	→	UB
		SH	→	AG

Remark The symbols of 6 categories of land cover refer to Table 4.

Source: Ratanasuwan (2001)

2.4 Numerical models

Numerical models can help flood management by providing warning of the likely extent, timing and location of flooding, before it occurs. Models can also be used to predict the effectiveness of different flood mitigation measures by trialing them under different flooding scenarios. Two types of models are important in flood modeling: hydrologic and hydraulic models, as described below.

2.4.1 Hydrologic model for study the rainfall-runoff relationships

Hydrologic models are commonly used for flow and flood estimation to serve several purposes in water resources projects. There are many hydrological models which can be divided into two categories - empirical and conceptual models (Carcano *et al*., 2008). An empirical model is based on a mathematical linkage between input and output series (e.g. rainfall and runoff data) considering the catchment as a lumped unit, with no physical characteristic of the basin. Examples of this type of model include classical AutoRegressive Moving Average (ARMA) models, initially developed by Box and Jenkins (1976) and all extensions, transfer function models (Hipel and McLeod, 1994), and Artificial Neural Networks (ANNs) (Cybenko, 1989). On the other hand, conceptual models describe relevant components of hydrological behaviour through simplified conceptualizations of the physical transportation processes associated with the hydrological cycle. There are various models developed under this concept, for example, the Soil Conservation Service (SCS) developed by USDA (1972), NAM (Nielsen and Hansen, 1973), TANK (Sugawara, 1974), HEC-HMS (Hydrologic Engineering Center (HEC), 2000), SWAT (Neitsch *et al*., 2005), TOPMODEL (Beven and Kirkby, 1979 and Beven *et al*., 1995), and IHACRES (Croke *et al*., 2003). The general background of these well-known models is summarized below, given that this thesis is concerned with conceptual based modeling.

The SCS model was developed by the United State Department of Agriculture in 1972. It is a versatile and widely used procedure for runoff estimation using the hydrologic soil cover complex method. Several important properties of the watershed such as soil permeability, land cover and antecedent soil water conditions are taken into consideration (USDA, 1972). This model therefore can be used to simulate various desired alternative forms of land development (Ragan and Jackson, 1980, Lewis *et al*., 2000; Xianzhao and Jiazhu, 2008). However in the model configuration, the infiltration rate will approach zero during a storm of long duration, which could cause overestimation in runoff estimates.

The NAM model was developed by the Danish Hydraulic Institute (DHI). Model theory includes various components of the rainfall–runoff process by continuously accounting for the water content in four different and mutually interrelated storages. These storages comprise snow, surface, lower zone (root zone), and groundwater storages to represent different physical elements of the catchment (Nielsen and Hansen, 1973). This model has been successfully used in various applications, especially for flood estimation (Refsgaard, 1997, and Butts *et al*., 2001). In 1995, this model was included in the MIKE11 software package and it is currently one of the most well-known and widely used commercial software packages available for hydrologic modelling (Havnø *et al*., 1995).

TANK is a linear conceptual model which uses a series of storage tank configuration to simulate the hydrological processes that occur in a catchment (Sugawara, 1974). It is simple to use but at the same time, capable of depicting the physical hydrological processes like evaporation, groundwater, infiltration, precipitation, and stream flow. Many researchers suggest that this model is suitable to be applied for flood forecasting purposes (Hayase and Kadoya, 1993, and Chen *et al*., 2003).

The HEC-HMS model, which was developed since 1998, comprises 4 sub-models to compute runoff volume, direct runoff (overland flow and interflow), baseflow, and channel flow, which represents each component of the runoff process.

This model can be used for runoff simulation in a catchment including reservoirs and dam-break effects (Hydrologic Engineering Center, HEC, 2000). There are several methods to be chosen from among the processes of infiltration, channel routing and baseflow in one catchment. It has been widely applied for flood estimation studies especially those incorporating GIS and RS to compute SCS curve numbers for each land cover type in a catchment (Shultz, 1997, and McColla and Aggett, 2006).

The Soil and Water Assessment Tool (SWAT) model was developed by the USDA Agricultural Research Service, Blackland Research Center in Texas (Neitsch *et al*., 2005) as a distributed model. It needs the data of land cover and soil type in GIS format to evaluate the Curve Number (CN) to be used later for loss estimation, which can be different between pixels. Runoff estimation at a particular pixel will be routed to another pixel using Manning's equation. The model can be used to predict the impact of land management practices on water, sediment, and agricultural chemical yields in large complex watersheds with varying soils, land cover and management conditions over long periods of time (Xue-song *et al.* (2003), and Pikounis *et al.* (2003)). The developers reported that the SWAT model is not designed to simulate single-event flood estimation but is suitable for long term flood and flow estimation.

TOPMODEL incorporates the influence of the earth's surface topography on runoff production (Beven and Kirkby, 1979 and Beven *et al.*, 1995). The model is categorized as a semi-distributed model in which the runoff factors can be derived from the topography of the basin under a Digital Elevation Model (DEM) and basic hydrological data, such as rainfall, evapotranspiration and soil moisture. This model succeeds in simulating the catchment runoff in many areas (Guo *et al.* (2000), and Xiong *et al.* (2002)). Although the model uses DEM to evaluate topographic differences between pixels, hydrological factors are determined using only rough averaging methods such as the Thiessen polygon method.

The IHACRES model which is applied in this thesis is a conceptual rainfall-runoff model consisting of two modules: a non-linear loss module to transform the measured rainfall to effective rainfall, and a linear routing module to compute a linear combination of antecedent streamflow values and effective rainfall. Despite its relatively recent development, IHACRES has been widely and quickly accepted in the hydrologic modelling community because of its structural simplicity that reduces parameter uncertainty, while at the same time attempting to represent more details of the internal processes than is typical for a distributed model (Croke *et al*., 2005). It has been successfully applied to investigate the hydrologic response for various catchments worldwide such as in Australia (Carlile *et al*., 2004), Thailand (Croke *et al*., 2003, and Taesombat and Sriwongsitanon, 2010), USA (Evans, 2003), UK (Littlewood *et al*., 1997), and South Africa (Dye and Croke, 2003).

The selection of which model to apply will vary according to the needs of the investigation. More complex models need more input data. Moreover, with increasing model complexity comes the cost of increasing calibration difficulty and uncertainty in the model outputs. Viney *et al.* (2005) conducted a study on an impact of land cover change in Dill River Basin in Germany using eleven different well known hydrological models (DHSVM, HBV, IHACRES, LASCAM, MIKE SHE, PRMS, RHESSys, SLURP, TOPLATS, SWAT, WASIM-ETH) applied to a common set of land cover change scenarios for the regional scale Dill catchment (693 km^2) in central Germany. All models were calibrated using observed streamflow data for the period 1983–1989 and model predictions were developed for the validation period 1990–1998. It was concluded that although the mean of models predicted annual streamflow changes are quite small, there is strong agreement among the models on the direction and magnitude of change for each scenario.

The semi-distributed models (HBV and LASCAM) were found to perform best during calibration and verification periods, but do not improve their fits during the less-demanding validation period as much as some of the distributed models (PRMS and DHSVM) that do not require as much calibration. However, a notable exception is that the most lumped model, IHACRES, also increases efficiency

quite significantly between calibration and validation. Thus, it seems that a lumped model such as IHACRES with fewer parameters can predict the effects of land cover change on hydrology potentially as well the semi-distributed and distributed models.

In most of Thailand river basins, there are insufficient streamflow data for effective application of hydrologic models. Rainfall, streamflow and temperature are generally widely available. It is therefore not meaningful to use the distributed models which need grid data generated from measurement data as input to these models which have many parameters that need to be calibrated and validated.

More complex models normally require more input data and are difficult to apply, especially for ungauged catchments where insufficient or no hydrologic data is available (Mapium and Sriwongsitanon, 2009). This study aims to select a simple model for estimation of runoff parameters as some catchments in the UPRB are ungauged. Of the mentioned models, only four consider the land cover component namely SCS, HEC-HMS, SWAT, and IHACRES. SCS, HEC-HMS and SWAT models were not chosen because their structures are based on the SCS unit hydrograph technique and loss estimation is based on SCS curves, an approach which is not suitable for flood estimation. IHACRES therefore was selected to investigate the effect of land cover change on flood characteristics in the UPRB in Northern Thailand.

An important factor is selecting IHACRES is that previously be used to successfully investigate the effect of land cover change on flood characteristics in Thailand river basin by Croke *et al.* (2003) who presented a simple hydrologic approach, using IHACRES to predict hydrologic response to land cover changes and the CATCHCROP model developed by Perez *et al.* (2002) to capture effects of land cover on infiltration and runoff. A simple regionalisation of streamflow response was tested for three gauged sub-catchments of the Mae Chaem catchment (Huai Phung, Mae Mu and Kong Kan sub-catchments) in Northern Thailand where the potential impacts of deforestation on hydrological response are of significant importance, but also a lack of stream gauge instrumentation. For the study, data were

collected over the period 1985–1995, and land units classified sub-catchments of the Mae Chaem catchment represent soil and topography were collected from the Land Development Department. Calibrated parameters from the largest catchment were used to infer parameters for regionalization of the models and showed good performance.

In applying hydrological models, model parameters need to be evaluated normally through calibration and verification procedures on gauged catchments. For ungauged catchments, model parameters have to be estimated, usually by formulating relationships between model parameters and catchment characteristics on nearby gauged catchments. For instance, Post and Jakeman (1996) found that some parameters of IHACRES model had been successfully related to catchment characteristic in sixteen small catchments in the Maroondah region of Victoria, Australia. Sefton and Howarth (1998) also successfully derived relationships between parameters of IHACRES model in terms of the physical catchment characteristics in 60 catchments in England and Wales using multiple regression techniques. Mapium and Sriwongsitanon (2009) demonstrated that relationships between the URBS model parameters and catchment characteristics can be confidently applied for flood estimation of the ungauged catchments within the catchment area of the eleven stations in the upper Ping river basin (UPRB), Northern Thailand.

Given these considerations in this thesis, the relationships between IHACRES model parameters and catchment characteristics were investigated for gauged catchments in the UPRB in order to allow IHACRES to estimate flooding on nearby ungauged catchments also within the UPRB. The sensitivity of model parameters was also checked at P.4A station to bring an understanding of how the model parameters affect the peak and volume of flood hydrograph.

2.4.2 Hydraulic model for flood routing investigation

Hydraulic models can be used to estimate the flow rate and water level at important locations in the channel system. These models are based on the Saint-Venant equations for one-dimensional flow that allow the flow rate and water level to be computed as functions of space and time (Chow *et al*., 1988). There are several hydraulic models that have been developed such as CE-QUAL-RIV1 (Environmental Laboratory, 1995), FLDWAV (Fread and Lewis, 1998), MIKE 11 (DHI, 2002), HEC-RAS (Brunner, 2002). FLDWAV and MIKE 11-HD proved to be effective to investigate flood routing on the UPRB (Taesombat and Sriwongsitanon, 2006). Moreover, FLDWAV has been implemented on complex river systems in USA applications in the Mississippi river (Ming and Sylvestre, 2001), Red river (Buan, 2003) and Susquehanna river (Sylvestre and Sylvestre, 2002), and also in China Yangtze delta area (Xu and Zhang, 2002) and many other applications.

FLDWAV (Fread and Lewis, 1998), a hydrodynamic public domain model, has been developed by the US National Weather Service (NWS). It replaces the DAMBRK and DWOPER models since it will allow the utilization of their combined capabilities, as well as provides new hydraulic simulation features. FLDWAV is based on an implicit finite-difference solution of the complete one-dimensional Saint-Venant equations of unsteady flow, coupled with an assortment of internal boundary conditions for simulating unsteady flows controlled by a wide spectrum of hydraulic structures.

Buan (2003) applied FLDWAV to the Red River of the North (USA) for real-time river forecasting. This model was calibrated using the 1996 and 1997 historic flood data and verified using 1999 and 2001 data. The results show that the FLDWAV model is capable of modeling the complex hydraulic effects experienced in the 1997 flood, such as the significant backwater, flood plain water storage and drainage conduit blockage in very large and flat flood plain areas. Future enhancements of this study will add additional model features to improve the forecasting of extreme events, as well as to aid in developing additional value-added

products derived from the model, such as flood inundation maps for communities along the Red river. The improved modeling accuracy attained with this model will lead the NWS to meeting future flood forecasting challenges.

Sylvestre and Sylvestre (2002) applied FLDWAV to 530-mile long of the Susquehanna river system in Pennsylvania including the Susquehanna river (320 miles) as the main stem with three dynamic tributaries, the Chemung river (177 miles), the west branch of the Susquehanna river (39 miles) and the Juniata river (48 miles). The Juniata River system in the vicinity of the town of Lewistown, Pennsylvania was selected as a test site for the NWS flood forecast mapping application. The model was calibrated using the 1996 and 1997 flood data and the results validated using the 1999 flood data. The RMSE for the 1999 flood was 0.61 ft, which indicates that accurate results will be obtained during forecast mode. The 1984 flood was also simulated using FLDWAV and the peak water surface profile has been mapped using the NWS flood forecast mapping application (FLDVIEW). The extent of flooding mapped by FLDVIEW compares well with the high water marks for the flood.

In this thesis, the effectiveness of FLDWAV for flood routing investigation in Thailand's Ping river basin was assessed and compared to the performance of MIKE 11-HD. MIKE 11 has been accepted worldwide and also applied in many Thai rivers. A particularly important recent project that MIKE 11 model was selected for is the Yangtze River Flood Control and Management Project in China (Clark *et al.*, 2004).

2.5 Remote sensing for land cover change and land cover classification

The use of LANDSAT-Thematic Mapper (TM) data to detect land use changes has been generally a success. Ratanopad and Kainz (2006) using remote sensing data from LANDSAT -5TM, accurately analyzed the land use change from 1995 to 2004 in Mahasarakham province of North-Eastern Thailand. GIS has also been used to determine physical descriptors of catchments like morphology, soil type, land cover type, climate indices etc (Sefton and Howarth, 1998). Digital image classification coupled with GIS has demonstrated its ability to provide comprehensive information on the direction, nature, rate, and location of land use changes as a result of rapid urbanization and deforestation (Weng, 2001). The ability of GIS to integrate spatial data from different sources, with different formats, structures, projections, or levels of resolution is especially useful in land use studies. Quantification of temporal change often involves use of such sources as historical maps, air photos, and satellite images. Changes in the spatial distribution of land classes can be summarized by overlaying maps of different dates and analyzing their spatial coincidence. Changes from one land class to another can be mathematically described as probabilities that a given pixel will remain in the same state or be converted into another state (Johnson, 1993).

LANDSAT-5TM, remotely sensed images from optical sensors were used in this thesis to classify land cover across UPRB. Both temporal and spatial annual changes of each land cover type were assessed for the period 1988-2005 which is the same period as the flood characteristics investigation by the numerical models were assessed. The relationship between land cover changes and flood characteristics for each sub-catchment of the UPRB were then examined. Land cover classification was derived by image processing of satellite images including ground verification and then land cover changes were compared using GIS.

2.6 Areal rainfall estimations using spatial interpolation technique

Rainfall plays an important role in the hydrologic cycle which controls our water supplies and water disasters. Knowing the nature and characteristics of rainfall, we can conceptualize and predict its effects in runoff, infiltration, evapotranspiration and water yield (Tang *et al.*, 2005). Many rainfall-runoff models were developed over the last few decades to estimate runoff characteristics, mainly using rainfall data as well as other catchment area and meteorological characteristics. Acquiring more accurate rainfall data is therefore crucial to improve the hydrograph prediction results. Since rainfall is never evenly distributed over the area of study, due to the topographic variability of the catchment areas, it is preferable to have as many rainfall stations as possible for estimating the areal rainfalls in order to represent the actual rainfalls over the basin. Unfortunately, it is not possible to install rainfall stations in as many locations as were hoped for due to limiting factors such as budget constraints, inaccessibility of certain areas, the lack of available equipment, etc.

Several areal rainfall estimation techniques are currently used for averaging rainfall depths collected at ground stations. Thiessen Polygon and Isohyetal Map are conventional techniques that are usually applied worldwide including Thailand basins to estimate the areal rainfall over the entire basin (Guillermo *et al*., 1985). However, the fundamental principles of applying these techniques can be the cause of inaccurate results being obtained due to the effects of topographical variation and, especially, the number of available rainfall stations. Alternative techniques were therefore needed to improve the accuracy of areal rainfall estimation.

Two of the most well-known alternative techniques that have been generally applied are the geostatistics and the Thin Plate Splines (TPS) techniques. The geostatistics, which is based on the theory of regionalized variables, has been accepted because it has an ability to assess spatial correlation among neighboring observations to predict attribute values at unsampled locations (Goovaerts, 2000). Several authors including Tabios and Salas (1985) and Phillips *et al.* (1992) concluded that the geostatistical prediction technique (kriging) provides better

estimates of rainfall than the conventional techniques such as Thiessen Polygon and Inverse Distance Weighting (IDW) techniques. However, Dirks *et al.* (1998) found that the kriging method does not show significantly improving the predictive skill compared to the simpler techniques, such as IDW technique, in the area with high-resolution networks (e.g. 13 raingauges over a 35 km^2 area).

Another alternative technique: the TPS, which was introduced by Hutchinson (1998a,b) can also be used to interpolate spatial rainfalls more accurately than the conventional techniques, especially for mountainous areas. This technique can generate meteorological surfaces using a trivariate function of latitude, longitude and elevation of meteorological stations together with the terrain elevation. It was proved to be a robust technique for dealing with noisy multivariate data and was applied in many countries such as Australia (Hutchinson, 1995a,b) and Canada (Price *et al.*, 1999) as well as in Thailand (Ekasingh and Kaewthip, 2000).

Hutchinson (1998a,b) illustrated that a small data set of daily rainfalls can be used to reliably calibrate topographic dependencies using the TPS technique. First of all, the elevation of rainfall stations derived from different resolutions of DEM data were used as input data for the TPS technique. In order to assess how well each resolution can be used to estimate rainfall data from 10 stations out of 100 stations were removed and estimated. A particular resolution of DEM data, which provided the minimum rainfall errors at those 10 stations, was then chosen for further study. The result showed that the 10 km resolution gave the least values of root mean square errors (RMSE). Subsequently, the TPS technique incorporating varying degrees of topographic dependence, namely slope and aspect, was also investigated to detect any accuracy improvement using the same removal of 10 rainfall data technique. The TPS technique with a consideration of elevation derived from a DEM resolution of 10 km together with slope and aspect, can significantly improve the accuracy of rainfall estimation rather than by considering only the elevation. The TPS technique with a consideration of topographic slope and aspect was then validated by removing rainfall data at 100 of the 467 stations; the predicted rainfall data at those 100 stations, using the TPS technique, were later compared to the measured data. The result revealed a

small value of RMSE and it can be concluded that the topographic slope and aspect have significant effects on estimated rainfall depths. Hutchinson also recommends further investigations into different rainfall types, such as convective rainfall and frontal rainfall, which can also affect rainfall depth estimation.

Price *et al.* (1999) also revealed that the TPS technique produced better results for elevation-dependent spatial interpolation of monthly climatic data from sparse weather station networks than did the statistical method called Gradient plus Inverse-Distance-Squared (GIDS). The selected climatic data used for the analysis comprised thirty-year monthly mean, minimum and maximum temperatures and precipitation data in Eastern and Western Canada.

Ekasingh and Kaewthip (2000) developed a spatial climatic database to include in the decision supporting system for crop production projects in the northern and central regions of Thailand. One of the objectives of that study was to select the most suitable method for spatial interpolating of meteorological data such as rainfall, air temperature and sunlight radiation. Four spatial interpolation methods comprising the Thiessen Polygon, Inverse Distance Weighting (IDW), Kriging and Thin Plate Spline (TPS) were applied. Monthly meteorological data from 305 daily rainfall stations, 73 air temperature stations and 12 sunlight radiation stations in Chiang Mai and Pitsanulok Provinces were collected from related government agencies. To test the performance of each method, predictions were generated for known locations by removing one data point at a time and calculating the value from neighboring stations. The results showed that the TPS technique which was used to generate the spatial meteorological data, together with the digital elevation model, gave the least RMSE values of climate spatial interpolation than other methods. Moreover, the generated data is in a grid layer which can be conveniently used to analyze different layers of the GIS.

Boer *et al.* (2001) applied four forms of kriging and three forms of thin plate splines to predict monthly maximum temperature and monthly mean precipitation in Jalisco State of Mexico. The trivariate regression-kriging and

trivariate thin plate spline showed the best performance. The authors also pointed that thin plate splines have an advantage over kriging according to the operational simplicity of this technique, which can be very significant from a practical point of view.

The ANUSPLIN software based on TPS technique was selected to be carried out to generate the daily areal rainfall estimations in the UPRB in the period of 1988-2006. These areal rainfall estimations were then input to the IHACRES model.

3. Theory and Technique for Calculation

The theory and technique for calculation of IHACRES, FLDWAV, RS, land cover detection, and TPS technique are described here as follows:

3.1 The IHACRES model

3.1.1 General description

The name IHACRES stands for “Identification of unit Hydrographs And Component flows from Rainfall, Evaporation, and Streamflow data”. It is a catchment-scale rainfall-runoff model that aims to characterize the dynamic relationship between rainfall and runoff. The first version of the model (Version 1.0) was developed in 1994 by the Institute of Hydrology (IH), Wallingford, UK (Littlewood and Jakeman, 1994). The model was later updated to Version 2.1 by the Centre for Resource and Environmental Studies (CRES), Australian National University, Australia. The updated version contained a non-linear loss module and alternative model calibration techniques (Croke *et al.*, 2003) compared with the previous version. Figure 7 shows the model structure, which comprises the modules of non-linear and linear relationships. The non-linear module represents a transformation of rainfall and temperature into the effective rainfall while the linear module converts the effective rainfall into runoff.

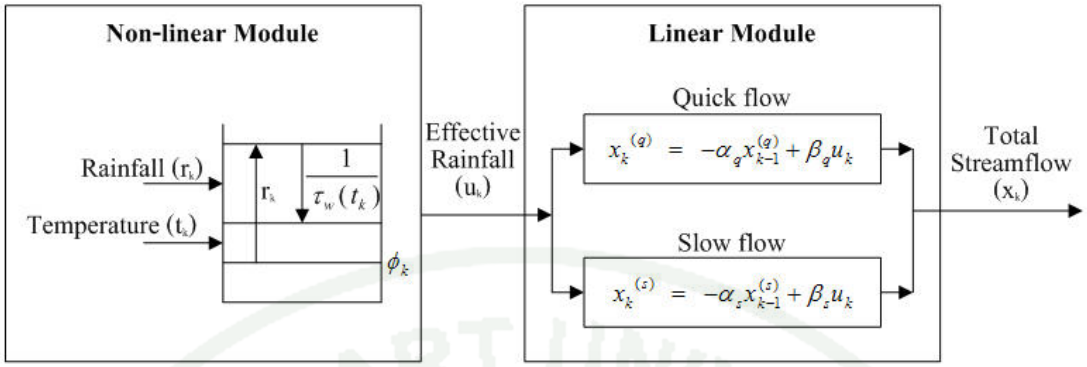

Figure 7 IHACRES model structure.

Source: Evans and Jakeman (1998)

3.1.2 Non-linear module

Eq. (1) shows a non-linear representation of the effective rainfall (u_k) in mm proposed by Ye *et al*. (1997).

$$u_k = \left[c\left(\phi_k - l\right)\right]^p r_k \qquad (1)$$

where, r_k is the observed rainfall in mm on day k, c is the mass balance, l is the soil moisture index threshold for producing flows, and p is the non-linear response term. The parameters l and p are typically only necessary for ephemeral catchments (Carcano *et al*., 2008). Soil moisture ϕ_k is described as in Eq. (2).

$$\phi_k = r_k + \left(1 - \frac{1}{\tau_k}\right)\phi_{k-1} \qquad (2)$$

where, τ_k is the drying rate given as shown in Eq. (3).

$$\tau_k = \tau_w e^{(0.062 f (t_r - t_k))} \quad (3)$$

where, t_k is the observed temperature in degrees Celsius, τ_w is the drying rate at reference temperature in degree Celsius, f is the temperature modulation in degree Celsius^{-1}, and t_r is the reference temperature in degrees Celsius, which is set to the local average air temperature. The parameter f relates to seasonal variation of evapotranspiration, which is mainly affected by climate, land cover, and land cover. The parameter τ_w affects the variation of soil drainage and infiltration rates.

The IHACRES Version 2.1 is a more general version than the original one (Version 1.0). However, users can switch from the Version 2.1 to the Version 1.0 by setting the parameter l to be zero and p to be one, and then the soil moisture index will be $s_k = c\phi_k$ as in the original version.

3.1.3 Linear module

In this module, the effective rainfall is converted into runoff using a linear relationship. There are two components in the flow routing – the quick flow and slow flow. These two components can be connected either in parallel or series. It was recommended in many applications to use the two components connected in parallel, except for semi-arid regions or in ephemeral streams where one component is usually sufficient (Ye *et al*., 1997). The parallel configuration of these two stores at time step k - quick flow ($x_k^{(q)}$) and slow flow ($x_k^{(s)}$) - are combined to yield the runoff (x_k) as presented in Eq. (4).

$$x_k = x_k^{(q)} + x_k^{(s)} \quad (4)$$

$$x_k^{(q)} = -\alpha_q x_{k-1}^{(q)} + \beta_q u_k \quad (5)$$

$$x_k^{(s)} = -\alpha_s x_{k-1}^{(s)} + \beta_s u_k \quad (6)$$

where, parameters α_q, β_q are time constants for the quick flow, and α_s, β_s for the slow flow. Dynamic response characteristics (DRCs) unit hydrographs for the quick flow and slow flow are calculated as shown in Eq. (7) and Eq. (8), respectively.

$$\tau_q = \frac{-\Delta}{\ln(-\alpha_q)} \quad (7)$$

$$\tau_s = \frac{-\Delta}{\ln(-\alpha_s)} \quad (8)$$

where, Δ is the time step, τ_q and τ_s are the recession time constants for quick flow and slow flow in days, respectively. The parameter τ_q is recommended to be less than time step (Δ). The relative volume of quick flow and slow flow can be calculated as presented in Eq. (9).

$$V_q = 1 - V_s = \frac{\beta_q}{1+\alpha_q} = 1 - \frac{\beta_s}{1+\alpha_s} \quad (9)$$

where V_q is the proportion of quick flow to total flow $(1-V_s)$.

3.2 FLDWAV

FLDWAV was used to simulate one dimensional unsteady flow situation in both channel and flood plain of the Ping and Mae Kuang rivers. Its basic equations are the Saint-Venant equations solved by the numerical method (finite-difference).

3.2.1 Saint-Venant equations

The Saint-Venant equations which are the one-dimensional unsteady open-channel flow. They are normally used as the basic equations for one dimensional dynamic wave models. These equations comprise the continuity and momentum equations which can be described mathematically as follows;

Continuity equation

$$\frac{\partial Q}{\partial x}+\frac{\partial A}{\partial t}-q=0 \tag{10}$$

Momentum equation

$$\frac{\partial Q}{\partial t}+\frac{\partial\left(\beta Q^{2}/A\right)}{\partial x}+gA\left(\frac{\partial h}{\partial x}+S_{f}+S_{e}\right)-\beta q v_{x}+W_{f}B=0 \tag{11}$$

where x is longitudinal distance along the channel, t is time, Q is discharge, A is cross-sectional area of flow, q is lateral inflow per unit length of the channel, h is water surface elevation, v_x is velocity of lateral flow in the direction of channel flow, S_f is friction slope, S_e is eddy loss slope, B is channel width, W_f is wind shear force, β is momentum correction factor, and g is gravitational acceleration.

3.2.2 Solution methods

The Saint-Venant equations are nonlinear partial differential equations with both spatial and time derivatives as shown in equations (10) and (11). These equations are the hyperbolic partial differential equations that cannot be solved using the analytical solution, but can be solved by numerical schemes. Each hydrodynamic model has different numerical solution schemes to solve these

equations such as the 6-point Abbott scheme used in the MIKE 11-HD model and weighted four points finite difference approximation used in the FLDWAV model.

3.2.3 FLDWAV Model Capabilities (Fread and Lewis, 1998)

FLDWAV model schematic is shown in Figure 8.

1) The input data structure has been arranged so that array sizes are determined internally based on the river system, thus eliminating the problem of running out of available time steps or number of cross sections.

2) FLDWAV can model river systems that have both a dendritic structure (both first and n^{th} order tributaries) and channel networks.

3) FLDWAV can simulate flows which overtop levees located along either or both sides of a main river and its principal tributaries.

4) FLDWAV can route unsteady flows occurring simultaneously in a system of interconnected rivers. Any of the rivers may have one or more structures (dams, bridges, levees, etc.) which control the flow and may breach if failure conditions are reached.

5) FLDWAV can handle subcritical, supercritical, critical or a combination of each, varying in space and time from one to another by using a new developed computational scheme (LPI) to model mixed flow.

6) The upstream boundary may be either a stage or discharge hydrograph for each river. The downstream boundary may be a stage/discharge hydrograph, tide, or a variety of rating curves.

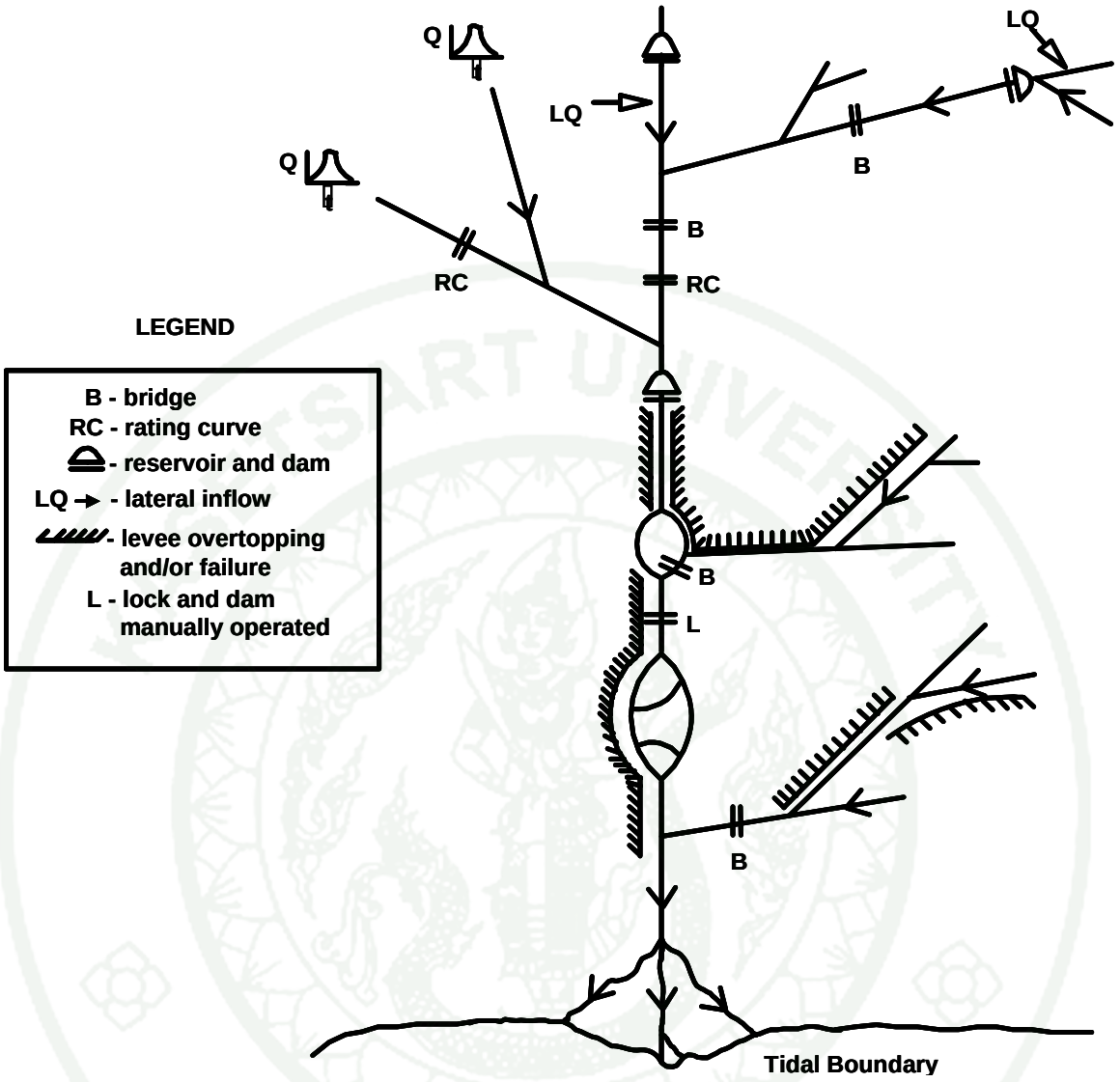

Figure 8 FLDWAV model schematic.

Source: Fread and Lewis (1998)

7) The initial conditions include the initial water surface elevations (WSEL) and discharges at each cross section locations. FLDWAV can start up in either a steady- state or an unsteady-state condition.

8) The initial computational time step may be user-defined or generated by the model. The model will determine the time to peak of each inflow hydrograph (upstream boundary) and divide the smallest value by 20. This value will be used throughout the run period until a breach failure mode is activated. The model will use the smallest value between failure time step(s) and the initial time step.

9) Manning n table is defined for each channel reach bounded by runoff stations and is specified as a function of either WSEL (h) or discharge (Q). Linear interpolation is used to obtain n for values of h or Q intermediate to the tabular values.

10) FLDWAV has an option for automatic calibration which allows the automatic determination of the Manning n so that the difference between computed WSELs (stage hydrographs) and observed hydrographs is minimized.

11) If a river has stage observations for more than two runoff stations, the Kalman filter may be turned on to update the predictions for each time step using observations. This option is applicable for real-time forecasting or when observed stage time series are available.

12) FLDWAV contains three techniques to determine the mud/debris related friction slope term due to the internal viscous dissipation of non-Newtonian fluids and granular sliding friction of coarse-grained debris surges.

3.2.4 Implicit Finite Difference Equations Solution scheme

The expanded Saint-Venant equations of conservation of mass and momentum with additional terms for the effect of expansion/contractions (Fread, 1978), channel sinuosity (DeLong, 1986 and 1989) and non-Newtonian flow (Fread, 1988) are shown as following; (Fread and Lewis, 1993);

$$\frac{\partial Q}{\partial x}+\frac{\partial s_c(A+A_o)}{\partial t}-q_L=0 \tag{12}$$

$$\frac{\partial(s_m Q)}{\partial t}+\frac{\partial(\beta Q^2/A)}{\partial x}+gA\left(\frac{\partial h}{\partial x}+\overline{S_f}+S_e+S_i\right)+L+W_f B=0 \tag{13}$$

where:

Q	=	discharge (flow)
A		wetted active cross-sectional area
A_o	=	wetted inactive off-channel (dead) storage area associated with topographical embankments or tributaries
B	=	the channel flow width,
s_c and s_m	=	depth-dependent sinuosity coefficients for mass and momentum, respectively that account for meander
β	=	the momentum coefficient for non-uniform velocity
q	=	lateral flow (inflow is positive, outflow is negative)
t	=	time
x	=	distance measured along the mean flow-path of the floodplain
g	=	the gravitational acceleration constant
h	=	the water-surface elevation

L	=	the momentum effect of lateral flows ($L=-qv_x$ for lateral inflow where v_x is the lateral inflow velocity in the x-direction, $L=-qQ/(2A)$ for seepage lateral outflows, $L= -qQ/A$ for bulk lateral outflows such as flows over levees)
S_f	=	the boundary friction slope ($S_f=(Qn/(1.49AR^{2/3}))^2$ where n is the Manning roughness coefficient and R is the hydraulic radius)
S_e	=	the slope due to local expansion-contraction (large eddy loss)
W_f	=	the wind term.

Equations (12) and (13) can be solved by either “explicit” or “implicit” finite-difference techniques in FLDWAV (Liggett and Cunge, 1975). Explicit methods, although simpler in application, are restricted by mathematical stability considerations to very small computational time steps. Such small time steps cause the explicit methods to be very inefficient in the use of computer time.

Based on the weighted four-point implicit finite-difference scheme, the continuous x-t (space-time) region in which solutions of h and Q are sought, is represented by a rectangular net of discrete points shown in Figure 9. The net points are determined by the intersection of lines drawn parallel to the x- and t-axes. Those parallel to the t-axis represent locations of cross sections; they have a spacing of Δx_i, which need not be constant. Those parallel to the x-axis represent time lines; they have a spacing of Δt_j, which also need not be constant. Each point in the rectangular network can be identified by a subscript (i) which designates the x-position and a superscript (j) which designates the particular time line. The time derivatives are approximated by a forward-difference quotient centered between the i^{th} and i+1 points along the x-axis, as showing in equation (14);

$$\frac{\partial \Psi}{\partial t} = \frac{\Psi_i^{j+1} + \Psi_{i+1}^{j+1} - \Psi_i^{j} - \Psi_{i+1}^{j}}{2\Delta t_j} \quad (14)$$

where Ψ represents any variable (Q, h, A, A_o, s_{co}, s_m, etc.)

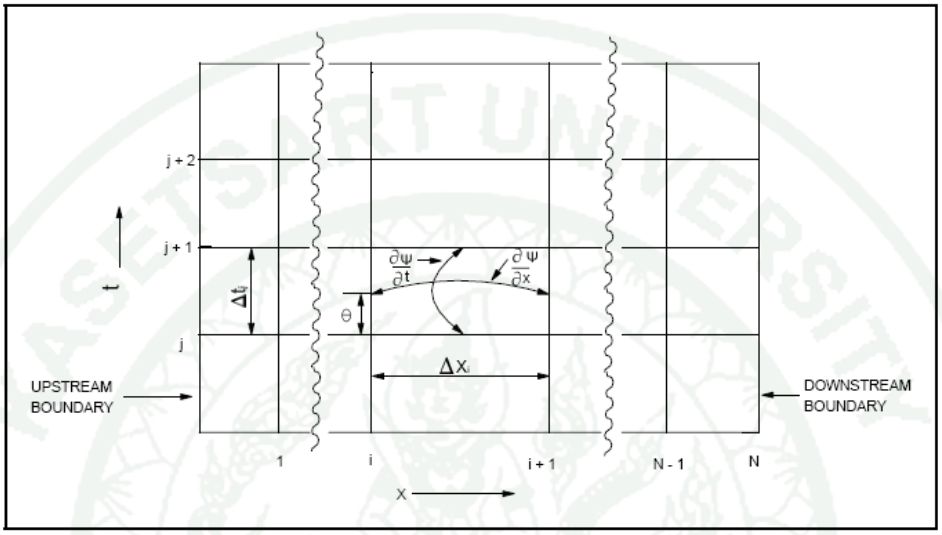

Figure 9 Discrete x-t Solution Domain.

Source: Fread and Lewis (1998)

The spatial derivatives are approximated by a forward-difference quotient positioned between two adjacent time lines according to weighting factors of θ and (1-θ), as following;

$$\frac{\partial \Psi}{\partial x} = \theta\left[\frac{\Psi_{i+1}^{j+1} - \Psi_i^{j+1}}{\Delta x_i}\right] + (1-\theta)\left[\frac{\Psi_{i+1}^{j} - \Psi_i^{j}}{\Delta x_i}\right] \quad (15)$$

Variables other than derivatives are approximated at the time level where the spatial derivatives are evaluated by using the same weighting factors, as following;

$$\Psi = \theta\left[\frac{\Psi_i^{j+1} + \Psi_{i+1}^{j+1}}{2}\right] + (1-\theta)\left[\frac{\Psi_i^{j} + \Psi_{i+1}^{j}}{2}\right] \quad (16)$$

A weighting factor (θ) of 1.0 yields the fully implicit or backward difference scheme used by Baltzer and Lai (1968). Usually, a weighting factor of 0.55 to 0.60 is used so as to minimize the loss of accuracy associated with greater values while avoiding the possibility of a weak or pseudo instability. However, θ may be user-specified other than the recommended value of 0.55 to 0.60 via the F1 parameter in the FLDWAV model.

Equations (14) to (16) are used to replace the derivatives and other variables in equations (12) and (13), the following weighted, four-point implicit, finite difference equations are obtained in equations (17) and (18):

$$\theta\left[\frac{Q_{i+1}^{j+1}-Q_i^{j+1}}{\Delta x_i}\right]-\theta\ q_i^{j+1}+(1-\theta)\left[\frac{Q_{i+1}^{j}-Q_i^{j}}{\Delta x_i}\right]-(1-\theta)q_i^{j}$$

$$+\left[\frac{s_{co_i}{}^{j+1}(A+A_0)_i^{j+1}+s_{co_i}{}^{j+1}(A+A_0)_{i+1}^{j+1}-s_{co_i}{}^{j}(A+A_0)_i^{j}-s_{co_i}{}^{j}(A+A_0)_{i+1}^{j}}{2\Delta t_j}\right]=0 \qquad (17)$$

$$\left[\frac{(s_{m_i}Q)^{j+1}+(s_{m_i}Q)^{j+1}-(s_{m_i}Q)^{j+1}-(s_{m_i}Q)^{j+1}}{2\Delta t_j}\right]+\theta\left[\frac{(\beta Q^2/A)_{i+1}^{j+1}-(\beta Q^2/A)_i^{j+1}}{\Delta x_i}\right.$$

$$\left.+g\overline{A}^{j+1}\left(\frac{h_{i+1}^{j+1}-h_i^{j+1}}{\Delta x_i}+\overline{S}_f^{j+1}+\overline{S}_e^{j+1}+\overline{S}_i^{j+1}\right)+L_i^{j+1}+(W_f\overline{B})_i^{j+1}-\right]$$

$$+(1-\theta)\left[\frac{(\beta Q^2/A)_{i+1}^{j}+(\beta Q^2/A)_i^{j}}{\Delta x_i}+g\overline{A}^{j}\left(\frac{h_{i+1}^{j}-h_i^{j}}{\Delta x_i}++\overline{S}_f^{j}+\overline{S}_e^{j}+\overline{S}_i^{j}\right)\right.$$

$$\left.+L_i^{j}+(W_f\overline{B})_i^{j}\ \right]\ =\ 0 \qquad (18)$$

where

$$\overline{A}\ =\ \frac{A_i+A_{i+1}}{2} \qquad (19)$$

$$\overline{S_f} = \left[\frac{n_i^2 \overline{Q|Q|}}{\mu^2 \overline{A}^2 \overline{R}^{4/3}} \right] = \frac{Q|\overline{Q}|}{\overline{K}^2} \quad (20)$$

$$\overline{Q} = \frac{Q_i + Q_{i+1}}{2} \quad (21)$$

$$\overline{R} = \frac{\overline{A}}{\overline{B}} \quad or \quad \overline{R} = \frac{\overline{A}}{\overline{P}} \quad (22)$$

$$\overline{B} = \frac{B_i + B_{i+1}}{2} \quad (23)$$

$$\overline{K} = \frac{K_i + K_{i+1}}{2} \quad (24)$$

$$\overline{P} = \frac{P_i + P_{i+1}}{2} \quad (25)$$

where P_i is the wetted perimeter given by the following:

$$P_{i_1} = B_{i_1} \quad (26)$$

$$P_{i_k} = P_{i_{k-1}} + 2\left[0.25\left(B_{i_k} - B_{i_{k-1}}\right)^2 + \left(h_{i_k} - h_{i_{k-1}}\right)^2\right]^{1/2} \quad (k = 2,3,...) \quad (27)$$

The hydraulic radius (R) used in equations (20) and (22) is normally evaluated within FLDWAV model as A/B or the hydraulic depth (D). This is satisfactory for almost all river channels since A/B ≈ A/P. For very narrow, deep channels (B<10D) this approximation is not as good. Therefore, a user-specified option for R = A/P is available in FLDWAV by providing a value of unity to the control parameter, KPRES. When this option is selected, the wetted perimeter (P) is computed from the user-specified top width (B_k) versus elevation (H_k) table according to equations (26) and (27).

The terms associated with the j^{th} time line are known from either the initial conditions or previous computations. The initial conditions refer to values of h_i^j and Q_i^j at each node along the x-axis for the first time line (j=1).

Equations (17) and (18) have four unknowns Q_i^{j+1}, h_i^{j+1}, Q_{i+1}^{j+1}, h_{i+1}^{j+1} and only two equations which are applied to each of the (N-1) rectangular grids shown in Figure 6 between the upstream and downstream boundaries, a total of (2N-2) equations with 2N unknowns can be formulated. Then, prescribed boundary conditions for subcritical flows, one at the upstream boundary and one at the downstream boundary, provide the necessary two additional equations required for the system to be determinate. The resulting system of 2N nonlinear equations with 2N unknowns is solved by the Newton-Raphson iterative method (Amein and Fang, 1970).

Computations for the iterative solution of the nonlinear system are begun by assigning trial values to the 2N unknowns. Substitution of the trial values into the system of nonlinear equations yields a set of 2N residuals. The Newton-Raphson method provides a means for correcting the trial values until the residuals are reduced to a suitable tolerance level, near zero. This is usually accomplished in one or two iterations through use of linear extrapolation for the first trial values. If the Newton-Raphson corrections are applied only once, such as no iteration, the nonlinear system of difference equations degenerates to the equivalent of a quasi-linear, finite-difference formulation (Barkau, 1985) of the Saint-Venant equations which often will require smaller time steps than the nonlinear formulation (used in FLDWAV) for the same degree of numerical accuracy.

A system of 2N x 2N linear equations relates the corrections to the residuals and to a Jacobian coefficient matrix composed of partial derivatives of each equation with respect to each unknown variable in that equation. The Jacobian (coefficient) matrix of the linear system has a banded structure as shown in Figure 10 which allows the system to be solved by a compact, quad-diagonal, Gaussian elimination algorithm (Fread, 1971 and 1985), which is very efficient with respect to computing time and storage. The required storage is reduced from 2Nx2N to 2Nx4 and the required number of computational steps is greatly reduced from $16/3N^3+8N^2+14/3N$ to approximately 38N.

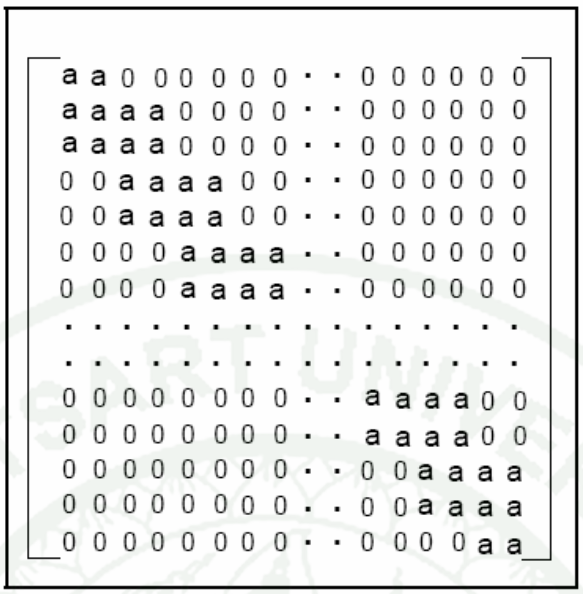

Figure 10 Jacobian Coefficient Matrix.

Source: Fread and Lewis (1998)

3.2.5 Local Partial Inertia (LPI) Technique

A Local Partial Inertial (LPI) technique (Fread *et al.*, 1996) is utilized in which a numerical filter (σ) modifies the extent of contribution of the inertial terms in the momentum equation such that its properties vary from dynamic to diffusion. The diffusion method's stability take advantage in the near-critical range of the Froude number ($F_r \cong 1$) or mixed flows with moving supercritical/subcritical interfaces and retain the accuracy of the dynamic method.

The momentum equation is modified by a numerical filter (σ) so that the inertial terms are partially or altogether omitted in some situations. The modified equation and numerical filter are:

$$\sigma\left[\frac{\partial\left(s_m\, Q\right)}{\partial t}+\frac{\partial\left(\beta Q^2 / A\right)}{\partial x}\right]+gA\left(\frac{\partial h}{\partial x}+S_f+S_e+S_i\right)+L+W_f B \;=\; 0 \qquad (28)$$

$$\sigma \;=\; \begin{cases} 1.0 \quad -F_r{}^m & \left(F_r \le 1.0; \quad m \ge 1\right) \\ 0 & \left(F_r > 1.0\right) \end{cases} \qquad (29)$$

in which the power m is a user-specified constant, usually $3 \le m \le 5$. Figure 11 shows the variation of σ with F_r and with the power (m). The σ numerical filter, which depends on F_r, has a variation that ranges from a linear function to the Dirac-delta function. Since the Froude number is determined at each computational point for each time, σ is a Local parameter. Therefore, portions of the routing reach with low Froude numbers will be modeled with all or essentially all of the inertial terms included, while those portions with F_r values in the vicinity of critical flow will be modeled with Partial Inertial effects included; and supercritical flow (F_r >1) will be modeled with no inertial effects. It is found that smaller values of the power (m) tend to stabilize the solution in some cases while larger values of m provide more accuracy. By using the σ filter, the FLDWAV model automatically changes from a dynamic model to a diffusion model as F_r approaches 1.0 and takes advantage of the stability of the diffusion model for those flows with F_r near the critical value of 1.0. Previously, a simple inertial filter ($1-F_r^2$) was proposed (Havnø and Brorsen,1986) however, it was not localized nor its error properties analyzed.

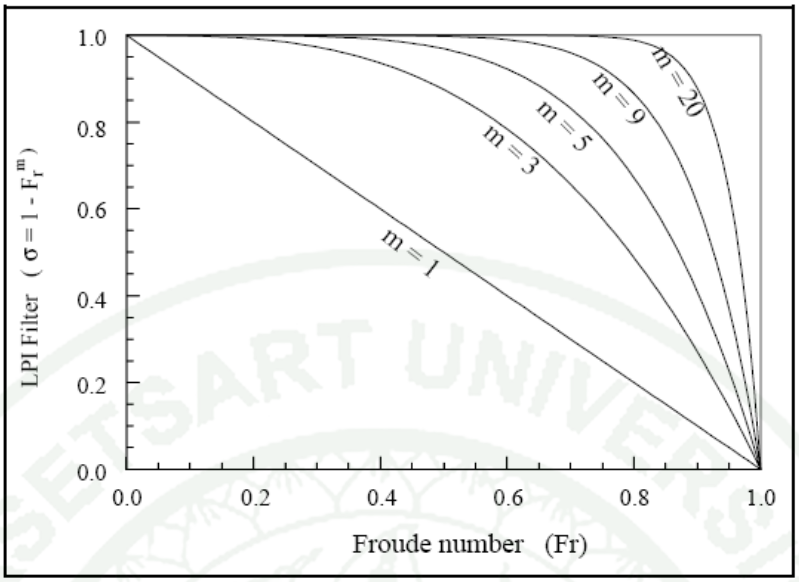

Figure 11 The LPI Filter (σ).

Source: Fread and Lewis (1998)

3.3 Evaluation of the numerical model performance

The numerical model performance can be evaluated by a comparison between the computed and the observed discharge and water level at different runoff stations. In this thesis, three statistical measures are used. They are a correlation coefficient (r), an efficiency index (EI) and a root mean square error ($RMSE$) according to equations (30) to (32).

3.3.1 Correlation coefficient (r) between the computed and the observed discharge data is shown as following;

$$r = \frac{\sum_{i=1}^{N}\left(Q_{oi}-\bar{Q}_o\right)\times\left(Q_{ci}-\bar{Q}_c\right)}{\left[\sum_{i=1}^{N}\left(Q_{oi}-\bar{Q}_o\right)^2\times\sum_{i=1}^{N}\left(Q_{ci}-\bar{Q}_c\right)^2\right]^{0.5}} \qquad (30)$$

where $\bar{Q}_o$ is the average of observed discharge or water level data

$\bar{Q}_c$ is the average of computed discharge or water level data

$\bar{Q}_{oi}$ is the observed discharge or water level at the time *i*

$\bar{Q}_{ci}$ is the computed discharge or water level at the time *i*

N is the number of data

3.3.2 Efficiency index (EI) between the computed and the observed discharge data is shown as following;

$$EI = \frac{\sum_{i=1}^{N}(Q_{oi} - \bar{Q}_o)^2 - \sum_{i=1}^{N}(Q_{oi} - Q_{ci})^2}{\sum_{i=1}^{N}(Q_{oi} - \bar{Q}_o)^2} \times 100\% \quad (31)$$

3.3.3 Root mean square error (RMSE) between the computed and the observed discharge data is shown as following;

$$RMSE = \sqrt{\frac{1}{N} \sum_{i=1}^{N}[Q_{oi} - Q_{ci}]^2} \quad (32)$$

These statistical indicators, *r* can be used to specify the strength and direction of a linear relationship between observed data and computed from the models. *r* valves are between -1 and 1. Higher *r* valves close to 1 indicate greater linear relationships. Higher *EI* valves close to 100 also indicate greater linear relationships. In addition, *RMSE* is used as indicator of the magnitude of extreme errors. Lower *RMSE* values indicate greater central tendencies and generally smaller extreme errors.

3.4 Remote sensing (RS)

RS is the collection of information about an object or system without coming into direct physical contact with it. That information is nearly always carried by electromagnetic radiation (EMR). A large number of Electromagnetic energy sensors are currently being operated from airborne and spaceborne platforms to assist in the inventorying, mapping, and monitoring of earth resources. These sensors acquire data on the way various earth surface features emit and reflect electromagnetic energy, and these data are analyzed to provide information about the resources under investigation (Lillesand *et al.*, 2004).

Two common types of remote sensors used for the study of the Earth's surface are optical and radar. Optical sensors use the visible, near-infrared, and short-wave infrared parts of the spectrum to form images of the Earth's surface by detecting solar radiation reflected from objects on the ground. Different materials reflect and absorb radiation differently at different wavelengths. Thus, objects such as bare rock, water, vegetation and soil types, etc., can be differentiated by their spectral reflectance signatures in the remotely sensed images (Chapman *et al*., 2005). Figure 12 illustrates electromagnetic spectrum both wavelength and frequency, Figure 13 illustrates the principle of optical remote sensing and Figure 14 illustrates spectral reflectance signature of soil, vegetation and water.

From Lillesand *et al.* (2004), the two basic processes in RS are 1) data acquisition and 2) data analysis. Figure 15 illustrates the generalized processes and elements involved in the electromagnetic remote sensing of earth resources.

From Liew (2006) The elements involved up to the data acquisition process are emission of a EM signal from (a) sources of energy, (b) propagation of energy through the atmosphere, (c) energy interactions with earth surface features, (d) retransmission of energy through the atmosphere, (e) airborne and/or spaceborne sensors, and (f) resulting in the generation of sensor data in pictorial and/or digital form.

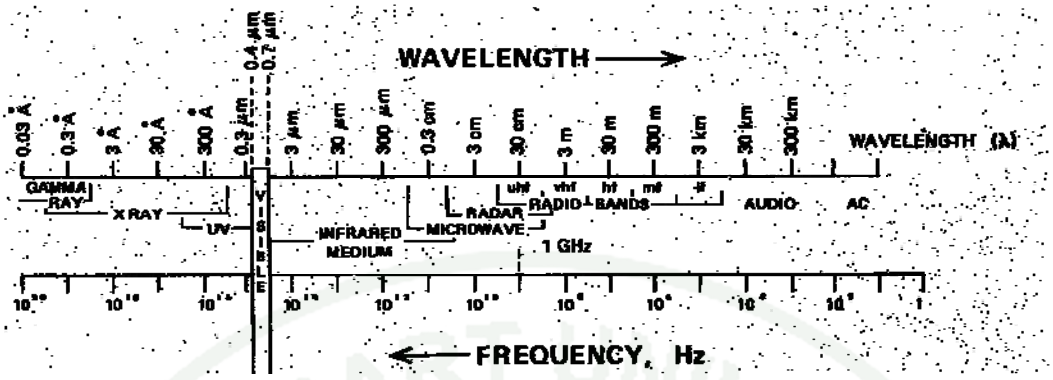

Figure 12 Electromagnetic spectrum.

Remark $\mu m = 10^{-6}$ m, $\overset{0}{A} = 10^{-10}$ m, cm = 10^{-2} m and km = 10^{3} m

Source: Preechachol (2006)

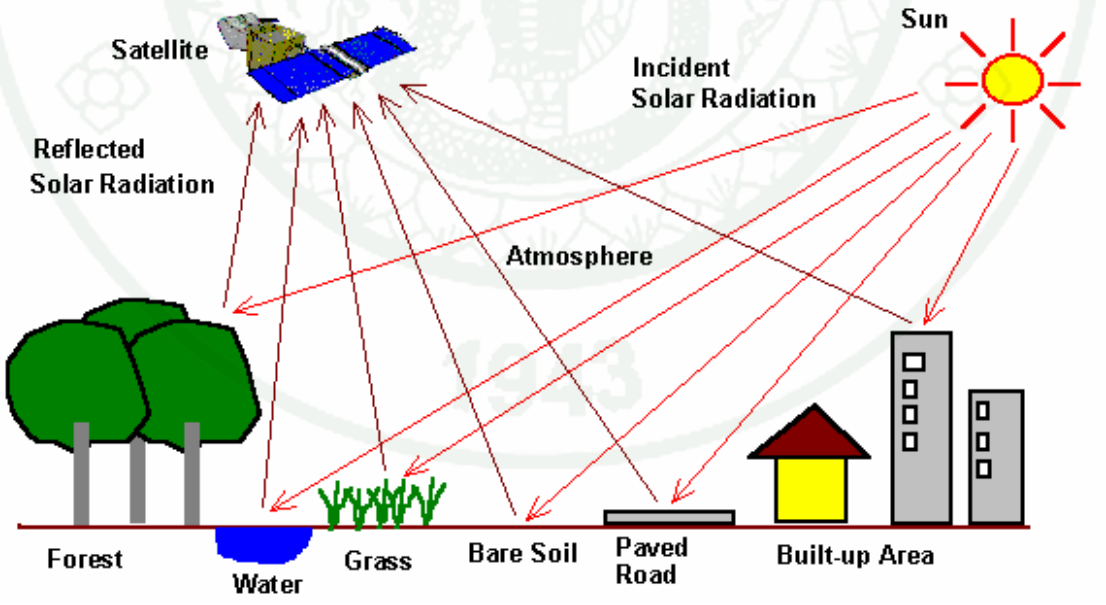

Figure 13 Principle of optical remote sensing.

Source: Liew (2006)

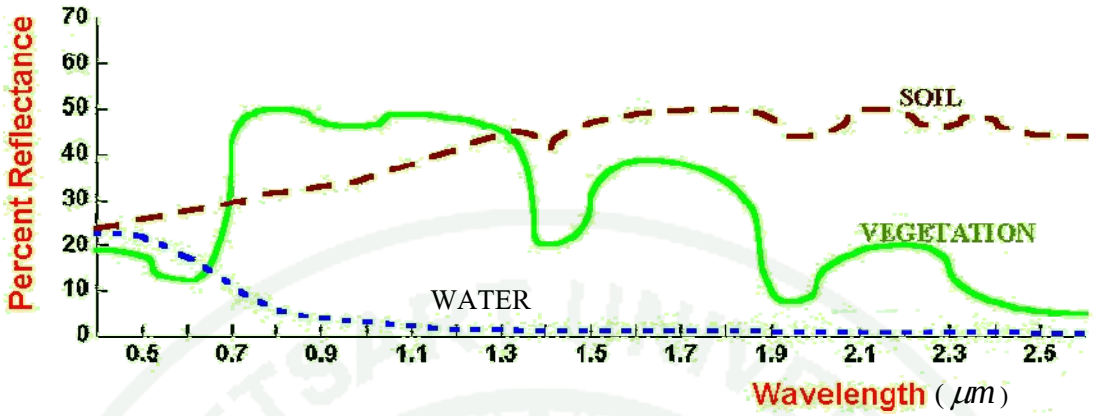

Figure 14 Spectral reflectance signature of soil, vegetation and water.

Source: Preechachol (2006)

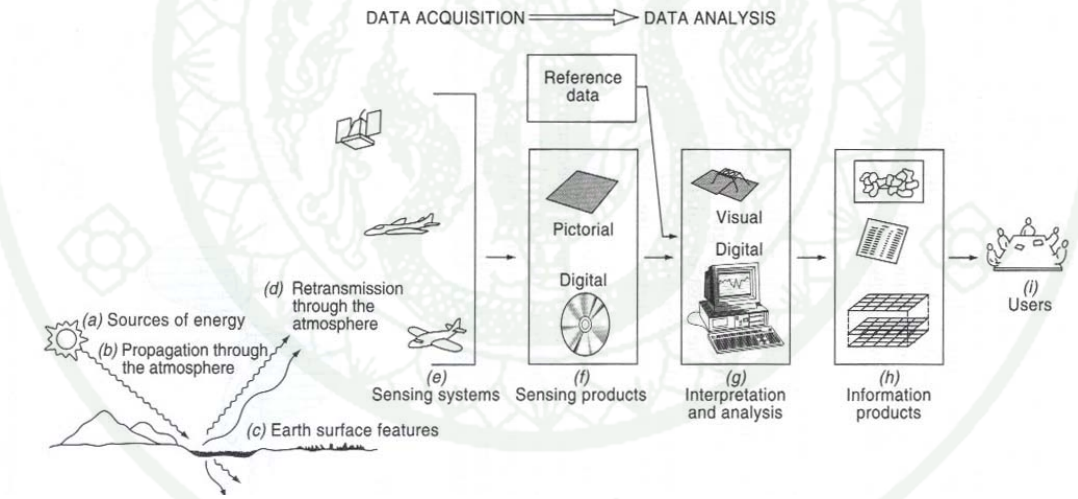

Figure 15 Electromagnetic remote sensing of earth resources.

Source: Lillesand *et al.* (2004)

The data analysis process (g) involves examining the data using various viewing and interpretation devices to analyze pictorial data and/or a computer to analyze digital sensor data. Reference data about the resources being studied (such as soil maps, crop statistics or field-check data) are used when and where available to assist in the data analysis which extracts information about the type, extent, location, and condition of the various resources over the collected sensor data. This information is then compiled (h), generally in the form of hardcopy maps and tables or as computer files that can be merged with other layer of information in GIS. Finally, the information is presented to users (i) who apply it to their decision-making process.

3.5 LANDSAT-5TM

LANDSAT is a satellite use to survey for natural resources of the United States of America under the National Aerospace Administration (NASA). The first satellite under the LANDSAT project was named Earth Resources Technology Satellite (ERTS) or LANDSAT-1 dated July 23, 1972 (Chalayonavin, 1998). LANDSAT-5 was launched in March 1, 1984. This satellite orbit has an altitude of 705 km, an inclination angle of 98.2^{o} (8.2^{o} from normal) with respect to the equator. This satellite crosses the equator on the north-to-south portion of each orbit at 9:45 A.M. local sun time. Each orbit takes approximately 99 minutes, with just over 14.5 orbits being completed in a day. LANDSAT-5 carries the instrument suites that include the Thematic Mapper (TM) imaging sensors and the Multi-Spectral Scanner (MSS). The design of LANDSAT-5 is shown in Figure 16.

Direct transmission of TM data to ground receiving stations is made possible via the X-band and S-band antennas onboard the satellite. The ground receiving stations are shown in Figure 17. The data transmission rate of TM is 85 megabits per second (Mbps).

MSS sensor has approximately the 79-m-resolution cell and collects four spectral bands. TM is a highly advanced sensor incorporating a number of spectral radiometric and geometric design improvements relative to the MSS. Spectral improvements include the acquisition of data in seven bands instead of four, with new bands in the visible (blue), mid-IR, and thermal portions of the spectrum. TM data are collected using a 30-m-ground-resolution cell (except thermal band (band 6), which has 120 m resolution). Table 6 lists the seven spectral bands of the TM along with a brief summary of the intended principal applications of each.

The continuous data record (since 1972) of the LANDSAT Program has proven to be an invaluable resource for researchers. The historical record of LANDSAT data provides documentable evidence on changes in the area extent of a process and rate of process change.

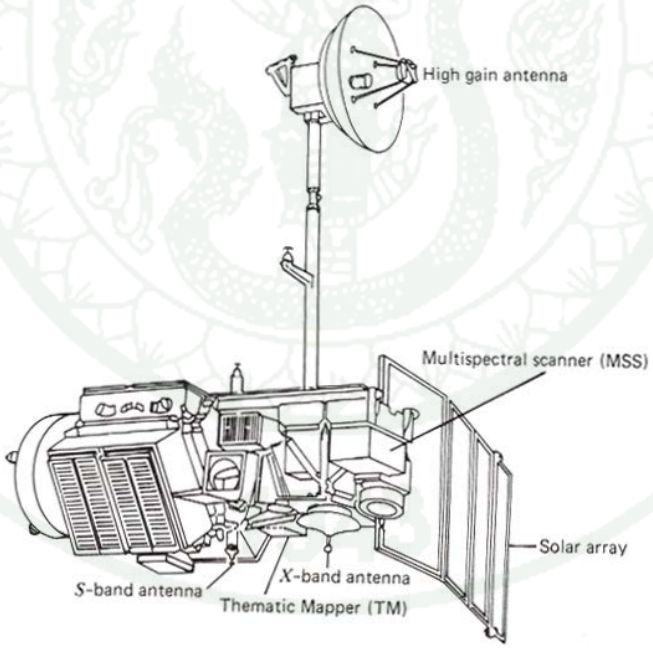

Figure 16 LANDSAT-5 observatory configuration.

Source: Lillesand *et al.* (2004)

Figure 17 LANDSAT-5 ground receiving stations.

Source: NASA (2004)

Table 6 LANDSAT-5 Thematic Mapper (TM) spectral bands.

Band	Wavelength (μm)	Nominal Spectral Location	Principal Applications
1	0.45-0.52	Blue	Designed for water body penetration, making it useful for coastal water mapping. Also useful for soil/vegetation discrimination, forest-type mapping, and cultural feature identification.
2	0.52-0.60	Green	Designed to measure green reflectance peak of vegetation for vegetation discrimination and vigor assessment. Also useful for culture feature identification.
3	0.63-0.69	Red	Designed to sense in a chlorophyll absorption region aiding in plant species differentiation. Also useful for culture feature identification.
4	0.76-0.90	Near IR	Useful for determining vegetation types, vigor, and biomass content, for delineating water bodies, and for soil moisture discrimination.
5	1.55-1.75	Mid IR	Indicative of vegetation moisture content and soil moisture. Also useful for differentiation of snow from clouds.
6[1]	10.4-12.5	Thermal IR	Useful in vegetation stress analysis, soil moisture discrimination, and thermal mapping applications.
7[1]	2.08-2.35	Mid IR	Useful for discrimination of mineral and rock types. Also sensitive to vegetation moisture content.

Remark [1] = Band 6 and 7 are out of wavelength sequence because band 7 was added to TM late in the original system design process.

Source: Lillesand *et al.* (2004)

In Thailand, the Remote Sensing Division (RSD), or internationally known as Thailand Remote Sensing Center (TRSC) was started in 1979 with the Thailand ground receiving station being established in 1982. (see Figure 17) Realizing the significant role of technology in remote sensing and GIS, and in monitoring and management of natural resources; a new organization, the Geo-Informatics and Space Technology Development Agency (Public Organization) or GISTDA was established on November 2, 2000.

GISTDA's main activities include direct reception of the data from earth observation satellites such as LANDSAT-5, RADARSAT, SPOT-2, 4 and 5; archiving and processing data in various forms, data analysis and integration with GIS, as well as distribution of such data to users worldwide. The resulting data is made available to all organizations concerned, both public and private. Figure 18 illustrates coverage of LANDSAT-5 image over Thailand.

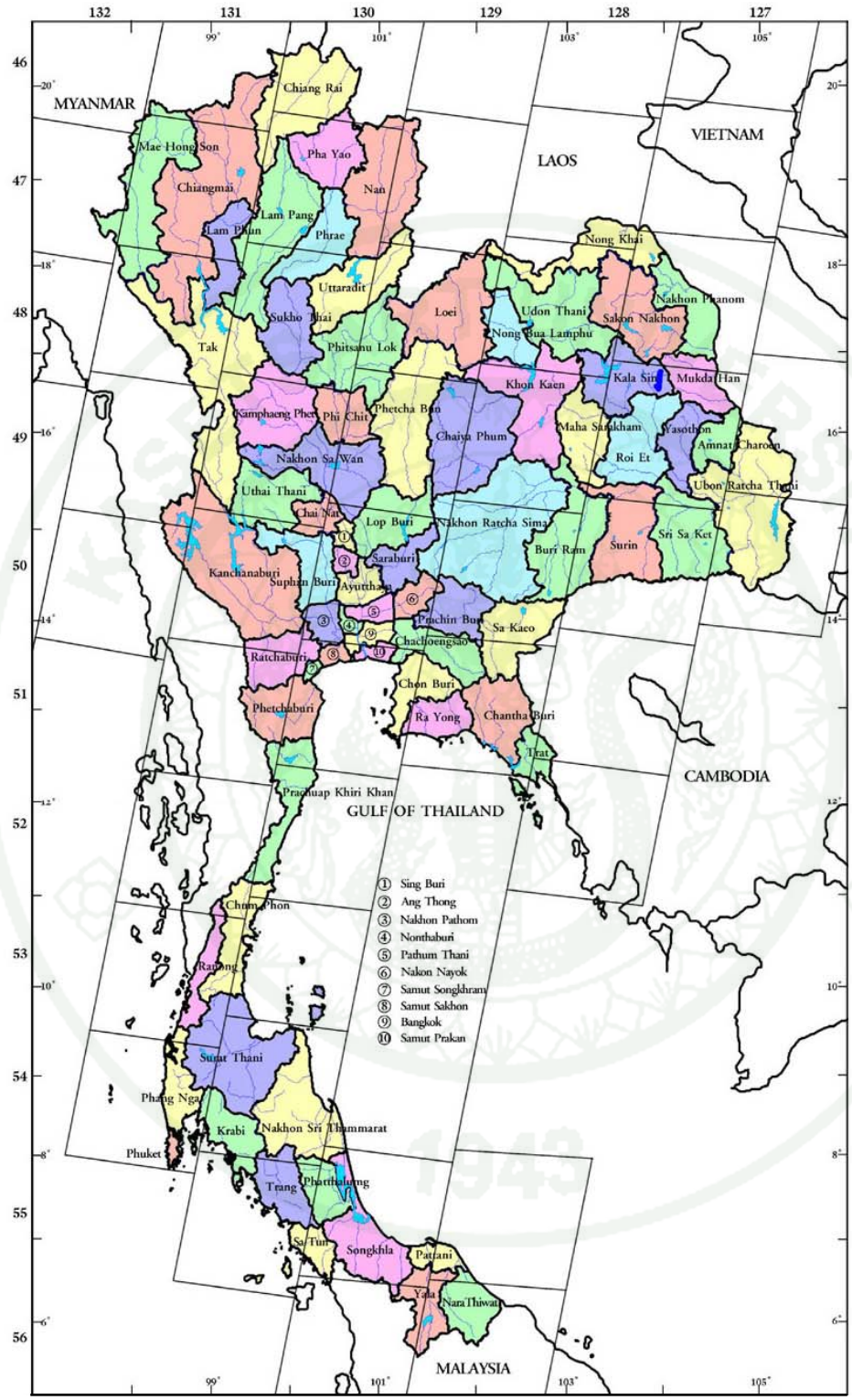

Figure 18 Coverage of LANDSAT-5 image over Thailand.

Source: GISTDA (2005)

3.6 Land cover change detection

Land cover change detection is necessary for the management of natural resources. The change is usually detected by comparison between two multi-date images, or sometimes between an old map and an updated remote sensing image (Japan Association of Remote Sensing, 2006). The method of change detection is divided into two methods as following.

- Comparison between two land cover maps which are independently produced

- Change enhancement by integrating two images into a color composite or principal component image. (see Figure 19)

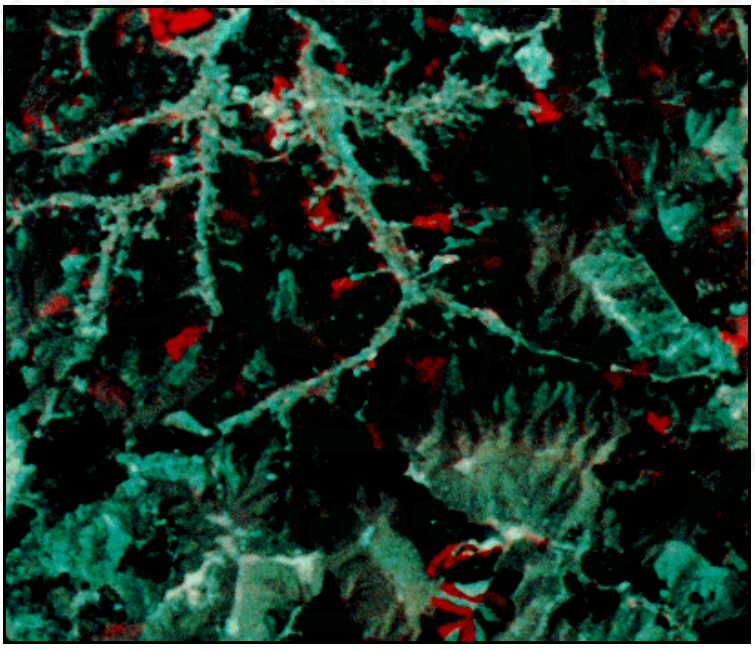

Figure 19 The changes over a 5 year period which were detected by using a color composite with blue assigned to an old image of LANDSAT-TM and red assigned to a new image of LANDSAT-TM.

Source: Japan Association of Remote Sensing (2006)

Land cover change can also be divided into two types;

- Seasonal change is that agricultural lands and deciduous forests change seasonally with a given year

- Annual change is that land cover or land cover changes which are real changes, for example deforested areas or newly built towns.

Usually elements of Seasonal and Annual change are present when comparing two different images.

3.7 Processes for the digital analysis of LANDSAT-TM

For the present study, RS analysis was applied to LANDSAT-5TM satellite imagery to categorize the land cover types. The detection was divided in two stages. First, two land cover maps in the same season of different years were compared. Second, change enhancement by integrating these two images into a color composite called as principal component image. This detected change in land cover consists of seasonal changes as agricultural lands or deciduous forests and annual change which reflect long term change like deforestation or newly built towns. Usually seasonal and annual change is mixed within the same image.

Digital image processing is carried out on the satellite imagery by a computer algorithm (Figure 20) which comprises of pre-processing, processing and post-processing. First is the pre-processing of satellite image data for radiometric and geometric corrections to remove respective distortions and image enhancement. Radiometric correction is also used to reconstruct the physically calibrated value from the observed data (Japan Association of Remote Sensing, 2006). Image enhancement is conducted to convert image quality to a better and more understandable level for feature extraction or image interpretation.

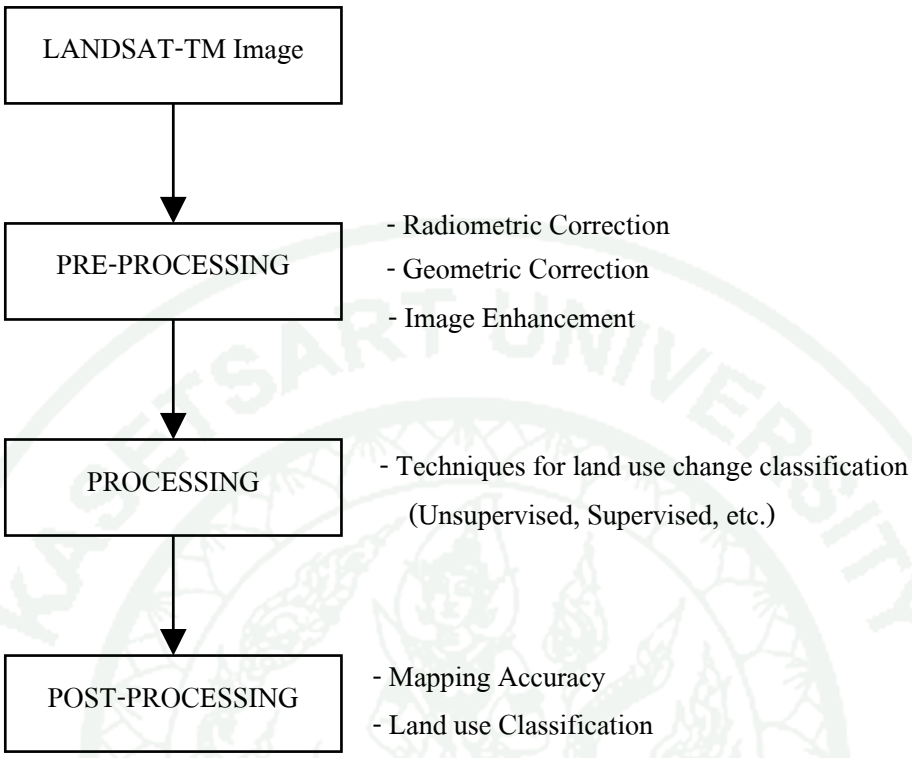

Figure 20 The processes of the digital analysis of LANDSAT-TM.

Source: Chalayonavin (1998)

Second is the classification of groups with homogeneous characteristics with the aim of discriminating multiple objects from each other within the image. Classification is executed on the basis of spectral or spectrally defined features, such as density, texture and so on by supervised or unsupervised learning on the training data sets.

False color composite based on the satellite bands for red (band 4), green (band 5) and blue (band 3) colors can be used to analyze the result of supervised technique. Alternatively, an algorithm of parallelepiped with maximum likelihood as a breaker can be used for the same purpose (PCI Geomatics Enterprises Inc., 2003).

Finally in post-processing, the accuracy of land cover classification results after the processing stage will be checked using the data fact and ground truth. The accuracy of the training data that can be prepared using unsupervised technique is checked using the kappa method (explained in the following section). Alternatively, the selected sample point of pixels checked by the ground truth can be used as a training area. Each selected training area will be used by the supervised technique together with the ground truth to detect the land cover type.

3.8 Accuracy assessment of supervised classification

The accuracy of supervised classification is assessed to know the accuracy of each land cover class. The assessment is done by comparing the relevant data extracted from the training area against the computer-processed results based on supervised technique. In assessing such accuracy, two statistical indicators, Cohen's Kappa and Overall Accuracy are used.

3.8.1 Cohen's Kappa

The Cohen's Kappa statistic (Jenness and Wayne, 2005) is used to measure the agreement between two sets of categorizations of a dataset while correcting for chance agreements between the two categories. This statistic is used for estimating the accuracy of supervised classification by measuring the agreement between sets of training area and classification results. The Kappa statistic makes use of both the overall accuracy of the supervised classification and the accuracies within each land cover type. This concept can best be understood by viewing the sets of training area and classification results for the land cover types in an error matrix (Figure 21).

In this matrix, the rows (j) represent the training area values while the columns (i) represent the classification result values. Each cell represents the number of land cover types (n) that were classified by using i and providing result as j. The diagonal where, represents the cases where the training area value agrees with

the classification result value. The off-diagonal cells contain misclassified values and the row and column describe exactly how these values were misclassified.

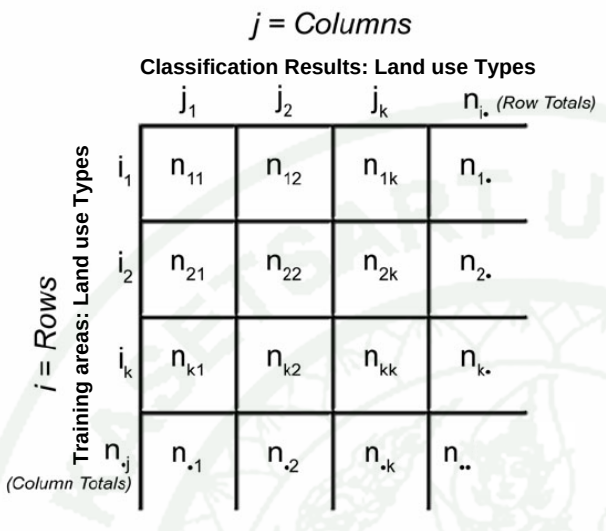

Figure 21 An error matrix of the sets of training area and classification results.

Source: Congalton and Green (1999)

The Kappa statistic provides a measure of agreement between the predicted values and the observed values and is calculated in the following equations (33) to (35);

$$n_{i\bullet} = \sum_{j=1}^{k} n_{ij} \tag{33}$$

$$n_{\bullet j} = \sum_{i=1}^{k} n_{ij} \tag{34}$$

$$Estimated\ Kappa = \frac{n_{\bullet\bullet}\sum_{i=1}^{k} n_{ii} - \sum_{i=1}^{k} n_{i\bullet}n_{\bullet j}}{n_{\bullet\bullet}^{2} - \sum_{i=1}^{k} n_{i\bullet}n_{\bullet j}} \tag{35}$$

where *n*, *i* and *j* are as defined above. The Classification is accepted if Estimated Kappa > 0.7.

3.8.2 Overall Accuracy

The overall accuracy of the model is simply defined as the total number of correct classifications divided by the total number of sample points and can be written in equation (36);

$$Overall\ Accuracy = \frac{\sum_{i=1}^{k} n_{ii}}{n_{\bullet\bullet}} \quad (36)$$

These two statistical indicators signify the accuracy of the results of land cover classification calculated using supervised classification. The classification is considered as acceptable if the Estimated Kappa value is higher than 0.7 and Overall Accuracy is greater than 70.

3.9 Areal Rainfall Estimation by using Thin Plate Spline method

The Thin Plate Spline technique is a general technique for smoothing a continuous surface such as elevation, water table, etc., by minimizing the curvature of the surface (Hutchinson, 1993). In this thesis, the thin plate spline technique was applied to interpolate daily rainfall data over the study area. To equilibrate the variance of the noise across the rainfall data network and to reduce the skew in the raw data, the square root transformation was applied to the observed rainfall values as shown in equation (37) (Sharples *et al.*, 2005).

$$r_i^{(1/2)} = f(x_i, y_i, h_i) + \varepsilon_i \qquad i = 1,2,..,n \quad (37)$$

where f is a smooth function of the longitude (x_i), latitude (y_i), and elevation (h_i); r_i is the rainfall recorded at the location i; n is the number of locations; ε_i are random error terms, including those associated with rainfall data measurement and the model deficiency, which are normally distributed with zero mean and variance σ^2. The unit of the observed rainfall is in mm and varies according to the longitude and latitude coordinates, which have the unit in degree, while the unit of elevation is in km. As a result, the elevation scale is around 100 times larger than horizontal coordinates (Hutchinson, 1995a).

The general thin-plate smoothing spline estimate of the function g is obtained by minimizing the equation (38) over a class of suitably smooth functions (Wahba, 1990).

$$\frac{1}{n}\sum_{i=1}^{n}\left[r_i^{(1/2)} - f(x_i, y_i, h_i)\right]^2 + \lambda J_m(f) \qquad (38)$$

The first term in the equation (38) is the average squared Euclidean distance between the observed data and fitted values, and the $J_m(f)$ term is the mth order roughness penalty consisting of the integral of squared mth order partial derivatives of f. In this thesis, the smoothness in terms of the second order partial derivatives of f and the term $J_m(f)$ were considered to be

$$J_2(f) = \iiint \left(f_{xx}^2 + f_{yy}^2 + f_{hh}^2 + 2f_{xh}^2 + 2f_{xy}^2 + 2f_{yh}^2\right) dx\, dy\, dh \qquad (39)$$

The smoothing parameter λ in equation (38) determines a balance between the fidelity to the data and the degree of smoothness of the fitted spline function f. This parameter is usually determined by minimizing the generalised cross validation (GCV). The GCV is an estimate of predictive error of the spline surface. It is calculated by removing each data point and summing the square of the difference of

each point from a surface fitted by all other data points (Hutchinson and Gessler, 1994).

In this thesis, the mentioned equations were carried out by applying the ANUSPLIN software, developed by Hutchinson (1993), to generate a surface of interpolated daily rainfalls in conjunction with observed elevations in the UPRB. Input data consists of the generated DEM data covering the UPRB, daily rainfall stations as well as their observed locations and elevations. The outputs from the ANUSPLIN software are areal rainfall surfaces which correspond to point rainfalls and DEM data. A summary of the statistical indicators can be printed to show the accuracy of point rainfall estimation using the cross-validation technique. The output of areal rainfall surfaces in the text file can be later imported to generate a grid format in the GIS environment.

MATERIALS AND METHODS

Materials

The materials for this thesis include the following:

1. Computer laptops and printers

2. IHACRES (Version 2.1), FLDWAV (Version 2.0.2.2) and MIKE11-HD (Version 2007) models for hydrologic and hydrodynamic analysis

3. ArcView GIS (Version 3.2) and MapInfo (Version 7.0) Softwares for GIS analysis and Garmin Vista for GPS analysis

4. PCI Geomatica Software (Version 9.1) for RS analysis

5. SPSS Software (Version 12) for Multiple regression analysis

6. ANUSPLIN software (Version 4.3) licensed for the Department of Water Resources Engineering, Faculty of Engineering, Kasetsart University.

7. Microsoft Office 2003 Software for editing this thesis and analyzing the results

Methods

The Methodology of this thesis can be illustrated by the conceptual framework shown in Figure 22. This conceptual framework includes the application of numerical models, and Geoinformatics in order to investigate the effects of annual land cover change on flooding in the UPRB. The methods can be summarized into 5 parts: 1) Data collection and processing, 2) Hydrologic and Hydrodynamic Modeling, 3) Land cover change investigation, 4) Examine relationships between flood characteristics and catchment characteristic, and 5) Prepare land use change scenarios. Each part is described as the following sequence.

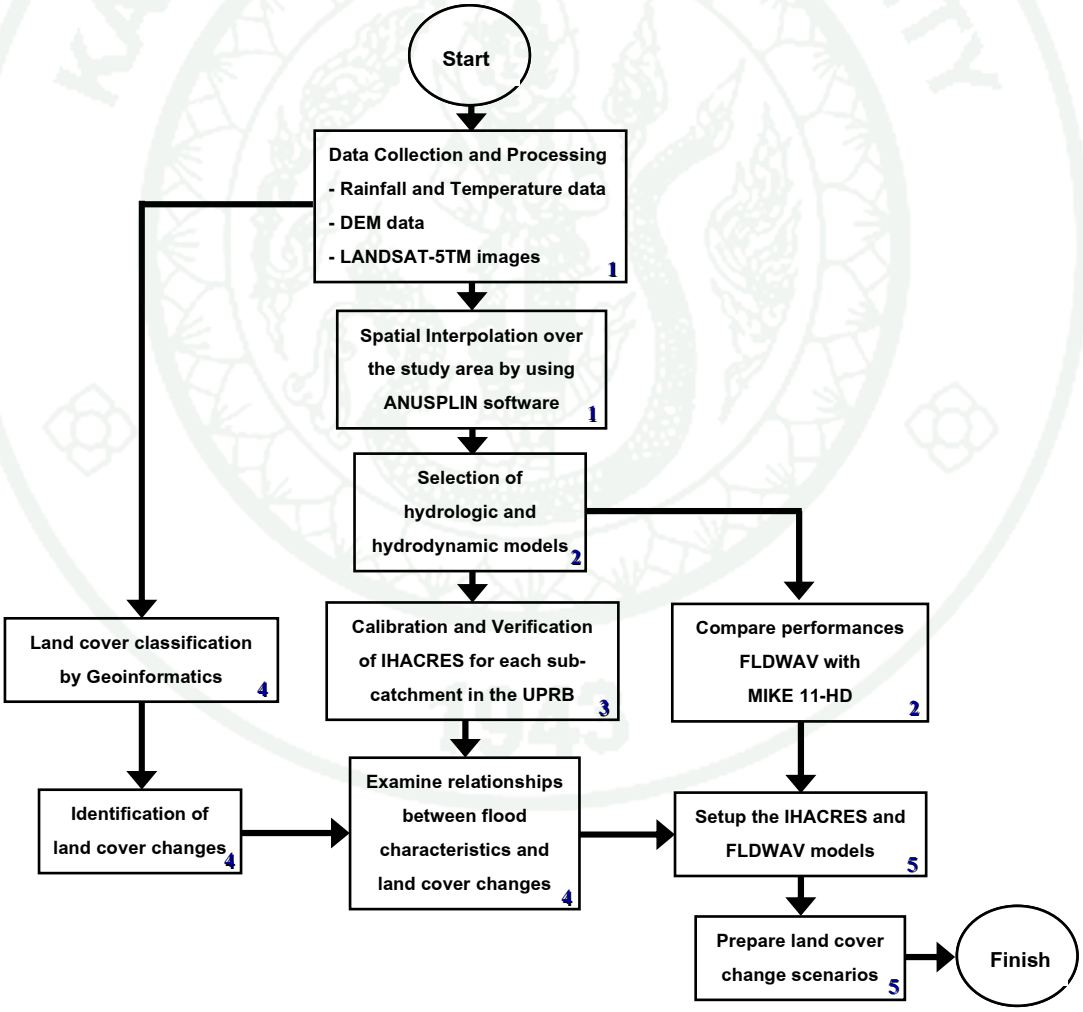

Figure 22 Conceptual Framework for this thesis.

Remark: number (1,2,3,4,5) identify each part of methods.

1. Data Collection and Processing

1.1 Data Collection

1.1.1 Rainfall data

Daily rainfall data was selected from a network of 123 rainfall stations located within and around the UPRB between 1988 and 2005. These data were collected by Department of Water Resources (DWR), Royal Irrigation Department (RID), Thai Meteorological Department (TMD), and Electricity Generating Authority of Thailand (EGAT). The consistency of the rainfall data was investigated using the double mass curve technique. Rainfall data at 68 rainfall stations were shown to be reliable. Areal rainfall estimation in this thesis was carried out using the TPS technique which provides more accurate results of rainfall estimation than the Isohyetal technique and particularly the Thiessen Polygon technique (Taesombat and Sriwongsitanon, 2009). These areal daily rainfall data were used as the input data for IHACRES to simulate flood hydrographs for eleven gauged catchments within UPRB. Figure 23 shows the locations of the 68 rainfall stations used in the study.

1.1.2 Meteorological data

Daily temperature data at three meteorological stations, which are located in Chiang Mai (CM-Met), Lamphun (LP-Met), and the Bhumibol Dam Site (BB-Met) were used as the input data for IHACRES. These stations are operated by the TMD. Figure 23 shows the locations of these three stations used in the study. All of meteorological stations also have data covering the period between 1988 and 2005 as runoff data used for the model application.

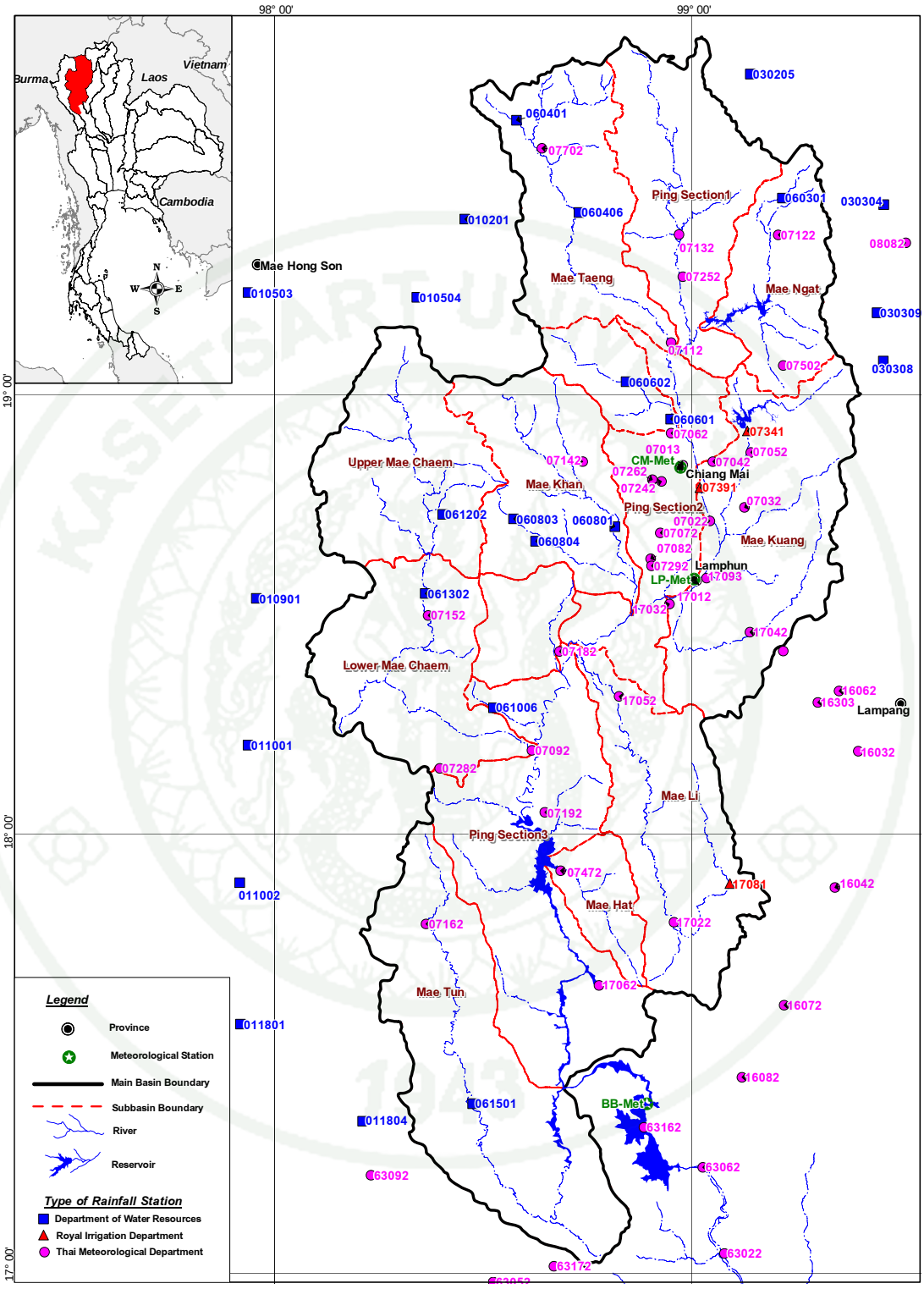

Figure 23 UPRB map showing the location of rainfall and meteorological stations.

1.1.3 Runoff data

Data between 1988 and 2005 was available for this thesis at 18 runoff stations in the UPRB operated by RID at the locations shown in Figure 24. However, some of these stations were unsuitable for the study of IHACRES model:

- P.56A station can be affected by backwater from the Mae Ngat reservoir so data from this station could be unreliable, especially during flood events.

- Stations P.75, P.67, P.1 and P.73 located along the Ping river and downstream of the Mae Ngat and Mar Kuang Reservoirs were not used as reservoir operations would be expected to affect flood behaviour at these stations. However, these stations were compared with the result of the FLDWAV model.

- Stations P.79 and P.80 only commenced operation in 2001, so insufficient data was available for use in this study

Runoff data were used for calibration and verification purpose. With these stations omitted, Table 7 summarises the features of the eleven remaining stations and their associated sub-catchments that were used in the analysis.

Table 7 Eleven runoff stations analyzed

Station	Area (km^2)	Rainfall Data No. of Stations	Rainfall Data Length of data	Mean Annual Rainfall (mm)	Mean Annual Discharge (mm)	Average %Runoff (runoff/rain)
P.4A	1,902	9	1988-2005	1,142	187	16.4
P.14	3,853	10	1988-2005	1,128	258	22.8
P.20	1,355	6	1988-2005	1,023	277	27.1
P.21	515	5	1988-2005	1,029	229	22.3
P.24A	460	5	1988-2005	1,043	290	27.8
P.42	315	3	1988-2001	862	103	12.0
P.64	336	2	1990-2005	1,056	434	41.1
P.65	240	2	1992-2005	1,162	508	43.7
P.71	1,771	12	1996-2005	1,088	161	14.8
P.76	1,541	4	2000-2005	828	130	15.7
P.77	547	4	1999-2005	922	146	15.8

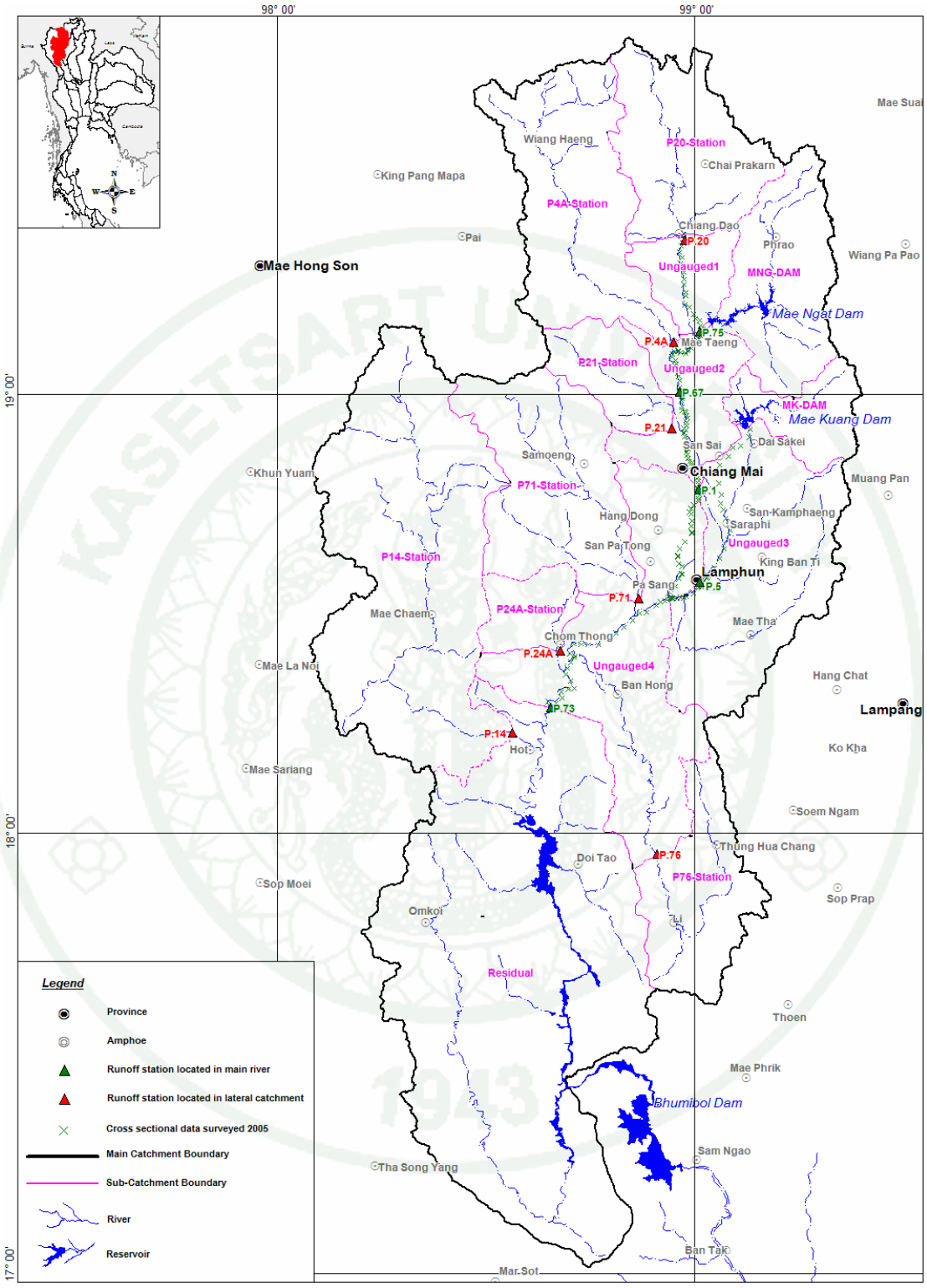

Figure 24 The map of sub-catchments and cross sectional data used in this river basin modeling (IHACRES and FLDWAV).

1.1.4 Cross section data

The data from 187 cross-sections were used - which are located along the Ping river between the upstream and downstream stations (P.20 to P.73), and along the Kuang river between the Mae Kuang Dam and the confluence of Mae Kuang and Ping river - as the input data for the FLDWAV model. These cross sections were surveyed by the RID and the DWR. Table 8 presents the number of cross-sections between particular locations which were collected at different time by these two government agencies.

Regarding to runoff and cross section data, Figure 24 illustrates the map of sub-catchments and cross sectional data used in this river basin modeling (IHACRES and FLDWAV). Furthermore, the river network schematic for river basin modeling in the UPRB is shown in Figure 25. Due to the FLDWAV boundary configuration, there are two upstream boundaries which are 1) daily discharge at P.20 station in the Ping river and 2) daily flows from MK-RE in Mae Kuang river. Downstream boundary is the rating curves at P.73 station in the Ping river. Regarding to Figure 25, there are seven sub-catchments having the available runoff stations and four sub-catchments which are also called ungauged catchment. Table 9 showed the detail of sub-catchments in the river network schematic for river basin modeling.

1.1.5 Hydraulic structures

Hydraulic structural characteristics in the Ping and Mae Kuang rivers are show in Table 10 and Table 11, respectively.

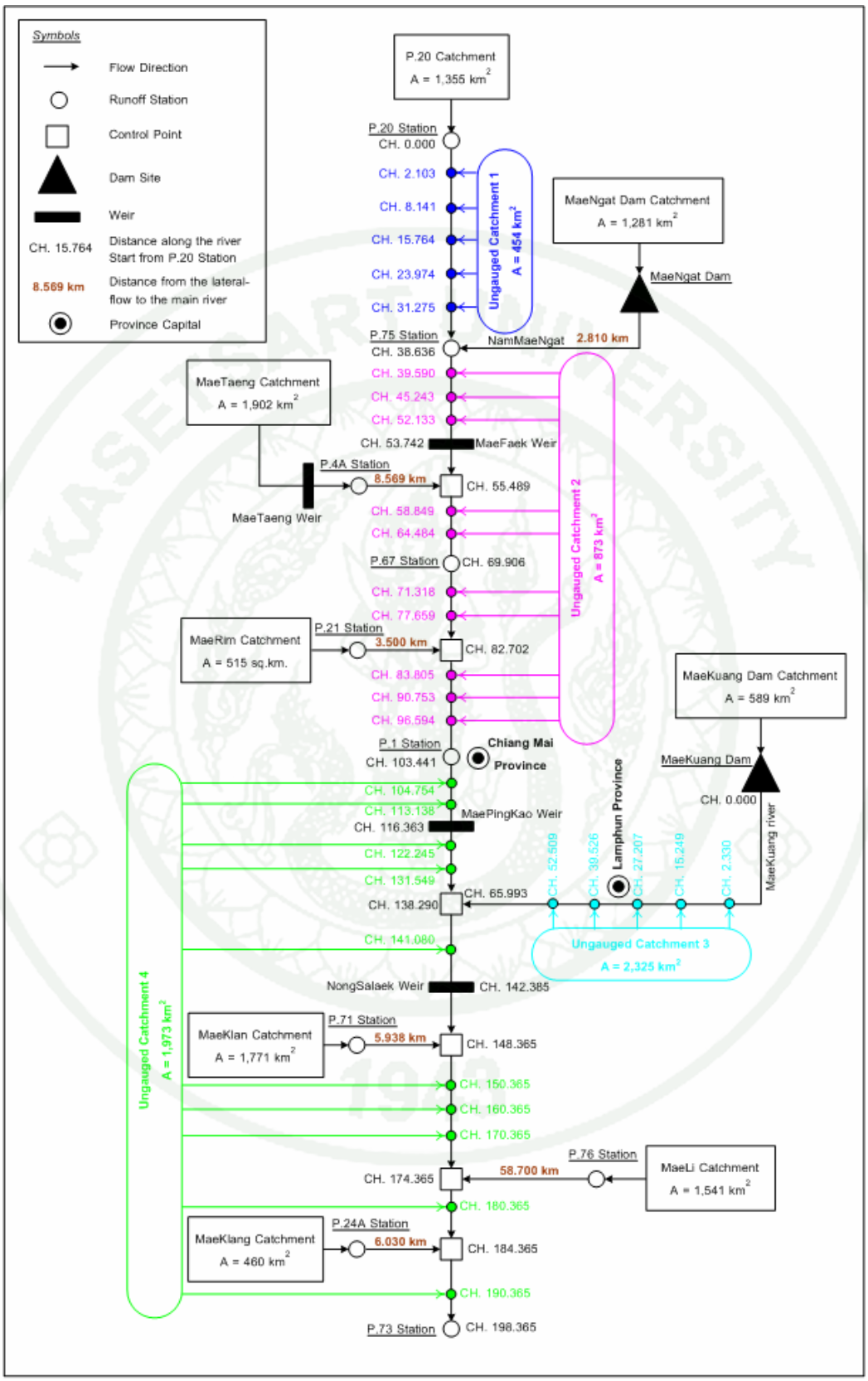

Figure 25 The river network schematic for river basin modeling in the UPRB.

Table 8 Detail of river cross section data in the study area.

River Name	Year of Survey	Number (sections)	Length of river (km)
Ping river			
• Between Amphoe Chiang Dao (P.20 station) to Nong Saleak Weir surveyed by RID	2005	94	138.4
• Between Nong Saleak Weir to Ban Son Soi, Amphoe Chomthong (P.73 station) surveyed by DWR	2005	31	60.0
Mae Kuang			
• Between Mae Kuang Dam to confluence of Main Ping river surveyed by RID	2005	32	64.0

Table 9 The detail of sub-catchments in the river network schematic for river basin modeling.

Order	Sub-catchment Names	Catchment Area (km^2)	Distance Along River		Remark Point	
			Start	End	Start	End
1	Upper Ping Sub-catchment	1,355	0.000	-	P.20	-
2	Upper Mae Ngat Sub-catchment	1,280	38.636	-	Mae Ngat Dam	-
3	Mae Taeng Sub-catchment	1,902	55.489	-	P.4A	-
4	Mae Rim Sub-catchment	515	82.702	-	P.21	-
5	Upper Mae Kuang Sub-catchment	557	0.000	-	Mae Kuang Dam	-
6	Mae Klan Sub-catchment	1,771	148.365	-	P.71	-
7	Mae Li Sub-catchment	1,541	174.365	-	P.76	-
8	Mae Klang Sub-catchment	460	184.365	-	P.24A	-
9	Mae Chaem Sub-catchment	3,853	-	-	P.14	-
10	Ungauged 1	454	0.000	38.636	P.20	P.75
11	Ungauged 2	873	38.636	103.441	P.75	P.1
12	Ungauged 3	2,325	0.000	65.993	Mae Kuang	Mae Ping Confluence
13	Ungauged 4	1,973	103.441	198.365	P.1	P.73
Total Area of the UPRB		**25,370**				

Remark: Distance along the Ping river is in the unit of km.

Table 10 Hydraulic structural characteristics in Ping river.

Order	Hydraulic Structure Name	Province	Length (m)	Height (m)	Type	Completed Year
1	Mae Ngat Dam	Chiang Mai	1,950	59	Earthfill Dam	1985
2	Mae Taeng Weir	Chiang Mai	80	5.50	Concrete	1973
3	Mae Faek Weir	Chiang Mai	89	3.00	Masonry	1936
4	Tha Sala Weir	Chiang Mai	130	2.00	Riprap	-
5	Nong Phung Weir	Chiang Mai	110	3.00	Riprap	-
6	Tha Wangtal Weir	Chiang Mai	130	2.00	Riprap	-
7	Mae Ping Kao Weir	Chiang Mai	105	2.00	Masonry	1941
8	Tha Mako Weir	Chiang Mai	67	3.00	Masonry, Concrete	1989
9	Sob Rong Weir	Chiang Mai	80	2.00	Riprap	1987
10	Phaya-Ut Weir	Lamphun	65	2.50	Masonry, Concrete	1989
11	Nong Saleak Weir	Lamphun	138	4.40	Concrete Weir	1999
12	Den Kha Weir	Lamphun	138	-	Riprap	-
13	Doi Noi Weir	Chiang Mai	125	4.00	Masonry, Concrete	1987
14	Wang Phan Weir	Lamphun	155	2.35	Concrete Weir	1990
15	Bhumibol Dam	Tak	486	154	Concrete Arch Dam	1964

Table 11 Hydraulic structural characteristics in Mae Kuang river.

Order	Hydraulic Structure Name	Province	Length (m)	Height (m)	Type	Completed Year
1	Mae Kuang Dam	Chiang Mai	610	68	Earthfill Dam	1993
2	Wang Tong Weir	Lamphun	30	3.85	-	1975
3	Ban Mae Rong Noi Weir	Lamphun	25	1.80	-	-

1.1.6 Satellite data

For the multi-temporal land cover classification, bands 3, 4, and 5 of nine predominately cloud-free LANDSAT-5TM images on path number 131 row 46 to 48 covering the UPRB were obtained from the Geo-Informatics and Space Technology Development Agency (GISTDA). They were taken at the beginning of the dry season (January - February) to ensure comparable conditions of soil moisture, vegetation development etc. which can mask the effects of seasonal change. Details of each image are summarized in Table 12.

Table 12 Details of nine LANDSAT-5TM imageries used in the study.

Year	Collecting date	Year	Collecting date
1988	Feb, 23	2000	Jan, 25
1993	Feb, 22	2001	Jan, 27
1994	Feb, 9	2002	Feb, 23
1995	Jan, 11	2005	Feb, 7
1996	Jan, 30		

1.1.7 Topographical maps

The topographical maps at scale of 1:50,000 (20 m contour interval) collected from the Royal Thai Survey Department. These data used for pre-processing satellite image in order to the geo-rectified process.

1.1.8 Land cover maps

Land cover maps in year 2000 collected by the Land Development Department (LDD) were collected. These data used as reference data for the cross-validation of land cover classification result in this thesis.

1.1.9 Digital Elevation Model (DEM) data

Two sources of DEM data covering an area of 53,100 km^2 in the UPRB and some parts of Myanmar between longitude 97.8° to 99.6° and latitude 16.9° to 19.85° were downloaded from NOAA-GLOBE (Hastings and Dunbar, 1998) and NASA-SRTM (Jarvis, 2006). The DEM data provided by these two organizations have different horizontal resolutions of around 1 km and 90 m, respectively. Hastings and Dunbar (1998) and Gorokhovich and Voustianiouk (2006) applied the DEM data from NOAA-GLOBE and NASA-SRTM, respectively, and they concluded that the vertical accuracy provided by these two data sources are around 20 and 16 m, respectively, which are not much different. By using these two sources of DEM data in the analysis, we can investigate whether the horizontal resolution of DEM data would have any impact on the accuracy of areal rainfall interpolation.

Regrading to generating flood inundation map, the DEM data was applied together with GIS software to generate the flood inundation map by using the calculated maximum water level profile along Ping and Kuang rivers from FLDWAV. The source of DEM data covering an area of 1,450 km^2 in the UPRB between longitude 98.6° to 99.1° and latitude 18.3° to 18.8° were collected from the Land Development Department. The DEM data has horizontal resolutions of around 1 m.

1.2 Spatial Interpolation over the study area by ANUSPLIN software

Regard to published manuscript (Taesombat and Sriwongsitanon, 2009), the materials and methods of this section were followed by that manuscript and shown as follow:

To be able to distinguish the effectiveness of each technique for areal rainfall interpolation, large amounts of rainfall show the results explicitly better than small amounts of rainfall (Hutchinson, 1998a,b).

Two periods of rainfall registered in August 2001 and September 2003, which had average rainfall depths over the data network of around 252.11 and 220.96 mm, respectively, were then chosen for further analysis. Number of rainfall station located within the 15 sub-basin areas of the UPRB and nearby area is shown in Table 13; average rainfall registered in August 2001 and September 2003 over each sub-basin is also presented. Figure 23 presents the locations of rainfall stations.

Table 13 Rainfall stations in each sub-catchment area in the UPRB and their average rainfall in August 2001 and September 2003.

Order	Sub-catchment	Area (km^2)	Number of Rainfall Station	Average Rainfall (mm)	
				Aug. 2001	Sep. 2003
1	Ping Section 1	1,972	2	309.55	291.85
2	Mae Ngat	1,282	3	223.97	237.70
3	Mae Taeng	1,956	4	293.38	257.20
4	Ping Section 2	1,723	10	291.46	291.74
5	Mae Rim	566	2	228.70	186.15
6	Mae Kuang	2,680	7	349.10	194.44
7	Mae Khan	1,732	4	310.35	271.50
8	Mae Li	2,080	3	222.43	186.10
9	Mae Klang	616	2	176.15	200.10
10	Ping Section 3	3,180	3	176.80	151.05
11	Upper Mae Chaem	1,965	1	435.40	273.70

Table 13 (Continued)

Order	Sub-catchment	Area (km^2)	Number of Rainfall Station	Average Rainfall (mm)	
				Aug. 2001	Sep. 2003
12	Lower Mae Chaem	1,930	3	248.93	197.70
13	Mae Hat	521	1	192.90	156.50
14	Mae Tun	3,167	2	129.50	191.65
15	Nearby Area	-	21	193.07	226.99
	Total Area	**25,370**	**68**	**252.11**	**220.96**

1.2.1 DEM Generation

To be able to easily compare the estimated areal rainfall produced by the two different DEM data together with rainfall data and TPS technique, DEM resolutions were transformed into 100 m using a nearest neighbour method in the ArcView GIS software (version 3.2) (ESRI, 2002). Ground elevation of those 68 selected rainfall stations can be later defined using these generated DEM data. The generated DEM data, rainfall locations and their ground elevations were later used as the input data for the ANUSPLIN software.

1.2.2 Investigation of topographical effect on rainfall depths

Rainfall depths generally vary with space and time and tend to increase with increasing elevations because of the orographic effect of mountainous terrain, which causes the air to be lifted vertically, and the condensation occurs due to adiabatic cooling (Goovaerts (2000) and Mirshahi *et al.* (2008). Hevesi et al.(1992a,b) revealed that there is a significant correlation of around 0.75 between average annual precipitation and their elevation recorded at 62 rainfall stations in Nevada and southeastern California. To prove this general understanding, the relationship between the average annual rainfall of each rainfall station between 1988 and 2006 and its elevation in the UPRB were plotted. If the results show a linkage between the two parameters, it is therefore possible to increase the accuracy of areal

rainfall interpolation by applying a topographic parameter (ground elevation of rainfall station) as proposed in this thesis.

1.2.3 Generate areal rainfall interpolation to input for IHACRES

An application of ANUSPLIN software Version 4.3 (Hutchinson, 2004) was carried out to generate the daily areal rainfall interpolation in the period of 1988-2005. These data would be later input to IHACRES for each sub-basin in the UPRB.

2. Selection of hydrologic and hydrodynamic public domain models

For this thesis, public domain mathematical models were searched and selected through the internet in order to get a set of well documental appropriate models widely used internationally for which model source code is available for improving users' understanding in the theory relevant to the model and its application according to the users' purposes. It is evident that this will lead to more advanced and greater model capacity in the future, enabling model users to be able to conduct in-depth research associated with the subjects in which these models are designed to serve.

As documented in manuscripts (Taesombat and Sriwongsitanon, 2006 and 2010a), internationally IHACRES and FLDWAV was selected, to calculate flood hydrographs at ungauged locations and to determine flood properties (flow rate and water level) at important locations, respectively, in the UPRB. The study river reach is between the gauging stations P.75 and P.73.

2.1 IHACRES model

IHACRES was used to estimate flow hydrographs for the ungauged catchments within the stations P.75 and P.73 as input data for the FLDWAV model. To do this, ungauged catchments were separated into three areas called the ungauged catchments 1, 2, and 3 which have the catchment areas of around 873, 2,325, and 1,973 km^2, respectively, as shown in Figure 26. Since these areas are ungauged, model parameters cannot be determined using the calibration and verification processes. Therefore, calibrated model parameters from neighboring gauged stations P.20, P.76, and P.77 which cover areas of 1355, 1541, and 547 km^2 respectively, were used to define model parameters for these ungauged catchments. Flood hydrographs at these three stations between August to November in 2001 and 2002 were used for model calibration and in 2003 and 2004 were used for model verification. Table 14 shows rainfall and meteorological stations used for model calibration and verification at these three runoff stations. Daily temperatures registered at each meteorological station and areal rainfall data were used as the input data for the IHACRES model.

Table 14 Rainfall and meteorological stations used for IHACRES calibration and verification.

Runoff station	Meteorological station	Rainfall station
P.20	CM-Met	07122, 07132, 07702, 030205, 060406
P.76	LP-Met	17022, 17062, 17081
P.77	LP-Met	07032, 07052, 17042

2.2 FLDWAV model

The FLDWAV model can be calibrated using unsteady flow characteristics to evaluate the suitable roughness coefficient (Manning's n) for both the channel and floodplain of each cross-section. For the UPR network between the stations P.75 and P.73 as shown in Figure 26, a flood event in 2001 (1-31 August) was selected to be used for model calibration. The maximum flow rate of this event at P.1 is around 450 cms which exceeds its channel capacity (350 cms). The suitable Manning's n for both channel and floodplain of each cross-section between the stations P.75 and P.73 were chosen by trial and error to obtain the best fit between calculated and observed flood hydrographs at stations P.67, P.1 and P.73. In the model verification procedure, selected values of Manning's n of each cross section were applied to another two flood events in 2003 (1-30 September), and 2004 (1-30 September). The maximum flow rates of these two events at P.1 are around 414 and 400 cms, respectively, which also exceed its channel capacity. Input data for the FLDWAV model used for routing flood water from P.75 to P.73 (see Figure 27) are as follows:

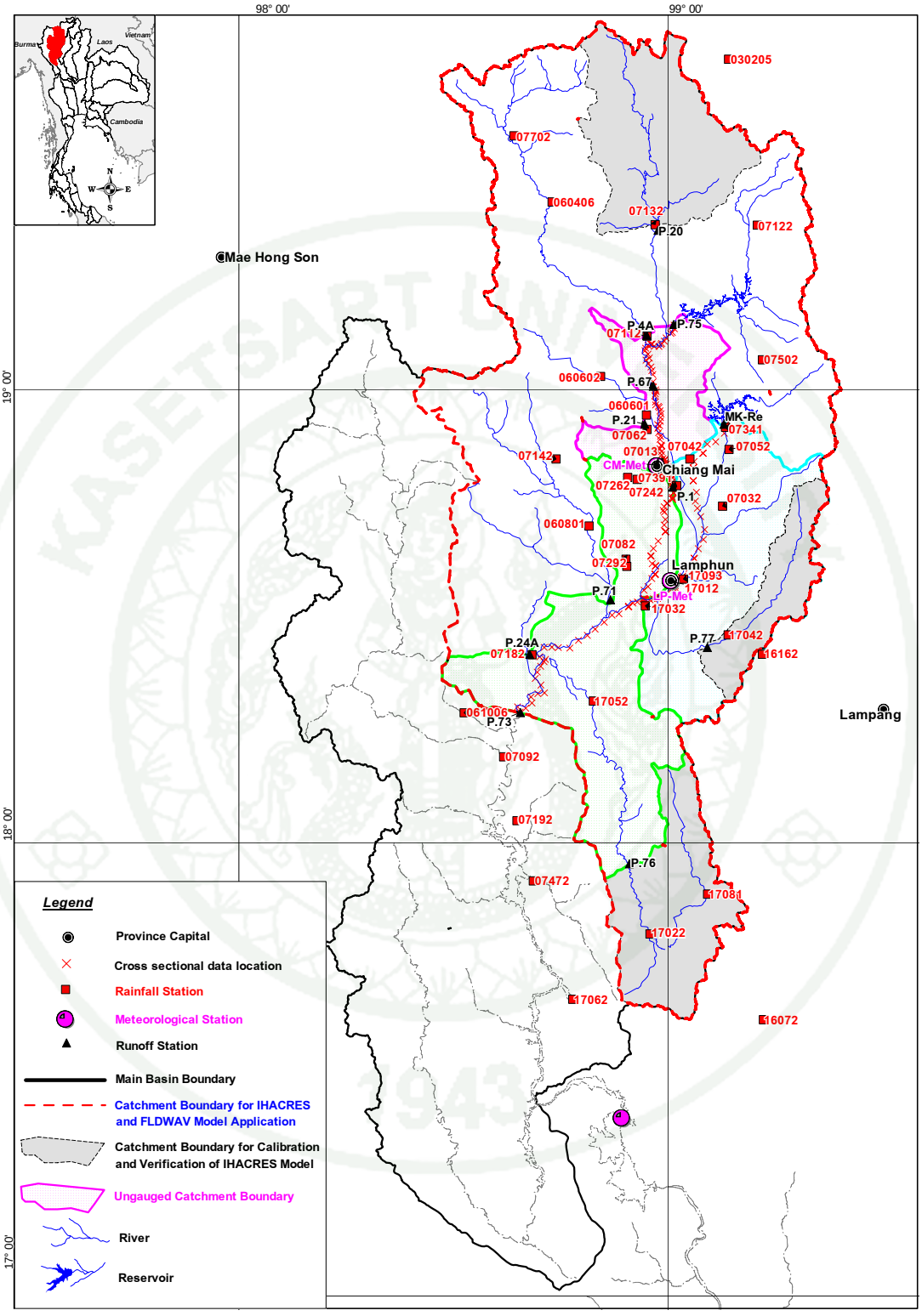

Figure 26 The UPRB and locations of rainfall, runoff, and meteorological stations for IHACRES-FLDWAV application.

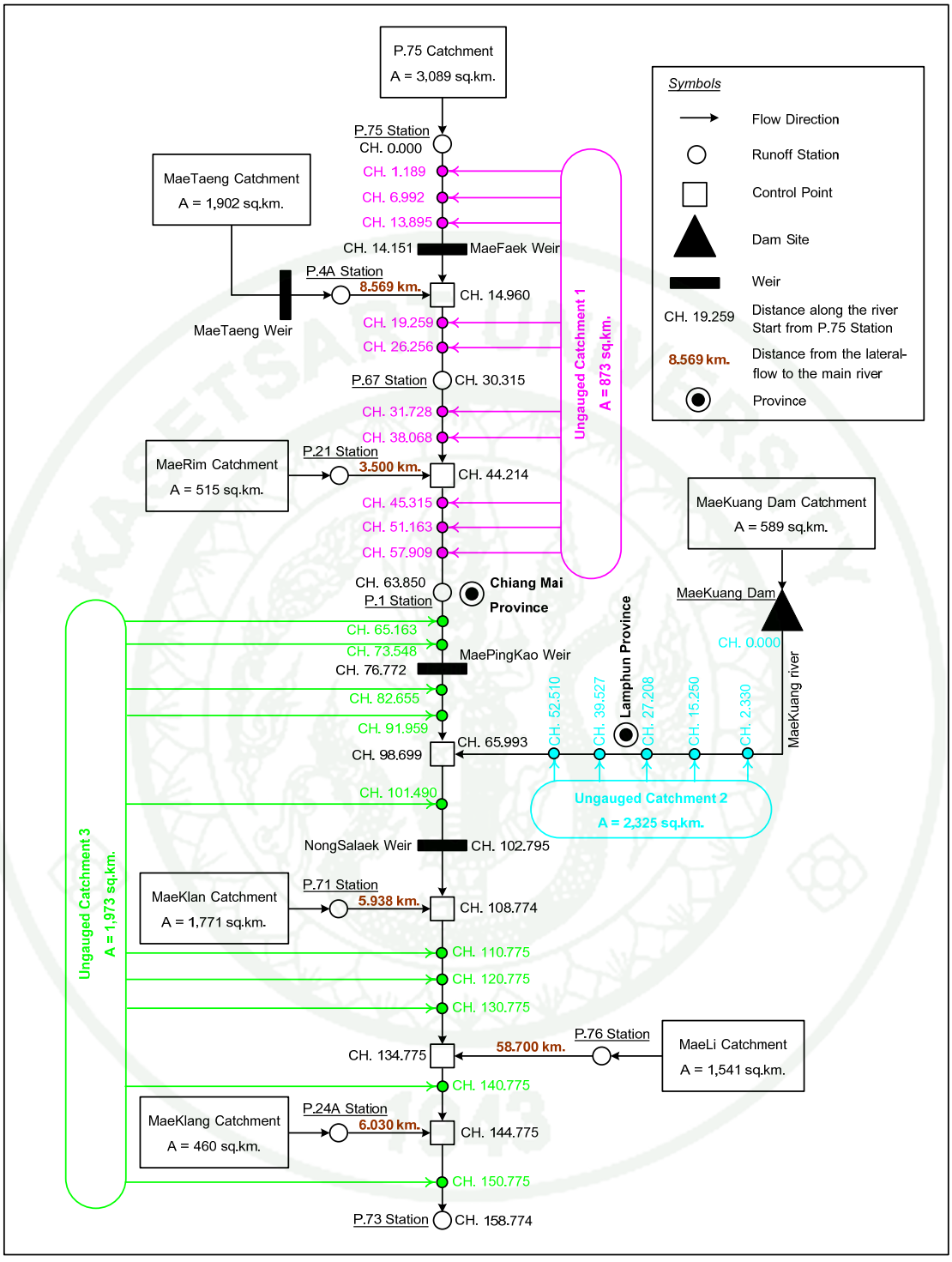

Figure 27 Schematic of the UPR network between P.75 and P.73.

1) Daily runoff data at all upstream locations of the river network comprising P.75, P.4A, P.21, P. 71, P.24A, and flow release from Mae Kuang Dam,

2) Local flows at 3 ungauged catchments were calculated using the IHACRES,

3) Observed rating curves at P.73 were observed in 2001, 2003, and 2004.

All calibration and verification results are shown in the Results and Discussion section.

3. Examine relationships between model parameters and catchment attributes

In this section, the relationships between IHACRES model parameters and catchment characteristics were investigated for gauged catchments in the UPRB in order to allow IHACRES to estimate flood characteristics on nearby ungauged catchments also within the UPRB. As described in Section 2.1, IHACRES was applied on eleven runoff stations: nine for calibration and two for verification to determine the model's ability in flood estimation and to derive relationships between model parameters and catchment characteristics. Following calibration, the sensitivity of model parameters was also checked at P.4A station to bring an understanding of how the model parameters affect the peak and volume of flood hydrograph. Details of this study are illustrated as follows.

3.1 Model Calibration at eleven runoff stations

To calibrate the model, firstly, the entire period of record for each catchment was divided into three year periods, each of which overlapped the previous period by one year. In this way, model parameters are exposed to some inter-annual variability, while ensuring that the hydrological response of the catchment does not change dramatically within the calibration period. The outcome of the calibration of

each period was used to determine suitable values of each model parameter for the years 1988-2005 for each sub-catchment. The calibration/verification results are illustrated in the Results and Discussion section. Figure 28 illustrates the location of selected runoff stations for IHACRES model calibration. Table 15 describes the details of the calibration periods for the selected runoff stations.

Table 15 Calibration periods for the selected runoff stations.

Runoff Station	Area	Calibration Period																
	(sq.km)	1988	1989	1990	1991	1992	1993	1994	1995	1996	1997	1998	1999	2000	2001	2002	2003	2004	2005
P4A	1,902																		
P14	3,853																		
P20	1,355																		
P21	515																		
P24A	460																		
P.42	315																		
P64	336																		
P65	240																		
P71	1,771																		
P76	1,541																		
P77	547																		

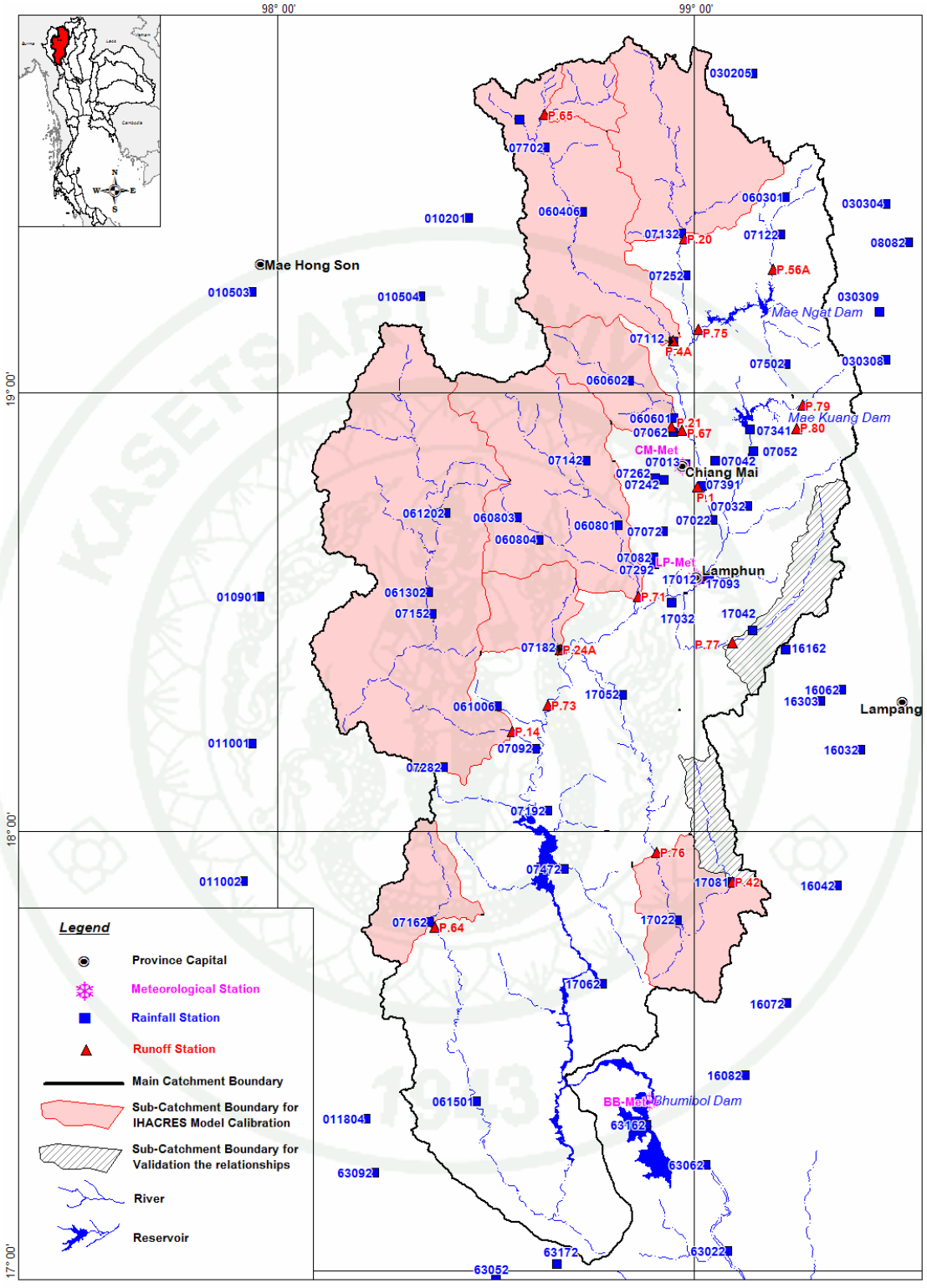

Figure 28 UPRB and the locations of rainfall, runoff, and meteorological stations for IHACRES calibration and verification.

3.2 Sensitivity Analysis of IHACRES model

The purpose of the sensitivity analysis was to understand how hydrograph outputs produced by the IHACRES model are affected by the six significant model parameters $c, \tau_w, f, \tau_s, \tau_q$, and V_s. If trends signifying how changing parameter values affect the characteristics of the hydrograph for the UPRB, a better understanding of how IHACRES represents catchment rainfall-runoff processes on the UPRB can be developed. The IHACRES model consists of 6 significant parameters; For the reference temperature (τ_s), it was recommended to use the average daily temperature, which is 25 degrees Celsius between 1988 and 2006. In addition, the guidelines for selecting each variable as illustrated in the user manual of IHACRES model are summarized in Table 16.

Sensitivity analysis of the hydrograph to changes of parameters was done by running the model across a range of values for each parameter independently, while other parameters remained constant at P.4A station. As parameter values were changed, increases or decreases of flood peak and flood volume were noted as detailed in the Results and Discussion section.

Table 16 Guideline for IHACRES model parameters.

	Model parameter name	Lower	Upper	Unit
1. Non-Linear Module				
c	Mass Balance	Unlimited		mm
f	temperature dependence of drying rate	1	50	celsius^{-1}
τ_w	Drying rate at reference temperature	2	100	day
2. Linear Module				
Delay	Relationship Rainfall and Streamflow	0,1		day
τ_s	slow flow response decay time constant	0	200	day
τ_q	quick flow response decay time constant	0	20	day
V_s	proportional volumetric contribution of slow flow to streamflow	0	1	-

3.3 Catchment Characteristics

Previous literature reviews (Post and Jakeman, 1996, and Sefton and Howarth, 1998) reveal that IHACRES parameters have relationships to the catchment characteristics.

With regard to catchment morphology, IHACRES considers four attributes. First, catchment size is given by the catchment area in km^2. Catchment shape is described by catchment elongation, defined as the ratio of the diameter of a circle with the same area as the catchment, to the catchment length (Schumm, 1956). Slope of catchment is defined by the angle formed by the catchment maximum vertical relief and channel length. Catchment drainage density is defined by Horton (1932) as the total length of streams per km^2. The descriptions of four catchment attributes are summarized in Table 17. Table 18 presents four catchment attributes which were derived for each of eleven sub-catchments in UPRB.

Table 17 Catchment characteristics description.

Catchment characteristics	**Catchment attribute details**	**Unit**
(1) Area	Catchment area	km^2
(2) Drainage density	Total length of streams per square kilometer	km^{-1}
(3) Slope	Angle formed by the catchment maximum vertical relief and channel length	degree
(4) Elongation	Ratio of the diameter of a circle with the same area as the catchment	-

Table 18 Derived catchment attributes for eleven sub-catchments in UPRB.

Station	Area (km^2)	Drainage (km^{-1})	Slope (degree)	Elongation
P.4A	1,902	0.40	7.84	0.06
P.14	3,853	0.43	8.13	0.04
P.20	1,355	0.33	8.01	0.09
P.21	515	0.38	7.23	0.13
P.24A	460	0.42	9.83	0.13
P.42	315	0.33	4.23	0.19
P.64	336	0.77	4.90	0.08
P.65	240	0.44	6.41	0.16
P.71	1,771	0.43	6.88	0.06
P.76	1,541	0.25	4.12	0.12
P.77	547	0.32	6.32	0.15

3.4 Relationships between model parameters and catchment attributes

To date, generalised relatonships between IHACRES parameters and physical catchment attributes have yet to be developed. Yet developing such relationships would greatly enhance the model's more widespread use (Sefton and Howarth, 1998). The relationships between calibrated model parameters and catchment attributes should ideally contain independent variables, be statistically significant and physically sensible whilst yielding good estimates of model parameters that can be shown to allow the model to reliably simulate observed discharge.

To determine if such relationships can be developed for the UPRB, linear and non linear multiple regression analysis were applied using SPSS Version 12 (SPSS Inc., 2008) to determine a set of equations suitable for estimating all six model parameters based on the catchment attributes for the nine sub-catchments used in calibration. Catchments of the P.42 and P.77 were not used for determining multiple

regression relationships as these catchments were used in validating the equations. Based on equations, each parameter was compared against the parameters obtained from the normal calibration in order to test the reliability of the equations that have been formulated from the multiple regression analysis. Outcomes of this analysis are illustrated in the Results and Discussion section.

4. Investigation of Land Cover Changes in the UPRB

The methods of this section were followed as documented in two manuscripts (Taesombat and Sriwongsitanon, 2010c and Taesombat *et al.* 2010). First, Geoinformatics was used to investigate the land cover changes in the UPRB. And, the relationships between land cover and flood characteristics were examined.

4.1 Classification of Land Cover Changes in the UPRB using the Geoinformatics

Regard to pending manuscript (Taesombat and Sriwongsitanon, 2010c), the processes for applying the Geoinformatics technique for this thesis are described as in the followings.

4.1.1 RS Analysis

Supervised classification together with the ground truth investigation which selected to be used in identifying land cover types are described as follows.

1) Application of false color composite with the following satellite bands: red color using band 4, green color using band 5, and blue color using band 3.

2) The algorithm selected for categorizing land cover types by means of a supervised classification technique is the parallelepiped with maximum likelihood as the breaker (PCI Geomatica Enterprises Inc., 2003).

4.1.2 Ground truth investigation

The user is required to designate a specific training area for entry into a computer program to classify land covers within the entire area. To define this training area, it is necessary to perform a ground truth investigation to acquire actual features of land cover which will then be compared with satellite imagery collected. Data observed from ground truth survey and that obtained from image comparison will be subsequently used to determine the training area for this study.

The ground truth survey in Chiang Mai and Lamphun Provinces was performed from March 28 to April 10, 2007, though this was a different year from the period during which the satellite image had been collected. A total of 63 sites scattered along 13 sub-basins of the UPRB were selected for conducting land cover classification survey. Results derived from the ground truth investigation were used to divide training areas into 23 categories. The 23 training sites were found to be providing an intensive computerized analysis of land covers and accurate end results. All the categories were further processed by supervised technique to get more than 100 pixels to the size of the training area. Subsequently, patterns of land cover identified through the 23 categories, were regrouped into six classes to make them more suitable for analyzing land cover changes afterward. These groupings are illustrated in Table 19 as follows. Figure 29 shows a map depicting sites under the ground truth survey.

Table 19 Details of Land cover class and training area.

Land cover class	Training Area	
1. Forest Area	1. Decidous forest	
	2. Evergreen forest	
	3. Forest plantation	
2. Disturbed Forest Area	4. Highland agriculture	
	5. Disturbed forest	
	6. Highland paddy fields	
3. Agriculture Area	7. Paddy fields	8. Longan
	9. Maize	10. Vegetable
	11. Soybean	12. Tobacco
	13. Potato	14. Pasture
	15. Garlic	16. Shallot
	17. Lychee	
4. Urban Area	18. Crushing plant	19. Urban
	20. Golf club	21. Road
5. Water body	22. Reservoir	
	23. River	
6. Other Area	24. Radiometric error*	

Remark: * is null class from 23 training areas

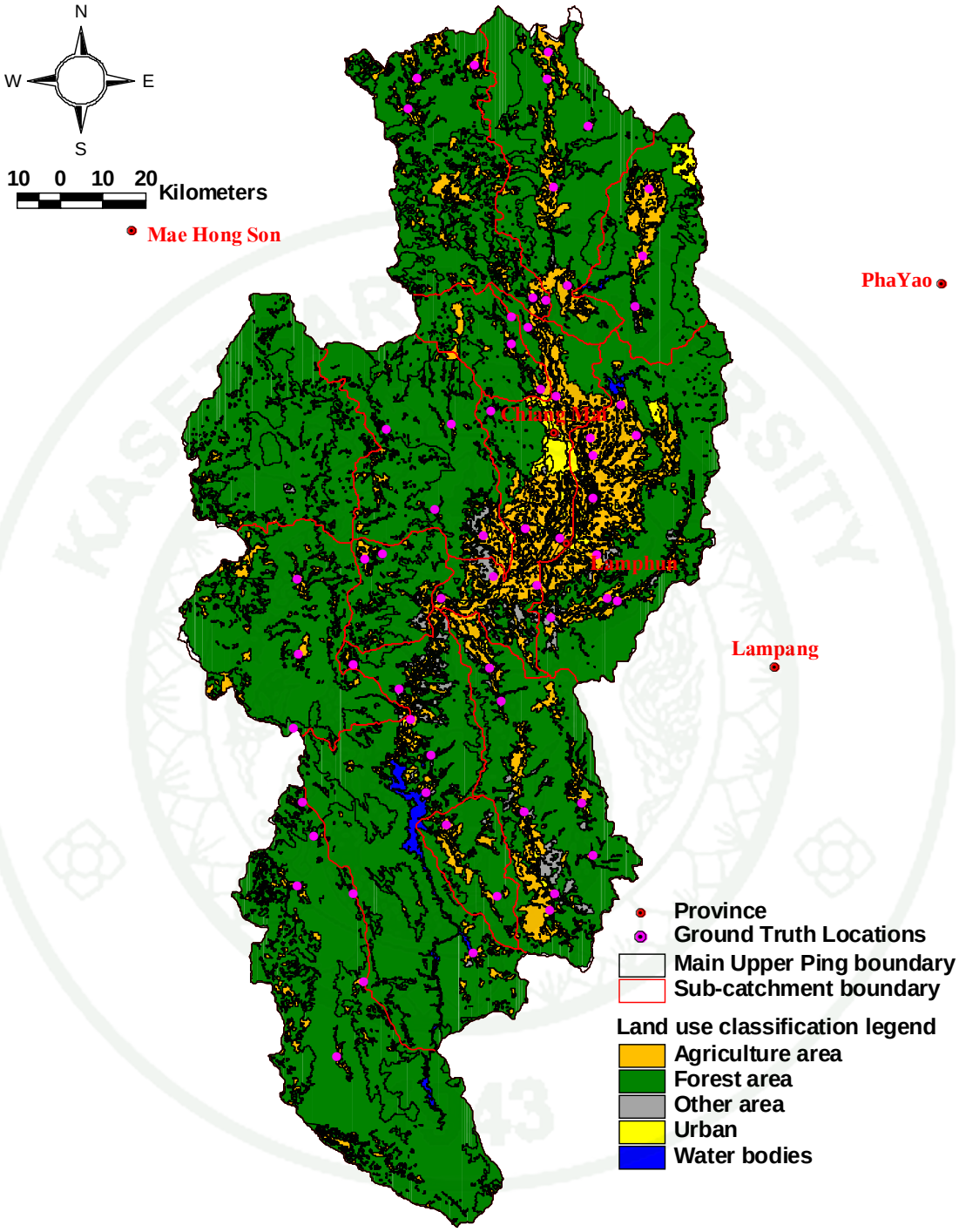

Figure 29 Map of land cover classification derived from LDD in year 2000 and the locations of ground truth survey in year 2007.

4.2 Examination of the Relationship between Land Cover and Flood Characteristics.

According to pending manuscript (Taesombat *et al.*, 2010), analyzing how land cover change impacts on flood events on each sub-catchment involved firstly determining the peak flow rate and the proportion of nett runoff to rainfall (the Rainfall Runoff Factor – RRF) associated with flood events for years during the study period when Landsat TM data were available. Correlation relationships between RRF and peak flow rate were then determined over the whole study period and from one year to the next for each sub-catchment. Next, RRF corresponding to peak flood events of 2, 5, 10 and 25 year Annual Recurrence Interval (ARI) were determined from the correlations for each year of the study period on each of the 11 sub-catchments. These peak flows standardized RRF were then correlated against the observed land cover changes. The methods of this section were described as in the followings.

4.2.1 Determination of RRF for flood events

Determination of the RRF for flood events on each sub-catchment was performed using standard flood analysis techniques on events with single peaked hydrographs in two steps:

1) Baseflow was removed from the flood hydrograph as it represents the contribution from antecedent precipitation rather than from the immediate event. This was done by constructing a trapezoid between the minimum flow points at the start and end of the event. RRF was then calculated as the area under the hydrograph divided by the sub-catchment area and the rainfall. (Note that no adjustments were made to peak flow rates.)

2) Rainfall related to a particular flood event was included when the discharge started to rise at the start of the event, until it started to fall at the end of the event.

4.2.2 Relationships between RRF and Peak Flow Rates for Flood Events

The RRF and the peak flow rate are the parameters that are most important in quantifying flood hydrology as they represent the proportion of rainfall transformed to runoff and the magnitude of a given flood event respectively. For a particular catchment, these two parameters would normally display well correlated, time independent relationships, unless some significant change takes place on the catchment such as changing land cover.

With this in mind, firstly RRF and peak flow were checked that they were overall well correlated for each sub-catchment. Next correlation relationships between RRF and peak flow rates were determined for each sub-catchment on a year by year basis to see if these relationships are changing over time.

The evidence were then looked for that the inter-annual changes in RRF to peak flow relationships were related to changes in land cover conditions. Our primary interest here is in flood event, however data available have only limited, so compromised by consider how flood hydrology might be affected by land cover for the 2, 5, 10 and 25 year ARI peak flows events (as determined by log Pearson III, statistics over the length of records available, 1954 to 2006 for most sub-catchments). These four peak flow values were applied to the RRF to the nine peak flow regression relationships relevant to each year in the study period for each of the 11 sub-catchment to determine a set of 297 RRF values that correspond to particular ARI flow rates for each year on each sub-catchment. Then how these RRF values were determined that they were correlated with the inter-annual changes in land cover: percentage forest cover, deforested areas, agricultural areas and urban areas for each sub-catchment. Under this approach, should correlations be evident between RRF and land cover, then change in hydrology can have some confidence that it is related to change in land cover.

4.3 Relationships between RRF and Land cover for Flow Events

In the previous section were realized that the relationships between RRF and peak flow rates for flood events (larger than around one year ARI) would differ from the relationships for flow events (less than approximately one year ARI). These differences would possibly depend on different soil moisture condition of the catchment between flow and flood hydrographs. With this in mind, the relationships between RRF and land cover for flow hydrographs were investigated, on the same 11 selected sub-catchments to see how effects on RRF and land cover on the continuous long period. Presumably for flow events, the catchment is in an unsaturated condition so this would make an interesting comparison with the result from the previous section.

For all runoff data within nine years between 1988 and 2005, all flow hydrographs were selected during the monsoonal period from May to October (6 months) except flood events which were analyzed within the previous section. For these flow hydrographs, the volume of rainfall and runoff (with base flow removed) was considered in order to determine the RRF and then the correlation between RRF and land cover under what would most likely be unsaturated catchment conditions. RRF were then determined for this period on each of the 11 sub-catchments and correlated these against the observed forest area and agriculture plus disturbed forest in each year.

5. Effects of Land Cover Changes on Flooding

In this section, the effects of land cover changes in this study were carried out by the derived relationships between RRF and land cover changes developed by Taesombat *et al.* (2010) in Section 4.2 and 4.3. These new approach can apply to determine how land use change will affect flooding by considering the ratio of the nett runoff volume generated to RRF. Section 4.2 and 4.3 were revealed the reliable relationships between land cover and RRF, for different magnitudes of peak flow during flood events. Two conditions identified were 1) flood events during the monsoonal period, strong relationships were found between RRF and land use particular forest area across the basin which indicates that increased forest area will increase runoff. 2) flow events where the result was opposite that shown in the flood events. With this in mind, suggested RRF should affect the same proportion of changes in the magnitude of flood hydrograph for each catchment. In Section 2., Taesombat and Sriwongsitanon (2010a) revealed that a combination model using IHACRES (rainfall-runoff model) and FLDWAV (hydrodynamic model) can be used for flood investigation in the river basin.

Based on all previous sections, through this thesis seek to improve the understanding of land cover changes on flooding by applying these models to consider how flooding may be affected under future land use change scenarios for the UPRB by: (1) applying the demonstrated relationships between RRF and observed land use changes from 1988 to 2005 determined in Section 4.2 and 4.3, (2) estimating flood hydrograph at ungauged catchments for the future scenarios using hydrographs derived by IHACRES, then by adjusting all sub-catchment hydrograph volumes according to the RRF relationships developed in Section 3., (3) simulating flood routing along the Ping river using the calibrated FLDWAV model for both channel and floodplain in Section 1.2 and 2. (4) testing the land cover change scenarios which were separated into two events, namely flood and flow events. They were used to predict the effect on the river basin by using the IHACRES and FLDWAV models.

5.1 Selecting flood and flow events

First of all, flood and flow hydrographs within the period 1988 to 2005 need to be selected for the events when nine land cover data are available. In this study, hydrographs with peak flow magnitude larger than around 1 year ARI was categorized as flood event and that of less than around 1 year ARI was categorized as flow event (Taesombat et al., 2010). These flood and flow events were later used to investigate the impact of deforestation and aforestation in the scenarios runs. Since the city of Chiang Mai, where the P.1 runoff station is located, has been suffering from flooding in the past decade. Flood events at this station were chosen as the reference to select flood and flow hydrographs for further study. The impact of deforestation and aforestation on the largest flood magnitude at P.1 station was selected. The largest flood event at P.1 station actually occurred in 2005. However, flood peak magnitudes at many of runoff stations used for developing the correlations between RRF and percentage of forest cover prepared in Section 4.2 happened to be below their peak magnitudes in 2005. Since the correlations between RRF and percentage of forest cover were further applied in this study, flood peak magnitudes in 2005 at many runoff stations were considered as the outliers. The second largest size of flood hydrograph in 2001 was therefore selected. Flow event also chosen within the same year. Table 20 shows periods of these selected flood and flow events as well as their flood peak magnitudes.

Table 20 Selected historical flood and flow events.

	Selected Flood Event			Daily Flood Peak	
Year	**Start**	**End**	**Duration (days)**	**Magnitude (cms)**	**Date of Occurred**
1. Flood events					
2001	1 August	31 August	31	450.8	13 August
2. Flow events					
2001	1 May	31 May	31	75.8	22 May

5.2 Flood and flow routing investigation along the Ping River

FLDWAV was applied in the UPRB main river network between the stations P.20 and P.73 (see Figure 25) to route those selected flood and flow events described in Section 5.1. Input data for FLDWAV application are: 1) daily runoff data at all upstream locations of the river network comprising P.20, P.4A, P.21, P.71, P.24A, P.76 and flow release from Mae Ngat Dam and Mae Kuang Dam, 2) local flows at four ungauged catchments estimated using IHACRES (see next section), 3) observed rating curve at P.73, and 4) Manning's n values for the channel and floodplain flows of the Ping river which are 0.035 and 0.070, respectively, evaluated in Section 2.

5.3 Flood Estimation for Ungauged catchments

Regarding to Figure 25, four ungauged catchments between P.20 and P.73 have the catchment areas of around 454, 873, 2325, and 1973 km^2, respectively. Since these areas are ungauged, model parameters cannot be determined using the calibration and verification processes. In this section, the model parameters for these catchments calculated by applying the relationships between IHACRES model parameters and catchment characteristics derived in Section 3.3 in the Results and Discussion (p.135) as showed in Table 32. Using these relationships and catchment characteristics of each ungauged catchment as presented in Table 21, model parameters for those four ungauged catchments can be evaluated as shown in Table 22. These model parameters and areal rainfall data during selected flood and flow events were input into IHACRES to generate flood and flow events for those ungauged catchments to be later input into FLDWAV.

Table 21 Derived catchment attributes for four ungauged catchments in UPRB.

Sub-catchment	Area (km^2)	Drainage (km^{-1})	Slope (degree)	Elongation
Ungauged 1	454	0.44	7.47	0.12
Ungauged 2	873	0.49	4.41	0.08
Ungauged 3	2325	0.36	4.14	0.06
Ungauged 4	1973	0.67	4.63	0.04

Table 22 IHACRES model parameters for four ungauged catchments.

Catchment	Area	Non-linear Module			Linear Module		
	(km^2)	c	τ_w	f	τ_s	τ_q	v_s
Ungauged 1	454	0.003437	41.55	11.79	47.18	1.87	0.67
Ungauged 2	873	0.002119	80.17	6.50	35.60	1.47	0.61
Ungauged 3	2325	0.001470	107.05	5.91	32.27	1.75	0.56
Ungauged 4	1973	0.001033	142.05	4.55	48.37	1.64	0.69

5.4 Impact of deforestation and aforestation on flood and flow hydrographs

5.4.1 Correlations between RRF and percentage of forest cover for flood and flow events

In this section, the correlation relationships reported in Table 38 in section 4.2 in Results and Discussion (p.148) were used to determine RRF values on the upstream sub-catchments (P.20, P.4A, P.21, P.71, P.76, and P.24A) in FLDWAV application for those selected flood peak event presented in Table 20 and correlated against the proportion of forest area (F) on each sub-catchment. Table 23 shows correlations for individual sub-catchments for the selected flood event. These generated relationships were later used to calculate RRF with different percentage of forest cover under scenarios runs for selected flood event.

In section 4.2 in Results and Discussion (p.148) also suggested that the relationships between RRF and peak flow rates for flood events (larger than ~1

year ARI) would differ from the relationships for flow events (less than ~1 year ARI). These differences would possibly depend on different soil moisture condition of the catchment between flow and flood hydrographs. Table 24 shows correlations of RRF and percentage of forest cover for the upstream sub-catchments (P.20, P.4A, P.21, P.71, P.76, and P.24A) in FLDWAV application for flow events. These relationships were later used to calculate RRF with different percentage of forest cover under scenarios runs for selected flow events.

Table 23 Correlations of RRF and percentage of forest cover for individual sub-catchments for selected flood event in 2001.

Runoff Station	**Flood peak (cms)**	**RRF = a + b (F)**		
		a	**b**	*r*
P.20	156	-0.77	0.0126	0.87
P.4A	124	-0.18	0.0041	0.62
P.21	37	-0.92	0.0133	0.82
P.71	194	-0.15	0.0049	0.72
P.76	65	-0.42	0.0077	0.82
P.24A	41	0.55	-0.0043	0.43

Table 24 Correlations of RRF and percentage of forest cover for individual sub-catchments for flow event.

Runoff Station	**RRF = a + b (F)**		
	a	**b**	*r*
P.20	0.579	-0.0057	0.53
P.4A	0.366	-0.0034	0.48
P.21	0.344	-0.0026	0.56
P.71	0.198	-0.0018	0.56
P.76	0.234	-0.0017	0.43
P.24A	0.300	-0.0023	0.54

5.4.2 Scenarios of deforestation and aforestation in the UPRB

In section 4.1 concluded that forest cover across the UPRB was generally decreasing from 1988 to 2005 at a rate of 1.86% annually (471 km^2/year). Conversely, for the corresponding period, areas under agriculture, disturbed forest, urbanized, and water bodies areas increased at annual rates of 0.60%, 0.84% 0.30% and 0.12% (151, 213, 77, and 30 km^2/year), respectively (see Figure 53). Since changes in percentage of forest cover is different in each sub-catchment and from year to year. Two scenarios for deforestation and one scenario for aforestation were proposed with different percentage changes in forest as presented in Table 25. For the scenario 1, flood event in 2001 was rerun using historical forest percentage in 2005. The selected flood event in the scenario 2 was rerun using hypothetical forest percentage in 2010 when the forest percentage reduced from 2005 at the same rate as historical percent reduction between 2000 and 2005. For the scenario 3, the selected flood event was rerun using hypothetical forest percentage in 2005 when the forest percentage increased at the same rate as it reduced between 2000 and 2005.

Forest percentage of each sub-catchment and each scenario as presented in Table 25 was substituted into corresponding correlation of RRF and percentage of forest cover of each sub-catchments and selected flood event. Table 26 presents percent changes in RRF for each scenario at upstream runoff stations for FLDWAV application. RRF at P.24A increased instead of reduced compared to other sub-catchments. This was the result of the correlations of RRF and forest cover show a negative trend while other sub-catchments show the positive trends (see Table 23). To be noted that flow release data from the Mae Ngat Dam (MN-RE) and Mae Kuang Dam (MK-Re) considered as upstream locations in FLDWAV application were kept unchanged because these flows were regulated and assumed to be unaffected by deforestation and aforestation.

Those three different scenarios were also applied on flow event in 2001. Forest percentage of each sub-catchment and each scenario as presented in Table 24 was substituted into corresponding correlation of RRF and percentage of forest cover

of each sub-catchment. Table 27 presents percent changes in RRF for each scenario at upstream runoff stations for FLDWAV application. Flow release data from the Mae Ngat Dam (MN-RE) and Mae Kuang Dam (MK-Re) were also kept unchanged as they were regulated.

The variation of these RRF at the upstream sub-catchments (P.20, P.4A, P.21, P.71, P.76, and P.24A) as presented in Tables 26 and 27 were used to adjust flood and flow hydrographs at each station for all scenarios runs and were routed by FLDWAV. Results of flood and flow hydrographs for each scenario were presented at P.75, P.67, P.1, and P.73 situated from the upstream to downstream locations along the main Ping river.

5.5 Preparation of flood inundation map

Flood map affected by river overflow from the main Ping river for the second largest flood event in 2001 were prepared for all scenarios compared to the baseline event in 2001. Flood inundation maps were prepared by GIS software using the input data of water level profiles determined by FLDWAV together with the DEM data of the basin. Extend and severity of flooding in 2001 can be evaluated using this flood inundation map.

Table 25 Percent changes in forest cover of each scenario for 2001 flood event.

Station	Scenarios	Forest Area (%)	Change in Forest (%)
P.20	Historical data	86.1	
	SN1: Deforestation in 2005	83.8	-2.37
	SN2: Deforestation in 2010	81.3	-4.87
	SN3: Aforestation in 2005	88.6	+2.50
P.4A	Historical data	83.1	
	SN1: Deforestation in 2005	81.0	-2.14
	SN2: Deforestation in 2010	79.0	-4.14
	SN3: Aforestation in 2005	85.1	+2.00
P.21	Historical data	79.6	
	SN1: Deforestation in 2005	78.2	-1.33
	SN2: Deforestation in 2010	77.2	-2.33
	SN3: Aforestation in 2005	80.6	+1.00
P.71	Historical data	81.1	
	SN1: Deforestation in 2005	78.9	-2.20
	SN2: Deforestation in 2010	76.9	-4.20
	SN3: Aforestation in 2005	83.1	+2.00
P.76	Historical data	70.6	
	SN1: Deforestation in 2005	69.4	-1.20
	SN2: Deforestation in 2010	68.4	-2.20
	SN3: Aforestation in 2005	71.6	+1.00
P.24A	Historical data	72.7	
	SN1: Deforestation in 2005	70.3	-2.43
	SN2: Deforestation in 2010	67.8	-4.93
	SN3: Aforestation in 2005	75.2	+2.50

Table 26 Percent changes in RRF for each scenario at upstream runoff stations for FLDWAV application on flood event scenarios in 2001.

Runoff Station	Historical data Flood Magnitude (cms)	SN1: Deforestation in 2005		SN2: Deforestation in 2010		SN3: Aforestation in 2005	
		Flood Magnitude (cms)	Changing in RRF (%)	Flood Magnitude (cms)	Changing in RRF (%)	Flood Magnitude (cms)	Changing in RRF (%)
P.20	156	141	-9.51	126	-19.51	172	+10.01
P.4A	124	118	-5.34	111	-10.34	130	+4.99
P.21	37	32	-13.06	29	-22.88	41	+9.82
P.71	194	186	-4.33	178	-8.27	202	+3.94
P.76	65	60	-7.51	56	-13.75	69	+6.24
P.24A	41	43	+4.48	45	+9.09	39	-4.61

Table 27 Percent changes in RRF for each scenario at upstream runoff stations for FLDWAV application on flow event scenarios in 2001.

Runoff Station	Historical data Flow Magnitude (cms)	SN1: Deforestation in 2005		SN2: Deforestation in 2010		SN3: Aforestation in 2005	
		Flow Magnitude (cms)	Changing in RRF (%)	Flow Magnitude (cms)	Changing in RRF (%)	Flow Magnitude (cms)	Changing in RRF (%)
P.20	23	27	+15.4	31	+31.7	20	-16.2
P.4A	65	71	+8.8	76	+17.0	60	-8.2
P.21	27	28	+2.5	28	+4.4	27	-1.9
P.71	60	65	+7.6	69	+14.6	56	-7.0
P.76	15	16	+1.8	16	+3.3	15	-1.5
P.24A	38	40	+4.2	41	+8.5	36	-4.3

RESULTS AND DISCUSSION

As explained in the materials and methods section, there were five parts taken to complete this thesis; the results and discussion are therefore presented according to this order whereby the areal rainfall estimations using spatial interpolation technique is described in the first part, followed by the selection of hydrologic and hydrodynamic public domain models, relationships between model parameters and catchment attributes, classification of land cover changes in the UPRB, relationships between flood behaviours and land cover change and preparation of land cover scenarios to see the effects of land cover changes on flooding are described in sequence as followings.

1. Areal rainfall estimations using spatial interpolation technique

1.1 DEM Generation

The elevations generated using the SRTM-DEM and GLOBE-DEM covering the selected area are between 26 to 2,520 m, and 33 to 2,487 m above mean sea level, respectively. Figure 30 shows the 3-D maps generated using the SRTM-DEM and GLOBE-DEM. The ground elevation at particular locations of each rainfall station can be specified from these two generated maps. Figure 31 shows a scatter plot of ground elevations of each rainfall station derived from SRTM-DEM and GLOBE-DEM. The accumulated different value of ground elevations generated from SRTM-DEM and GLOBE-DEM at the same rainfall stations presented by the mean errors (ME) is shown to be approximately -0.58 m. This different value is not so great when compared to the resolution differences of these two data sources that are quite large (90 m for SRTM-DEM and 1 km for GLOBE-DEM). It can be concluded that two different horizontal resolutions of DEM data used In this thesis did not have much impact on the vertical accuracy.

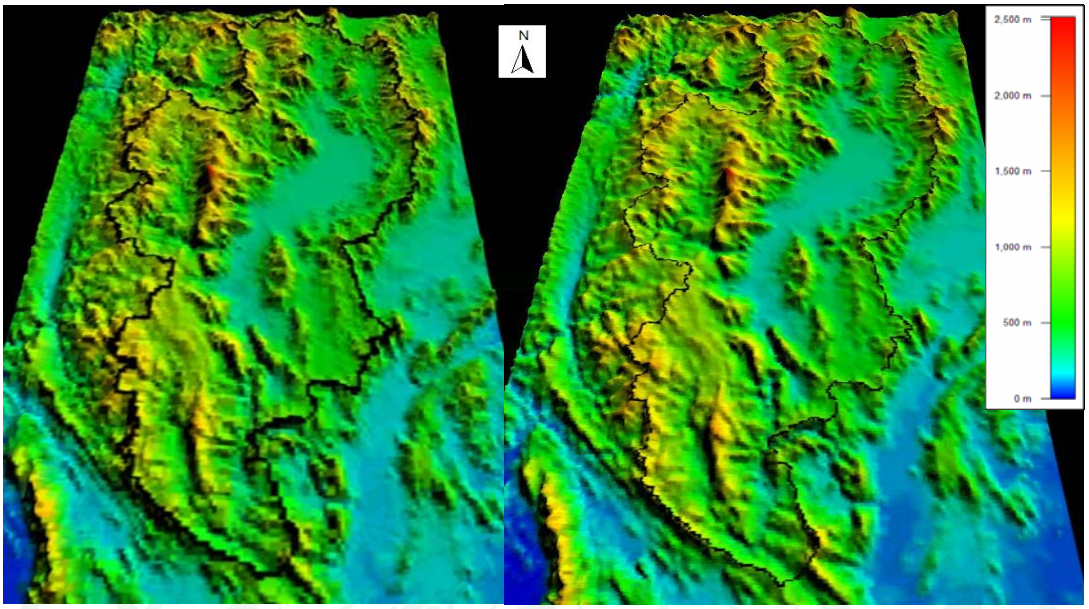

3-D Map of SRTM-DEM **3-D Map of GLOBE-DEM**

Figure 30 3-D maps generated using SRTM-DEM and GLOBE-DEM.

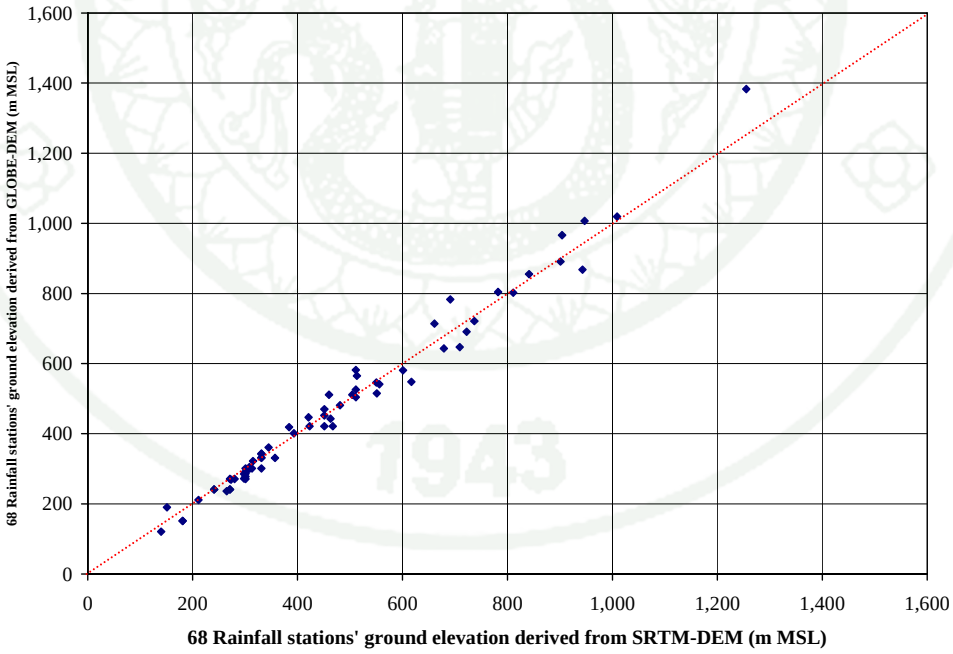

Figure 31 Ground elevations of each rainfall station derived from SRTM-DEM and GLOBE-DEM.

1.2 Relationship between rainfall depths and observed locations

The relationships between the average annual rainfall of each rainfall station between 1988 and 2006 and its elevation are plotted as shown in Figure 32. The figure shows that the average annual rainfalls tend to increase with increasing observed elevations with a coefficient of determination around 0.6918. It can be seen that rainfall stations located in the UPRB and nearby area, show the same tendency between rainfall depths and their station locations.

1.3 Areal rainfall estimations using TPS technique

Annual areal rainfall depths generating by TPS technique comparing with Thiessen Polygon technique over the UPRB that occurred in period of water year 1988 to 2005 were created and shown as histograms in Figure 33.

In addition, maps of maximum daily areal rainfalls that occurred on August 11, 2001 and September 13, 2003 were generated using these three different techniques and are illustrated in Figures 34 and 35, respectively. There are three different maps shown on this figure. Figures (a) is maps of areal rainfall depths generated by the TPS technique together with SRTM-DEM, while figures (b) and (c) were generated by the Isohytal and Thiessen Polygon techniques, respectively. It found that TPS technique provided more accurate results of rainfall estimation than the Isohyetal technique and particularly the Thiessen Polygon technique. (Taesombat and Sriwongsitanon, 2009)

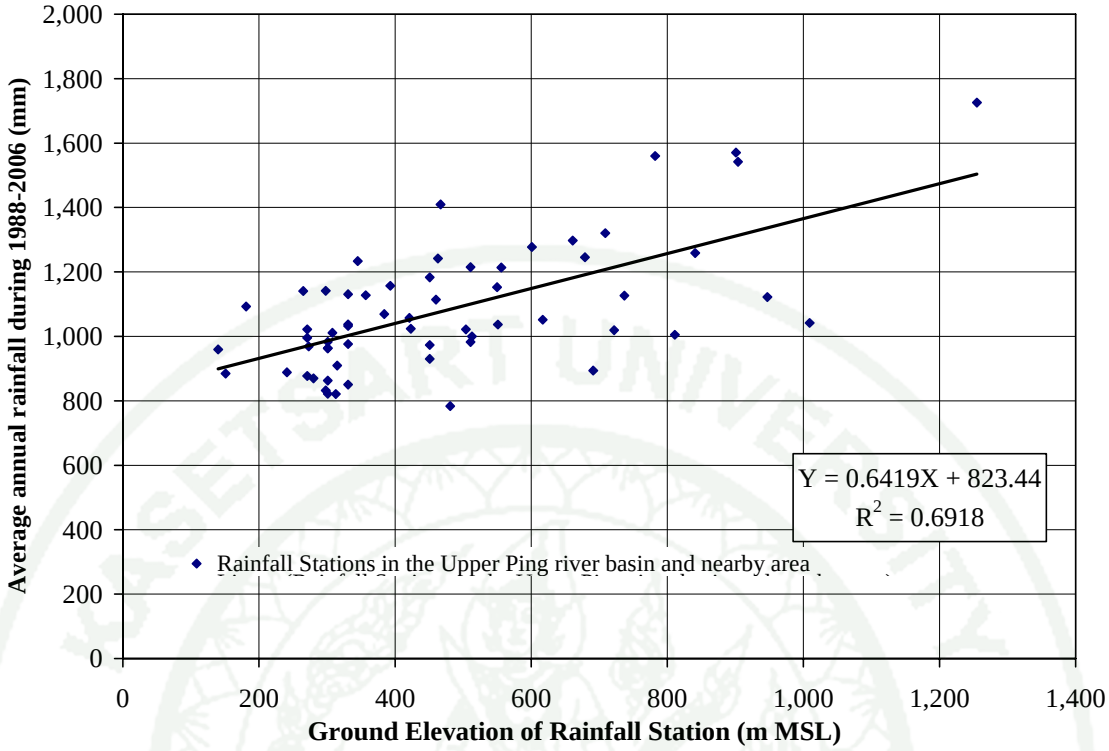

Figure 32 Relationship between the average annual rainfall of each rainfall station and its elevation in the UPRB.

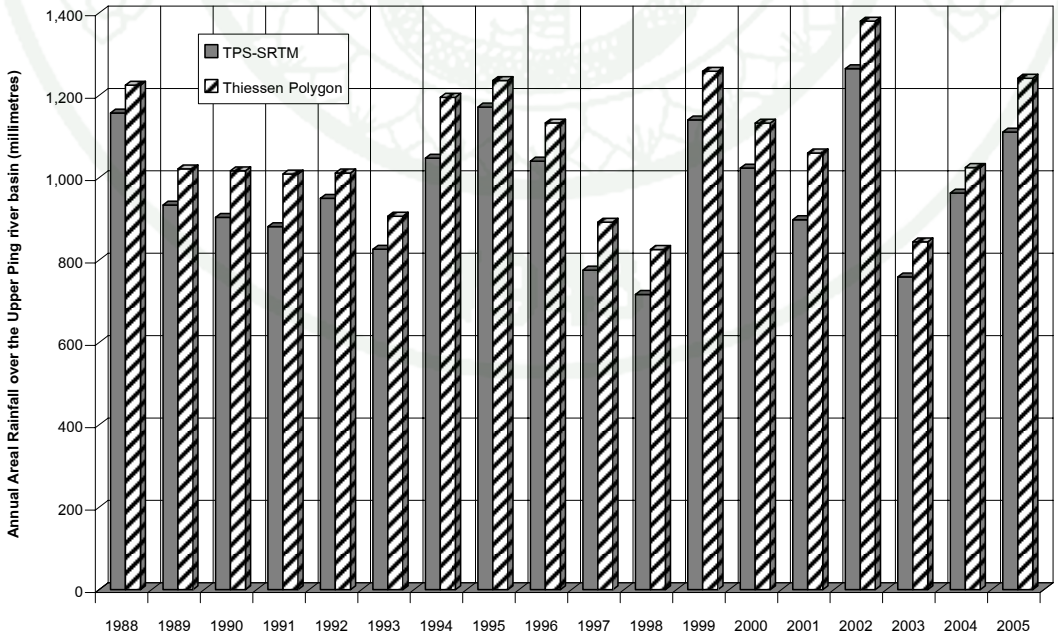

Figure 33 Histograms of annual areal rainfall depths in water year 1988-2005.

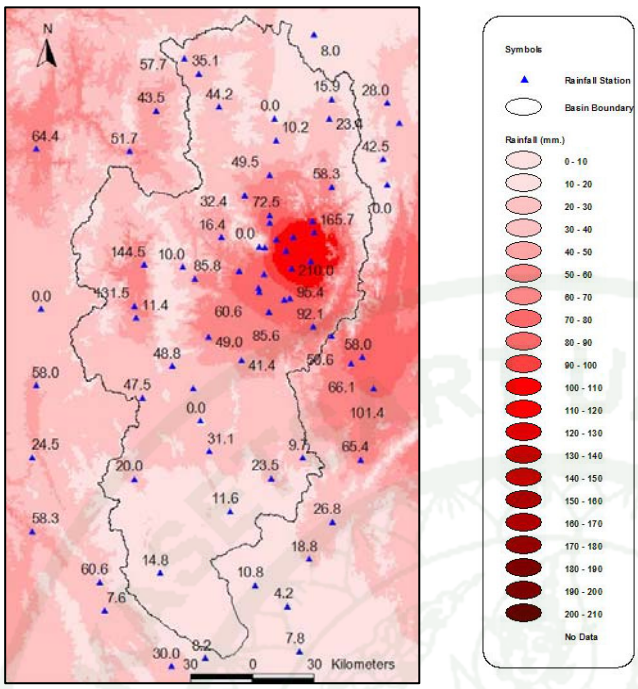

(a) TPS-SRTM technique

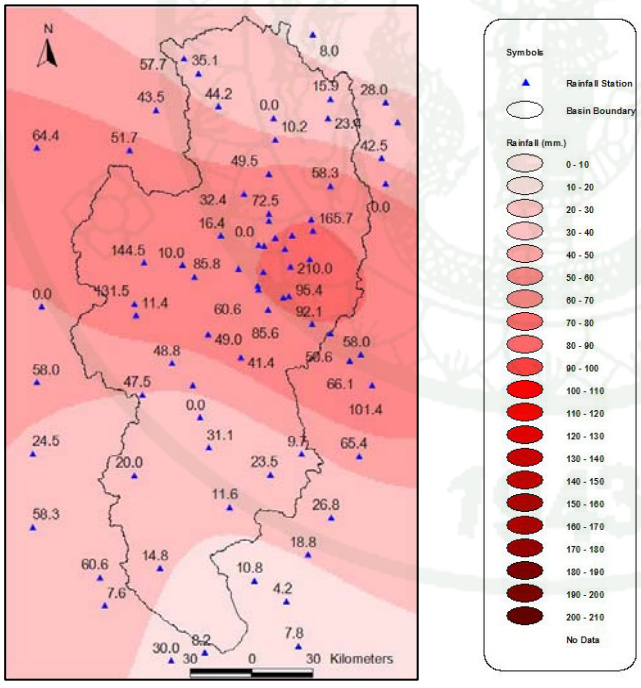

(b) Isohyetal technique

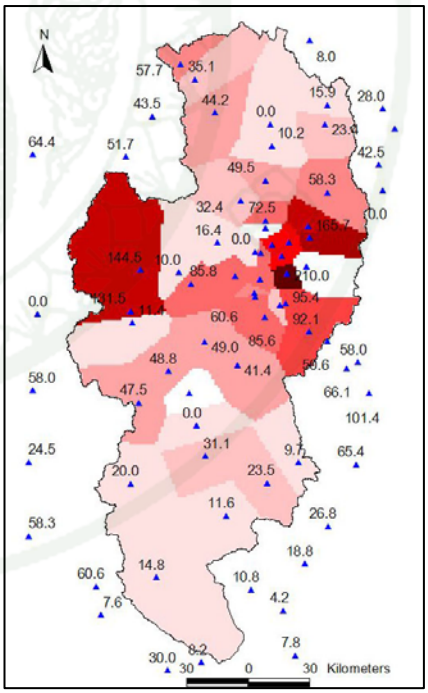

(c) Thiessen Polygon technique

Figure 34 Maps of daily areal rainfall depths in the UPRB on August 11, 2001 generated by three different techniques.

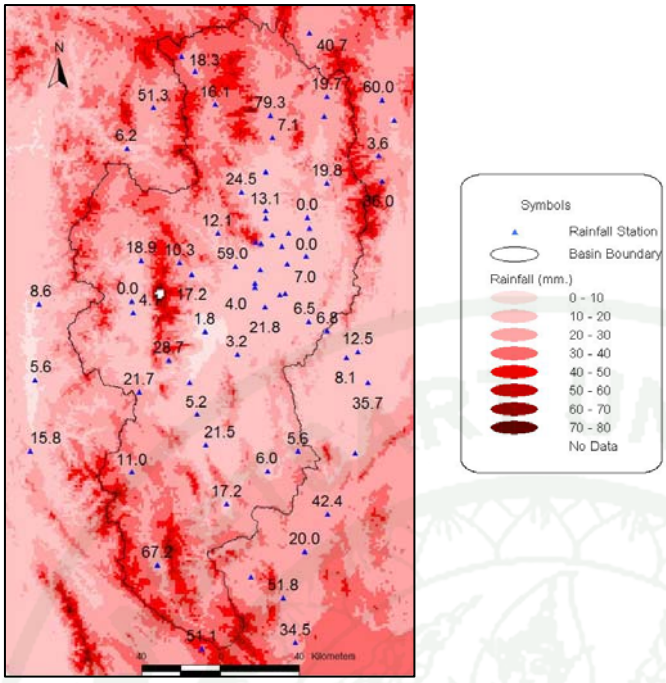

(a) TPS-SRTM

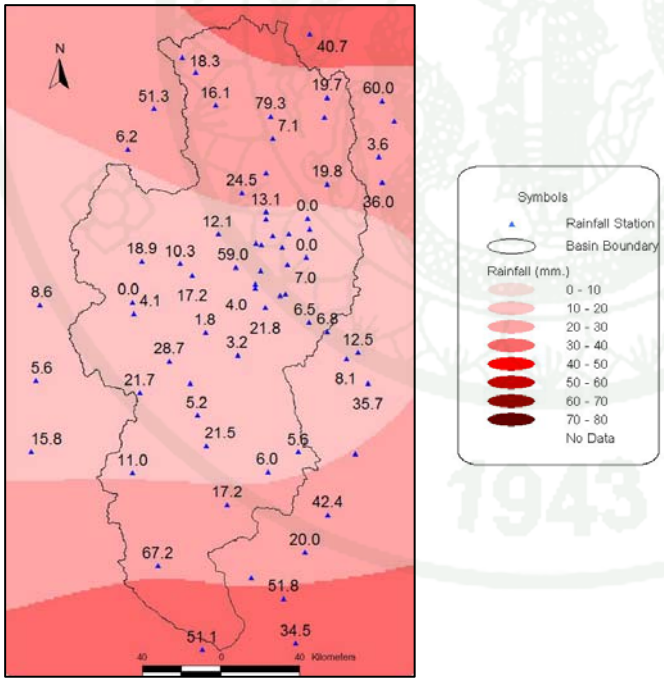

(b) Isohyetal technique

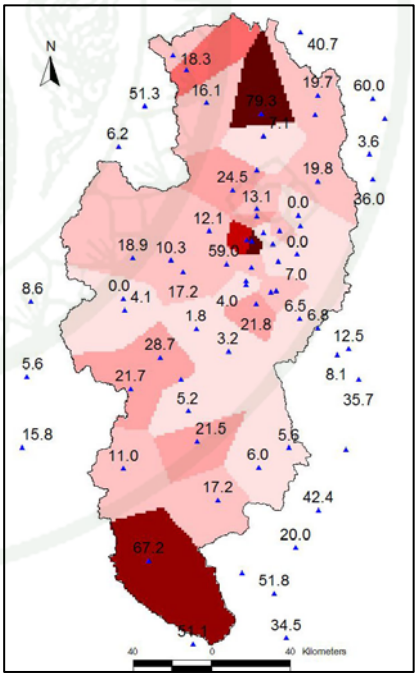

(c) Thiessen Polygon technique

Figure 35 Maps of daily areal rainfall depths in the UPRB on September 13, 2003 generated by three different techniques.

2. Selection of hydrologic and hydrodynamic public domain models

There were two main steps of model application taken to complete this section; Details of each step are shown in the following items.

2.1 Calibration and Verification of IHACRES model

The suitable model parameters at the stations P.20, P.76, and P.77 are presented in Table 28. By applying these parameters, the values of statistical indicators comparing the calculated and observed hydrographs for these runoff stations are presented in Table 29. The table shows that the r values are between 0.75 and 0.93 with the average of 0.85, the EI values are between 81% and 94% with the average of 88%, and RMSE are between 0.8 and 13.1 cms with the average of 7.0 cms. These values are within the acceptable range. These parameters at the stations P.20, P.77, and P.76 can therefore be applied to the ungauged catchments 1, 2, and 3, respectively. Figures 36 to 38 show the comparison between calculated and observed hydrographs at these 3 stations.

During the calibration and verification processes, The results revealed that the parameters in the non-linear module (c, τ_w and f) have significant direct effects on volume and peak of flow hydrograph. The parameters in the linear module (τ_s, τ_q and ν_s) affect the peak of the hydrograph, but not its volume. The parameter τ_q has a direct effect while τ_s and ν_s have indirect effects on peak flow.

Table 28 IHACRES model parameters for the stations P.20, P.76, and P.77.

Runoff Station	Area (km^2)	Non-linear Module			Linear Module		
		c	τ_w	f	τ_s	τ_q	v_s
P.20	1,355	0.012584	5	11	24.23	1.13	0.766
P.76	1,541	0.007422	37	16	63.10	3.05	0.540
P.77	547	0.001939	15	1	28.31	1.39	0.287

Table 29 Values of statistical indicators evaluated at 3 stations for 4 flood periods for IHACRES calibration and verification.

Flood Period	P.20			P.76			P.77		
	r	EI (%)	RMSE (cms)	r	EI (%)	RMSE (cms)	r	EI (%)	RMSE (cms)
2001	0.80	87	9.1	0.87	88	6.5	0.89	87	3.4
2002	0.78	90	7.9	0.91	92	13.1	0.83	82	4.9
2003	0.75	81	11.3	0.93	94	6.2	0.89	89	0.8
2004	0.83	91	9.7	0.80	90	9.9	0.90	88	1.5

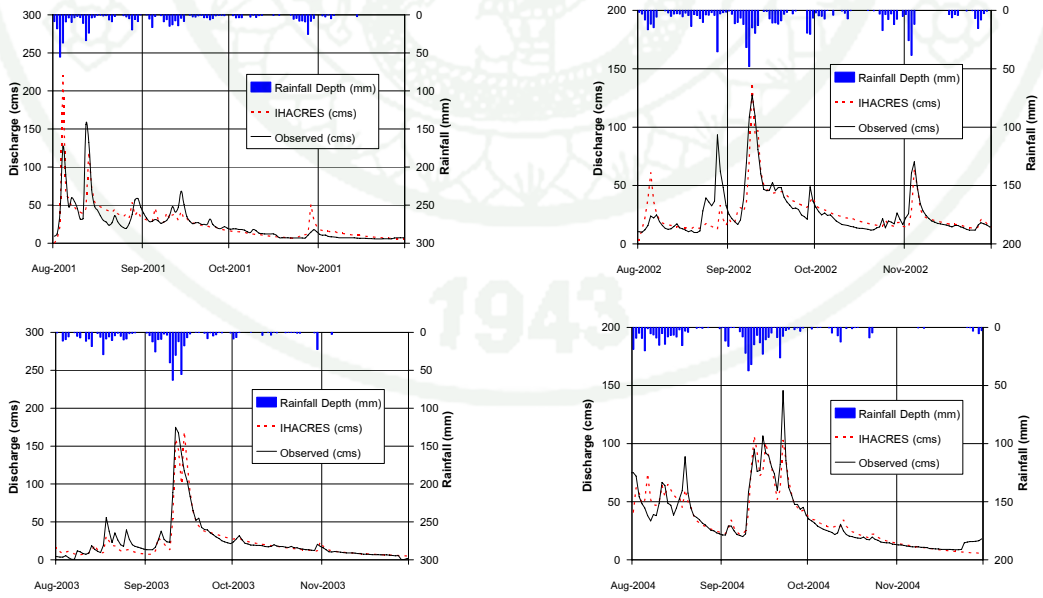

Figure 36 Comparison of calculated and observed flood hydrographs at P.20.

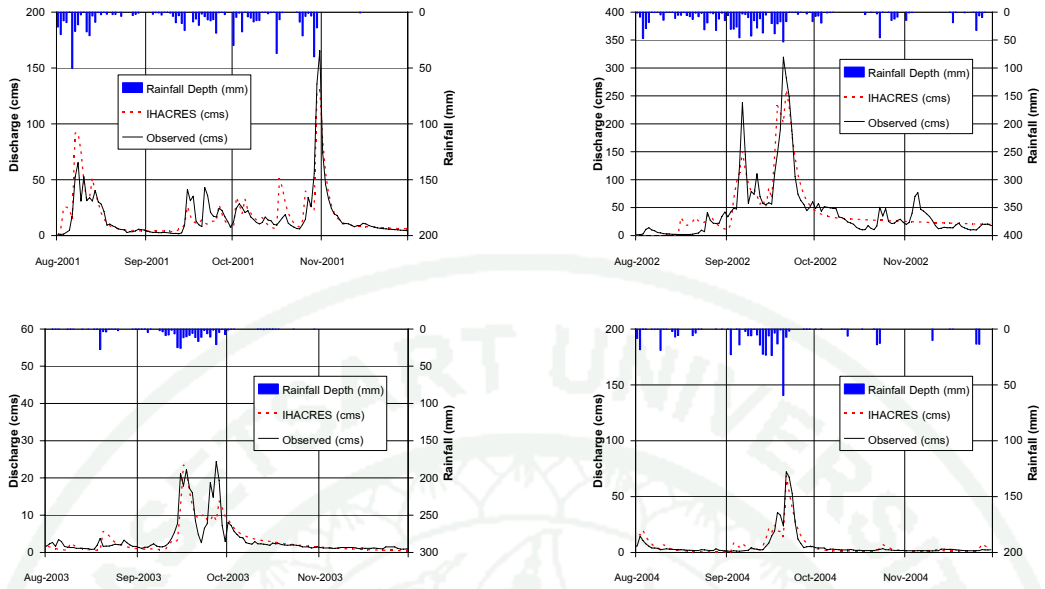

Figure 37 Comparison of calculated and observed flood hydrographs at P.76.

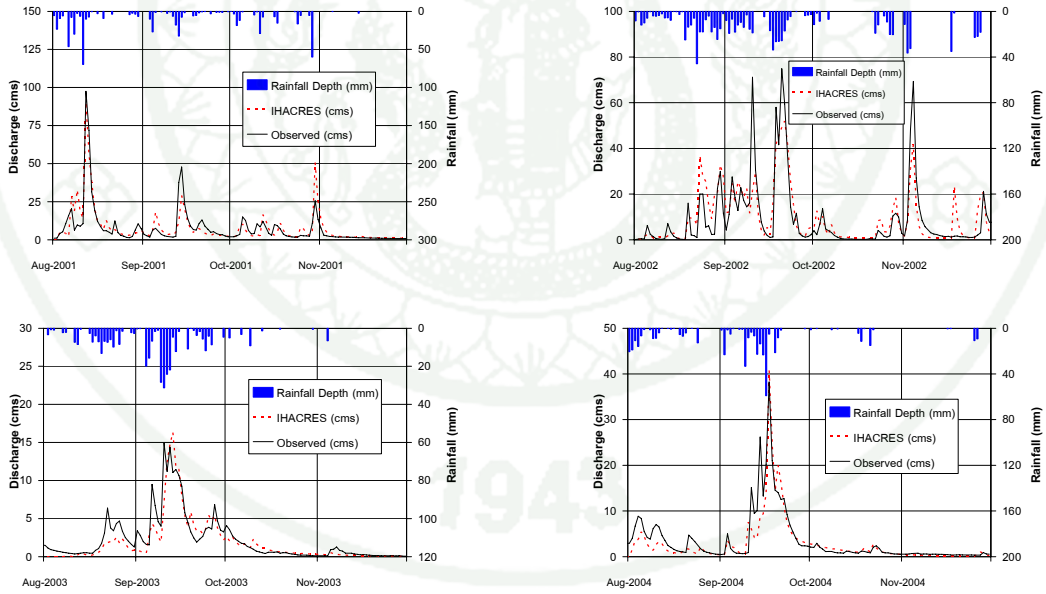

Figure 38 Comparison of calculated and observed flood hydrographs at P.77.

2.2 Calibration and Verification of FLDWAV model

The suitable Manning's n values for channel and floodplain flows of the Ping river are 0.035 and 0.070, respectively. Increased Manning's n values will result in reducing the flow magnitude and increasing the travel time. Using these values provided the best fit between observed and calculated flood hydrographs of all three flood events at the runoff stations P.67, P.1 and P.73 located along the Ping river from upstream to downstream. Table 30 presents the statistical values resulting from model calibration and verification of these flood events. The r values are between 0.91 and 0.99 with the average of 0.97, the EI values are between 97% and 99% with the average of 99%, and RMSE are between 4.0 and 33.8 cms with the average of 15.7 cms. These values are also within the acceptable range. The Manning's n values applied in the model are therefore suitable to be used for other application purposes. Figures 39 to 41 show the comparison between calculated and observed hydrographs at these three stations for each flood event.

Table 30 Statistical indicators evaluated for FLDWAV model performance.

Flood	**P.67**			**P.1**			**P.73**		
Period	**R**	**EI (%)**	**RMSE (cms)**	**r**	**EI (%)**	**RMSE (cms)**	**r**	**EI (%)**	**RMSE (cms)**
2001	0.97	99	6.9	0.97	99	9.7	0.93	99	33.8
2003	0.99	99	6.0	0.99	99	4.0	0.91	99	29.6
2004	0.97	99	8.1	0.97	96	24.2	0.98	99	17.9

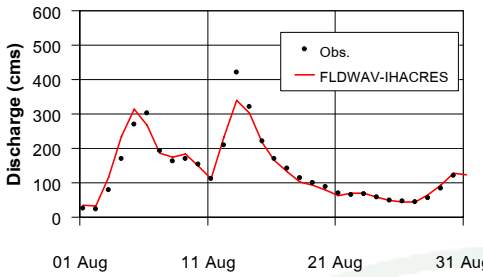

(a) Flood discharges at P.67

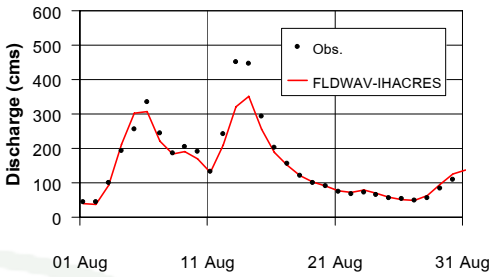

(b) Flood discharges at P.1

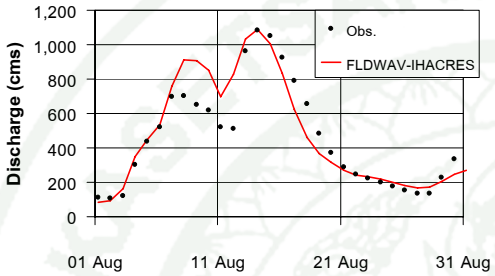

(c) Flood discharges at P.73

Figure 39 Comparison of calculated and observed flood hydrographs in 2001.

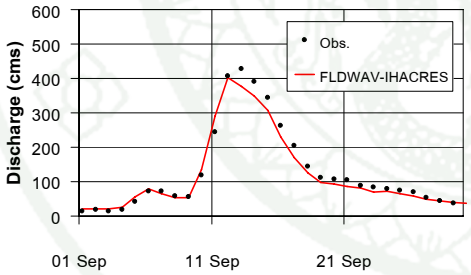

(a) Flood discharges at P.67

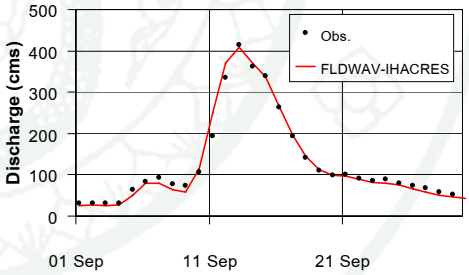

(b) Flood discharges at P.1

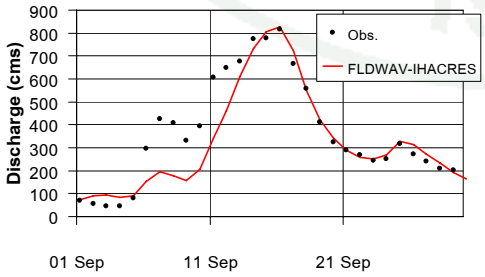

(c) Flood discharges at P.73

Figure 40 Comparison of calculated and observed flood hydrographs in 2003.

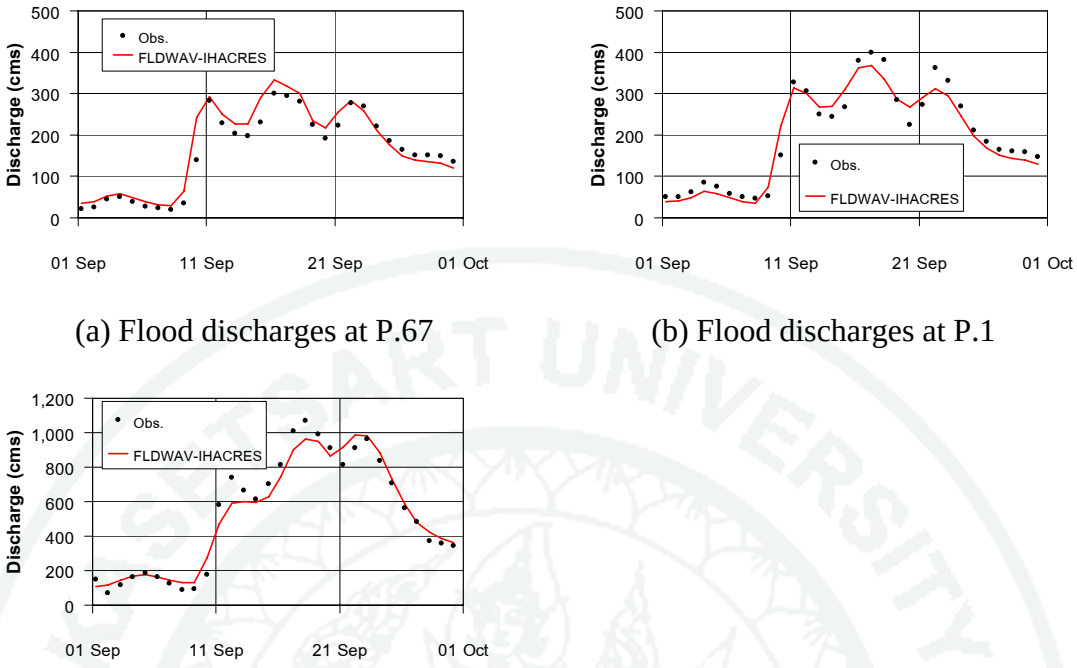

(a) Flood discharges at P.67 (b) Flood discharges at P.1

(c) Flood discharges at P.73

Figure 41 Comparison of calculated and observed flood hydrographs in 2004.

3. Examine relationships between model parameters and catchment attributes

3.1 Calibration of IHACRES model

A comparison between the outcomes of the calibration of discharge as derived from the calculation of IHACRES model during the years 1988-2005 and the actual observation is illustrated by the regression coefficient (r), Efficiency Index (EI), and Root Mean Square Error ($RMSE$) is shown in Figure 42. Examples of the model calibration results for two runoff stations are shown in Figures 43 and 44.

3.2 Sensitivity Analysis of IHACRES model

By varying values of each parameter individually while keeping other parameters constant for the catchment of P.4A station, sensitivity analysis was performed to see their effects on flood peaks and flood volumes of the hydrograph. The period of September, 1-30, 2003 were selected for the calibration of IHACRES. Over this period, best fit parameters as determined in the calibration phase were c=0.005579, τ_w=2, f=2, τ_s=12.361, τ_q=1.945, and V_s=0.081. The results associated with the sensitivity of flood peaks and flood volumes to change of six parameters: c, τ_w, f, τ_s, τ_q, and V_s are shown in Table 31 and Figure 45.

With regard to the sensitivity characteristics of parameters, the parameters in the non-linear module (c, τ_w and f) were found to have significant effects on volume and peak of flow hydrograph. The parameters in the linear module (τ_s, τ_q and v_s) also affect the peak, shape and volume of the hydrograph.

(a) Correlation coefficient (*r*)

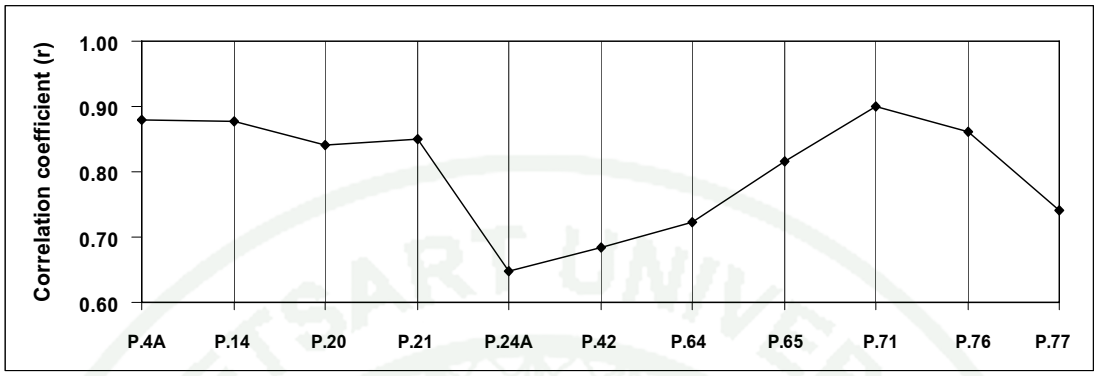

(b) Efficiency index (*EI*)

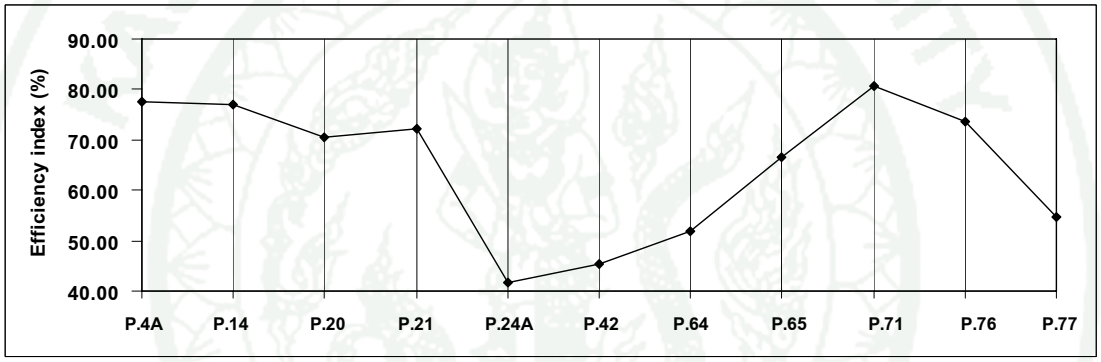

(c) Root mean square error (*RMSE*)

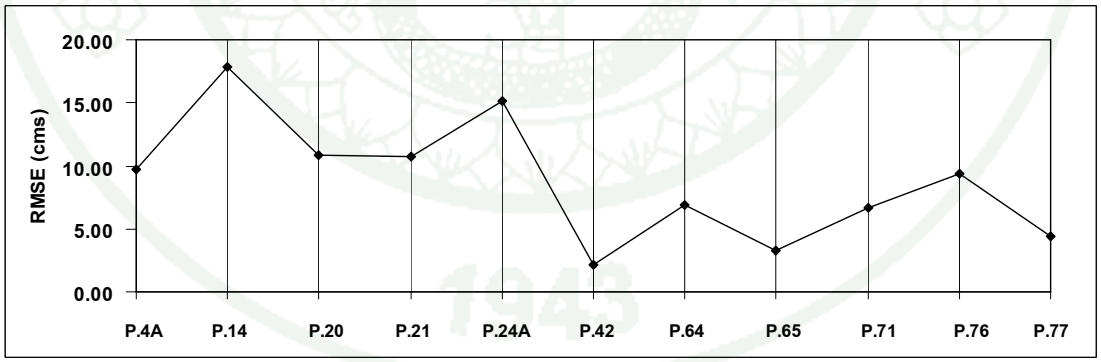

Figure 42 Statistical indicators evaluated the calibration result.

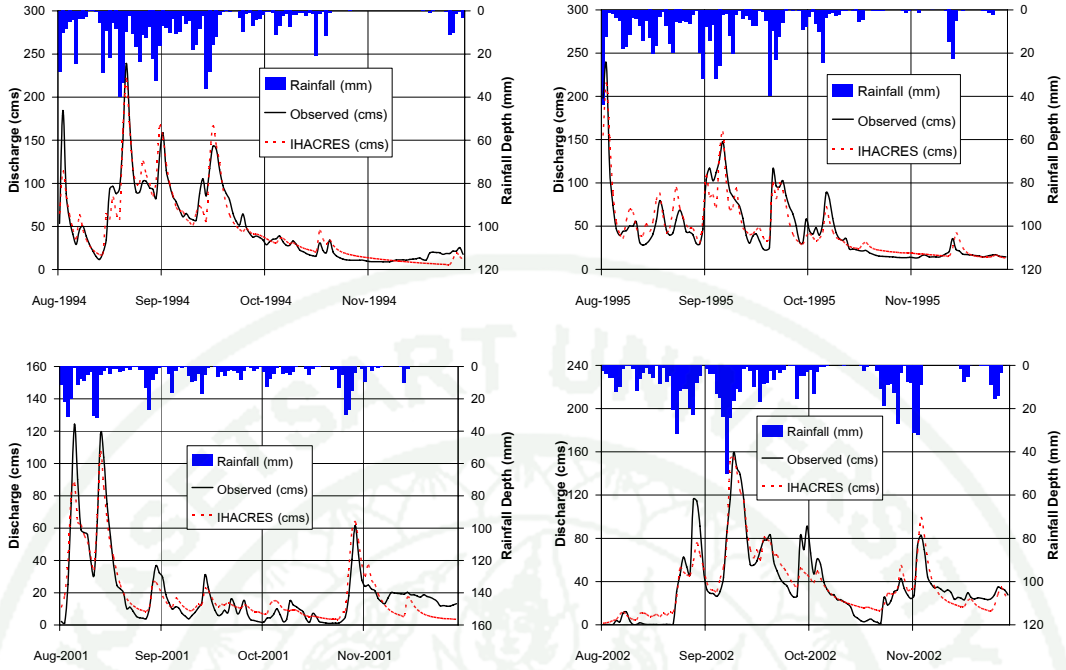

Figure 43 The model calibration results for the P.4A runoff station.

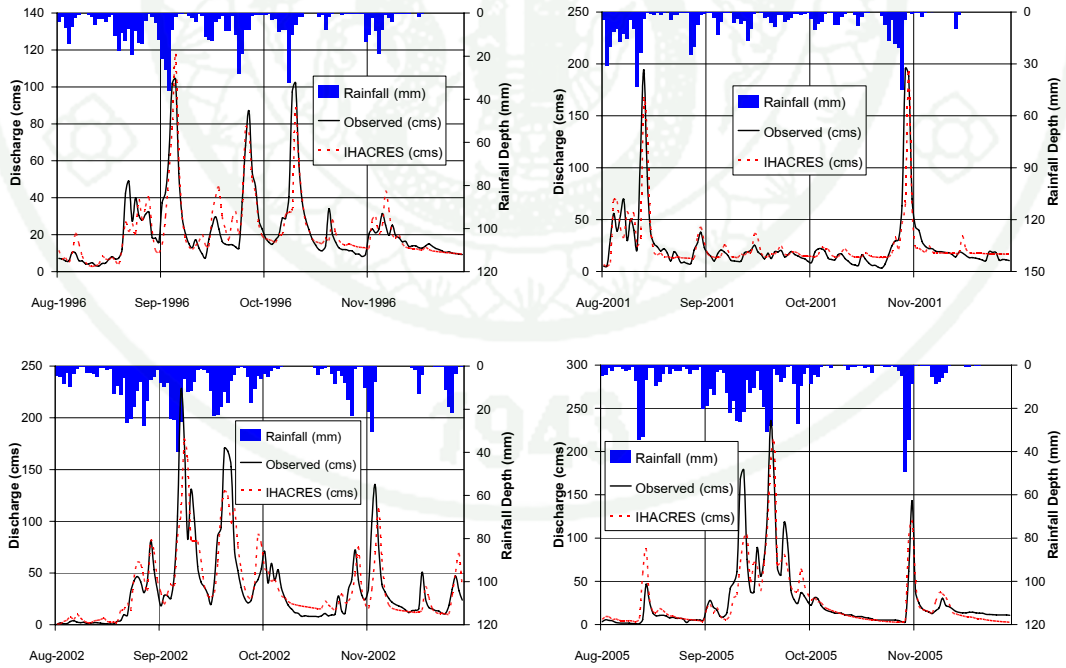

Figure 44 The model calibration results for the P.71 runoff station.

Table 31 Sensitivity results on IHACRES model parameters at P.4A station.

(a) Non-linear module

Change	C		Change	τ_w		Change	f	
Parameter	**Peak (%)**	**Volume (%)**	**Parameter**	**Peak (%)**	**Volume (%)**	**Parameter**	**Peak (%)**	**Volume (%)**
0.003	-46.2	-46.2	1	-42.6	-40.0	1	3.5	4.2
0.004	-28.3	-28.3	3	36.2	32.0	3	-3.6	-4.1
0.006	7.6	7.6	4	65.4	59.8	4	-7.4	-8.3
0.007	25.5	25.5	5	89.6	84.9	5	-11.3	-12.5
0.008	43.4	43.4	6	110.3	108.1	6	-15.4	-16.6
0.009	61.3	61.3	7	128.7	130.0	7	-19.4	-20.5
0.010	79.3	79.3	8	145.3	150.6	8	-23.6	-24.1
0.011	97.2	97.2	9	160.6	170.2	9	-27.7	-21.2

(b) Linear module

Change	τ_s		Change	τ_q		Change	V_s	
Parameter	**Peak (%)**	**Volume (%)**	**Parameter**	**Peak (%)**	**Volume (%)**	**Parameter**	**Peak (%)**	**Volume (%)**
2	116.4	21.7	0.5	39.8	0.3	0.02	3.8	1.2
5	57.7	18.3	1.0	17.3	0.2	0.04	2.6	0.8
10	11.7	6.0	1.5	5.8	0.2	0.10	-1.2	-0.4
20	-22.9	-16.5	3.0	-12.0	-0.6	0.20	-7.5	-2.4
35	-42.5	-36.6	5.0	-29.2	-2.9	0.40	-20.0	-6.4
50	-51.7	-48.1	7.0	-40.7	-6.8	0.60	-32.6	-10.5
100	-63.9	-65.2	10.0	-51.9	-13.5	0.80	-45.2	-14.5
200	-70.8	-75.7	15.0	-62.7	-24.0	0.95	-54.6	-17.5

(a) c parameter

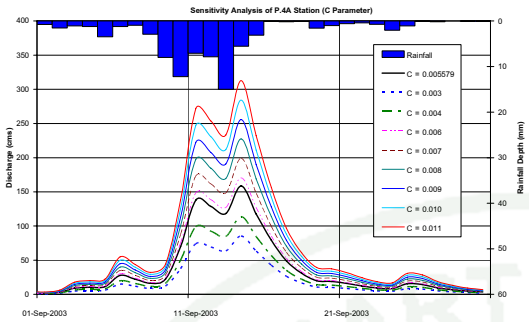

(b) τ_w parameter

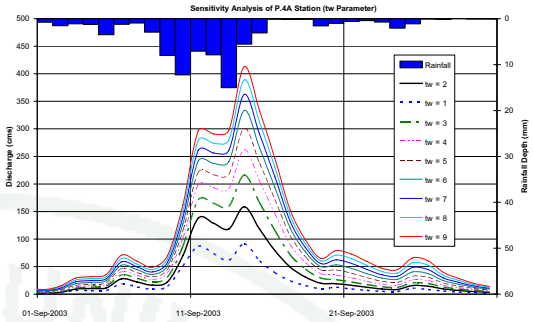

(c) f parameter

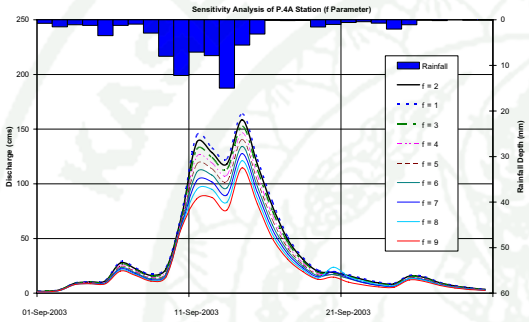

(d) τ_s parameter

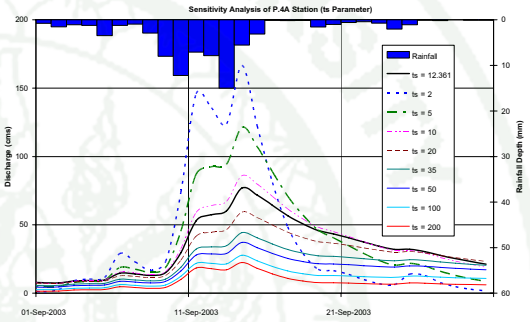

(e) τ_q parameter

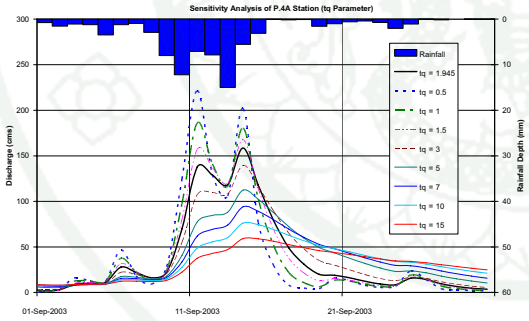

(f) V_s parameter

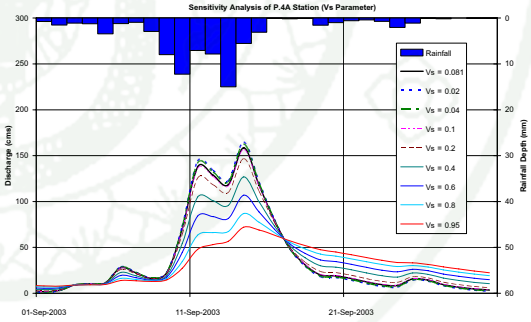

Figure 45 Sensitivity results on IHACRES model parameters at P.4A station.

3.3 Multiple Regressions between IHACRES parameters and Catchment Attributes

Multiple regression analysis was used to determine equations relating the six IHACRES model parameters to the catchment attributes. It was found that non-linear multiple regressions gave higher correlation coefficients than linear regression. Most regression relationships had satisfactory values of correlation coefficient, between 0.6 and 0.85 and are shown in Table 32. It shows that the *c* parameter, which is the mass balance, has significant relationships only with catchment size (A) and catchment shape (EG). While other five parameters show good correlations with all four catchment attributes.

Table 32 Equations derived from the relationship between model parameters and catchment attributes.

Relationship Equation	*r*
$1/c = 14.628 \times A^{0.236} EG^{-0.733}$	0.85
$f = 5.256 \times A^{1.515} D^{2.908} S^{0.684} EG^{3.52}$	0.64
$\tau_w = 5.047 \times A^{3.703} D^{7.133} S^{-0.503} EG^{6.458}$	0.66
$\tau_q = 0.078 \times A^{3.505} D^{6.518} S^{0.615} EG^{6.685}$	0.80
$\tau_s = 6.729 \times A^{0.208} D^{0.717} S^{0.813} EG^{0.173}$	0.78
$1/V_s = 2.043 \times A^{-0.207} D^{-0.667} S^{-0.242} EG^{-0.418}$	0.71

3.4 Validation of relationship between model parameters and catchment attributes

The relationship between the model parameters and catchment attributes were validated by applying them to estimate the model parameters for the nine calibration sub-catchments. Comparisons of parameter values derived from the regression relationships and from the normal calibration are shown in Figure 46. It appears that the estimation of parameters based on the proposed equations gave a satisfactory result for a certain degree or, in other words, produces the parameters of values quite close to those obtained from the normal calibration.

Next, verification of these equations was performed on sub-catchments; P.42 and P.77. Following this, the parameters obtained from the regression equations for P.42 and P.77 were then applied to IHACRES to estimate the discharge time series as if these two sub-catchments were ungauged. The calculated discharges were then compared with the earlier estimates based on the parameters derived from the normal calibration (gauged approach). Examples of the comparison between gauged and ungauged approaches at these two stations are presented in Figures 47 and 48. The outcomes of the values of r, EI, and $RMSE$ which compared these two types of hydrographs at these two stations presented in Table 33 are satisfactory.

Table 33 Statistic indicators for the validated stations.

Station	**Year**	r		EI **(%)**		$RMSE$ **(cms)**	
		Gauged	**Ungauged**	**Gauged**	**Ungauged**	**Gauged**	**Ungauged**
P.42	2000	0.65	0.63	57.7	52.3	1.8	2.3
	2001	0.83	0.82	68.2	66.6	2.9	3.0
P.77	2000	0.86	0.82	73.8	65.3	3.0	3.5
	2001	0.88	0.85	77.0	69.2	5.5	6.4

(a) parameter, c (b) parameter, τ_w

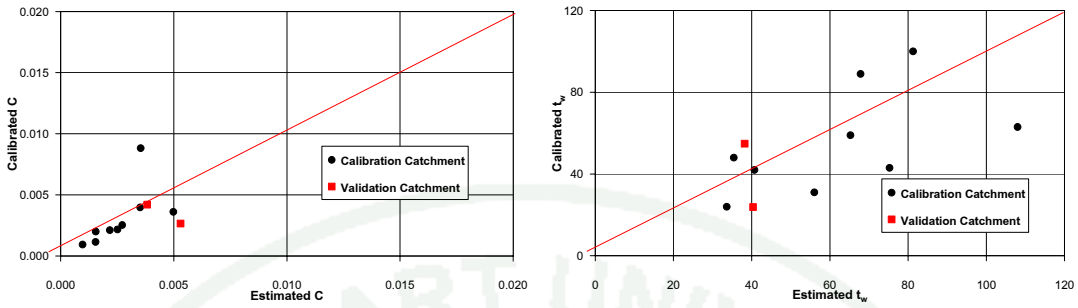

(c) parameter, f (d) parameter, τ_s

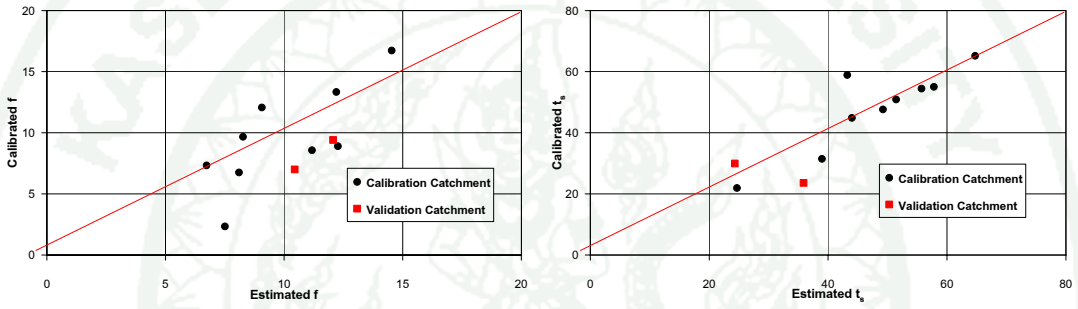

(e) parameter, τ_q (f) parameter, V_s

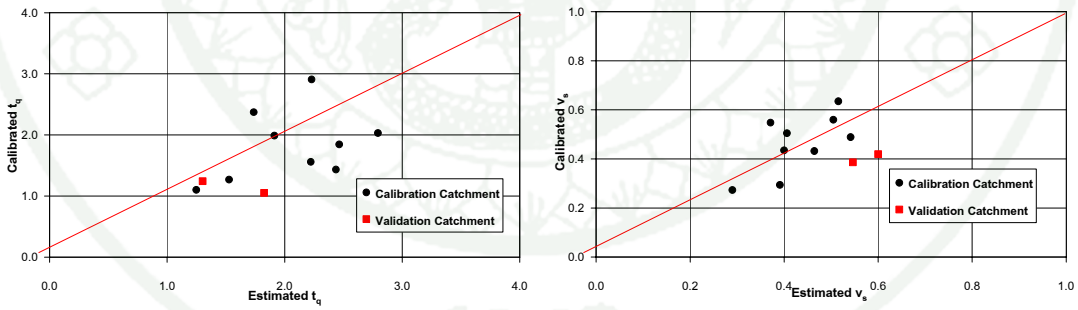

Figure 46 Scatter plot showing the relationship between model results where the model parameters were determined directly as best fit cases (calibrated) and were estimated by regression (estimated) cases for nine calibration and two validation catchments.

(a) Year 2000

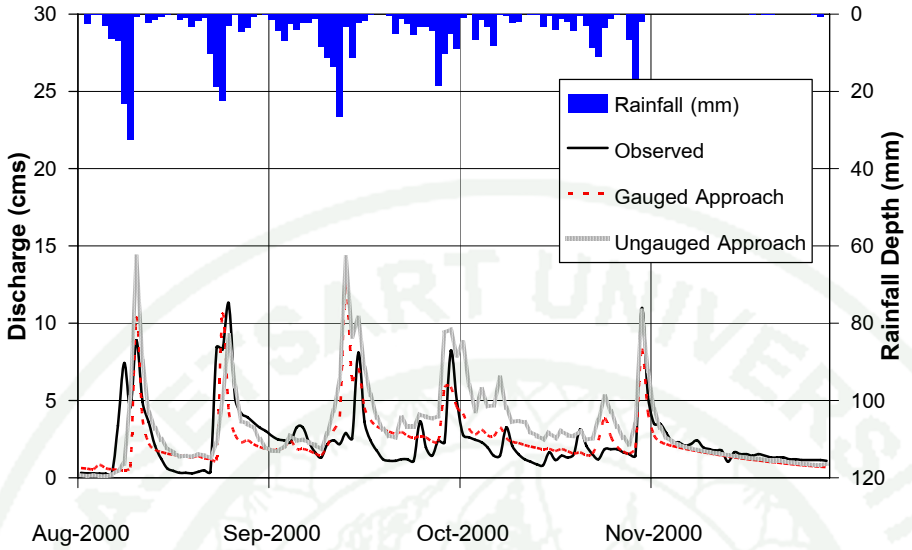

(b) Year 2001

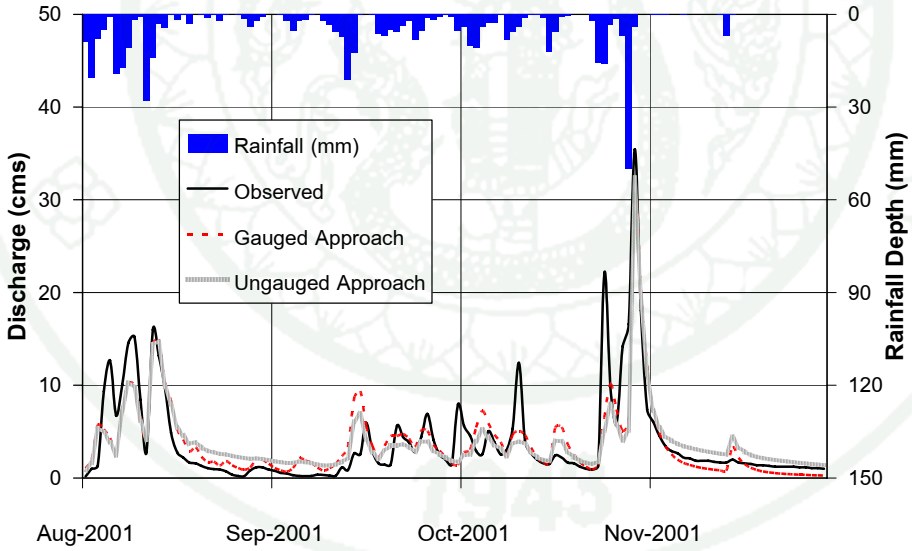

Figure 47 Observed and calculated flood hydrographs at P.42 station.

(a) Year 2000

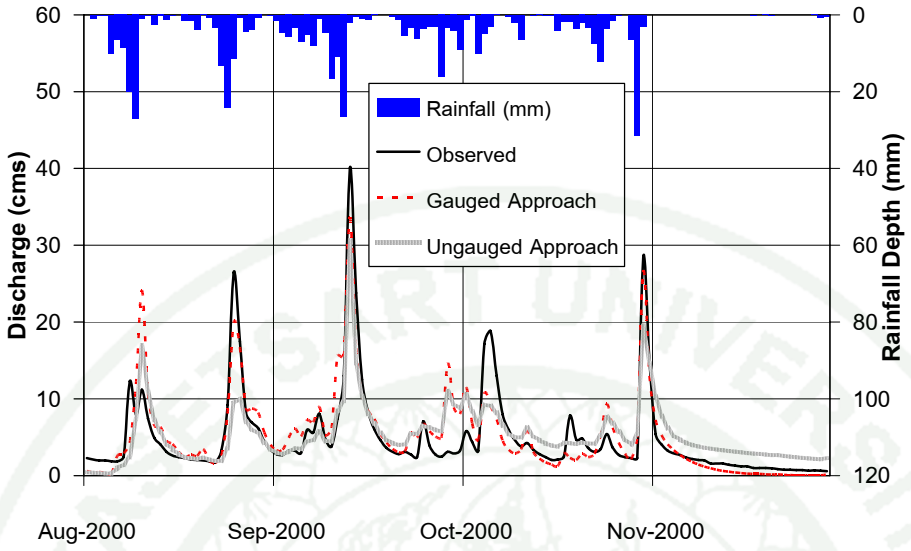

(b) Year 2001

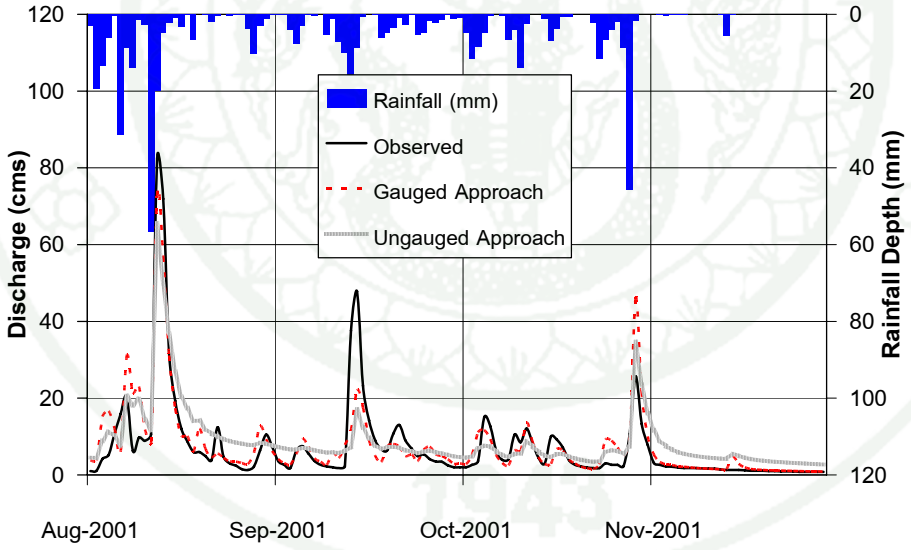

Figure 48 Observed and calculated flood hydrographs at P.77 station.

4. Investigation of Land Cover Changes in the UPRB

This section discusses the results of 1) the investigation of land cover changes in the UPRB using Geoinformatics, and 2) the examination of the relationships between land cover and flood characteristics.

4.1 Classification of Land Cover Changes in the UPRB

4.1.1 Land Cover Classification

According to land cover classification as shown in Table 34 and Figures 49 and 50, forest area covering the UPRB is declining every year, changing to other functions particularly agriculture to expansion of urbanized community. Note in particular that forest cover across the UPRB was generally decreasing from 1988 to 2005; forest cover decreased at a rate of 1.86% annually (471 km^2/year). Areas under agriculture, disturbed forest, urbanized, water bodies areas increased at annual rates of 0.60%, 0.84% 0.30% and 0.12% (151, 213, 77, and 30 km^2/year), respectively. In the year 2005, the most recent satellite images was available, the forest area in the UPRB remains at 75.5% (19,477 km^2) while the agriculture and urban areas account for 18.3% and 4.6% (4,634 and 1,188 km^2) respectively. General land cover trends for the UPRB are shown in Figures 51 and 52.

Table 34 Land cover classification results.

Land cover type	Percentage of each land cover type								
	1988	**1993**	**1994**	**1995**	**1996**	**2000**	**2001**	**2002**	**2005**
1. Forest	88.4	85.3	81.9	81.7	81.3	86.5	77.1	74.7	75.5
2. Disturbed forest	1.4	3.9	4.9	7.5	6.6	2.5	7.7	9.9	1.3
3. Agriculture	8.8	9.8	11.3	8.3	9.4	8.5	12.8	11.4	18.3
4. Urban	1.1	1.0	1.7	1.9	1.9	2.0	2.0	3.0	4.6
5. Water bodies	0.3	0.0	0.1	0.5	0.7	0.4	0.4	0.6	0.3
6. Other	0.0	0.0	0.1	0.1	0.1	0.1	0.0	0.4	0.0
Total	**100.0**	**100.0**	**100.0**	**100.0**	**100.0**	**100.0**	**100.0**	**100.0**	**100.0**

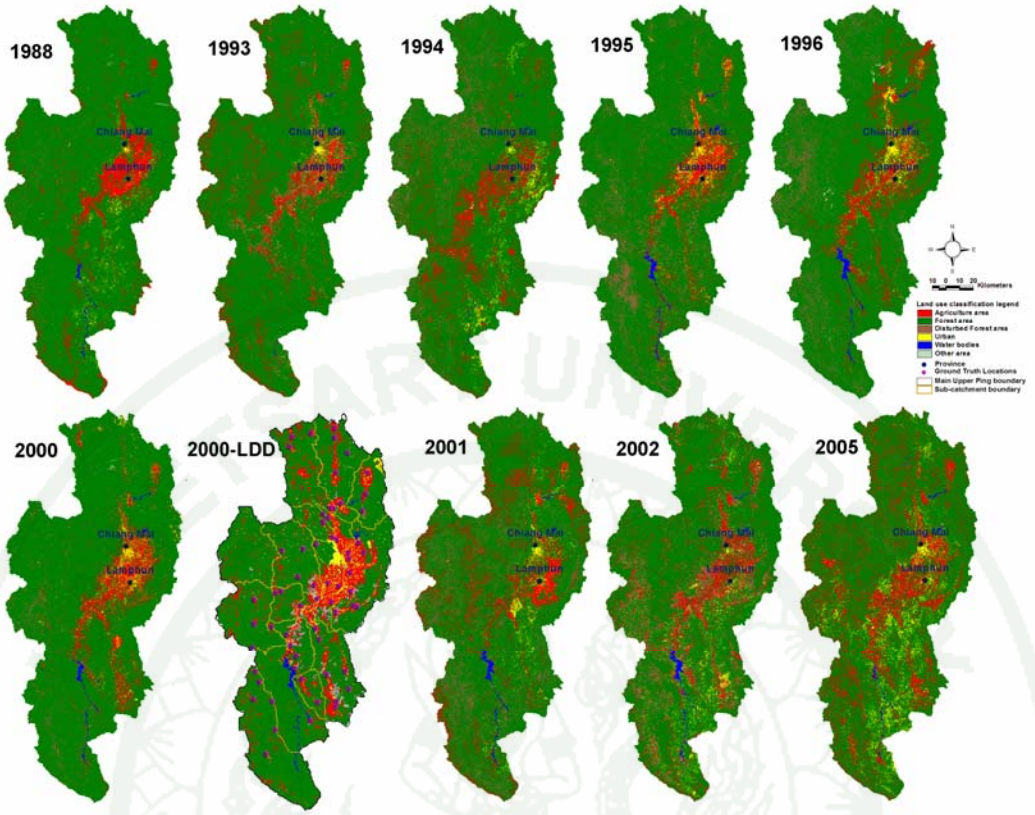

Figure 49 Annual land cover derived from LANDSAT-5TM.

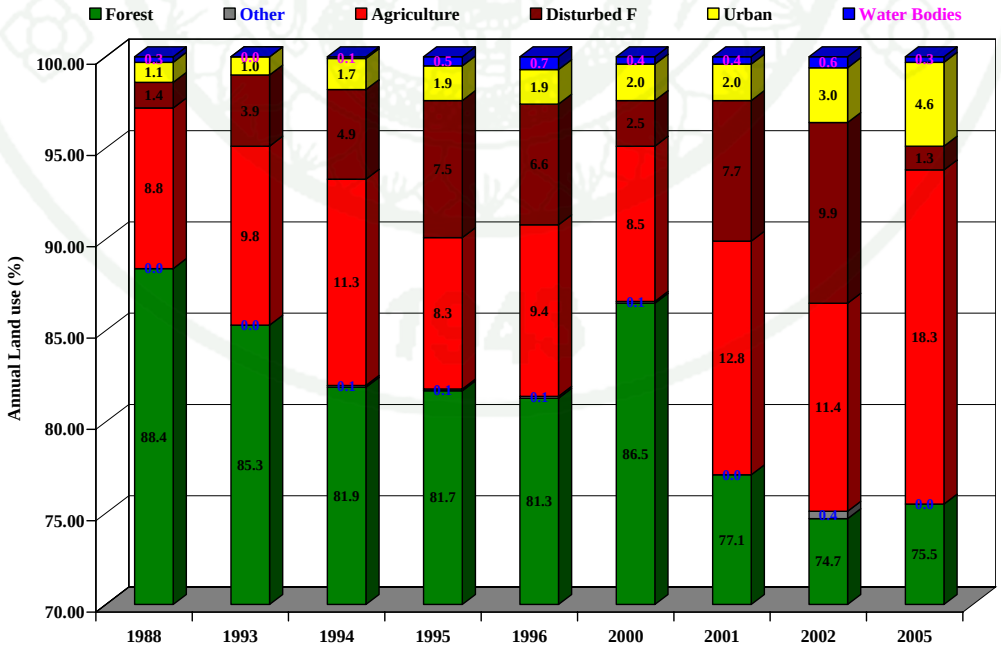

Figure 50 Histogram of annual land cover derived from LANDSAT-5TM.

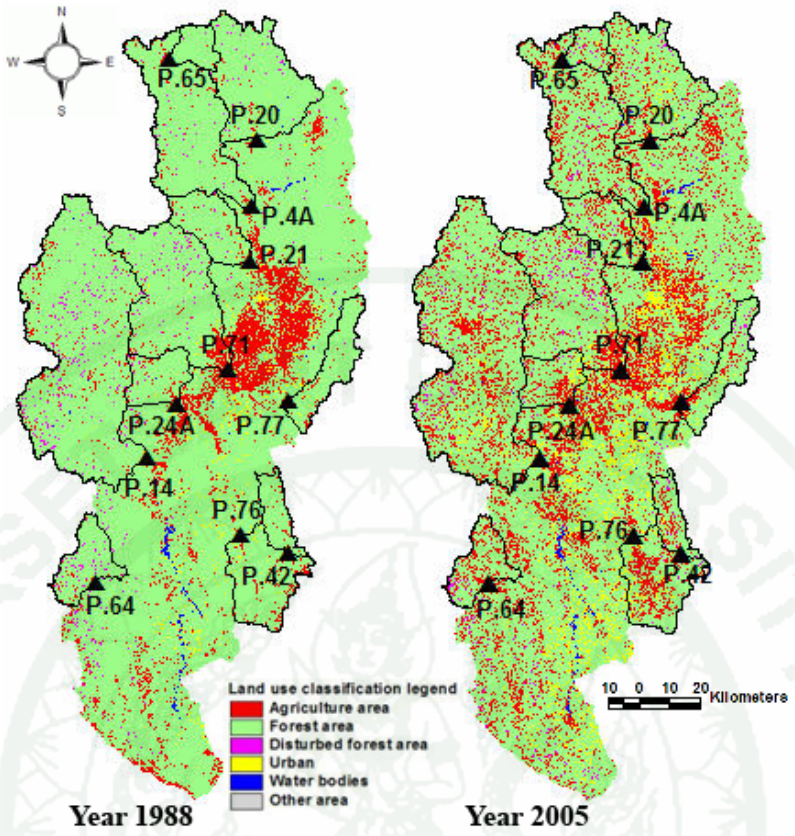

Figure 51 Annual land cover for the UPRB from LANDSAT-5TM, 1988 to 2005.

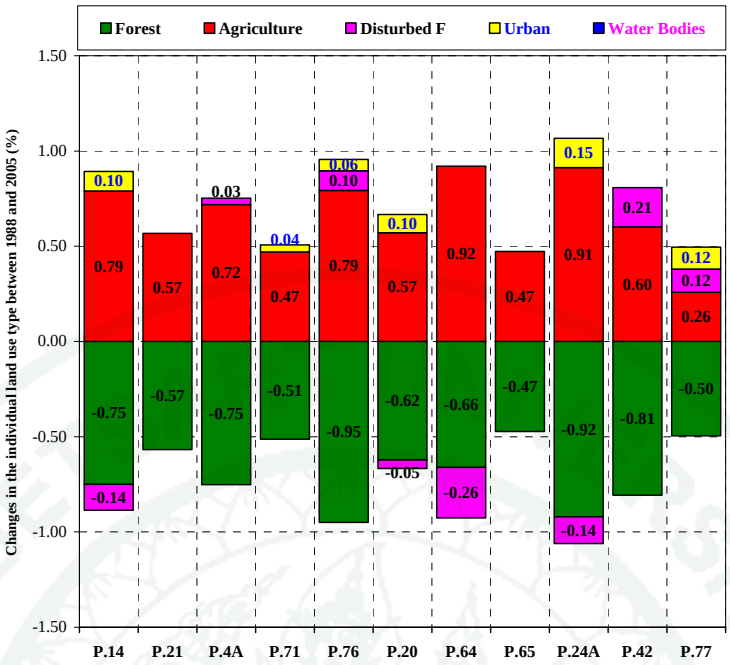

Figure 52 Changes in annual land cover for UPRB subcatchments, from 1988 to 2005.

Table 35 Accuracy assessment of land cover classification results.

Indicators	Annual land cover classification result								
	1988	**1993**	**1994**	**1995**	**1996**	**2000**	**2001**	**2002**	**2005**
1. Kappa	0.85	0.78	0.81	0.81	0.84	0.81	0.74	0.86	0.72
2. Overall Accuracy	83.56	76.40	87.44	82.37	83.28	81.78	74.29	85.50	73.07

Regarding to Table 35, Kappa and Overall Accuracy values obtained were acceptable, being above criterion of > 0.7 and 70 respectively. Despite the acceptable statistics, some problems still persist when there is an attempt to classify the land cover features particularly between agriculture and forest areas due to the diversity of plants. The problem of land cover classification arising in the year 1994 involves how to distinguish false colour composite images between forest and agriculture areas. There is a possibility that these two classes of land cover are represented by certain colours with almost identical tones. For example, hill evergreen forest and crop plants get the same orange-red tone with the only difference being that

the hill evergreen forest resides in the mountainous area at a moderate altitude of 1,500 m above sea level whereas crop plants usually grow on plain land. As a result, it appears the forest area has receded while the agriculture area increased.

There are some problems of classification here as urban area with shelters and the agriculture area with shelters built over plants have similar colour tone. An example of plants growing in shelters are the vegetations or the flowers of cold regions that have been planted on mountains, making it look like a roof of dwelling place usually found scattered in the UPRB such as Mae Chaem and Mae Rim Districts.

Overall water body areas have not significantly increased except in the years following 1994 that shows abrupt change as a result of the construction of Mae Kuang Dam (of capacity 263 million m^3) that started to store water in that year. In addition, water body areas in the year 2001 were larger than in 2005 due to a greater quantity of water storage at the Bhumibol Dam than usual.

4.1.2 Cross Validation

Cross Validation refers to an act of validating land cover classification data obtained from this study with the field observations of the LDD. In normal practice, LDD updates the observed information every five years on average. It is worth pointing that the data of the LDD is more accurate and specific than that derived in this thesis because of the method of visual image interpretation with ground truth used by the LDD. However for this study, RS data was required more frequent basis.

Cross validation of the derived classification result against that observed by LDD for the year 2000 is shown in Table 36 (LDD has up to now only released the observed data for year 2000). Observed data for the other years were not in digital form and so could not be used. Therefore only the classification results for the year 2000 have been used in this thesis. The satellite image shows that the two

largest classes of land cover, forest and agriculture covers, show similar false colour composite results because of almost identical tone which results in misclassification between derived and observed results. The same amount of misclassification occurred in the year 1994. Although the digital observed data is not available for this year, the misclassification can be seen in Figure 49. The percentage agricultural area is reduced from 11.3% to 8.5% however the Kappa estimator shows close values for these years, reflecting the misclassification between the agricultural and forest areas. On the same line, the amount of misclassification can be seen visibly from Figure 49 for the nine years and quantified from Tables 34 and 35.

Table 36 Comparison of land cover type derived from LDD and this study in year 2000.

Source	**Land cover type**				
	Agriculture	**Urban**	**Other**	**River**	**Forest**
Derived	11.0*	2.0	0.1	0.4	86.5
LDD	15.1	3.1	1.5	0.8	79.5

Remark *Agricultural area derived In this thesis is an area combination of agriculture and disturbed forest.

4.2 Correlations between Land Cover Change and Peak Flow Rates

Strong nonlinear correlations that were well fitted by power relationships were found between RRF and peak flow (~1 to 288 year ARI) for individual sub-catchments as shown in Table 37 with two examples plotted in Figure 53 for sub-catchments P.4A, and P.21. The coefficient of correlation (r) for these relationships varied between 0.74 and 0.93 and the average was around 0.83. The values of the power parameter b of each sub-catchment varied between 0.39 and 0.91, while the multiplier, parameter a significantly varied from 0.0009 to 0.0228. Peak flow of course scales strongly with the sub-catchment area so peak flows were divided by sub-catchment area as shown in Table 37; which narrowed the range of parameter a values to between 0.4219 and 2.0492 across the sub-catchments.

As expected, these RRF to peak flow relationships varied from year to year on each sub-catchment as shown in Table 38. For each year in which land cover data was available there was generally a distinct nonlinear correlation relationship between RRF and flood peak. The r coefficients varied from 0.80 to 0.96 and the average value was 0.88. Two typical examples of these correlations are plotted in Figure 54 for sub-catchments P.4A and P.21.

The peak flows for the 2, 5, 10 and 25 year ARI events on each catchment are shown in Table 39. Using the correlation relationships reported in Table 38, RRF values for these 2, 5, 10 and 25 year ARI events on each sub-catchment were determined and correlated against the proportion of forest area (F), disturbed forest area (DF), agricultural area (Ag) and the combined area of disturbed forest plus agriculture (DF+Ag) on each sub-catchment as shown in Table 40. Two examples of the correlations between RRF values and the proportion of forest area (F), as well as the combined area of disturbed forest plus agriculture (DF+Ag) are plotted for P.4A and P.21 in Figures 55 and 56, respectively. Note that urban areas and areas of water bodies on the sub-catchments changed by such small amounts that they were not considered for this study.

Table 37 Correlations of RRF and peak flood runoff for individual sub-catchments on the UPRB.

Runoff Station	No. of selected flood events	Range of peak (yr ARI)	RRF = a (Peak) ^{b}			RRF = a (Peak/Area) ^{b}		
			a	b	*r*	a	b	*r*
P.4A	30	~1-15	0.0228	0.39	0.74	0.4219	0.39	0.74
P.14	67	~1-10	0.0009	0.91	0.78	1.6256	0.91	0.78
P.20	56	~1-86	0.0036	0.87	0.86	1.8918	0.87	0.86
P.21	49	~1-15	0.0181	0.63	0.74	0.9126	0.63	0.74
P.24A	29	~1-6	0.0133	0.77	0.79	1.4903	0.77	0.79
P.42	28	~1-2	0.0177	0.83	0.91	2.0492	0.83	0.91
P.64	48	~1-4	0.0124	0.85	0.76	1.5606	0.81	0.76
P.65	43	~1-10	0.0110	0.90	0.93	1.5178	0.90	0.93
P.71	31	~1-16	0.0058	0.75	0.89	1.1247	0.71	0.89
P.76	20	~1-11	0.0057	0.71	0.89	1.4714	0.75	0.89
P.77	25	~1-4	0.0165	0.71	0.81	1.4105	0.72	0.81

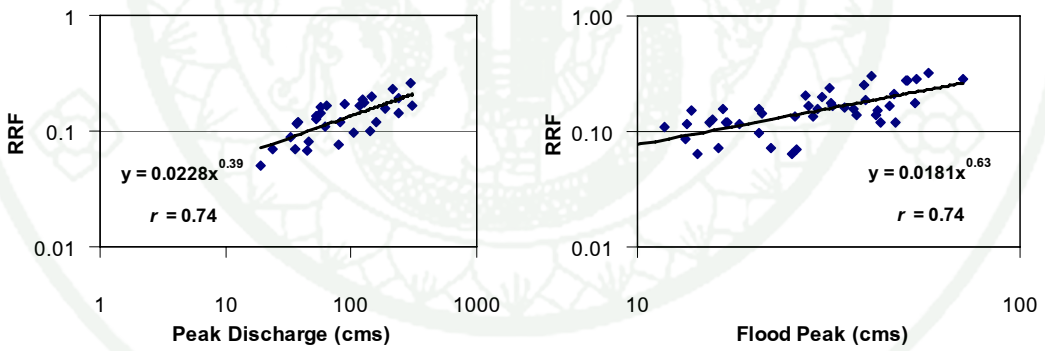

(a) P.4A (b) P.21

Figure 53 Typical relationships between the RRF and peak flood runoff for sub-catchments in the UPRB.

Table 38 Interannual Comparison of Runoff to Peak Flow Relationships for individual sub-catchments on the UPRB.

Runoff Station	Non-linear regression RRF = a (Peak) ^{b}				Non-linear regression RRF = a (Peak/Area) ^{b}			
	Range of a	Range of b	*r*		Range of a	Range of b	*r*	
			Range	Average			Range	Average
P.4A	0.0031-0.0252	0.40-0.72	0.69-0.89	0.80	0.51-1.33	0.40-0.72	0.69-0.89	0.80
P.14	0.0002-0.0068	0.51-1.23	0.72-0.97	0.89	0.44-4.91	0.51-1.23	0.72-0.97	0.89
P.20	0.0003-0.0287	0.50-1.39	0.82-0.99	0.89	1.09-7.70	0.50-1.39	0.82-0.99	0.89
P.21	0.0003-0.0531	0.29-1.81	0.73-0.98	0.86	0.33-22.21	0.29-1.81	0.73-0.98	0.86
P.24A	0.0001-0.0203	0.68-2.19	0.79-0.99	0.87	1.10-12.81	0.68-2.19	0.79-0.99	0.87
P.42	0.0005-0.0277	0.66-2.34	0.91-0.99	0.96	1.23-350.00	0.66-2.34	0.91-0.99	0.96
P.64	0.0001-0.0565	0.46-2.81	0.65-0.99	0.88	0.84-255.44	0.46-2.81	0.65-0.99	0.88
P.65	0.0019-0.0134	0.79-1.37	0.84-0.99	0.92	1.04-8.94	0.79-1.37	0.84-0.99	0.92
P.71	0.0045-0.0082	0.67-0.81	0.75-0.99	0.83	1.05-1.88	0.67-0.81	0.75-0.99	0.83
P.76	0.0011-0.0089	0.61-1.29	0.91-0.97	0.94	0.76-14.89	0.61-1.29	0.91-0.97	0.94
P.77	0.0086-0.0280	0.50-0.91	0.84-0.88	0.86	0.66-2.68	0.50-0.91	0.84-0.88	0.86
			Average	0.88			Average	0.88

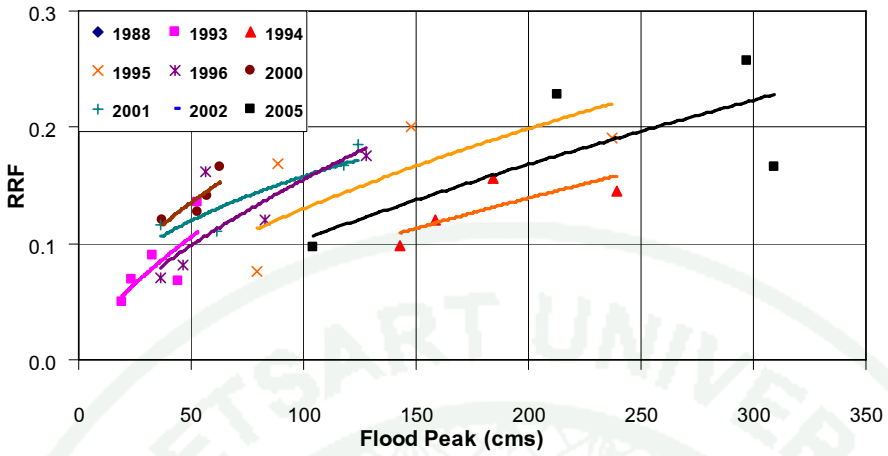

(a) P.4A

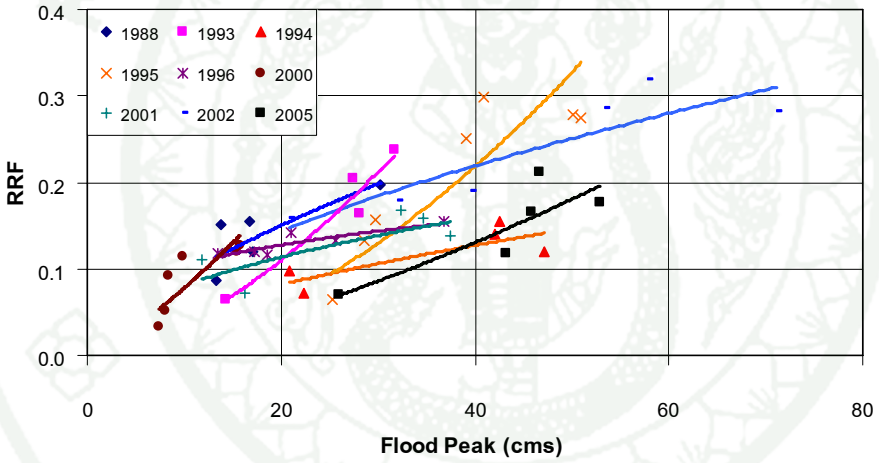

(b) P.21

Figure 54 Examples of interannual correlations of RRF to flood peak relationships for UPRB sub-catchments.

Table 39 Flood peak of ARI standardised events for each sub-catchment.

Runoff station	Flood peak (cms)			
	2 yr ARI	5 yr ARI	10 yr ARI	25 yr ARI
P.4A	129	208	277	385
P.14	271	418	528	681
P.20	118	205	272	366
P.21	44	59	68	78
P.24A	74	112	139	176
P.42	27	41	50	60
P.64	85	138	170	208
P.65	30	47	59	75
P.71	155	203	226	248
P.76	109	220	310	437
P.77	74	140	190	255

Table 40 Relationships between RRF and land cover for flood events in the UPRB.

Runoff station	Given flood peak (years)	Forest area RRF = a + b (F)			Disturbed forest area RRF = a + b (DF)			Agricultural area RRF = a + b (Ag)			DF+Ag area RRF = a + b (DF+Ag)		
		a	b	*r*	a	b	*r*	a	b	*r*	A	b	*r*
P.4A	2	-0.18	0.0042	0.62	0.17	-0.0006	0.09	0.19	-0.0034	0.50	0.23	-0.0041	0.59
	5	-0.26	0.0058	0.68	0.23	-0.0013	0.14	0.25	-0.0044	0.51	0.32	-0.0057	0.65
	10	-0.31	0.0069	0.69	0.28	-0.0018	0.17	0.30	-0.0050	0.50	0.38	-0.0069	0.67
	25	-0.38	0.0085	0.69	0.35	-0.0026	0.20	0.37	-0.0059	0.48	0.47	-0.0086	0.68
Average				**0.67**			**0.15**			**0.49**			**0.65**
P.14	2	-0.12	0.0033	0.69	0.16	-0.0011	0.22	0.17	-0.0021	0.44	0.20	-0.0032	0.66
	5	-0.36	0.0071	0.68	0.25	-0.0027	0.24	0.26	-0.0041	0.40	0.34	-0.0068	0.64
	10	-0.56	0.0102	0.67	0.32	-0.0041	0.26	0.33	-0.0057	0.37	0.45	-0.0099	0.63
	25	-0.88	0.0150	0.66	0.42	-0.0066	0.28	0.42	-0.0079	0.35	0.60	-0.0145	0.62
Average				**0.68**			**0.25**			**0.39**			**0.64**
P.20	2	-0.45	0.0080	0.67	0.29	-0.0110	0.41	0.31	-0.0085	0.53	0.40	-0.0135	0.81
	5	-1.25	0.0193	0.94	0.44	-0.0025	0.05	0.59	-0.0219	0.80	0.70	-0.0250	0.87
	10	-2.00	0.0295	0.91	0.55	0.0091	0.12	0.82	-0.0350	0.81	0.95	-0.0349	0.77
	25	-3.21	0.0458	0.84	0.68	0.0314	0.26	1.19	-0.0569	0.79	1.33	-0.0503	0.66
Average				**0.84**			**0.21**			**0.73**			**0.78**
P.21	2	-1.22	0.0173	0.80	0.34	-0.0199	0.48	0.42	-0.0181	0.64	0.47	-0.0163	0.75
	5	-1.97	0.0272	0.76	0.50	-0.0337	0.49	0.61	-0.0282	0.60	0.71	-0.0261	0.72
	10	-2.49	0.0339	0.74	0.61	-0.0433	0.49	0.74	-0.0351	0.58	0.86	-0.0328	0.71
	25	-2.81	0.0382	0.73	0.68	-0.0495	0.49	0.82	-0.0395	0.57	0.96	-0.0372	0.70
Average				**0.76**			**0.49**			**0.60**			**0.72**
P.24A	2	0.99	-0.0079	0.66	0.29	0.0188	0.81	0.28	0.0063	0.42	0.18	0.0104	0.81
	5	1.31	-0.0091	0.56	0.48	0.0255	0.80	0.51	0.0054	0.26	0.37	0.0117	0.67
	10	1.37	-0.0077	0.29	0.64	0.0280	0.54	0.74	0.0015	0.05	0.58	0.0097	0.34
	25	1.18	-0.0021	0.04	0.89	0.0282	0.29	1.13	-0.0082	0.13	0.97	0.0026	0.05
Average				**0.39**			**0.61**			**0.21**			**0.47**
P.42	2	0.77	-0.0057	0.43	0.25	0.0047	0.42	0.28	-0.0016	0.10	0.21	0.0056	0.41
	5	1.18	-0.0090	0.41	0.35	0.0069	0.37	0.40	-0.0013	0.05	0.28	0.0089	0.40
	10	1.42	-0.0110	0.40	0.41	0.0082	0.36	0.46	-0.0011	0.03	0.32	0.0109	0.40
	25	1.70	-0.0134	0.40	0.42	0.0098	0.34	0.53	-0.0009	0.02	0.37	0.0133	0.39
Average				**0.41**			**0.37**			**0.05**			**0.40**
P.64	2	-10.21	0.1420	0.64	1.93	-0.0583	0.30	1.92	-0.0938	0.36	3.99	-0.1420	0.64
	5	-43.46	0.5854	0.65	6.77	-0.2564	0.32	6.31	-0.3572	0.33	15.08	-0.5854	0.65
	10	-80.50	1.0772	0.65	12.01	-0.4787	0.33	10.99	-0.6448	0.33	27.22	-1.0772	0.65
	25	-142.57	1.9000	0.65	20.71	-0.8523	0.33	18.71	-1.1230	0.32	47.44	-1.9000	0.65
Average				**0.65**			**0.32**			**0.34**			**0.65**
P.65	2	0.65	0.0104	0.47	0.29	-0.0017	0.10	0.33	-0.0149	0.48	0.39	-0.0104	0.47
	5	-1.50	0.0220	0.49	0.50	-0.0050	0.14	0.56	-0.0267	0.43	0.70	-0.0220	0.49
	10	-2.23	0.0317	0.50	0.65	-0.0081	0.16	0.73	-0.0360	0.41	0.94	-0.0317	0.50
	25	-3.33	0.0461	0.50	0.87	-0.0127	0.18	0.96	-0.0491	0.38	1.28	-0.0461	0.50
Average				**0.49**			**0.15**			**0.42**			**0.49**
P.71	2	-0.12	0.0041	0.75	0.24	-0.0023	0.25	0.29	-0.0069	0.85	0.28	-0.0039	0.71
	5	-0.15	0.0051	0.72	0.29	-0.0030	0.25	0.36	-0.0084	0.80	0.35	-0.0047	0.68
	10	-0.17	0.0055	0.70	0.31	-0.0033	0.25	0.39	-0.0090	0.78	0.37	-0.0051	0.66
	25	-0.18	0.0060	0.69	0.34	-0.0035	0.25	0.41	-0.0097	0.76	0.40	-0.0055	0.65
Average				**0.72**			**0.25**			**0.80**			**0.67**
P.76	2	-0.89	0.0153	0.72	0.34	-0.0138	0.54	0.24	0.0008	0.04	0.86	-0.0288	0.75
	5	-2.38	0.0388	0.63	0.78	-0.0431	0.58	0.41	0.0074	0.12	2.09	-0.0742	0.66
	10	-3.77	0.0604	0.59	1.18	-0.0722	0.59	0.52	0.0150	0.15	3.20	-0.1161	0.63
	25	-5.96	0.0943	0.57	1.80	-0.1197	0.60	0.65	0.0283	0.17	4.93	-0.1817	0.61
Average				**0.63**			**0.58**			**0.12**			**0.66**
P.77	2	-0.38	0.0085	0.67	0.35	-0.0027	0.17	0.45	-0.0146	0.76	0.48	-0.0101	0.71
	5	-2.38	0.0388	0.63	0.78	-0.0431	0.58	0.41	0.0074	0.12	2.09	-0.0742	0.66
	10	-2.08	0.0323	0.82	0.76	-0.0171	0.34	1.02	-0.0447	0.75	1.19	-0.0376	0.85
	25	-3.12	0.0463	0.85	0.97	-0.0263	0.37	1.31	-0.0615	0.74	1.57	-0.0538	0.88
Average				**0.78**			**0.29**			**0.75**			**0.81**
Overall Average				**0.64**			**0.33**			**0.45**			**0.63**

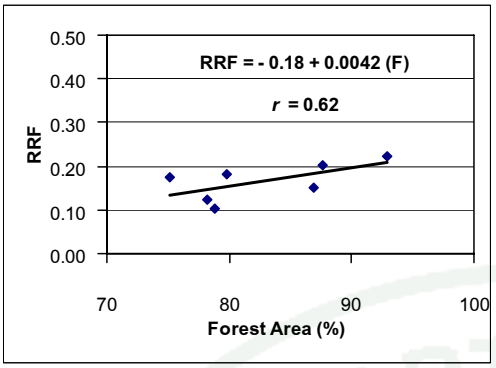

(a) 2 year return period

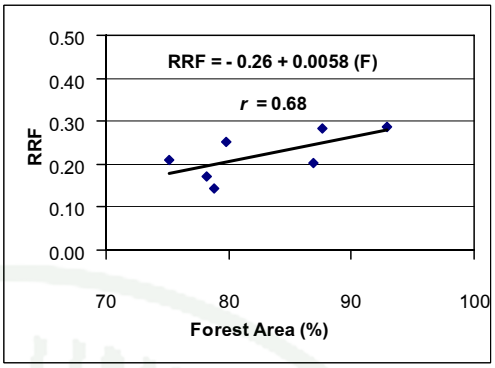

(b) 5 year return period

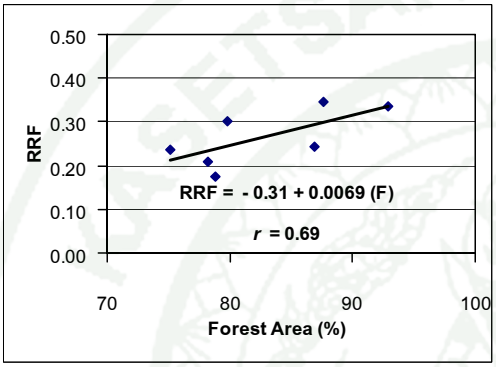

(c) 10 year return period

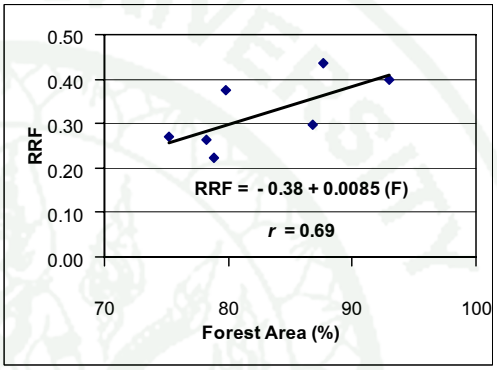

(d) 25 year return period

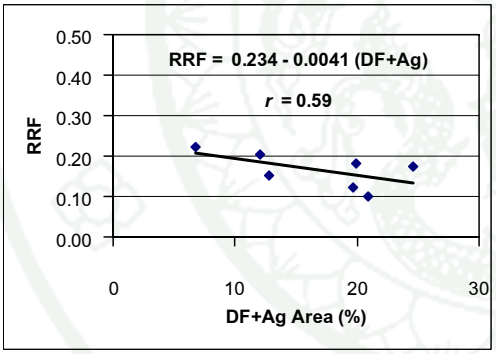

(a) 2 year return period

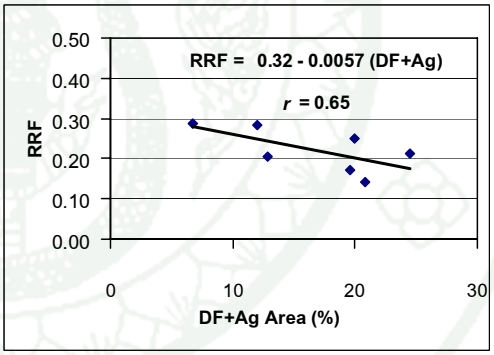

(b) 5 year return period

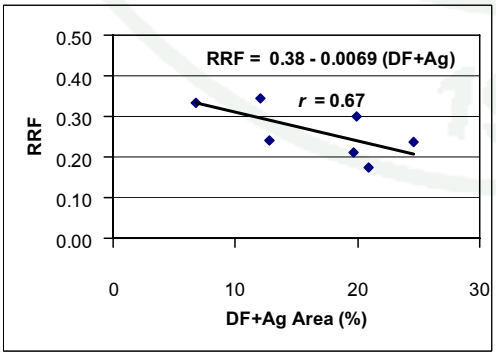

(c) 10 year return period

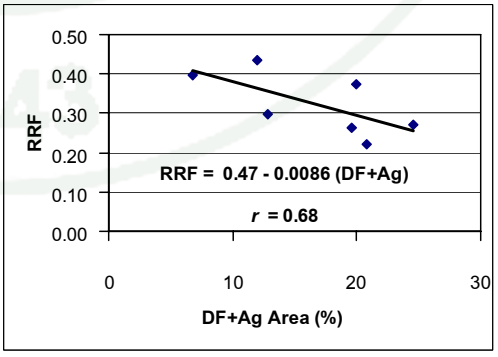

(d) 25 year return period

Figure 55 Relationships between RRF and land cover for flood events for P.4A catchment.

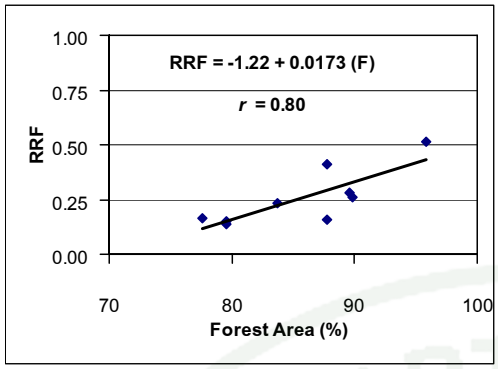

(a) 2 year return period

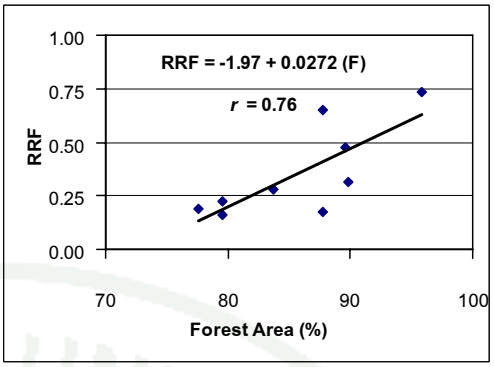

(b) 5 year return period

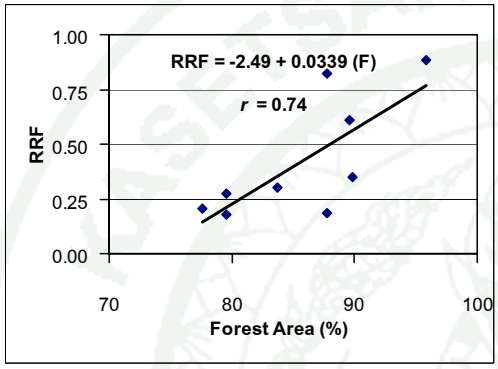

(c) 10 year return period

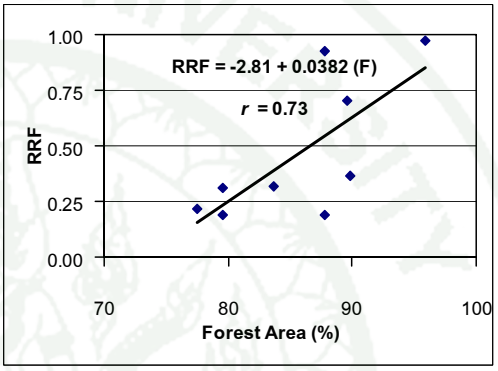

(d) 25 year return period

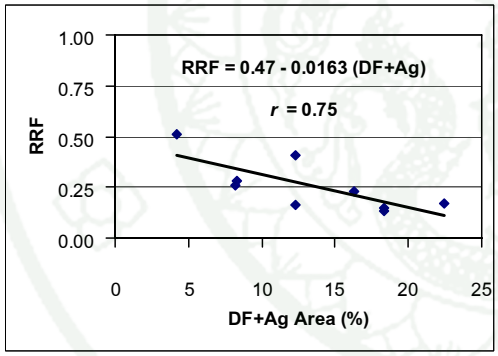

(a) 2 year return period

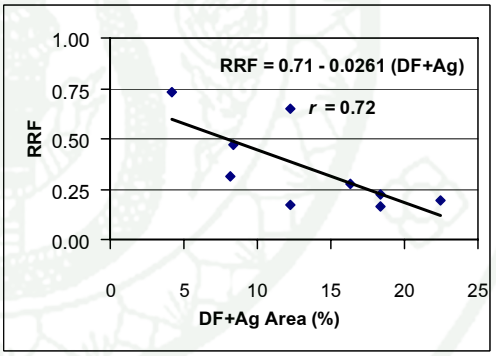

(b) 5 year return period

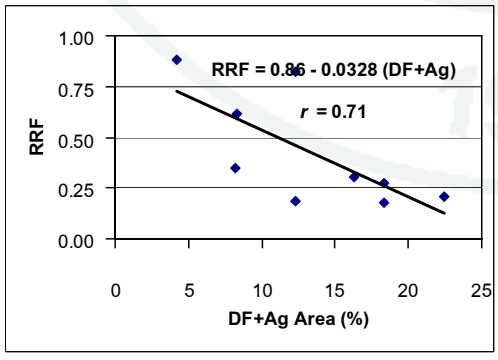

(c) 10 year return period

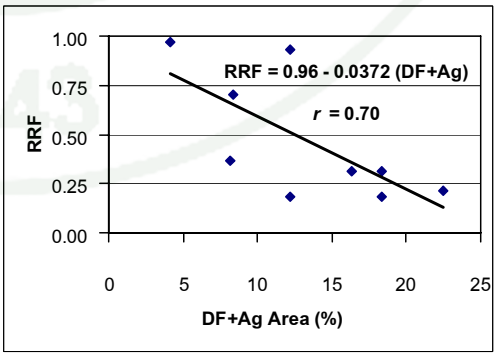

(d) 25 year return period

Figure 56 Relationships between RRF and land cover for flood events of P.21 catchment.

Table 40 shows that good linear correlation relationships were generally obtained between RRF and land cover. The relationships between RRF and forest area almost universally have a positive slope (multiplier "*b*" values were positive) for all of the sub-catchments except P.24A and P.42 (nine out of eleven sub-catchments). A positive slope on these correlations means that the RRF increases with increasing forest proportion for a particular peak flow event on each sub-catchment. The *b* values also tended to increase with increasing return period of flood peaks for those ten sub-catchments. The average r coefficient was around 0.64. Even for runoff stations with low r; all stations still show a positive slope, except P.24A and P.42. Evidently a higher proportion of forest on a catchment area means that a higher proportion of rainfall is converted to runoff for a flood event with a particular peak discharge.

Table 40 also shows that the relationships between RRF and the proportion of disturbed forest on the sub-catchment have a negative slope (*b* values were negative) for most of the sub-catchments. A similar result was found when RRF values were correlated against the proportion of agricultural areas on the sub-catchments. The average r coefficients for both cases were around 0.33 and 0.45, respectively, which were quite low but they still showed the same negative trend. The relationships between RRF and the combined area of disturbed forest plus agriculture were calculated. As expected, the relationships between the RRF values and agriculture plus disturbed forest showed a negative slope (*b* values were negative) for most of the catchments except P.24A and P.42. The average r coefficients for these relationships increased compared to individual case with the average value of around 0.63. The *b* values also tend to increase with increasing return period of flood peaks for those sub-catchments. So that when peak flow is kept constant, but as land cover changes, RRF decreases with increasing agricultural plus disturbed forest proportion on each sub-catchment. The more agricultural plus disturbed forest proportion will bring less runoff percentage over the same rainfall depth (lower RRF) at a particular flood peak flow.

It should be noted that in this section flood events only were investigated. Under such flood events, we expect that soil and vegetation would be saturated across all land cover types. However, the forest areas typically have the highest degree of vegetation and so are able to hold more moisture than agricultural disturbed forest areas. It appears that less rainfall loss rate occurs for flood events in areas with a high proportion of forest cover, causing flood volumes to be larger for the same flood peak on sub-catchments with a high proportion of forest area and the opposite trend presented in the agriculture and disturbed forest areas.

However, the result in this section does not conclude that increasing forest area would bring more runoff for the catchment for general rainfall events. Of course as forest cover increases on catchments, more rainfall will be lost to infiltration and evapotranspiration on an annual basis. However, at the commencement of a flood event, soil moisture and vegetation will be saturated, so forest areas could retain moisture from the early part of the storm better than agricultural and disturbed forest areas. As such, it is possible that a relatively higher proportion of rainfall is transformed from rainfall to runoff compared to the peak flow in highly forested catchments for flood events. More flood volume can be expected during these circumstances over the forest area. Results gained from the next section would be able to prove this assumption.

4.3 Correlations between RRF and Land cover for Flow Events

Moderately strong linear correlations were found between RRF and forest area (F) for individual sub-catchments under flow conditions as shown in Table 41. The coefficient of correlation (r) varies between 0.42 and 0.57 across the sub-catchments with an average of around 0.51. The values of parameter b of each sub-catchment vary between -0.0126 and -0.0014, while parameter a significantly vary between 0.160 and 1.303.

Similarly good linear correlations were found between RRF and disturbed forest plus agriculture area (DF+Ag), the r coefficient varies between 0.26 and 0.59

with an average of around 0.50. However, as expected, the values of the parameters were the opposite with the value for parameter *b* on each sub-catchment varying between 0.0016 and 0.0127, while parameter *a* significantly varied between -0.003 and 0.232. Two examples plotted are shown in Figure 57.

The result for all stations for the flow events is opposite that shown in the results in previous section which considered only flood events. It appears as if that the catchment is unsaturated at low flows, so losses from smaller rainfall events are relatively high. Of course, there would be many factors on the catchment contributing to this effect such as infiltration and evapotranspiration processes, which would significantly affect to the flood behaviours. However, when the catchment becomes saturated under flood events, flood behaviours in particularly runoff volume is found to increase when the forest area increasing.

These results are consistent with studies such as Stekauerova *et al.* (2006) who found that moisture content of soils is much greater in forest areas than in agricultural areas in the Bodiky and Bac regions in Slovakia. Likewise the expect above ground stores of water at and above ground level to be much higher in forest areas due to the much large amounts of vegetation and detritus present in these areas.

Table 41 Correlations of RRF and land covers for flow events for individual sub-catchments on the UPRB.

Runoff Station	**RRF = a + b (F)**			**RRF = a + b (DF+Ag)**		
	a	**b**	*r*	**a**	**b**	*r*
P.4A	0.366	-0.0034	0.48	0.034	0.0030	0.43
P.14	0.160	-0.0014	0.49	0.017	0.0016	0.52
P.20	0.579	-0.0057	0.53	-0.003	0.0079	0.59
P.21	0.344	-0.0026	0.56	0.082	0.0032	0.58
P.24A	0.300	-0.0023	0.54	0.077	0.0024	0.51
P.42	0.191	-0.0017	0.42	0.013	0.0018	0.42
P.64	0.623	-0.0038	0.57	0.232	0.0039	0.57
P.65	1.303	-0.0126	0.54	0.035	0.0127	0.54
P.71	0.198	-0.0018	0.56	0.016	0.0017	0.56
P.76	0.234	-0.0017	0.43	0.070	0.0018	0.26
P.77	0.325	-0.0027	0.47	0.050	0.0031	0.47
Average			**0.51**			**0.50**

a) P.4A

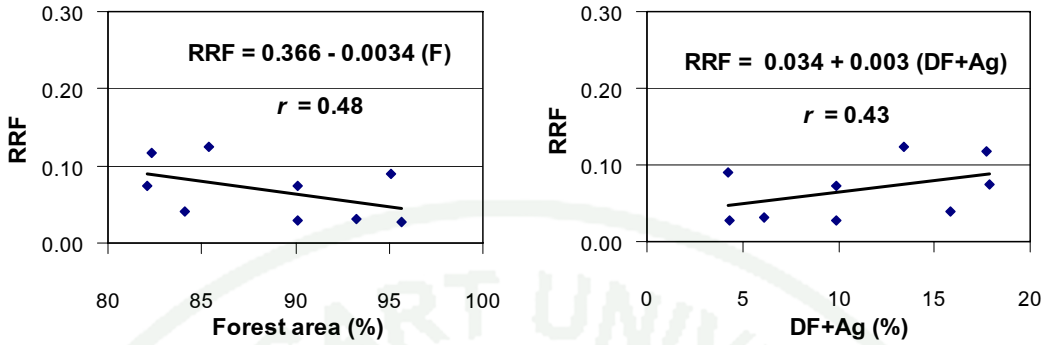

b) P.21

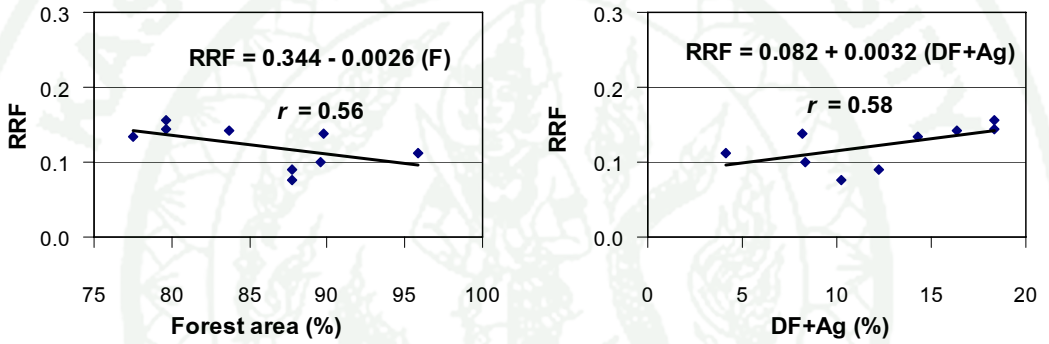

Figure 57 Typical relationships between RRF and land cover for flow events of P.4A and P.21 sub-catchments.

5. Effects of Land Cover Changes on Flooding

The results of the effects of land cover changes on flooding are discussed as follows.

5.1 Impact of deforestation and aforestation on flood hydrographs

Two scenarios of deforestation in 2005 and 2010 and one scenario of aforestation in 2005 were applied on selected flood event in 2001. Result of flood hydrographs at P.1 station in 2005 and 2010 calculated using FLDWAV based on three scenarios compared to flood hydrograph calculated based on forest cover in 2001 (baseline event) are presented in Figure 58. Table 42 shows the comparisons between flood peak and flood volume under each scenario and that of the baseline event in 2001.

Table 42 shows that flood peak and flood volume at all four stations along the main Ping river under the scenario 1 (in which flood event in 2001 was rerun using historical forest percentage in 2005) reduced at the same average rate of 4.9% compared to that of the baseline flood event in 2001. Percentage of flood peak reduction reduced from the most upstream at P.75 at the rate of 6.7% to the most downstream at P.73 at the rate of 1.7%. It was also the same pattern for the percentage of flood volume which reduced from the most upstream at P.75 at the rate of 6.1% to the most downstream at P.73 at the rate of 2.1%.

Similar results as the scenario 1 also presented in the scenario 2 in which the flood event in 2001 was rerun using hypothetical forest percentage in 2010 when the forest percentage reduced from 2005 at the same rate as historical percent reduction between 2000 and 2005. To be expected, flood peak and flood volume at all four stations along the main Ping river under the scenario 2 reduced at higher average rates of 9.8% and 9.7% compared to that of the baseline flood event in 2001, respectively. Percentage of flood peak and flood volume reduction also reduced from the most upstream at P.75 to the most downstream at P.73.

The results of the scenario 3, in which the selected flood event was rerun using hypothetical forest percentage in 2005 when the forest percentage increased at the same rate as it reduced between 2000 and 2005, came opposite those the scenarios one and two. Flood peak and flood volume at all four stations under the scenario 3 increased at the average rates of 4.9% and 4.8% compared to that of the baseline flood event in 2001, respectively. Percentage of flood peak increment also decreased from the most upstream at P.75 at the rate of 7.1% to the most downstream at P.73 at the rate of 1.4%. It was also the same way for the percentage of flood volume which reduced from the most upstream at P.75 at the rate of 6.4% to the most downstream at P.73 at the rate of 2.0%.

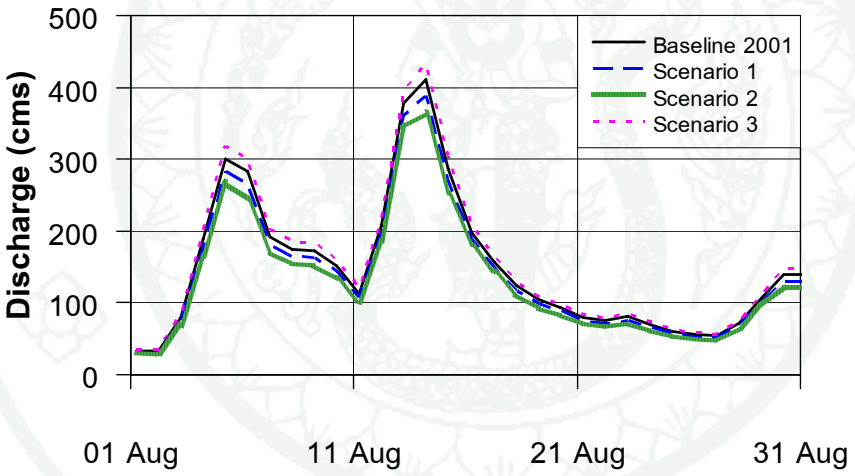

Figure 58 Flood hydrographs at P.1 based on three scenarios compared to that of the baseline event in 2001.

Table 42 Results of flood peak and flood volume under each scenario compared to that of the historical flood event in 2001.

Station	Baseline flood event in 2001	Scenario 1		Scenario 2		Scenario 3	
		Value	(%)	Value	(%)	Value	(%)
1. Flood peak (cms)							
P.75	203	189	-6.7	175	-13.8	217	+7.1
P.67	392	370	-5.6	348	-11.1	413	+5.4
P.1	411	388	-5.6	365	-11.1	433	+5.5
P.73	1,133	1,114	-1.7	1,097	-3.2	1,149	+1.4
	Average		**-4.9**		**-9.8**		**+4.9**
2. Flood volume (MCM)							
P.75	199	187	-6.1	175	-12.4	212	+6.4
P.67	382	360	-5.8	338	-11.4	403	+5.6
P.1	398	376	-5.5	355	-10.9	419	+5.3
P.73	1,316	1,288	-2.1	1,262	-4.1	1,342	+2.0
	Average		**-4.9**		**-9.7**		**+4.8**

5.2 Impact of deforestation and aforestation on flow hydrographs

Three different forest cover scenarios also applied on the selected flood event in 2001. Result of flow hydrographs at P.1 station in 2005 and 2010 calculated using FLDWAV based on three scenarios compared to flow hydrographs calculated based on forest cover in 2001 (baseline event) are presented in Figure 59. Results of peak flow and flow volume under each scenario are compared to that of the baseline event in 2001 as shown in Table 43.

Table 43 shows that peak flow and flow volume at all four stations along the main Ping river under the scenario 1 increased at the average rates of 5.8% and 6.7% compared to that of the baseline flow event in 2001. Percentage of peak flow increment reduced from the most upstream at P.75 at the rate of 6.4% to the most downstream at P.73 at the rate of 5.0%. It was also the same pattern for the percentage of flow volume which reduced from the most upstream at P.75 at the rate of 7.9% to the most downstream at P.73 at the rate of 4.8%.

Peak flow and flow volume at all four stations under the scenario 2 also increased at higher average rates of 11.6% and 13.7% compared to that of the baseline flow event in 2001, respectively. Percentage of peak flow and flow volume reduction also reduced from the most upstream at P.20 to the most downstream at P.73.

The results of the scenario 3 came opposite those the scenarios one and two as expected. Peak flow and flow volume at all four stations under the scenario 3 reduced at the average rates of 5.9 and 6.9% compared to that of the baseline event in 2001, respectively. Percentage of peak flow reduction also decreased from the most upstream at P.75 at the rate of 7.5% to the most downstream at P.73 at the rate of 4.8%. It was also the same way for the percentage of flow volume which reduced from the most upstream at P.75 at the rate of 8.5% to the most downstream at P.73 at the rate of 4.8%.

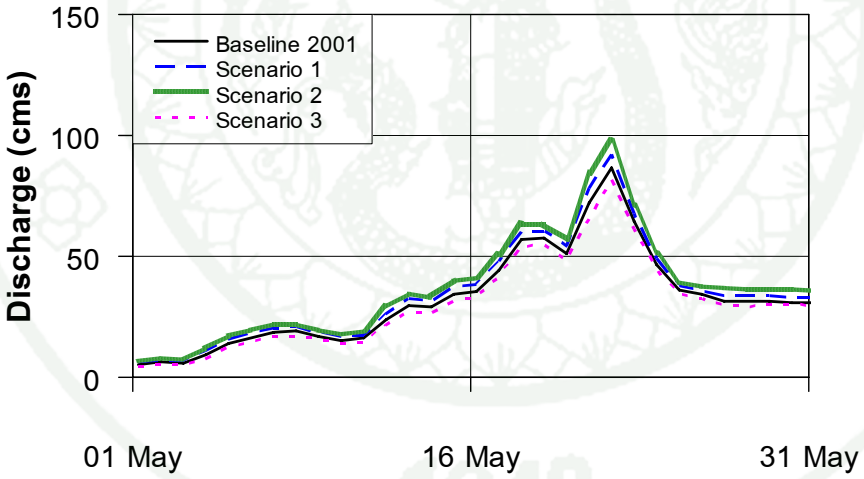

Figure 59 Flow hydrographs at P.1 based on three scenarios compared to that of the baseline event in 2001.

Table 43 Results of peak flow and flow volume under each scenario compared to that of the baseline event in 2001.

Station	Baseline flow event in 2001	Scenario 1		Scenario 2		Scenario 3	
		Value	(%)	Value	(%)	Value	(%)
1. Peak flow (cms)							
P.75	49	52	+6.4	56	+13.3	45	-7.5
P.67	95	100	+5.7	105	+10.8	89	-5.4
P.1	86	92	+6.2	97	+12.8	81	-5.9
P.73	165	174	+5.0	181	+9.6	157	-4.8
	Average		**+5.8**		**+11.6**		**-5.9**
2. Flow volume (MCM)							
P.75	42	46	+7.9	49	+16.8	39	-8.5
P.67	79	85	+7.1	91	+14.2	74	-7.2
P.1	80	86	+7.1	91	+14.2	74	-7.2
P.73	154	162	+4.8	169	+9.5	147	-4.8
	Average		**+6.7**		**+13.7**		**-6.9**

5.3 Flood inundation maps under 3 scenarios compared to the baseline flood map

Flood inundation maps for the 3 scenarios and the baseline flood event in 2001 were prepared by GIS software using the input data of the maximum water level at each cross-section determined by FLDWAV together with the DEM data of the basin. Since these flood inundation maps were generated using the maximum water levels of each cross section, they are not really presented in the real situation but only used as the upper limit of each flood scenario for easy comparison between scenarios. Figure 60 shows flood inundation maps of the three extreme flood events: the scenario 2 1 and 3 for the minimum, moderate and maximum flood events, respectively. Flood effects for all cases covered partial parts of five districts in Chiang Mai Province comprising Muang Chiang Mai, Hang Dong, San Kamphaeng, Mae Wang, and Chom Thong Districts, as well as three districts in Lamphun Province comprising Muang Lamphun, Pa Sang, and Ban Hong Districts.

However flood inundation areas of the two extreme events shown in Figure 60 are not significantly difference. Table 44 therefore prepared to show flood inundation areas for each flood depth under each scenario compared to the baseline event in 2001. As we can see in the table that flood area reduced for 2.9% and 5.0% for the scenarios 2 and 3, respectively, and increased for 3.5% for the scenario 3 compared to the baseline flood event in 2001 which showed flood area of 417.5 km^2. Flood depth also reduced for 1.1% and 3.2% for the scenarios 2 and 3, respectively, and increased for 1.3% for the scenario 3 compared to the baseline flood event in 2001 which showed flood depth of 1.75 m. Flood areas of the higher flood depths in the scenario 1 reduced compared to the baseline flood in 2001 and reduced further in the scenario 2. On the other hand, flood areas of the lower flood depths in the scenario 1 increased compared to the baseline flood in 2001 and increased further in the scenario 2. However, the results came opposite the scenario 3 in which forest percentage increased instead of reduced as the cases for the scenarios 1 and 2. The results can be seen clearly in Figure 61 which shows flood inundation areas for each flood depth of each scenario and the baseline event. It also shows the changes in flood area of each flood depth compared to that of the baseline event in 2001.

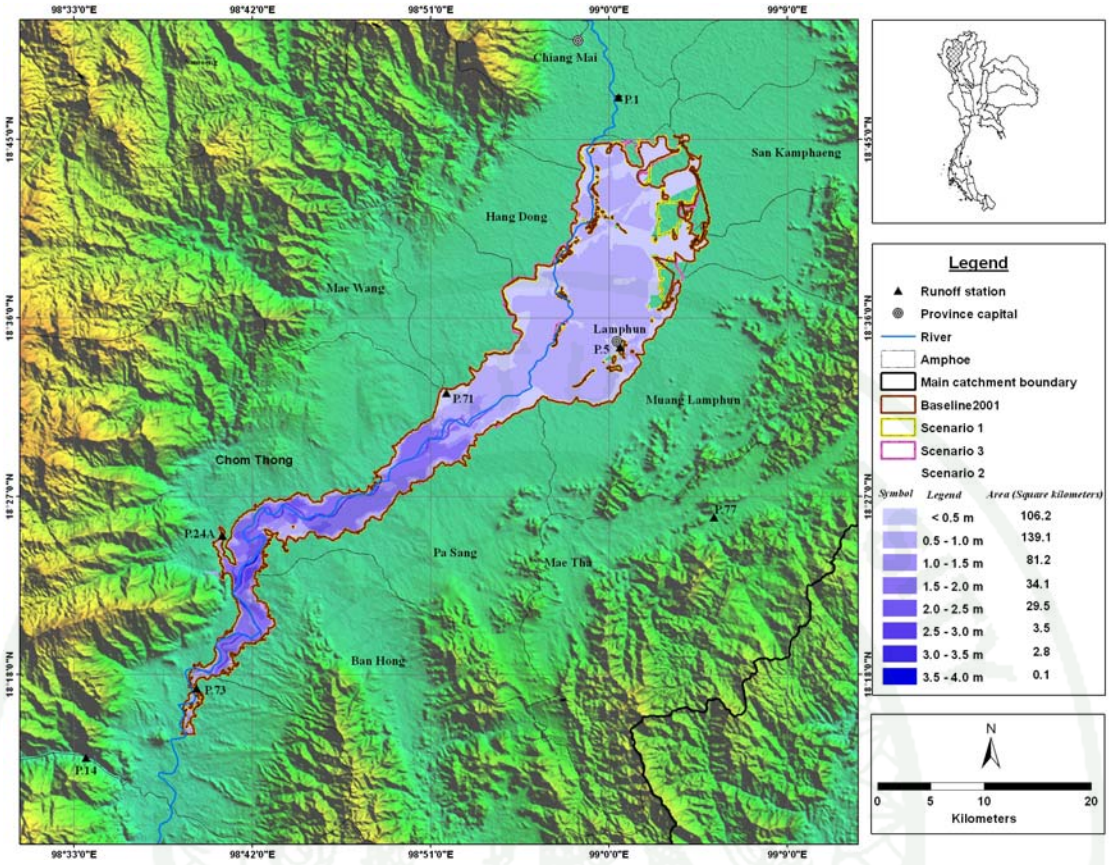

Figure 60 Flood inundation maps of the three extreme flood events of the scenarios 1 2 and 3.

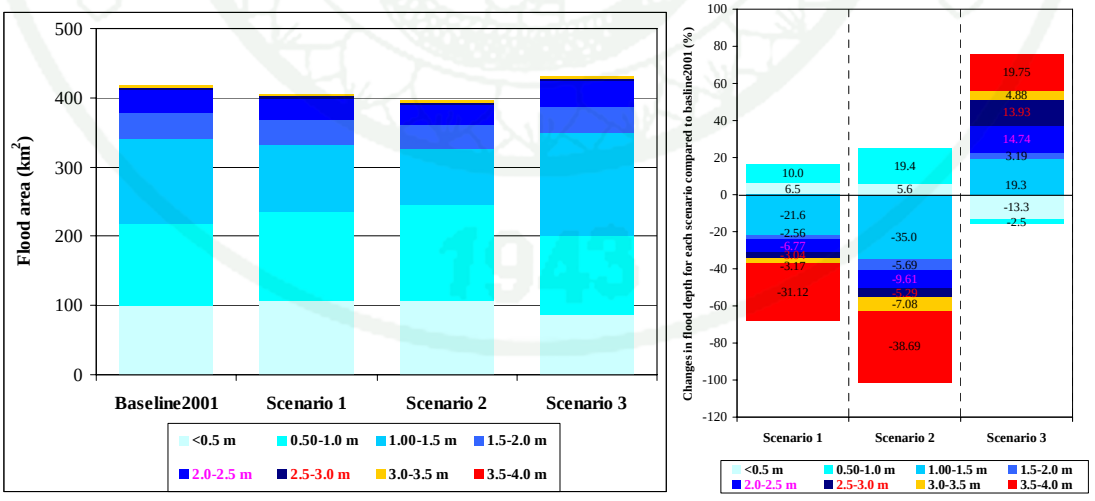

(a) Flood inundation areas for each flood depth of each scenario and the baseline event

(b) Changes in flood area of each flood depth compared to that of the baseline event

Figure 61 Comparisons of histograms of flood inundation area under each scenario and the baseline event in 2001.

Table 44 Comparison of flood inundation area in square kilometers for each flood depth under each scenario and the baseline event in 2001.

Description	Flood inundation area in km^2 for each flood depth (m)									Average Flood Depth (m)
	<0.5 m	0.5-1.0 m	1.0-1.5 m	1.5-2.0 m	2.0-2.5 m	2.5-3.0 m	3.0-3.5 m	3.5-4.0 m	Total	
Baseline2001	100.5	116.5	124.8	36.2	32.6	3.7	3.0	0.2	417.5	1.75
Scenario 1	107.0	128.1	97.8	35.2	30.4	3.6	2.9	0.1	405.3	1.73
(% change)	(6.5)	(10.0)	(-21.6)	(-2.6)	(-6.8)	(-3.0)	(-3.2)	(-31.1)	(-2.9)	(-1.1)
Scenario 2	106.2	139.1	81.2	34.1	29.5	3.5	2.8	0.1	396.5	1.70
(% change)	(5.6)	(19.4)	(-35.0)	(-5.7)	-9.6	(-5.3)	(-7.1)	(-38.7)	(-5.0)	(-3.2)
Scenario 3	87.1	113.6	149.0	37.3	37.4	4.2	3.2	0.2	432.0	1.77
(% change)	(-13.3)	(-2.5)	(19.3)	(3.2)	14.7	(13.9)	(4.9)	(19.7)	(3.5)	(1.3)

CONCLUSION AND RECOMMENDATION

This thesis addresses the relationship between the land cover changes and flood characteristics in the UPRB. This river basin is increasingly facing flooding problems due to land cover changes associated with long term continuing development. The approach which has been selected to carry out in this thesis is summarized as follows: (1) To apply suitable hydrologic and hydrodynamic public domain models for flood characteristic investigation, and (2) To use Geoinformatics to monitor and investigate land cover changes in the UPRB by analyzing LANDSAT-5TM satellite imagery taken during January and February for a set of nine years between 1988 and 2005. The historical relationships between land cover changes and flood characteristics were examined using the multiple regression technique. Land cover change scenarios were investigated to see their effects on flood characteristics. Finally, land cover change scenarios were prepared to alleviate possible flooding that would occur in the UPRB for the sustainable development in the basin.

In the first part of this section, the results and findings of this thesis are summarized and discussed in the form of five objectives. In last part, recommendation for further development is presented.

1. Results and Findings: Discussion and Conclusion

1.1 Objective 1: *To study the theory and concept of the well known hydrologic and hydrodynamic public domain models and to choose the suitable models to suit Thailand river basins to be used for flood estimation and flood routing investigation for the UPRB.*

In other countries the hydrological and hydrodynamic public domain models are at present available for users through free on-line downloading associated with their copyrights. For example, IHACRES, HEC-HMS, etc. are hydrological models while the hydrodynamic models include FLDWAV, CE-QUAL-RIV1, HEC-RAS, etc.

In this thesis, public domain mathematical models were identified and selected to get a set of appropriate models widely used in other countries. It is assured that they are provided with user manuals and theoretical-information manuals, as well as model source code for purposes of users' better understanding in the theory relevant to the model and its application according to users' purposes.

The hydrological model selected was IHACRES from Australia. This model is used in estimating flood hydrograph in sub-catchments using rainfall and temperature data. The hydrodynamic model selected is FLDWAV from the United States of America, which is a distributed flow routing model starting at the upstream portion of interest and ending at the downstream portion of interest in both river channels and flood plains of the Ping and Kuang rivers. FLDWAV uses the Saint-Venant Equation for one-dimensional unsteady flow to determine hydraulic characteristics of flood waves. Changes in water flow and its level can be calculated over the temporal and spatial domains.

In order to ensure that the public domain models selected are as effective as the commercial models commonly used in Thailand, MIKE 11-NAM/HD – a package of hydrological and hydrodynamic models developed by DHI Water and Environment, Denmark – was selected to examine the same flood events in the UPRB. Comparison of the estimated flood hydrograph generated by these two models are plotted according to the observed data from 2 runoff stations – P.67 and P.1 stations – located in Ping river and their effectiveness is revealed. (Taesombat and Sriwongsitanon, 2006)

After comparing the selected public domain models (which is free of copyright-related charge in the UPRB), the results have been found to be satisfactory suggesting the applicability of the models. These public domain models can be utilized reliably in the future studies of flood in any Thailand river basin.

1.2 Objective 2: *To setup the hydrologic and hydrodynamic models for the study basin for an investigation of flood hydrograph characteristics at each runoff station and downstream areas for the flood events from 1988 to 2005. Hydrologic and hydraulic parameters were examined for their differences within these flood events.*

Areal rainfall estimation is an important input for a hydrological model. Acquiring accurate areal rainfall is therefore crucial to improve the model prediction results. Moreover, the geography of the UPRB is generally mountainous. Hence, the conventional techniques such as Thiessen Polygon, and Isohyetal techniques that are usually applied to estimate the areal rainfall over the entire basin, their accuracies are decreased by topographical effects. Therefore, instead of these techniques, Thin Plate Spline (TPS) technique was selected to be used for areal rainfall estimation over the study basin. The TPS technique was introduced by Hutchinson (1998a,b) to interpolate spatial rainfalls more accurately, especially for mountainous areas. This technique can generate meteorological surfaces using a trivariate function of latitude, longitude and elevation of meteorological stations together with the terrain elevation.

In this thesis, the ANUSPLIN software Version 4.3 was applied to generate a surface of interpolated point rainfalls in conjunction with observed elevations in the UPRB during 1988-2005. The input data were 1) the generated SRTM-DEM data with a resolution of 30 m covering the UPRB and nearby areas and 2) daily rainfall data at 68 stations as well as their observed locations and elevations. The output from the ANUSPLIN software produces areal rainfall surfaces which correspond with point rainfalls and SRTM-DEM data. The output of areal rainfall surfaces were imported in the text file to generate a grid format in the GIS environment. They were summarized for each sub-catchment in order to provide input for the calibration and verification of IHACRES model.

Finally, the IHACRES and FLDWAV models were setup for model calibration and verification for the same nine years period in which satellite images were acquired. Calibration of the IHACRES model was carried out in nine runoff stations and results were verified at another 2 station. Six IHACRES model

parameters for each runoff station following calibration/verification relationships relationships between the catchment attributes and the physical conditions.

1.3 Objective 3: *To apply the technique of Geoinformatics (RS, GIS, and GPS) to investigate annual land cover changes from 1988 to 2005 in the study basin. Future land cover changes were predicted using the historical recorded data.*

Geoinformatics technology was used to monitor and investigate land cover changes across the entire UPRB by analyzing LANDSAT-5TM satellite imagery taken during January and February during the nine years period. A Supervised classification technique was applied with the ground truth investigation in order to classify land cover features across the basin. GIS was used to process land cover classification results to identify annual land cover changes in the study area. forest cover across the UPRB was found to be generally decreasing from 1988 to 2005; forest cover decreased at a rate of 1.86% annually (471 km^2/year). Areas under agriculture, disturbed forest, urbanized, and water bodies areas increased at annual rates of 0.60%, 0.84% 0.30% and 0.12% (151, 213, 77, and 30 km^2/year), respectively.

Patterns of land cover identified through the 23 categories, are regrouped in to six classes to make them more suitable for analyzing land cover changes afterward. These groupings comprise forest area, disturbed forest area, agriculture area, urban area, water body, and other area which is null class from 23 categories.

1.4 Objective 4: *To investigate the historical relationship between annual land cover change and flood characteristics in the study basin. These relationships were used to predict future flooding using the predicted future land cover changes in the basin.*

Strong nonlinear relationships between RRF and peak flow for all flood events at each sub-catchment were found for all eleven sub-catchments. Once RRF correlates in the positive trend to flood peak, higher RRF also means higher flood peak.

RRF to peak flow correlation relationships changed predictably and significantly over the nine years of this study for each sub-catchment; however the regression relationships were different from one year to the next.

Changes in hydrology are strongly linked to changes in land cover within each sub-catchment as significant correlation relationships between land cover (proportions of forest, disturbed forest, agriculture, and agriculture plus disturbed forest proportion) and RRF when peak flow is held constant at the 2, 5, 10 and 25 year ARI events.

Relationships between RRF and forest area have a positive slope for ten out of eleven sub-catchments with high r values. This shows that with peak flow held constant, RRF will tend to increase with increasing forest proportion for all but one sub-catchment. These increases are more significant for larger flood peaks since generally the slopes tend to increase with increasing flood peaks.

The relationships between RRF and disturbed forest plus agriculture proportion showed negative slope across the sub-catchments with quite good correlations (high r values). This means that RRF will decrease with increasing agricultural plus disturbed forest proportion for a particular peak flow event on each sub-catchment for events with the same peak magnitude. These reductions will be

more for larger flood peaks since the negative slopes tend to increase with increasing return period of flood peaks.

1.5 Objective 5: *To prepare land cover change scenarios to alleviate possible flooding that would occur in the UPRB.*

The second largest size of flood hydrograph in 2001 at P.1 was selected from flood and flow events between 1988 and 2005 when land cover data in the UPRB were available to investigate the effect of forest cover on flood and flow hydrographs. FLDWAV was used to investigate flood and flow routing between the most upstream station at P.20 and the downstream station at P.73. Flood inundation map for the baseline flood event in 2001 were prepared by GIS software using the input data of the maximum water level at each cross-section determined by FLDWAV together with the DEM data of the basin.

Two scenarios for deforestation and one scenario for aforestation with different percentage changes in forest were set to see the effect of forest cover changes on flood and flow hydrographs. For the scenario 1, flood and flow events in 2001 were rerun using historical forest percentage in 2005. For the scenario 2, flood and flow events in 2001 were rerun using hypothetical forest percentage in 2010 when the forest percentage reduced from 2005 at the same rate as historical percent reduction between 2000 and 2005. For the scenario 3, the selected flood and flow events were rerun using hypothetical forest percentage in 2005 when the forest percentage increased at the same rate as it reduced between 2000 and 2005.

The correlations between RRF and peak flow rates for flood and flow events suggested by Taesombat et al. (2010) were used to determine RRF values on the upstream sub-catchments (P.20, P.4A, P.21, P.71, P.76, and P.24A) in FLDWAV application for those selected flood peak and peak flow events. These RRF were correlated against the proportion of forest area on each sub-catchment. Flood and flow hydrographs at all upstream sub-catchments of each scenario were adjusted by the corresponding updating RRF to be input into FLDWAV application. Flood inundation

map of each scenario was then prepared by GIS software using the updating input data of the maximum water level at each cross-section determined by FLDWAV together with the DEM data of the basin of each scenario run.

Flood inundation maps for these three scenarios and the baseline flood event in 2001 were compared for their extent and severity. The result of flood maps revealed that deforestation tend to relieve flooding for both flood peak magnitude as well as flood volume but aforestation showed a reverse effect. The more degree of deforestation, the less flooding was presented as can be seen by the comparison between flood maps based on the scenarios 1 and 2. The impact of deforestation and aforestation on flow hydrograph showed an opposite direction as presented within flood events. Flood and flow hydrographs can be properly managed by another step of understanding on catchment saturation conditions within the basin.

For flood events, it appears that soil and vegetation on forested catchments reach a point where they becomes saturated, so highly forested catchments produce a relatively higher proportion of runoff for flood events (larger than ~1 year ARI) with the same peak flow rate compared to agricultural and disturbed forest areas. The opposite case was seen to apply for small flood events (lower than ~1 year ARI) where a trend of decreasing RRF with increasing forest area was seen. Presumably in the forested areas infiltration and evapotranspiration lead to higher proportional losses, particularly for highly forested catchments where losses to infiltration and evapotransporationcan be expected to be higher than agriculture and disturbed areas. This finding helps us to understand the response of flood behaviour to different land cover within the basin, which can be highly useful for flood management of river basins generally.

2. Recommendations

The influence of land cover change on flood characteristics has been an area of interest for hydrologists in recent years. This thesis is an example of a successful approach to river basin modeling which can be used to study the impact of land cover changes. However, there are some as follows.

2.1 Relationships between flood characteristics and land cover changes in the other river basins should be considered to cross validation with the relationships derived from the UPRB.

2.2 TPS accounting for elevation should be used ahead of the Polygon and Isohytal mapping to detect areal rainfall distributions as it is clearly superior. More investigation to use of slope and aspect as input into the method to further improve the technique.

2.3 IHACRES is suitable for modeling rainfall – runoff processes across UPRB. More work relating catchment characteristics to IHACRES parameters is needed.

2.4 FLDWAV is suitable for modeling channel hydraulics. Both IHACRES and FLDWAV are recommenced for future modeling due to the ease with which they can be calibrated and as they are publish domain.

2.5 Both significant flood events and flow events show relationships to land cover to use but they are depend on their nature: RRF increases with forest cover for large events while decreasing for flow event. Evidence for such difference behaviour based on event magnitude should be further examined both the UPRB and elsewhere.

LITERATURE CITED

Adamson. 2005. **Overview of the Hydrology of the Mekong Basin, Mekong River Commission.** Vientiane, Lao PDR

Amein, M. and C.S. Fang, 1970. Implicit Flood Routing in Natural Channels. **Journal of Hydraulics Division, ASCE.** 96 (HY12): 2481-2500.

Austin, S.A. 1999. **Streamflow Response to Forest Management: A Meta-analysis Using Published Data and Flow Duration Curves.** Unpublished M.Sc. thesis. Colorado State University, Fort Collins, CO, USA.

Baltzer, R.A. and C. Lai. 1968. Computer Simulation of Unsteady Flow in Waterways. **Journal of Hydraulics Division, ASCE.** 94 (HY4): 1083-1117.

Barkau, R.L. 1985. **A mathematical model of unsteady flow through a dendritic network.** Ph.D. Dissertation, Department of Civil Engineering, Colorado State University, Ft. Collins, CO, USA.

Beven, K. and M. J. Kirkby. 1979. **A physically based, variable contributing area model of basin hydrology.** Hydrological Sciences Bulletin. n.p.

Beven, K., R. Lamb, P. Quinn, R. Romanowicz and J. Freer. 1995. **TOPMODEL,** pp. 627–668. *In* Singh, V.P. (Ed.), Computer Models of Watershed Hydrology. Water Resources Publications, Colorado,

Boer, E.P.J., K.M. de Beursl and A.D. Hartkampz. 2001. Kriging and thin plate splines for mapping climate variables. **J Appl Genet** 3(2): 146-154.

Bosch, J.M. and J.D. Hewlett. 1982. A review of catchment experiments to determine the effect of vegetation changes on water yield and evapotranspiration. **Journal of Hydrology** 55: 3–23.

Box, G.E.P. and Jenkins, G.M. 1976. **Time Series Analysis: Forecasting and Control.** Holden-Day, San Francisco, CA, USA.

Bradshaw, C.J.A., Sodi, N.S., Peh, K.S.H., and Brook, B.W. (2007) Global evidence that deforestation amplifies flood risk and severity in the developing world. Global Change Biology, 13: 2379–2395.

Brunner, G.W. 2002. **HEC-RAS River Analysis System: Hydraulic Reference Manual Version 3.1.** US Army Corps of Engineer, Hydrologic Engineering Center (HEC), USA. 363 p.

Buan, S.D. 2003. **NWS FLDWAV MODEL - A one-dimensional unsteady flow model for the Red river of the north.** 1st International Water Conference. Red River Basin Institute, Moorhead, Minnesota, USA.

Buttle, J.M., and Metcalfe, R.A. (2000) Boreal forest disturbance and streamflow response, Northeastern Ontario. Canadian Journal of Fisheries and Aquatic Sciences 57 (Suppl. 2): 5–18.

Butts, M.B., Klinting, A., van Kalken, T., Cadman, D., Fenn, C. and Høst-Madsen, J., 2001. **Design and development of an Internet-based flood forecasting system using real-time rainfall, radar, and river flow data.** In: Falconer, R.A. and Blain, W.R., Editors, 2001. Proceedings of River Basin Management 2001, Cardiff, WIT Press, pp. 139–148.

Calder, IR and B Aylward (2006) “Forest and Floods: Moving to an Evidence-based Approach to Watershed and Integrated Flood Management”, Water International, Volume 31, Number 1.

Carcano E.C., Bartolini P., Muselli M., and Piroddi L. 2008. **Jordan recurrent neural network versus IHACRES in modelling daily streamflows.** J. Hydrol. 362(3-4): pp. 291-307.

Carlile, P.W., Croke, B.F.W., Jakeman, A.J. and Lees, B.G. 2004. **Development of a semi-distributed catchment hydrology model for simulation of land-use change streamflow and groundwater recharge within the Little river catchment, NSW.** In: Roach I.C. ed. 2004. Regolith 2004. CRC LEME, Australia. pp. 54-56.

Carlson, T.N. and Traci Arthur, S. (2000) The impact of land use-land cover changes due to urbanization on surface microclimate and hydrology: a satellite perspective. Global Planetary Change 25: 49–65.

Chalayonavin, V. 1998. **Application of Remote Sensing and GIS for planning and management of Huai Nongkop-Huai Nongbon watershed basin Changwat Kanchanaburi.** Ph.D. Dissertation, Department of Forestry, Kasetsart University, Bangkok, Thailand. 204 p.

Chapman, A.D., Munoz, M.E.S. and Koch, I. 2005. **Environmental information: Placing biodiversity phenomena in an ecological and environmental context.** Biodiversity Informatics, 2, 2005, Australia. pp. 24-41

Chen, R.S., Pi, L.C., and Huang, Y.H. 2003. **Analysis of rainfall-runoff relation in paddy fields by diffusive tank model.** Hydrol. Process. 17: pp. 2541–2553.

Chow, V.T., Maidment, D.R., and Mays, L.W. 1988. **Applied Hydrology.** McGraw-Hill Science. 572 p.

Clark, S.Q., Markar, M.S., Min Yaowu and Wu Daoxi. 2004. **Overview of hydraulic modelling of the Yangtze river for flood forecasting purposes.** 8th National Conference on hydraulics in water engineering, ANA Hotel Gold Coast, Australia.

Congalton, R.G. and K. Green. 1999. **Assessing the Accuracy of Remotely Sensed Data: Principles and Practices.** Lewis Publishers. 137 pp.

Connecticut Geology. 2005. **Duration of stream flow.** Wesleyan University, Connecticut, USA. Available source http://www.wesleyan.edu/ctgeology/ StreamFlowDuration/ StreamFlowDuration.html, Febuary 1, 2006.

Cosandey, C., Andre ´assian, V., Martin, C., Didon-Lescot, J.F., Lavabre, J., Folton, N., Mathys, N., and Richard, D. (2005) The hydrological impact of the mediterranean forest: a review of French research. Journal of Hydrology 301: 235–249.

Croke, B.F.W., Merritt, W.S. and Jakeman, A.J. 2003. **A dynamic model for predicting hydrologic response to land cover changes in gauged and ungauged catchments.** Journal of Hydrology 291 (2004), USA. pp. 115–131.

Croke, B.F.W., Andrews, F., Jakeman, A.J., Cuddy, S. and Luddy, A. 2005. **Redesign of the IHACRES rainfall-runoff model.** 29th Hydrology and Water Resources Symposium, 21-23 Febuary 2005, Canberra, Australia. pp. 1-7.

Cybenko, G. 1989. **Approximation by superposition of a sigmoidal function.** Math. Control. Signals. Syst. 2, pp. 303–314.

DeLong, L.L. 1986. **Extension of the unsteady one-dimensional open-channel flow equations for flow simulation in meandering channels with flood plains.** Selected Papers in Hydrologic Science, U.S. Geological Survey Water Supply Paper 2220, USA, pp. 101-105.

DeLong, L.L. 1989. **Mass Conservation: 1-D open channel flow equations.** Journal of Hydraulics Division, Vol. 115, No. 2, USA. pp. 263-268.

Department of Disaster Prevention and Mitigation. (2005) Typhoon Damrey Damage Summary. Available source: http://www.dmr.go.th/ewt_news.php?nid=5247& filename=news_dmr.

Department of Water Resources (DWR). 2006. **Early Warning System**, Completion Report, 257 p.

DHI Water & Environment. 2003. **Flood management solutions and services**. Hørsholm, Denmark.

DHI Water & Environment. 2002. **MIKE11-A Modelling System for Rivers and Channels: Reference Manual.** Hørsholm, Denmark, 504 p.

Dirks, K.N., Hay, J.E., Stow, C.D., and Harris, D. 1998. **High-resolution studies of rainfall on Norfolk Island Part II: interpolation of rainfall data.** J. Hydrol. 208(3-4), 187–193.

Dye, P.J. and Croke, B.F.W. 2003. **Evaluation of streamflow predictions by the IHACRES rainfall-runoff model in two South African catchments.** Environmental Modelling & Software 18 (2003), USA. pp. 705–712.

Dyhr-Nielsen, M. (1986) Hydrological effect of deforestation in the Chao Phraya basin in Thailand. In Proceedings of the International Symposium on Tropical Forest Hydrology and Application, Chiangmai, Thailand, 12 pp.

Ekasingh, M. and Kaewthip, J. 2000. **Spatial weather data development in rice decision support system.** In: Decision support system for crop production project: rice in the Northern, Final Report, The Thailand Research Fund, pp. 41-76.

Environmental Laboratory. 1995. **CE-QUAL-RIVI User's Manual:** A Dynamic, One-Dimensional (Longitudinal) Water Quality Model for Streams. US Army Corps of Engineer, Waterways Experiment Station, USA. 290 p.

Environmental Systems Research Institute, Inc (ESRI). 2002. **ArcView GIS Version 3.2-User Manual**, 385 pp.

Evans, J.P. and Jakeman, A.J. 1998. **Development of a simple, catchment-scale, rainfall-evapotranspiration-runoff model.** Environmental Modelling and Software 13. pp. 385-393.

Evans, J.P. 2003. **Improving the characteristics of streamflow modeled by regional climate models.** J. Hydrol. 284 (2003), pp. 211–227.

Fread, D.L. 1971. **Discussion of Implicit Flood Routing in Natural Channels.** by Amein M. and Fang C. S., Journal of Hydraulics Division, ASCE, Vol. 97, No. HY7, USA. pp. 1156-1159.

Fread, D.L. 1978. **Theoretical development of implicit dynamic routing model.** HRL-113, Hydrologic Research Laboratory, National Weather Service, Silver Spring, Md, USA.

Fread, D.L. 1985. **Breach: An Erosion Model for Earthen Dam Failures.** Hydrologic Research Lab, USA. 34 p.

Fread, D.L. 1988. **The NWS DAMBRK model: Theoretical background/user documentation.** HRL-256, Hydrologic Research Laboratory, National Weather Service, Silver Spring, Md, USA, 315 p.

Fread, D.L. and Lewis, J.M. 1993. **Selection of Δx and Δt computational steps for four-point implicit nonlinear dynamic routing models.** Proceedings of ASCE National Hydraulic Engineering Conference, San Francisco, California, USA, July 26-30, pp.1569-1573.

Fread, D.L., Jin, M. and Lewis, J. M. 1996. **An LPI numerical implicit solution for unsteady mixed-flow simulation.** North American Water and Environment Congress 1996, ASCE, Anaheim, California, June 22-28, USA.

Fread, D.L. and Lewis, J.M. 1998. **NWS-FLDWAV Model: Theoretical description and User documentation.** Hydrologic Research Laboratory, Office of Hydrology, National Weather Service (NWS), NOAA, Silver Spring, Maryland, USA. 334 p.

Geo-Informatics and Space Technology Development Agency (Public Organization): GISTDA. 2005. **The index of LANDSAT-5 image over Thailand.** Available source http://www.gistda.or.th/Gistda/HtmlGistda/Html/Index1.htm, January 25, 2006.

Goovaerts, P. 2000. **Geostatistical approaches for incorporating elevation into the spatial interpolation of rainfall.** J. Hydrol. 228(1-2), 113–129.

Gorokhovich, Y. and Voustianiouk, A. 2006. **Accuracy assessment of the processed SRTM-based elevation data by CGIAR using field data from USA and Thailand and its relation to the terrain characteristics.** Remote Sensing of Environment, Vol.104, pp. 409–415.

Grey, W.M.F., Luckman, A.J. and Holland, D. (2003) Mapping urban change in the UK using satellite radar interferometry. Remote Sens. Environ. 87: 16–22.

Guillermo, Q., Tabios, G.Q. III and Salas, J.D. 1985. **A Comparative analysis of techniques for spatial interpolation of precipitation.** Journal of the American Water Resources Association, Vol. 21, Issue 3, pp. 365-380.

Guo, F., Liu, X. R., and Ren, L.L. 2000. **A topography based hydrological model: TOPMODEL and its widened application.** Advances in Water Science. 11(3): pp. 296–301. (in Chinese)

Hastings, D.A. and Dunbar, P.K. 1998. **Development and Assessment of the Global Land One-km Base Elevation Digital Elevation Model (GLOBE).** Proceeding in the International Society of Photogrammetry and Remote Sensing (ISPRS) Symposium, Vol.32, number 4, pp. 218-221.

Havnø, K. and Brorsen, M. 1986. **A general mathematical modeling system for flood forecasting and control.** Proceeding of International Conference on Hydraulics of Floods and Flood Control, Cambridge, UK; BHRA, Stevenage.

Havnø, K., Madsen, M.N. and Dørge, J. 1995. **MIKE 11 - a generalized river modelling package.** In: Singh, V.P., Editor, 1995. Computer Models of Watershed Hydrology, Water Resources Publications, Colorado, pp. 733–782.

Hayase, Y., and Kadoya, M. 1993. **Diffusive tank model for flood analysis and its fundamental characteristics: runoff analysis by the diffusive tank model in low-lying drainage basin (I).** Trans. Jpn. Soc. Irrigat., Drainage and Reclam. Eng. 165: pp. 75–84. (in Japanese)

Hevesi, J.A., Flint, A.L., and Istok, J.D. 1992a. **Precipitation estimation in mountainous terrain using multivariate geostatistics. Part I: structural analysis.** J. Appl. Meteor. 31, 661–676.

Hevesi, J.A., Flint, A.L., and Istok, J.D. 1992. **Precipitation estimation in mountainous terrain using multivariate geostatistics. Part II: Isohyetal maps.** J. Appl. Meteor. 31, 677–688.

Hipel, K.W. and McLeod, A.I. 1994. **Time series modelling of water resources and environmental systems.** Dev. Water Sci. 45, 1–1013, Elsevier.

Horton, R.E. 1932. **Drainage basin characteristics**, Trans. Am. Geophys. Union 13, 350.

Hutchinson, M.F. 1993. **On Thin Plate Smoothing Splines and Kriging.** Computing and Science in Statistics 25, 55-62.

Hutchinson, M.F. and Gessler, P.E. 1994. **Splines more than just a smooth interpolator.** Geoderma 62, 45-67.

Hutchinson, M.F. 1995a. **Interpolating mean rainfall using thin plate smoothing splines.** International Journal of Geographical Information Systems 9 (4). pp. 385–403.

Hutchinson, M.F. 1995b. **Stochastic space-time weather models from ground based data.** Agric. For. Meteorol. 73, 237-264.

Hutchinson, M.F. 1998a. **Interpolation of rainfall data with thin plate smoothing splines: I two dimensional smoothing of data with short range correlation.** Journal of Geographic Information and Decision Analysis 2(2). pp. 152-167. Available source http://publish.uwo.ca/~jmalczew/gida_4.htm, March 2, 2006.

Hutchinson, M.F. 1998b. **Interpolation of rainfall data with thin plate smoothing splines: II analysis of topographic dependence.** Journal of Geographic Information and Decision Analysis 2(2). pp. 168-185.

Hutchinson, M.F. 2004. **ANUSPLIN Version 4.3 User Guide**, Centre for resource and environmental studies, The Australian National University, Canberra, Australia. 54 pp.

Hydrologic Engineering Center (HEC). 2000. **User's Manual HEC-HMS Hydrologic Modeling System Version 2.0**, US Army Crop of Engineer,U.S.A. 427 p.

Jakeman, A.J. and Hornberger, G.M. 1993. **How much complexity is warranted in a rainfall-runoff model.** Water Resources Research 29 (8). pp. 2637–2649.

Japan Association of Remote Sensing. 2006. **Remote Sensing Tutorials.** Available source http://www.profc.udec.cl/~gabriel/tutoriales/rsnote/contents.htm, February 22, 2006.

Jarvis A., H.I. Reuter, A. Nelson, E. Guevara. 2006. **Hole-filled seamless SRTM data V3.** International Centre for Tropical Agriculture (CIAT), USA. Available source http://srtm.csi.cgiar.org, May 2, 2007.

Jenness, J. and J.J. Wynne. 2005. **Kappa analysis (kappa_stats.avx) extension for ArcView 3.x.** Jenness Enterprises. Available: http://www.jennessent.com/ arcview/kappa_stats.htm, May 22, 2008.

Johnson, C. 1993. **Introduction to quantitative methods and modelling in community, population, and landscape ecology.** In Environment Modelling with GIS (M. F. Goodchild, B.O.Parks and L.T. Steyaert, eds), Oxford University Press. pp. 276–283.

Kern Mediation Group. 2006. **The hydrologic cycle.** Environmental science studies website, Urban Watershed Project, USA. Available source: http://www.kernsite.com/uwp/waterqua.htm, February 21, 2006.

Lewis, M.J., Singer, M.J. and Tate, K.W. 2000. **Applicability of SCS curve number method for a California Oak Woodlands Watershed.** Journal of Soil and Water Conservation. 55 (2): pp. 226–230.

Liew, S.C. 2006. **Optical Remote Sensing.** Principle of Remote Sensing, Centre for Remote Imaging, Sensing and Processing (CRISP), National University of Singapore, Singapore. Available source http://www.crisp.nus.edu.sg/~research/ tutorial/optical.gif, Febuary 16, 2006.

Liggett, J.A. and Cunge J.A. 1975. **Numerical methods of solution of the unsteady flow equations.** In unsteady flow in Open Channel, edited by K. Mahmood and V. Yevjevich, Vol. I, Chapter 4, Water Resources Publications, Ft. Collins, CO, USA.

Lillesand, T.M., Kiefer, R.W. and Chipman J.W., 2004. **Remote Sensing and Image Interpretation.** Fifth Edition, John Wiley and Sons, Inc., New York, USA, 763 p.

Lin, Y., and Wei, X. (2008) The impact of large-scale forest harvesting on hydrology in the Willow watershed of Central British Columbia. Journal of Hydrology 359: 141-149.

Littlewood, I.G. and Jakeman, A.J. 1994. **A new method of rainfall-runoff modelling and its applications in catchment hydrology.** Environmental Modelling, P. Zannetti (Ed.), Computational Mechanics Publications, Southampton, 2. pp. 143-171.

Littlewood, I.G., Down, K., Parker, J.R. and Post., D.A. 1997. **The PC version of IHACRES for catchment-scale rainfall - streamflow modelling Version 1.0 User Guide - April 1997.** Institute of Hydrology, Centre for Ecology and Hydrology, Wallingford, Oxon, UK. 97 p.

Liu, S., Wu, C. and Shen, H. (2000) A GIS-based model of urban land use growth in Beijing. Acta Geogr. Sin. 55: 407–416.

Mapiam, P.P., and Sriwongsitanon, N. 2009. **Estimation of the URBS model parameters for flood estimation of ungauged catchments in the upper Ping river basin, Thailand.** ScienceAsia 35(1), 49-56.

McColla, C., and Aggett, G. 2006. **Land-use forecasting and hydrologic model integration for improved land-use decision support.** Journal of Environmental Management. 84 (4): pp. 494-512.

Ming, J. and Sylvestre, J. 2001. **River flood forecast of the Mississippi-Illinois-Missouri river system using NWS FLDWAV model.** Theme C Proceedings of 29th International Association of Hydraulic Engineering and Research (IAHR), Sept. 16-21, 2001, Chinese Hydraulic Engineering Society (CHES), China. pp. 136-141.

Mirshahi, B., Onof, C., and Wheater, H. 2008. **Spatial-temporal daily rainfall simulation for a semi-arid area in Iran:** a preliminary evaluation of Generalised Linear Models. In: Sustainable Hydrology for the 21st Century, Proc. 10th BHS National Hydrology Symposium, Exeter, UK. pp. 145–152.

NASA (National Aerospace Administration). 2004. **LANDSAT-5.** Available source http://www.earth.nasa.gov/history/landsat/landsat5.html, July 12, 2005.

Neitsch, S.L., Arnold, J.G., Kiniry, J.R., and Williams, J.R. 2005. **Soil water assessment tool theoretical document, version 2005.** Grassland, Soil and Water Research Laboratory, Agricultural Research Service, 808 East Blackland Road, Temple, TX.

Nielsen, S.A. and Hansen, E., 1973. **Numerical simulation of the rainfall runoff process on a daily basis.** Nordic Hydrol. 4, pp. 171–190.

Noonan, G.R. 2003. **GIS technology: A powerful tool for entomologists.** Insight 1, Australia. pp.1-98.

O'Connor, J.E. and Costa, J.E. 2004. **The world's largest floods, past and present-Their causes and magnitudes.** U.S. Geological Survey Circular 1254, 13 p.

PCI Geomatics Enterprises Inc. 2003. **Geomatica Focus User Guide.** PCI Copyright and Trademarks. 352 pp.

Perez, P., Ardlie, N., Kuneepong, P., Dietrich, C. and Merritt, W.S. 2002. **CATCHCROP: modelling crop yield and water demandfor integrated catchment assessment in Northern Thailand.** Environmental Modelling and Software 17 (3). pp. 251–259.

Phillips, D.L., Dolph, J., and Marks, D. 1992. **A comparison of geostatistical procedures for spatial analysis of precipitations in mountainous terrain.** Agr. Forest Meteor. 58, 119–141.

Pikounis M., Varanou E., Baltas E., Dassaklis A. and Mimikou M. 2003. **Application of the SWAT model in the Pinios river basin under different land use scenarios.** Global Nest: the International Journal. 5 (2): pp. 71-79

Post, D., and Jakeman, A.J. 1996. **Relationships between catchment attributes and hydrological response characteristics in small Australian mountain ash catchments.** Hydrolog Process. 10: 877-892.

Preechachol, A. 2006. **Principle of Remote Sensing.** Training Document of the Fundamental of Remote Sensing, February, 1-10, 2006, The Institute of Space Knowledge-Based Development, Geo-Informatics and Space Technology Development Agency (Public Organization).

Price, D.T., McKenney, D.W., Nalder, I.A., Hutchinson, M.F. and Kesteven, J.L. 1999. **A comparison of two statistical methods for spatial interpolation of Canadian monthly mean climate data.** Agricultural and Forest Meteorology, vol.101, pp. 81–94.

R-Can Environmental Inc. 2006. **Water quality training course, Water Fundamentals.** Sterilight, Ultraviolet Disinfection System for the new Millenium, Ontario, Canada. Available source http://www.r-can.com/home.asp, February 20, 2006.

Ragan, R.M., Jackson, T.J., 1980. **Runoff synthesis using Landsat and SCS model.** Journal of Hydrologics Division, ASCE 106 (HY5), pp. 667–678.

Ratanasuwan, A. 2001. **Application of GIS and Remote Sensing for studying impact of land use change on streamflow quantity in the Mae Chaem watershed, Changwat Chiang Mai.** Master of Science (Forestry) Thesis, Kasetsart University, Bangkok, 100 p.

Ratanopad, S. and Kainz, W. (2006) Land Cover Classification and Monitoring in Northeast Thailand Using Landsat 5 TM Data. In Proceedings of the ISPRS Vienna 2006 Symposium Technical commission II, Vienna, Austria, pp. 137-144.

Refsgaard, J.C. 1997. **Validation and intercomparison of different updating procedures for real-time forecasting.** Nordic Hydrology 28, pp. 65–84.

Resource Planning and Development Commission. 2003. **Chapter 3: water quantity and quality, wetlands, aquatic health and groundwater.** State of the environment (SoE) report in Tasmania, Australia. Available source http://www.rpdc.tas.gov.au/soer/index/contents.php, February 14, 2006.

Royal Forestry Department. 2005. **The comparison of forest cover during the period of 1993-1997.** Available source http://www.dnp.go.th/Research/Knowledge/T_area1.htm, January 25, 2006.

Royal Forest Deparment. 2006. Table 2 - Forest Land Assessment by Province in 2004-2006. Availiable source http://www.forest.go.th/stat/stat50/TAB2.htm, 3 November 2008.

Royal Irrigation Department (RID). 2006. **Study and Installation of Telemetry System in the Upper Ping river basin for Flood Forecasting and Warning**, Completion Report, 380 p.

Rungsipanich, A. 2000. **Optimum technique for land use change detection.** Master of Science (Forestry) Thesis, Kasetsart University, Bangkok, 146 p.

Schultz, G.A. 1995. **Changes on flood characteristics due to land use changes in a river basin.** Paper prepared for the U.S.- Italy Research Workshop on the Hydrometeorology, Impacts, and Management of Extreme Floods, Perugia, Italy, November 1995. pp.1-13.

Schumm, S.A. 1956. **The evolution of drainage system and slopes in badlands at Perth**, Amboy, New Jersey, Geol. Soc. Am. Bull., 67, 597.

Sefton, C.E.M. and Howarth, S.M., 1998. R**elationships between dynamic response characteristics and physical descriptors of catchments in England and Wales.** J. Hydrol., 211 (1998), pp. 1–16.

Seker, D.Z., Kabdasli, S. and Rudvan, B. 2001. **Risk assessment of a dam-break using GIS technology.** Istanbul Technical University, civil engineering faculty, Maslak, Istanbul, Turkey.

Sharples, J.J., Hutchinson, M.F., and Jellett, D.R. 2005. **On the Horizontal Scale of Elevation Dependence of Australian Monthly Precipitation.** J Appl Meteorol 44(12), 1850-1865.

Shen, Y., Xiao, J., Kondoh, A. and Tateishi, R. (2003) Influence of land use and land cover change due to urbanization on hydrological environments: a case study. In: Proceedings of The CEReS International Symposium on Remote Sensing: Monitoring of Environmental Change in Asia, Chiba University, Japan December 16–17, pp. 25–28.

Shultz G.A. 1997. **Use of remote sensing data in a GIS environment for water resources management,** in Remote Sensing and GIS for Design and Operation of Water Resources Systems, edited by Baungartner M, Schultz G. A. and Johnson A. I., IAHS Press, Institute of Hydrology, Wallingford, Oxfordshire, UK.

SPSS Inc. 2008. **SPSS, Data Mining, Statistical Analysis Software, Predictive Analysis, Predictive Analytics, Decision Support Systems.** Available source http://www.spss.com/, August 19, 2008.

Stekauerova, V., Nagy, V., and Kotorova, D. 2006. **Soil water regime of agricultural field and forest ecosystems.** Biologia, Bratislava. 61(19): S300—S304. Source: http://147.213.145.2/biohydrology/Biologia2006Papers/Stekauerova.pdf

Sugawara, M., 1974. Tank model and its application to Bird Creek, Wollombi Brook, Bikin Rive, Kitsu River, Sanaga River and Namr Mune. Research Note of the National Research Center for Disaster Preventions 11, pp. 1–64.

Sylvestre, J. and Sylvestre, P. 2002. **FLDWAV application – transitioning from calibration to operational mode**. National Weather Service, NOAA, Silver Spring, MD, USA.

Tabios, G.Q. III, and Salas, J.D. 1985. **A comparative analysis of techniques for spatial interpolation of precipitation.** Water Resour. Bull. 21(3), 365–380.

Taesombat, W. and Sriwongsitanon, N. 2006. **An Evaluation of the Effectiveness of Hydrodynamic Models Application for Flood Routing Investigation in the Upper Ping River Basin.** Engineering Journal Kasetsart. Vol.20, No.60, pp. 74-82.

Taesombat, W. and Sriwongsitanon, N. 2009. **Areal Rainfall Estimations using Spatial Interpolation Techniques** ScienceAsia 35(3), 268-275.

Taesombat, W. and Sriwongsitanon, N. 2010. **Flood Investigation for the upper Ping river basin using the Mathematical Models** Kasetsart Journal (Natural Science) 44(1): 152-166.

Tang, Z., Engel, B.A., Lim, K.J., Pijanowski, B.C., and J. Harbor. 2005. **Minimizing the impact of urbanization on long term runoff.** J Am Water Resour Assoc. 41(6), 1347-1359.

Tangtham, N. 1994. **The hydrological roles of forests in Thailand.** TDRI Quarterly Review Vol. 9 No. 3 September 1994, Thailand. pp. 27-32.

United States Department of Agriculture, Soil Conservation Service (USDA). 1972. **Hydrology. In: National Engineering Handbook.** Section 4. Washington DC: US Govt. Printing office.

Unit for Social and Environmental Research (USER). 2006. **ERA Upper Ping.** Faculty of Social Sciences, Chiang Mai University, Chiang Mai, Thailand. Available source http://www.sea-user.org/uweb.php?pg=28, February 25, 2006.

Viney, N.R., Croke, B.F.W., Breuer, L., Bormann, H., Bronstert, A., Frede, H., Graff, T., Hubrechts, L., Huisman, J.A., Jakeman, A.J., Kite, G.W., Lanini, J., Leavesley, G., Lettenmaier, D.P., Lindstrom, G., Seibert, J., Sivapalan, M. and Willems, P. 2005. **Ensemble modelling of the hydrological impacts of land use change.** In Zerger, A. and Argent, R.M. (eds), MODSIM 2005 International Congress on Modelling and Simulation. Modelling and Simulation Society of Australia and New Zealand, December 2005. pp. 2967-2973.

Wahba, G. 1990. **Spline Models for Observational Data.** CBMS-NSF Regional Conference Series in Applied Mathematics. SIAM Philadelphia, PA, 169 pp.

Weng, Q. 2001. **Land use change analysis in the Zhujiang Delta of China using satellite remote sensing, GIS and stochastic modeling**. Journal of Environmental Management 64: 273–284.

Weng, Q.H. (2002) Land use change analysis in the Zhujiang Delta of China using satellite remote sensing, GIS and stochastic modelling. J. Environ. Manage. 64: 273–284.

Wilk, J., Andersson, L., and Plermkamon, V. (2001) Hydrological impacts of forest conversion to agriculture in a large river basin in northeast Thailand. Hydrological Processes 15: 2729-2748.

Xianzhao, L. and Jiazhu, L. 2008. **Application of SCS model in estimation of runoff from small watershed in Loess Plateau of China.** Chinese Geographical Science. 18 (3): pp. 235-241

Xiao, J., Shen, Y., Ge, J., Tateishi, R., Tang, C., Liang, Y. and Huang, Z. (2006) Evaluating urban expansion and land use change in Shijiazhuang, China, by using GIS and remote sensing. Landsc. Urban Plann. 75: 69–80.

Xiong, L.H., Guo, S. L., and Hu, C.H. 2002. **Application and studies of TOPMODEL in runoff simulation on different watersheds.** Hydrology. 22(5): pp. 5–8. (in Chinese)

Xu, X. and Zhang J. 2002. **The Improvement of NWS FLDWAV Hydraulic Model and Connection with WASP5.** Proceeding of 5th International Conference on Hydro-Science and -Engineering (ICHE-2002), September 18-21, 2002, Warsaw, Poland.

Xue-song, Z., Fang-hua, H., Hong-guang, C., and Dao-feng, L. 2003. **Application of swat model in the upstream watershed of the Luohe River.** Chinese Geographical Science. 13 (4): pp. 334-339.

Ye, W., Bates, B.C., Viney, N. R., Sivapalan, M. and Jakeman, A.J. 1997, **Performance of conceptual rainfall-runoff models in low-yielding ephemeral catchments.** Water Resources Research, volume 33, pp 153-166.

APPENDIX

Appendix Table 1 List of the rainfall stations in the UPRB and the surroundings.

No.	Sta. Code	Station Name	Province	Gov.	Latitude	Longitude	Period
1.	07013	A. Muang	Chiang Mai	TMD	18° 50' 23"	98° 58' 32"	1952 - con.
2.	07022	A. Sarapi	Chiang Mai	TMD	18° 42' 48"	99° 02' 29"	1952 - con.
3.	07032	A. San Kamphaeng	Chiang Mai	TMD	18° 44' 39"	99° 07' 28"	1952 - con.
4.	07042	A. San Sai	Chiang Mai	TMD	18° 50' 51"	99° 02' 54"	1952 - con.
5.	07052	A. Doi Saket	Chiang Mai	TMD	18° 52' 08"	99° 08' 22"	1952 - con.
6.	07062	A. Mae Rim	Chiang Mai	TMD	18° 54' 47"	99° 56' 52"	1952 - con.
7.	07072	A. Hang Dong	Chiang Mai	TMD	18° 41' 10"	98° 55' 19"	1952 - con.
8.	07082	A. San Pa Tong	Chiang Mai	TMD	18° 37' 37"	98° 53' 56"	1952 - con.
9.	07092	A. Hot	Chiang Mai	TMD	18° 11' 26"	98° 36' 52"	1952 - con.
10.	07112	A. Mae Taeng	Chiang Mai	TMD	19° 07' 08"	98° 56' 52"	1952 - con.
11.	07122	A. Phrao	Chiang Mai	TMD	19° 21' 52"	99° 12' 17"	1952 - con.
12.	07132	A. Chiang Dao	Chiang Mai	TMD	19° 21' 53"	98° 58' 00"	1952 - con.
13.	07142	A. Samoeng	Chiang Mai	TMD	18° 50' 52"	98° 44' 09"	1952 - con.
14.	07152	A. Mae Chaem	Chiang Mai	TMD	18° 29' 54"	98° 21' 54"	1952 - con.
15.	07162	A. Omkoi	Chiang Mai	TMD	17° 47' 45"	98° 21' 36"	1952 - con.
16.	07182	A. Chom Thong	Chiang Mai	TMD	18° 24' 57"	98° 40' 47"	1952 - con.
17.	07192	Ban Aen, A. Doi Tao	Chiang Mai	TMD	18° 03' 00"	98° 38' 43"	1959 - con.
18.	07232	Doi Chiang Dao Develop Settlement	Chiang Mai	TMD	19° 15' 36"	98° 55' 19"	1961 - 1972
19.	07242	Doi Suthep-Pui National Park	Chiang Mai	TMD	18° 48' 10"	98° 55' 30"	1961 - con.
20.	07252	Doi Chiang Dao Watershed Research	Chiang Mai	TMD	19° 16' 07"	98° 58' 32"	1964 - con.
21.	07262	Phuphing Ratchaniwet Palace	Chiang Mai	TMD	18° 48' 24"	98° 54' 12"	1965 - con.
22.	07272	Huai Khok Ma Watershed Research	Chiang Mai	TMD	18° 50' 00"	98° 52' 00"	1966 - 1977
23.	07282	Doi Bo Kaeo Seed-Multiplication, A. Hot	Chiang Mai	TMD	18° 09' 01"	98° 23' 35"	1966 - con.
24.	07292	San Pa Tong Rice Experimental Station	Chiang Mai	TMD	18° 36' 40"	98° 54' 02"	1962 - con.
25.	07304	Mae Cho Agrometeorological Station, A. San Sai	Chiang Mai	TMD	18° 53' 48"	99° 00' 39"	1973 - con.
26.	07331	Kaeng Kut (P.13), A. Mae Taeng	Chiang Mai	RID	19° 12' 45"	98° 52' 12"	1952 - 1980
27.	07341	Mae Kuang (P.25), A. Doi Saket	Chiang Mai	RID	18° 55' 04"	99° 07' 50"	1964 - con.
28.	07391	R.I.D. Office Unit 1, A. Muang	Chiang Mai	RID	18° 47' 21"	99° 01' 01"	1971 - con.
29.	07420	Huai Mae Faek Siphon, A. San Sai	Chiang Mai	RID	18° 59' 44"	98° 59' 00"	1952 - con.
30.	07430	Huai Mae Cho Siphon	Chiang Mai	RID	18° 54' 06"	99° 01' 14"	1952 - con.
31.	07440	Huai Kaeo Siphon	Chiang Mai	RID	19° 02' 33"	98° 58' 52"	1952 - con.
32.	07450	Huai Mae Tao Hai Siphon	Chiang Mai	RID	18° 55' 57"	99° 00' 02"	1952 - con.
33.	07460	Tail Regulator Of Mae Faek Project	Chiang Mai	RID	18° 52' 40"	99° 05' 08"	1960 - con.
34.	07472	Bhumiphol Dam Develop Settlement	Chiang Mai	TMD	17° 55' 00"	98° 41' 00"	1969 - con.
35.	07480	Sinthukit Pricha Weir (Mae Faek Proj.)	Chiang Mai	RID	19° 06' 08"	98° 57' 21"	1952 - con.
36.	07502	Mae Ho Phra Forest Plantation, A. Mae Taeng	Chiang Mai	TMD	19° 04' 00"	99° 13' 00"	1972 - con.
37.	07510	Ping River Old Project	Chiang Mai	RID	18° 41' 22"	98° 58' 20"	1977 - con.
38.	07520	Mae Taeng Headwork	Chiang Mai	RID	19° 09' 16"	98° 55' 22"	1977 - con.
39.	07530	Mae Hong Hak Siphon, A. Doi Saket	Chiang Mai	RID	18° 52' 35"	99° 08' 48"	1974 - con.
40.	07540	Mae Pong Siphon, A. Doi Saket	Chiang Mai	RID	18° 49' 17"	99° 10' 32"	1974 - con.
41.	07550	Ban Lom Wua Daeng, A. San Kamphaeng	Chiang Mai	RID	18° 44' 26"	99° 09' 37"	1959 - con.
42.	07562	Samoeng Mine Industry Centre	Chiang Mai	RID	18° 49' 14"	98° 34' 26"	1976 - 1978
43.	07581	Huai Mae Lai (P.36) A. San Kamphaeng	Chiang Mai	RID	18° 51' 26"	99° 17' 12"	1977 - 1985
44.	07591	Ban Pang Toem (P.41) A. San Pa Thong	Chiang Mai	RID	18° 37' 00"	98° 44' 43"	1979 - 1999
45.	07605	Muang Khong, A. Chiang Dao	Chiang Mai	OTH	19° 23' 00"	98° 43' 06"	1972 - 1994
46.	07615	Kut Project, A. Mae Taeng	Chiang Mai	OTH	19° 13' 48"	98° 48' 48"	1972 - 1994
47.	07625	Huai Mae Ka, A. Mae Chaem	Chiang Mai	OTH	18° 17' 21"	98° 19' 12"	1971 - 1979
48.	07635	Mae Chaem, A. Mae Chaem	Chiang Mai	OTH	18° 29' 52"	98° 21' 47"	1970 - 1981

Appendix Table 1 (Continued).

No.	Sta. Code	Station Name	Province	Gov.	Latitude	Longitude	Period
49.	07645	Kaeng Ob Luang, A. Mae Chaem	Chiang Mai	OTH	18° 13' 30"	98° 28' 00"	1971 - 1991
50.	07665	Mae Ngat Dam	Chiang Mai	OTH	19° 09' 00"	99° 02' 00"	1983 - con.
51.	07670	Mae Ngat Project (P.28A)	Chiang Mai	RID	19° 10' 10"	99° 03' 09"	1984 - con.
52.	07680	Ban Mae Thalob (G.7), A.Fang	Chiang Mai	RID	19° 42' 40"	99° 12' 50"	1986 - 1992
53.	08082	A. Wiang Pa Pao	Chiang Rai	TMD	19° 20' 47"	99° 30' 40"	1952 - con.
54.	08252	A.Pa-Daet	Chiang Rai	TMD	19° 31' 37"	99° 01' 44"	1989 - con.
55.	16032	A. Ko Kha	Lampang	TMD	18° 11' 21"	99° 23' 50"	1953 - con.
56.	16042	A. Sop Prap	Lampang	TMD	17° 52' 45"	33° 20' 26"	1953 - con.
57.	16062	A. Hang Chat	Lampang	TMD	18° 25' 00"	99° 13' 00"	1952 - con.
58.	16072	A. Thoen	Lampang	TMD	17° 36' 39"	99° 13' 08"	1952 - con.
59.	16082	A. Mae Phrik	Lampang	TMD	17° 26' 49"	99° 07' 04"	1956 - con.
60.	16162	Thung Kwian Forest Plantation, A. Hang Chat	Lampang	TMD	18° 25' 00"	99° 13' 00"	1970 - con.
61.	16303	Lampang Agrometeorogical Station	Lampang	TMD	18° 18' 00"	99° 18' 00"	1985 - con.
62.	17012	A. Muang	Lamphun	TMD	18° 34' 38"	99° 00' 34"	1952 - con.
63.	17022	A. Li	Lamphun	TMD	17° 48' 01"	98° 57' 17"	1955 - con.
64.	17032	A. Pa Sang (Pak Bong)	Lamphun	TMD	18° 31' 25"	98° 56' 38"	1955 - con.
65.	17042	A. Mae Tha	Lamphun	TMD	18° 27' 35"	99° 08' 14"	1952 - con.
66.	17052	A. Ban Hong	Lamphun	TMD	18° 18' 52"	98° 49' 21"	1962 - con.
67.	17062	Ban Ko, A. Li	Lamphun	TMD	17° 39' 20"	98° 46' 30"	1959 - con.
68.	17081	Ban Don Mun (P.42), A. Thung Hua Chang	Lamphun	RID	17° 53' 16"	99° 05' 20"	1978 - con.
69.	17093	Lamphun Agrometeological Station	Lamphun	TMD	18° 35' 00"	99° 02' 00"	1980 - con.
70.	17101	Ban Nong Hoi (P.44), A. Muang	Lamphun	RID	18° 35' 12"	99° 09' 27"	1983 - 1998
71.	17111	Mae Khanat (P.53) A. Mae Tha	Lamphun	RID	18° 23' 11"	99° 00' 37"	1986 - 1987
72.	20012	A. Muang	Mae Hong Son	TMD	19° 17' 53"	97° 58' 05"	1952 - con.
73.	20022	A. Mae Sariang	Mae Hong Son	TMD	18° 09' 24"	97° 56' 05"	1952 - con.
74.	20032	A. Khun Yuam	Mae Hong Son	TMD	18° 49' 45"	97° 56' 22"	1952 - con.
75.	20042	A. Pai	Mae Hong Son	TMD	19° 21' 29"	98° 26' 32"	1953 - con.
76.	20062	A. Mae La Noi	Mae Hong Son	TMD	18° 22' 45"	97° 56' 13"	1970 - con.
77.	20075	Ban Mae Suat, A. Mae Sariang	Mae Hong Son	OTH	17° 53' 30"	97° 57' 48"	1983 - 1995
78.	20095	Ban Mae Ngao, A. Sop Moei	Mae Hong Son	OTH	17° 51' 18"	97° 58' 12"	1984 - con.
79.	20105	Ban Wang Khan, A. Mae La Noi	Mae Hong Son	OTH	18° 23' 18"	97° 58' 11"	1984 - con.
80.	20111	Nam Pai (Sw.5A), A. Muang	Mae Hong Son	RID	19° 16' 10"	97° 56' 55"	1986 - con.
81.	20121	Mae Sariang (Sw.9), A. Mae Sariang	Mae Hong Son	RID	18° 09' 45"	97° 57' 20"	1986 - 1989
82.	63022	A. Ban Tak	Tak	TMD	17° 02' 46"	99° 04' 34"	1952 - con.
83.	63052	A. Mae Ramat	Tak	TMD	16° 58' 50"	98° 31' 14"	1952 - con.
84.	63062	A. Sam Ngao	Tak	TMD	17° 14' 32"	99° 01' 28"	1952 - con.
85.	63073	Bhumibol Dam	Tak	TMD	17° 14' 30"	99° 03' 45"	1959 - con.
86.	63092	A. Tha Song Yang	Tak	TMD	17° 13' 28"	98° 13' 41"	1967 - con.
87.	63111	Wang Kra Chao (P.12), A. Sam Ngao	Tak	RID	17° 14' 30"	99° 00' 45"	1952 - 1962
88.	63162	Ban Samong, A. Sam Ngao	Tak	TMD	17° 20' 00"	98° 53' 00"	1968 - con.
89.	63172	Ban Um Wab, A. Sam Ngao	Tak	TMD	17° 01' 00"	98° 40' 00"	1977 - con.
90.	PNR.1	Ban Teen That	Chiang Mai	DWR	19° 26' 54"	99° 12' 54"	1979 - con.
91.	PNR.13	Ban Nong Gai	Chiang Mai	DWR	19° 01' 48"	98° 50' 24"	1988 - con.
92.	PNR.2	San Pa Tong	Chiang Mai	DWR	18° 42' 00"	98° 48' 48"	1961 - con.
93.	PNR.3	Ban Mae Mut	Chiang Mai	DWR	18° 40' 12"	98° 39' 18"	1972 - 1991
94.	PNR.34	Ban Mae Mu	Chiang Mai	DWR	18° 43' 42"	98° 24' 00"	1987 - con.
95.	PNR.37	Ban San Pa Sak	Chiang Mai	DWR	19° 24' 54"	98° 43' 36"	1987 - con.
96.	PNR.39	Ban Mae Sapok (Upstream)	Chiang Mai	DWR	18° 40' 00"	98° 37' 24"	1989 - con.

Appendix Table 1 (Continued)

No.	Sta. Code	Station Name	Province	Gov.	Latitude	Longitude	Period
97.	PNR.40	Mae Mae	Chiang Mai	DWR	19° 19' 36"	98° 56' 24"	1988 - con.
98.	PNR.41	Ban Pha Lat	Chiang Mai	DWR	18° 17' 18"	98° 31' 18"	1990 - con.
99.	PNR.44	Chiang Mai	Chiang Mai	DWR	18° 56' 42"	98° 56' 48"	1977 - con.
100.	PNR.45	Ban Thung Luang	Chiang Mai	DWR	18° 43' 06"	98° 34' 12"	1974 - con.
101.	PNR.5	Ban Na Mon	Chiang Mai	DWR	19° 37' 30"	98° 34' 36"	1980 - con.
102.	PNR.6	Ban Kong Kan	Chiang Mai	DWR	18° 32' 54"	98° 21' 30"	1982 - con.
103.	PNR.8	Ban Pa Kha	Chiang Mai	DWR	17° 23' 12"	98° 28' 18"	1978 - con.
104.	GNR.43	Ban Huai Phai Yai	Chiang Mai	DWR	19° 43' 48"	99° 80' 18"	1970 - con.
105.	PNR.30	Ban Ko Thung	Lamphun	DWR	17° 35' 13"	98° 48' 40"	1988 - con.
106.	SWNR.4	Ban Na Chalong	Mae Hong Son	DWR	19° 24' 00"	98° 27' 12"	1986 - con.
107.	SWNR.5	Ban Mae Na	Mae Hong Son	DWR	19° 25' 54"	98° 24' 06"	1986 - con.
108.	SWNR.29	Ban Mae Suya	Mae Hong Son	DWR	19° 32' 06"	98° 07' 00"	1986 - con.
109.	SWNR.1	Sop Mae Samat (Pha Bong)	Mae Hong Son	DWR	19° 14' 00"	97° 56' 00"	1966 - con.
110.	SWNR.2	Ban Pang Mu	Mae Hong Son	DWR	19° 21' 30"	97° 57' 54"	1966 - con.
111.	SWNR.3	Nam Pai Dam Site	Mae Hong Son	DWR	19° 13' 18"	98° 20' 18"	1970 - con.
112.	SWNR.23	Ban Mae La Luang	Mae Hong Son	DWR	18° 32' 12"	97° 57' 12"	1967 - con.
113.	SWNR.10	Ban Tha Rua Pha Lae	Mae Hong Son	DWR	17° 53' 24"	97° 54' 48"	1969 - con.
114.	SWNR.11	Sop Han	Mae Hong Son	DWR	18° 12' 12"	97° 56' 00"	1966 - con.
115.	SWNR.14	Salween	Mae Hong Son	DWR	17° 58' 48"	97° 44' 24"	1970 - con.
116.	SWNR.16	Ban Tha Song Yang	Tak	DWR	17° 34' 06"	97° 54' 54"	1970 - con.
117.	SWNR.17	Mae Ramat	Tak	DWR	16° 58' 24"	98° 28' 42"	1971 - con.
118.	SWNR.19	Ban Dae Pha Tho Tha	Tak	DWR	17° 15' 48"	98° 14' 24"	1981 - con.
119.	SWNR.20	Ban Pho No Tha Tai	Tak	DWR	17° 20' 48"	98° 12' 30"	1986 - con.
120.	SWNR.28	Mae Charao	Tak	DWR	16° 58' 54"	98° 39' 30"	1987 - con.
121.	GNR.19	Mae Pun Luang	Chiang Rai	DWR	19° 26' 00"	99° 27' 30"	1972 - con.
122.	GNR.22	Ban Huai Muang	Chiang Rai	DWR	19° 04' 36"	99° 27' 24"	1979 - con.
123.	GNR.34	Ban Thung Yao	Chiang Rai	DWR	19° 11' 12"	99° 26' 30"	1980 - con.

Remark: con. = continous measurement until present.

Gov. = government agencies; DWR = department of Water Resources, RID = Royal Irrigation department, TMD = Thai Meteorology department

OTH = other government agencies

Appendix Table 2 List of the runoff stations in the UPRB.

No.	Sta. Code	Station Name	Province	Gov.	Area	Latitude	Longitude	Period
1.	P.1	Ping River at Nawarat Bridge	Chiang Mai	RID	6,355	18° 47' 09"	99° 00' 29"	1952 - con.
2.	P.4A	Mae Taeng at Mae Taeng	Chiang Mai	RID	1,902	19° 07' 15"	98° 56' 51"	1955 - con.
3.	P.4B	Mae Taeng at Ban Huai Hia	Chiang Mai	RID	1,833	19° 10' 20"	98° 55' 05"	1957 - 1964
4.	P.5	Nam Mae Kuang at Tha Sing Phithak Bridge	Lamphun	RID	1,569	18° 34' 32"	99° 00' 34"	1951 - 1992
5.	P.5A	Nam Mae Kuang at Ban Tha Chak	Lamphun	RID	1,740	18° 32' 32"	98° 58' 17"	1993 - 1994
6.	P.13	Mae Taeng at Kaeng Kut	Chiang Mai	RID	1,765	19° 12' 38"	98° 52' 20"	1952 - 1980
7.	P.14	Nam Mae Chaem at Kaeng Ob Luang	Chiang Mai	RID	3,853	18° 13' 49"	98° 33' 35"	1970 - con.
8.	P.14A	Nam Mae Chaem at Hot	Chiang Mai	RID	3,909	18° 12' 02"	98° 37' 01"	1958 - 1968
9.	P.19A	Ping River at Ban Tha Sala	Chiang Mai	RID	14,023	18° 25' 19"	98° 42' 11"	1958 - 1992
10.	P.20	Ping River at Chiang Dao	Chiang Mai	RID	1,355	19° 21' 09"	98° 58' 25"	1954 - con.
11.	P.21	Nam Mae Rim at Mae Rim	Chiang Mai	RID	515	18° 55' 29"	98° 56' 34"	1954 - con.
12.	P.22	Nam Mae Sa at Ban Mae Sa Noi	Chiang Mai	RID	135	18° 53' 45"	98° 57' 12"	1954 - 1968
13.	P.23	Nam Mae Khan at Ban Mae Khan	Chiang Mai	RID	1,777	18° 31' 37"	98° 51' 42"	1954 - 1987
14.	P.24	Nam Mae Klang at Ban Sop Tia	Chiang Mai	RID	616	18° 23' 15"	98° 40' 51"	1954 - 1973
15.	P.24A	Nam Mae Klang at Pracha Uthit Bridge	Chiang Mai	RID	460	18° 25' 01"	98° 40' 29"	1973 - con.
16.	P.24B	Muang Mai Canal at Ban Muang Klang	Chiang Mai	RID	-	18° 28' 05"	98° 39' 48"	1978 - 1988
17.	P.24C	Muang Luang Canal at Ban Muang Klang	Chiang Mai	RID	-	18° 28' 03"	98° 39' 41"	1978 - 1988
18.	P.25	Nam Mae Kuang at Ban Pha Taek	Chiang Mai	RID	572	18° 55' 04"	99° 07' 50"	1964 - 1968
19.	P.27	Huai Mae Nai at Ban Pa Muang	Chiang Mai	RID	24	18° 54' 23"	98° 54' 59"	1965 - 1969
20.	P.27A	Huai Mae Nai at Ban Mae Nai	Chiang Mai	RID	18	18° 53' 18"	98° 55' 00"	1967 - 1979
21.	P.28	Nam Mae Ngat at Ban Mai	Chiang Mai	RID	1,261	19° 10' 07"	99° 03' 01"	1966 - 1979
22.	P.29	Nam Mae Li at Ban Hong	Lamphun	RID	1,970	18° 18' 35"	98° 49' 35"	1969 - 1987
23.	P.30	Nam Mae Kuang at Ban Kiang Kha Mai	Chiang Mai	RID	466	18° 56' 35"	99° 08' 20"	1967 - 1979
24.	P.34	Nam Mae Kuang at Ban Pha Taek	Chiang Mai	RID	566	18° 56' 22"	99° 07' 25"	1974 - 1982
25.	P.36	Nam Mae Lai at Ban Huai Kaeo	Chiang Mai	RID	35	18° 51' 26"	99° 17' 12"	1977 - 1983
26.	P.37	Huai Mae Phaem at Ban Huai Kaeo	Chiang Mai	RID	14	18° 50' 48"	99° 16' 22"	1977 - 1983
27.	P.38	Nam Mae San at Ban Cham Khi Mot	Lamphun	RID	34	18° 30' 41"	99° 08' 09"	1977 - 1982
28.	P.41	Nam Mae Wang at Ban Pang Toem	Chiang Mai	RID	426	18° 37' 00"	98° 44' 43"	1978 - 1990
29.	P.42	Nam Mae Li at Ban Mae Bon Mai	Lamphun	RID	315	17° 53' 16"	99° 05' 20"	1978 - con.
30.	P.44	Nam Mae Tip at Ban Nong Hoi	Lamphun	RID	35	18° 35' 12"	99° 09' 27"	1982 - 1985
31.	P.48	Nam Mae Sapuat at Ban Mae Sapuat Nai	Lamphun	RID	74	18° 25' 21"	99° 05' 15"	1983 - 1988
32.	P.53	Nam Mae Khanat at Ban Mae Khanat	Lamphun	RID	146	18° 23' 11"	99° 00' 37"	1983 - 1987
33.	P.63	Nam Mae Tun at Ban Mae Tun	Chiang Mai	RID	45	18° 32' 31"	98° 42' 22"	1987 - 1990
34.	P.64	Nam Mae Tun at Ban Luang	Chiang Mai	RID	503	17° 47' 01"	98° 22' 31"	1990 - con.
35.	P.65	Mae Teang at Ban Muang Pog	Chiang Mai	RID	224	19° 38' 10"	98° 38' 19"	1993 - con.
36.	P.67	Ping River at Ban Mae Tae	Chiang Mai	RID	5,289	18° 54' 59"	98° 58' 19"	1996 - con.
37.	P.71	Nam Mae Klang at Ban Klang	Chiang Mai	RID	1,771	-	-	1996 - con.
38.	P.73	Ping River at Ban Sop Soi	Chiang Mai	RID	16,815	-	-	1997 - con.
39.	P.75	Ping River at Ban Cho Lae	Chiang Mai	RID	3,090	-	-	1998 - con.
40.	P.76	Nam Mae Li at Ban Mae E Hai	Lamphun	RID	1,541	-	-	1999 - con.
41.	PN.1	Nam Mae Ngat at Ban Teen That	Chiang Mai	DWR	81	19° 26' 54"	99° 12' 54"	1976 - con.
42.	PN.4	Huai Mae Suk at Ban Mae Suk	Chiang Mai	DWR	87	18° 33' 36"	98° 19' 42"	1977 - con.
43.	PN.5	Huai Mae Hat River at Ban Na Mon	Chiang Mai	DWR	79	19° 37' 30"	98° 34' 36"	1979 - con.
44.	PN.6	Nam Mae Chaem at Ban Kong Kan	Chiang Mai	DWR	1,950	18° 32' 54"	98° 21' 30"	1979 - con.
45.	PN.8	Nam Mae Tun at Ban Pa Kha	Chiang Mai	DWR	1,470	17° 23' 12"	98° 28' 18"	1976 - con.

Appendix Table 2 (Continued).

No.	Sta. Code	Station Name	Province	Gov.	Area	Latitude	Longitude	Period
46.	PN.10	Nam Mae Puai at Ban Huai Pong (us)	Chiang Mai	DWR	41	18° 38' 00"	98° 40' 06"	1982 - con.
47.	PN.11	Nam Mae Ya at Ban Hua Sua	Chiang Mai	DWR	90	18° 27' 06"	98° 38' 00"	1981 - con.
48.	PN.12	Nam Mae Klang at Ban Sop Hat	Chiang Mai	DWR	92	18° 32' 24"	98° 35' 42"	1981 - con.
49.	PN.13	Nam Mae Rim at Ban Nong Gai	Chiang Mai	DWR	163	19° 01' 48"	98° 50' 24"	1981 - con.
50.	PN.14	Nam Mae Chaem at Ban Huai Phung	Chiang Mai	DWR	1,270	18° 39' 18"	98° 22' 48"	1981 - con.
51.	PN.15	Huai Ma Kliang at Ban Pa Miang Pang Bong	Chiang Mai	DWR	5	18° 58' 57"	99° 20' 22"	1982 - con.
52.	PN.17	Nam Mae Lai at Ban Pa Miang Pang Kae	Chiang Mai	DWR	24	18° 51' 59"	99° 19' 48"	1982 - con.
53.	PN.18	Huai Mae Tia at Ban Som Poi	Chiang Mai	DWR	26	18° 21' 45"	98° 32' 06"	1982 - con.
54.	PN.19	Huai Mae Tae at Sop Mae Tae (US)	Chiang Mai	DWR	33	18° 24' 00"	98° 36' 00"	1982 - con.
55.	PN.20	Huai Mae Ton at Mae Wan Pang Klang	Chiang Mai	DWR	38	18° 58' 12"	99° 19' 12"	1982 - con.
56.	PN.21	Nam Mae Saluam at Ban Thung Ku	Chiang Mai	DWR	44	19° 22' 24"	99° 14' 54"	1985 - con.
57.	PN.22	Nam Mae Wan a Ban Mae Wan	Chiang Mai	DWR	53	18° 57' 54"	99° 16' 36"	1982 - con.
58.	PN.23	Huai Mae Tia at Ban Yang Mae Tia	Chiang Mai	DWR	65	18° 23' 24"	98° 37' 00"	1982 - con.
59.	PN.24	Nam Mae Pam at Sop Huai Mae Hat (DS)	Chiang Mai	DWR	203	19° 29' 12"	99° 03' 36"	1982 - con.
60.	PN.25	Nam Mae Wang at Ban Sop Win	Chiang Mai	DWR	343	18° 39' 06"	98° 41' 30"	1982 - con.
61.	PN.26	Nam Mae Khan at Sop Mae Samoeng (US)	Chiang Mai	DWR	548	18° 47' 42"	98° 43' 00"	1982 - con.
62.	PN.27	Nam Mae Khan at Ban Piang	Chiang Mai	DWR	1,170	18° 36' 39"	98° 51' 16"	1982 - con.
63.	PN.28	Nam Mae Kampong at Ban Mae Kampong	Chiang Mai	DWR	6	18° 51' 48"	99° 20' 42"	1983 - con.
64.	PN.31	Huai Ban at Ban Yang Huai Ban	Chiang Mai	DWR	12	19° 22' 36"	98° 44' 36"	1984 - con.
65.	PN.32	Huai Mae Phlaem at Ban Mae Phlaem (DS)	Chiang Mai	DWR	20	19° 23' 00"	98° 40' 48"	1984 - con.
66.	PN.33	Huai Tham Oe at Sop Huai Tham Oe	Chiang Mai	DWR	34	19° 25' 42"	98° 42' 30"	1984 - con.
67.	PN.34	Nam Mae Mu at Ban Mae Mu	Chiang Mai	DWR	71	18° 43' 42"	98° 24' 00"	1984 - con.
68.	PN.35	Nam Mae Rim at Ban Kad Hao	Chiang Mai	DWR	169	19° 01' 24"	98° 52' 48"	1984 - con.
69.	PN.36	Nam Mae Khong at Sop Huai Ban (US)	Chiang Mai	DWR	194	19° 23' 18"	98° 44' 18"	1984 - con.
70.	PN.37	Nam Mae Taeng at Ban San Pa Sak	Chiang Mai	DWR	835	19° 24' 54"	98° 43' 36"	1984 - con.
71.	PN.38	Nam Mae Pang at Ban Thung Pa Khao	Chiang Mai	DWR	30	19° 13' 6"	99° 13' 36"	1985 - con.
72.	PN.39	Nam Mae Sapok at Ban Mae Sapok (US)	Chiang Mai	DWR	35	18° 40' 00"	98° 37' 24"	1981 - con.
73.	PN.40	Nam Mae Mae at Ban Mae Na	Chiang Mai	DWR	47	19° 19' 36"	98° 56' 24"	1985 - con.
74.	PN.41	Nam Mae Pae at Ban Pha Lat	Chiang Mai	DWR	40	18° 17' 18"	98° 31' 18"	1990 - con.
75.	PE1	Nam Mae Taeng at Ban Sop Kai	Chiang Mai	EGAT	1,636	19° 13' 48"	98° 48' 48"	1972 - 1994
76.	PE5	Huai Mae Taman at Ban Mae Ta Man	Chiang Mai	EGAT	43	19° 12' 09"	98° 53' 11"	1985 - 1995
77.	PE6	Nam Mae Taeng at Ban Mae Ta Man	Chiang Mai	EGAT	1,692	19° 11' 48"	98° 53' 12"	1986 - 1995
78.	PE2	Mae Nam Ping at Ban Kong Hin	Chiang Mai	EGAT	18,932	18° 10' 30"	98° 36' 00"	1970 - con.
79.	PE3	Nam Mae Chaem at Obb Luang	Chiang Mai	EGAT	3,735	18° 13' 30"	98° 28' 00"	1968 - 1987
80.	PE4	Nam Mae Chaem at Ban Mae Ka	Chiang Mai	EGAT	3,286	18° 17' 21"	98° 19' 12"	1970 - 1979

Remark: con. = continous measurement until present.

Area = catchment area of runoff station in the unit of square kilometers

Gov. = government agencies; DWR = department of Water Resources, RID = Royal Irrigation department,

EGAT = Electricity Generating Authority of Thailand

CURRICULUM VITAE

NAME : Mr. Wisuwat Taesombat

BIRTH DATE : March 10, 1977

BIRTH PLACE : Amphoe Muang, Phitsanulok, Thailand

EDUCATION :

YEAR	INSTITUTION	DEGREE
1998	Kasetsart Univ.	B.Eng. (Irrigation Engineering)
2003	Kasetsart Univ.	M.Eng. (Water Resources Engineering)

POSITION/TITLE : Lecturer

WORK PLACE : Department of Irrigation Engineering, Faculty of Engineering at Kamphaengsaen, Kasetsart University, Kamphaengsaen Campus, Kamphaengsaen District, Nakorn Pathom, Thailand 73140.

SCHOLARSHIP/AWARD : The graduate school at Kasetsart University Thesis and dissertation support fund